



**HAL**  
open science

## Structural heterogeneities and mechanical behavior of amorphous alloys

J.C. Qiao, Qiang Wang, J.M. Pelletier, H. Kato, R. Casalini, D. Crespo, E. Pineda, Y. Yao, Y. Yang

► **To cite this version:**

J.C. Qiao, Qiang Wang, J.M. Pelletier, H. Kato, R. Casalini, et al.. Structural heterogeneities and mechanical behavior of amorphous alloys. *Progress in Materials Science*, 2019, 104, pp.250-329. 10.1016/j.pmatsci.2019.04.005 . hal-02405434

**HAL Id: hal-02405434**

**<https://hal.science/hal-02405434>**

Submitted on 22 Oct 2021

**HAL** is a multi-disciplinary open access archive for the deposit and dissemination of scientific research documents, whether they are published or not. The documents may come from teaching and research institutions in France or abroad, or from public or private research centers.

L'archive ouverte pluridisciplinaire **HAL**, est destinée au dépôt et à la diffusion de documents scientifiques de niveau recherche, publiés ou non, émanant des établissements d'enseignement et de recherche français ou étrangers, des laboratoires publics ou privés.



Distributed under a Creative Commons Attribution - NonCommercial 4.0 International License

## **Structural heterogeneities and mechanical behavior of amorphous alloys**

**J.C. Qiao<sup>a,b,c,\*</sup>, Q. Wang<sup>d</sup>, J.M. Pelletier<sup>c</sup>, H. Kato<sup>e</sup>, R. Casalini<sup>f</sup>, D. Crespo<sup>g</sup>, E. Pineda<sup>g</sup>, Y. Yao<sup>a,\*</sup>, Y. Yang<sup>b,h,\*</sup>**

*<sup>a</sup>School of Mechanics, Civil Engineering and Architecture, Northwestern Polytechnical University, Xi'an 710072, China*

*<sup>b</sup>Department of Mechanical Engineering, College of Engineering, City University of Hong Kong, Kowloon Tong, Kowloon, Hong Kong SAR, China*

*<sup>c</sup>Université de Lyon, MATEIS, UMR CNRS5510, Bat. B. Pascal, INSA-Lyon, F-69621 Villeurbanne cedex, France*

*<sup>d</sup>Laboratory for structures, Institute of Materials Science, Shanghai University, Shanghai, 200072, China*

*<sup>e</sup>Institute for Materials Research, Tohoku University, Sendai 980-8577, Japan*

*<sup>f</sup>Chemistry Division, Naval Research Laboratory, Code 6120, Washington D.C. 20375-5342, United States*

*<sup>g</sup>Departament de Física, Barcelona Research Center in Multiscale Science and Technology & Institut de Tècniques Energètiques, Universitat Politècnica de Catalunya, 08860-Castelldefels, Barcelona, Spain*

*<sup>h</sup>Department of Materials Science and Engineering, College of Engineering, City University of Hong Kong, Kowloon Tong, Kowloon, Hong Kong SAR, China*

**Ms. Ref. No.: PMS-D-18-00241**

**Submitted to *Progress in Materials Science***

**(Revised Version: April 17, 2019)**

\*Corresponding author:

Dr. J.C. Qiao

E-mail address: qjczy@hotmail.com

Dr. Y. Yao

E-mail address: yaoy@nwpu.edu.cn

Dr. Y. Yang

E-mail address: yonyang@cityu.edu.hk

## **Abstract**

Although the atomic structure of amorphous alloys, which lacks long-range translational symmetry, may appear homogeneous at the macroscopic scale, their local dynamic and/or static properties however vary significantly according to the recent experimental and simulation results. In the literature of amorphous alloys, the nature of such local heterogeneities is currently an issue under debate. More importantly, since amorphous alloys are in a thermodynamically nonequilibrium state, their local structures constantly evolve during structural relaxation, physical aging and mechanical deformation. As such, local structural heterogeneities, which vary with the thermal and mechanical history of amorphous alloys, could provide a key to understand the structural origin of their mechanical behavior, such as anelasticity, viscoelasticity, plasticity and fracture. In this review article, we first review mechanical spectroscopy or dynamic mechanical analyses as an important tool to study the relaxation dynamics in amorphous alloys, with a focus on the possible correlation between the secondary (also called  $\beta$ ) relaxation and the local structural heterogeneities of amorphous alloys. After that, we discuss the recent advances on the understanding of structural heterogeneities in metallic supercooled liquids and the influence of the structural heterogeneities on the overall mechanical properties of the corresponding amorphous alloys. Finally, we briefly discuss the further development of research on this subject.

## **Keywords**

Amorphous alloys; Metallic glass; Structural heterogeneity; Mechanical relaxation; Mechanical properties; Glass transition

# Contents

1. Introduction.....	1
2. Relaxation dynamics and structural heterogeneities in amorphous alloys .....	6
2.1 Mechanical relaxation of amorphous alloys .....	6
2.1.1 The $\alpha$ relaxation spectrum .....	12
2.1.2 Secondary relaxations .....	25
2.2 Mechanical relaxation behavior and physical properties of liquids and glasses. ....	40
2.2.1 Structural relaxation, glass transition and crystallization .....	40
2.2.2 Diffusion and microscopic dynamics.....	45
2.2.3 Mechanical behavior .....	47
3. Characterization of structural heterogeneity in amorphous alloys .....	56
3.1. High-energy X-ray diffraction method .....	57
3.2. High-rate Nanoindentation method.....	65
3.3. Atomic Force Microscopy (AFM) .....	69
3.3.1. Dynamic atomic force microscopy (DAFM) and nano-scale energy dissipation: theoretical analysis .....	69
3.3.2. DAFM analysis of dynamical structural heterogeneity in metallic glasses .....	70
3.3.3. The thermal annealing-induced evolution of nanoscale dynamical heterogeneity in metallic glasses .....	73
3.3.4. Plasticity-induced evolution of nanoscale dynamical heterogeneity in metallic glasses .....	78
3.3.5. Atomic force acoustic microscopy (AFAM) and local elastic properties of metallic glasses .....	81
3.4. Computational simulation of nanoscale structural heterogeneity in metallic glasses .....	81
4. Theoretical understanding of structural heterogeneity and relaxation dynamics in amorphous alloys .....	96
4.1. Physical origin of structural heterogeneity .....	96
4.2. Understanding relaxation dynamics from the perspective of defects .....	100
5. Structural heterogeneity and mechanical properties of amorphous alloys .....	125
5.1 Elastic constants and structural heterogeneity in amorphous alloys.....	125
5.2. Yield strength and structural heterogeneity in amorphous alloys .....	131
5.3. Ductility and structural heterogeneity in amorphous alloys .....	136
5.4. Tuning structural heterogeneity for enhanced mechanical properties ....	146
5.4.1 Cryogenic thermal cycling.....	147
5.4. 2 Surface treatment .....	150
5.4.3 Liquid-liquid phase separation.....	152
5.4.4. Nanograined amorphous alloy (nano-glass) .....	154
6. Summary and outlook .....	158
Acknowledgements.....	161
References.....	161

## 1. Introduction

After about six decades from their discovery, amorphous alloys or metallic glasses (MGs) still remain as one of the most active research topics in condensed matter physics and materials science [1-9]. Due to the rapid quenching of supercooled metallic liquids, amorphous alloys possess a disordered atomic structure and usually exhibit a unique combination of physical and mechanical properties [10-15]. Yet, challenging issues also arise for amorphous alloys as a result of this structural amorphousness, such as the room-temperature embrittlement, which severely hinders their application as a structural material [16, 17]. Therefore, understanding of the amorphous structure in amorphous alloys is of great importance even though it may appear overall featureless and was usually considered as “homogeneous” in the early literature [18, 19]. However, the recent research results clearly demonstrate that the atomic structure of amorphous alloys contains local structural heterogeneities, which can be characterized by either local static and/or dynamic properties [20, 21]. Nowadays, understanding of the physical and mechanical behavior of amorphous alloys from the perspective of local structural heterogeneities has become a very active research topic [22-27].

In principle, local structural heterogeneities could be linked to density and chemical fluctuations in an amorphous alloy for the minimization of its free energy locally [28-31]. As a result of the different local environments of atomic packing, some regions appear topologically unstable (or “liquid-like”) or stable (or “solid-like”)[32]. Nevertheless, the characteristics of such structural heterogeneities in an amorphous alloy is not well understood and still under debate [20, 33]. It is challenging to characterize the heterogeneities, if any, in an amorphous structure using the traditional characterization tools, which were early designed mainly for crystalline structures [34].

Being thermodynamically out-of-equilibrium, the atomic structure of amorphous

alloys is always inclined to evolve towards low energy configurations, as seen in the phenomena of structural relaxation and physical aging common to all sorts of glasses. Conversely, the atomic structure of amorphous alloys can be also rejuvenated by mechanical processes reaching very high energy configurations on their potential energy landscape. Consequently, the local structural heterogeneities of an amorphous alloy can be altered or modified during a thermal or mechanical treatment. Should there be a significant alteration of the local heterogeneities, a corresponding change should occur in the overall mechanical and physical behavior of amorphous alloys, such as mechanical relaxation, physical aging, crystallization, glass transition and plastic deformation. In other words, taking local structural heterogeneities as an intermediate “variable”, one may envision numerous structure-property correlations since the thermal and mechanical history of an amorphous alloy could be “encoded” in its heterogeneous atomic structure, which in turn determines the overall thermal or mechanical response of the alloy. More importantly, it should be kept in mind that these correlations could be time dependent, given the evolving disordered atomic structure or the dynamic nature of structural heterogeneities in amorphous alloys.

In the current review paper, we will first review the experimental and simulation results which are focused on mechanical (or stress) relaxation of amorphous alloys. These results are important, as provide the direct evidences that can be linked to the dynamic heterogeneities of amorphous alloys. In particular, we will discuss the correlations between the secondary (also called  $\beta$ ) relaxations and local structural heterogeneities of amorphous alloys. After that, we will shift to the recent advances on the understanding of structural heterogeneities of amorphous alloys, which are followed by the study of the influence of the structural heterogeneities on their mechanical and physical properties. Finally, we will briefly talk about our perspectives on the further development of the subject.

The outline of the current review paper is as follows: Part 1 is the introduction section in which we will discuss the importance of structural heterogeneities in

amorphous alloys for understanding their mechanical and physical properties. Part 2 deals with the macroscopic approach that lays out the foundation for the correlation of the mechanical relaxation and physical properties of amorphous alloys. A fundamental aspect of the physics of glass transition for different types of amorphous materials (i.e. amorphous polymers, glassy oxides and metallic glasses) will be briefly discussed in this part. The dynamical properties of glass formers are generally determined by measuring the relaxation behavior with techniques like dielectric and mechanical spectroscopies. The spectra usually show two relaxations: (i) the main (or  $\alpha$ ) relaxation observed at the glass transition temperature  $T_g$ , which is a universal feature of amorphous materials and attributed to the cooperative motion of molecules or atoms; and (ii) the secondary ( $\beta$ ) relaxation detected at a lower temperature (or a higher frequency), whose intensity is often much smaller than that of the  $\alpha$  process but is not always evident in all amorphous materials. According to the recent works [35-38], both  $\alpha$  and  $\beta$  relaxation could be detected in amorphous alloys, and connected to the alloys' physical, thermal and mechanical properties. In Part 3, we focus on the characterization of local structural heterogeneities based on the experimental data and atomistic simulations obtained by directly probing the local volumes or areas in an amorphous alloy. In Part 4, we review various theories and models for understanding structural heterogeneities in amorphous materials and, in particular, their connections with the  $\beta$  relaxations in amorphous alloys. These include the theories and models for supercooled liquids and glass transition [39], such as the Addams Gibbs theory [40], the random first order transition theory (RFOT) [41-45], the two-order parameter model [46-48], and the fractal twinkling theory [49, 50], and those for relaxation dynamics, such as the interstitialcy model [51, 52], the quasi-point defect model [53, 54] and flow unit model [55, 56]. In this section, these classic and new physical models as well as their experimental support will be discussed and compared in details. Compared to crystalline alloys, defining "defects" of an amorphous alloy is non-trivial and often controversial, it is however important

and can be linked with the local heterogeneities of the amorphous alloy. In Part 5, we will review the possible correlations between structural heterogeneities and mechanical properties of amorphous alloys and the possible routes to alter the structural heterogeneities for enhanced mechanical properties of amorphous alloys, such as sub- $T_g$  annealing and cryogenic thermal cycling. Finally, we will make a summary in Part 6 and discuss the future development of this subject.

To further assist understanding of the topics we are discussing, **Fig. 1** illustrates the structure of the current review. At the fundamental level, structural heterogeneity in amorphous alloys can be attributed to the thermodynamics of supercooled metallic liquids and glass transition [57, 58]. According to the theories [59, 60], structural heterogeneities arise in supercooled liquids in order to minimize their free energy, which are inherited by the corresponding glass as frozen-in structural features during glass transition. Below the glass transition temperature  $T_g$ , secondary  $\beta$  relaxations are observed in dynamic mechanical analysis (DMA) experiments [35, 36, 61-65] as a response of the heterogeneous amorphous structure to thermal stimuli. Interestingly, in the literature [35, 38, 66], these secondary relaxations were also considered as a precursor or elementary process to many important physical/mechanical phenomena observed on amorphous alloys, such as yielding and diffusion.

Here, it is worth mentioning that, in the classic literature of metallic glasses, plastic deformation in metallic glasses was proposed to be triggered by atom rearrangements in local regions involving several tens or hundreds of atoms, termed shear transformation zones (STZs) [67]. In theory, STZ can be considered as an energy barrier crossing event or a local plasticity event [67]; on the other hand, STZs can be also considered as a group of atoms within a relative loosely packed region undergoing configurational transformation [68]. Interestingly, computer simulations revealed that STZs are “liquid-like” in the sense they contain atomic clusters resembling those commonly found in super cooled liquids [69-75]. As a result of STZ activation, shear bands could form in stressed amorphous alloys through the

percolation of STZs [76-78]. In principle, stress relaxation and plasticity in amorphous alloys could be both attributed to the response of a heterogeneous amorphous structure to different external stimuli (thermal versus mechanical); therefore, they should be intrinsically correlated and the establishment of such correlations is of great importance to the study of amorphous alloys [79].

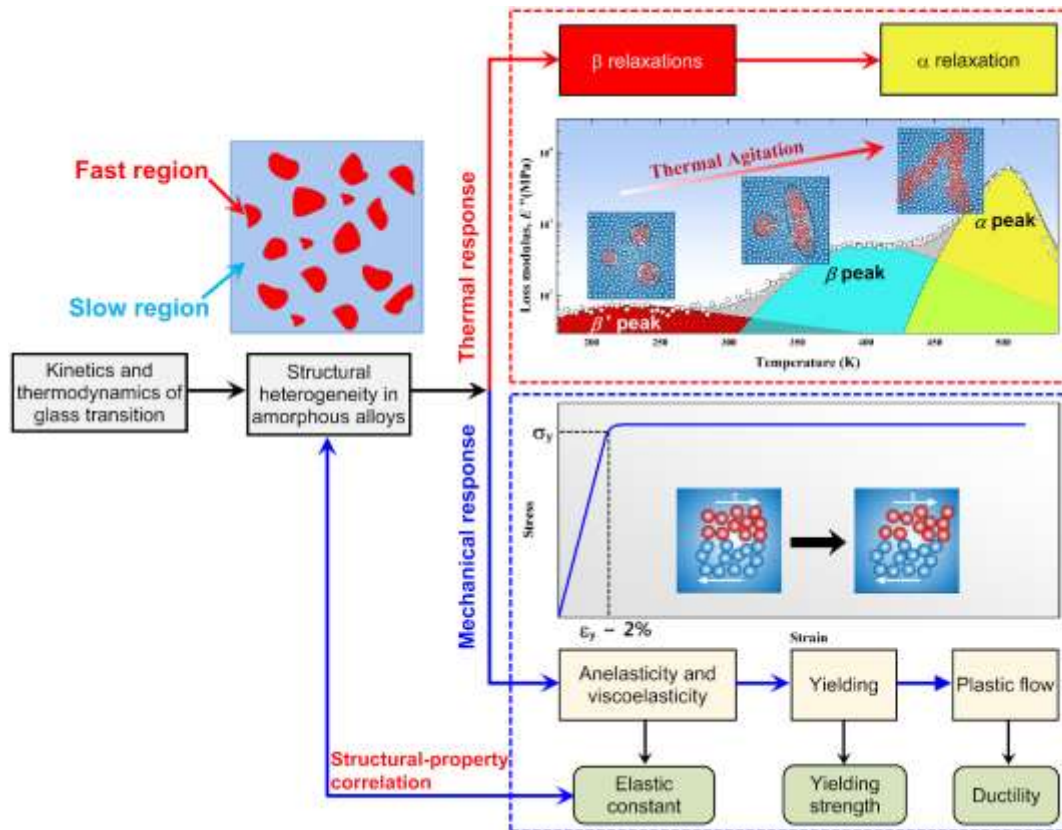


**Fig. 1.** The correlation between mechanical relaxations and mechanical properties of amorphous alloys. The mechanical spectrum adapted from reference[61]. Reprinted by permission from Macmillan Publishers Ltd: Nature Communications, reference[61], copyright (2015).

## **2. Relaxation dynamics and structural heterogeneities in amorphous alloys**

From the dynamics viewpoint, metallic supercooled liquids and glasses can be both characterized by complex structural dynamics which may be keyed to their basic properties. Structural dynamics involve processes implying a change of the inner configuration of an amorphous structure, from isolated and short-ranged atom jumps, as in solid-state atom diffusion, to collaborative and long-ranged atomic movements as in the flow of highly viscous supercooled melts. Some of these dynamic processes may entail a change in the overall energy state, like structural relaxation observed during physical aging of glasses, while some others may not, as the local structural rearrangements or stress relaxation after a temporal perturbation of temperature or external force in the supercooled liquid state or in a well-annealed glass. By a glass state, we consider all configurations sharing the same intrinsic properties like enthalpy, specific volume or relaxation time. When the relaxation of glass does not involve a change of the glass state, that is, when there is no irreversible structural change in the glass along the relaxation process, we will call this process relaxation in iso-configurational glass.

One of the main tools to probe the dynamic structural features of metallic glasses is to explore their mechanical relaxation behavior, i.e. how the system responds to the perturbation of an external stress [80, 81]. In this chapter, we will first summarize the main features observed in dynamic mechanical relaxation experiments of metallic glasses. Secondly, we will describe the relationship between the observed mechanical relaxation behavior and some basic physical properties like diffusion, physical aging and mechanical properties.

### **2.1 Mechanical relaxation of amorphous alloys**

Although glass transition has been traditionally viewed as a kinematic phenomenon, according to the recent theories and simulations [82] it also involves

changes in the underlying microstructure of the supercooled liquid as in a typical thermodynamic process. When a liquid is cooled rapid enough to avoid crystallization, its viscosity,  $\eta$ , increases sharply. By convention, the glass transition temperature  $T_g$  is defined as the temperature at which the timescale of the atomic/molecular motion – i.e. the main structural relaxation time – is 100 s, and viscosity reaches a value of  $10^{12}$  Pa·s. From the classic thermodynamic point of view, glass transition may not be a phase transition, as there is no discontinuity in any of the measurable physical properties such as specific volume or enthalpy – **Fig. 2** –. As such, the glass transition temperature depends on the cooling rate. Slower cooling rates allow a longer time for configurational sampling, and thus  $T_g$  decreases as the cooling rate decreases. Glasses obtained at slower cooling rates have a better atomic packing and a higher density.

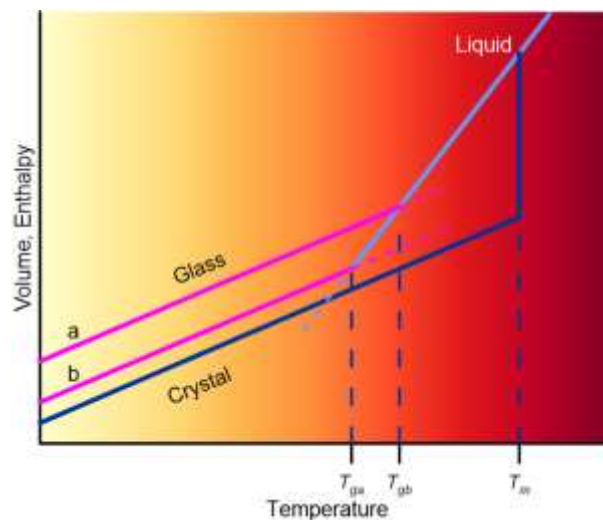


**Fig. 1.** Sketch of glass formation. Volume and enthalpy decrease as the liquid is cooled. For a high cooling rate glass transition takes place at a higher temperature –  $T_{ga}$  – than for a lower quenching rate –  $T_{gb}$  –. Reprinted by permission from Nature, reference [83], copyright (2001).

Viscosity is the main property describing the relaxation dynamics of glasses and liquids, therefore, it is worth to remember here some of the basic features of its behavior approaching the glass transition. **Fig. 3** shows the viscosity behavior of several metallic and non-metallic glass-formers, compared to the viscosity of the

strong  $\text{SiO}_2$  glass and that of a fragile pure metal [84]. In the silica glass, viscosity shows a thermally activated behavior, given by an Arrhenius temperature dependence. As shown in **Fig. 3**, the viscosity of glass-forming liquids deviates from this behavior and is better described by the Vogel-Fulcher-Tamman (VFT) law [85]. **The degree of this deviation is measured by the so called *glass fragility*  $m$  [85-87], defined as**

$$m = \left. \frac{d \log_{10} \eta}{d(T_g/T)} \right|_{T=T_g} \quad (2-1)$$

which in facts measures the steepness of the viscosity when approaching  $T_g$ , that is, the rate of decrease of the atomic mobility when approaching the glass transition. It is worth to mention that fragility is quite sensible to the chemical composition and the number of elements in multicomponent alloys.

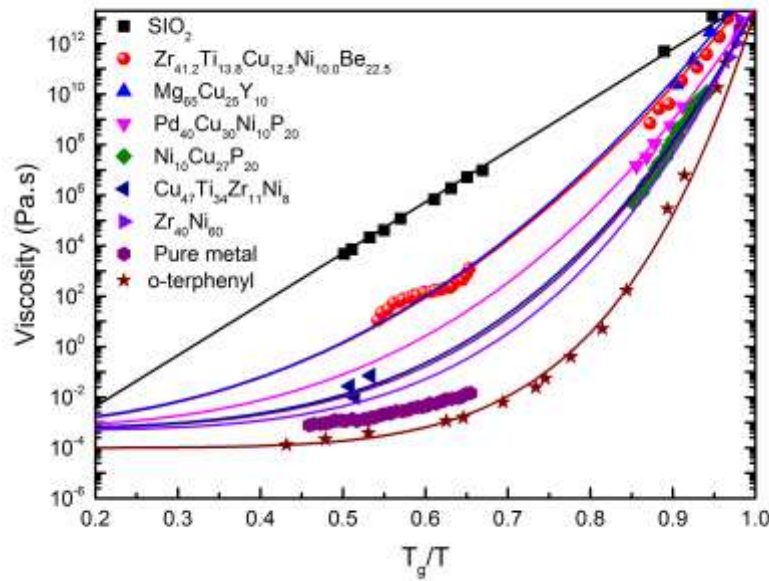


**Fig. 2.** Angell plot comparing the viscosities of different types of glass-forming liquids. Reprinted by permission from ref. [84], Copyright (2007) Cambridge University Press.

Liquids with a low fragility approach the Arrhenius behavior, and are termed

*strong*, while *fragile* liquids have a high  $m$  value. Indeed, the fragility of the liquid is related to its structural dynamics and the properties of the subsequent glass. The structure of strong liquids changes very little upon cooling towards the glass transition, opposite to that of fragile liquids [88]. The fragility of the precursor liquid correlates with the Poisson ratio of the glass [89], and that with the brittleness of the material [90]; as a consequence *strong liquids become brittle glasses while fragile liquids become ductile glasses*. This correlation is not strict, as the mechanical behavior of the glass depends also strongly on the state achieved during the quenching process, but is an overall tendency observed in metallic glasses. Thus, relaxation phenomena in the liquid state envisage the mechanical behavior of the subsequent glass. Park *et al.* [91, 92] showed that glass heterogeneity and mechanical properties such as plasticity is controlled by both the addition of minor elements and by the cooling rate, the former affecting also the fragility of the liquid while the latter controlling the particular glassy configuration in which the system is frozen-in after the quenching.

Mechanical relaxation experiments monitor the stress  $\sigma$  and strain  $\varepsilon$  of the material. According to linear viscoelasticity the distribution function of relaxation or retardation times is reflected in the time or frequency dependence of the elastic modulus  $M=\sigma/\varepsilon$  or the mechanical compliance  $J=\varepsilon/\sigma$ . Quasi-static experiments of stress relaxation or creep give the temporal evolutions  $M(t)$  or  $J(t)$  respectively, while dynamic probes obtain the complex responses  $M(\omega)=M'(\omega)+iM''(\omega)$  or  $J(\omega)=J'(\omega)-iJ''(\omega)$  composed by the storage (real) and loss (imaginary) parts. Typical dynamic or quasi-static experiments allows us to probe relaxation times from milliseconds to hours. This time-frequency window, although much narrower than that explored by dielectric spectroscopy for non-metallic glasses, covers most of the relevant structural dynamics characterizing the liquid/glass behavior at temperatures below and around the glass transition.

**Figs. 4** and **5** show experimental  $M(t)$  and  $M(\omega, T)$  obtained for  $\text{La}_{60}\text{Ni}_{15}\text{Al}_{25}$  amorphous alloys,  $T_g=461$  K, taken here as an example of the mechanical relaxation

behavior observed in metallic glasses. **Fig. 4** shows how the average relaxation time of the stress decay shortens as temperature increases,  $\tau \sim 100$  s is the time corresponding to the change from glass to liquid dynamics for typical laboratory heating/cooling rates ( $5\text{-}20 \text{ K min}^{-1}$ ) [93]. The  $M(\omega, T)$  behavior, shown in **Fig. 5**, is characterized by the main  $\alpha$  relaxation visualized by the main peak of loss modulus and the complete decay of storage modulus which determines the dynamic elastic-to-viscous transition. The  $\alpha$  peak is observed above the calorimetric  $T_g$  for frequencies higher than 0.01 Hz and typical experimental heating rates. In addition to the main relaxation, **Fig. 5** shows the presence of a secondary relaxation at lower temperature, these secondary processes have been reported in many metallic glass systems. The increase of storage and loss moduli at temperatures above the  $\alpha$  peak, corresponds to crystallization [94].

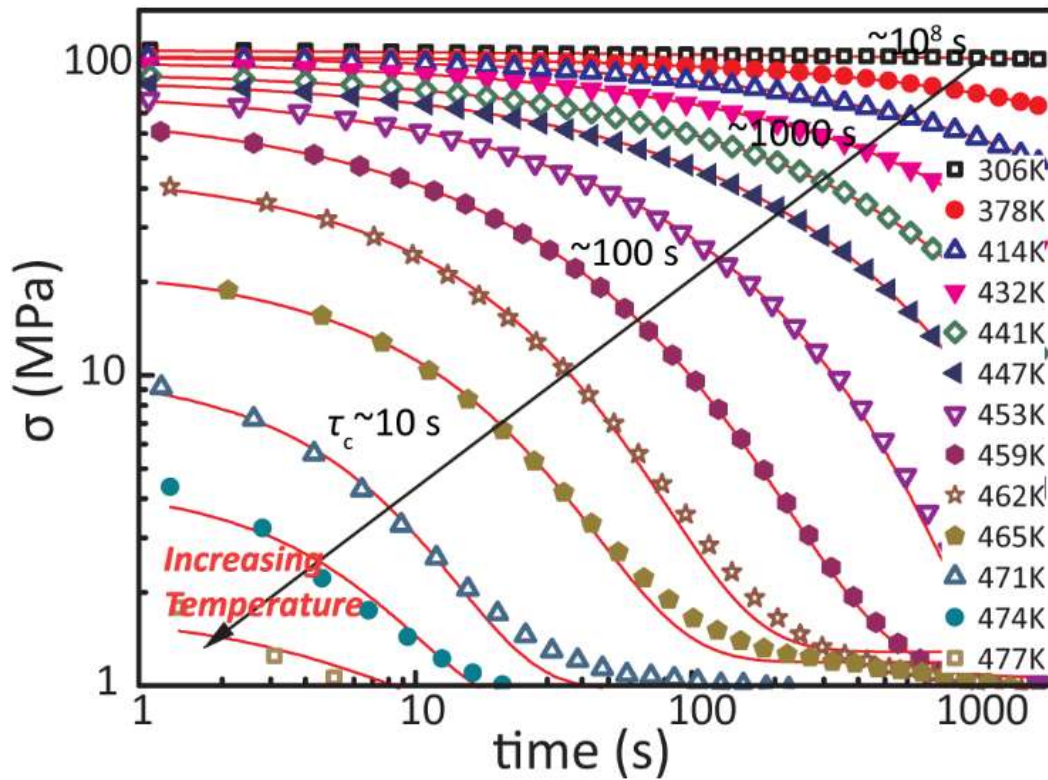


**Fig. 3.** Evolution of stress relaxation as function of temperature of  $\text{La}_{60}\text{Ni}_{15}\text{Al}_{25}$  metallic glass, taken from reference [95]. Reprinted by permission from Nature

Communations, reference [95], copyright (2014).

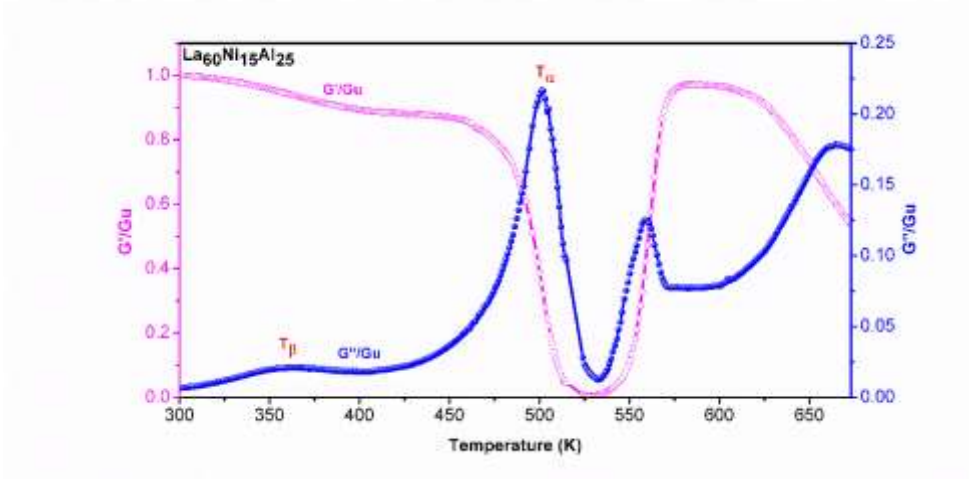


**Fig. 4.** Storage modulus and loss modulus of a  $\text{La}_{60}\text{Ni}_{15}\text{Al}_{25}$  metallic glass as a function of temperature. Reprinted from [94], with the permission of AIP Publishing.

Quasi-static stress relaxation give access to the relaxation function  $\phi(t)$  by

$$M(t) = \sigma(t)/\varepsilon = (\Delta\sigma\phi(t) + \sigma_r)/\varepsilon \quad (2-2)$$

where  $\Delta\sigma$  is the stress decay during the relaxation,  $\sigma_r$  the remnant stress and  $\varepsilon$  the applied constant strain. The relaxation function describes how the system losses the memory of the initial state and returns to internal equilibrium after being excited by an external force. On the other hand, dynamic experiments give access to the complex relaxation function  $\chi(\omega)$  through

$$M(\omega) = M_u - \Delta M\chi(\omega) \quad (2-3)$$

where  $M_u$  is the unrelaxed elastic modulus and  $\Delta M$  the intensity of the relaxation. The shape of both  $\phi(t)$  and  $\chi(\omega)$  give us access to the underlying time relaxation spectrum as will be discussed below. The storage modulus  $M'$  is proportional to the

amount of energy that is stored and released (in-and-out energy) within one load cycle, while the loss modulus  $M''$  is proportional to the energy dissipated due to viscous frictional loss and/or phase transformation within one load cycle.

Dynamic measurements of internal friction  $\tan\delta = Q^{-1} = M''/M'$  and creep experiments obtaining  $J(t)$  were some of the first results of mechanical relaxation reported for amorphous alloys [96-99]. Kimura et al. [100], later reviewed by Chen [101], showed that the  $J(t)$  obtained from creep of amorphous alloys can be well described by a viscoelastic model, i.e. with a stress exponent nearly to unity. Early internal friction measurements already observed the presence of secondary peaks at temperatures below the main  $\alpha$  relaxation, as shown in Fig. 6. We will now proceed to discuss some of the basic features observed for the  $\alpha$  relaxation of amorphous alloys and the different types of secondary relaxations reported in literatures.

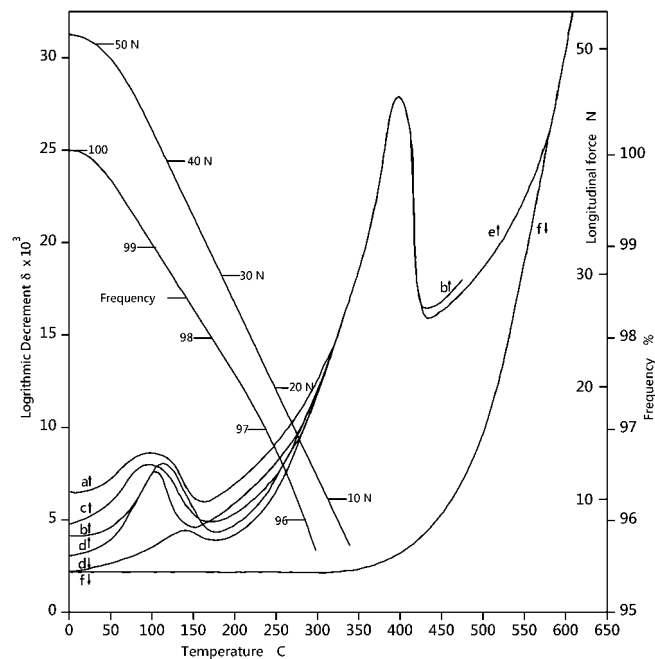


**Fig. 5.** Internal friction of Fe-based metallic glass from Hettwer et al. published in 1982 [102]. Reprinted From ref. [102], copyright (1982), with permission from Elsevier.

### 2.1.1 The $\alpha$ relaxation spectrum

Structural dynamics of amorphous alloys are characterized by a main relaxation time  $\tau_\alpha$ , related to the viscosity as  $\tau_\alpha \sim \eta/G$ , where  $G$  is the high-frequency shear modulus at the corresponding temperature. This main structural relaxation is characterized by two main features; the temperature behavior of the main relaxation time  $\tau_\alpha(T)$  and the shape of the relaxation responses  $\phi(t)$  or  $\chi(\omega)$ . The  $\tau_\alpha(T)$  behavior is described by a VFT law in the equilibrated super-cooled liquid in the  $T_g-1.2T_g$  region (relaxation times from  $10^2-10^3$  s to  $10^{-2}$  s) and it can be described by Arrhenius behaviors in the out-of-equilibrium glass below  $T_g$  (times longer than  $10^3$  s) [80, 103]. The fragility parameter  $m$ , the VFT parameters  $B$  and  $T_0$  or the apparent activation energy near the glass transition,  $E_{\alpha,liquid} = mRT_g \ln 10$ , are equivalently used to describe the  $\tau_\alpha(T)$  behavior above  $T_g$ . The Arrhenius activation energy is the main parameter describing the sub- $T_g$  behavior of iso-configurational glasses [104].

The shape of the relaxation response is associated with the expected participation of a distribution of relaxation times in the structural dynamics of disordered systems. The relation between  $\chi(\omega)$  and  $\phi(t)$ , obtained from quasi-static and dynamic mechanical relaxation respectively, is given by the transformation

$$\chi(\omega) = \int_0^{\infty} [-d\phi(t)/dt] e^{-i\omega t} dt \quad (2-4)$$

For the  $\alpha$  relaxation, which conducts the transition from elastic to viscous media, we expect  $\Delta M = M_u$  and  $\sigma_R = 0$  in equations 2-1 and 2-2. The experimental characterization of the glass and liquid relaxation is usually done by fitting empirical functions to the experimental  $\chi(\omega)$  and  $\phi(t)$ , in this way obtaining both the relaxation times and the shape-parameters of the relaxation functions. In the case of the frequency domain, the Havriliak-Negami (HN) function [105]:

$$\chi(\omega) = [1 + (i\omega\tau)^\alpha]^{-\gamma} \quad (2-5)$$

is commonly used as fitting function in many studies. The HN function produces an asymmetric peak of the loss modulus with high and low-frequency wings behaving as

$$\begin{aligned}\chi''(\omega) &\propto (\omega\tau)^\alpha & \omega \ll \tau \\ \chi''(\omega) &\propto (\omega\tau)^{-\alpha\gamma} & \omega \gg \tau\end{aligned}\quad (2-6)$$

Therefore, the values of  $\alpha$  and  $\gamma$  parameters determine the broadness and asymmetry of the relaxation peak. The symmetric Cole-Cole function [106] is obtained by fixing  $\gamma=1$  while the asymmetric Cole-Davidson function is obtained if  $\alpha=1$ , a discussion of the diverse empirical functions used to fit the relaxation behavior can be found in ref. [107]. In the time domain it is common to describe the decay of  $\phi(t)$  by a Kohlrausch-Williams-Watts (KWW) function [108, 109]:

$$\phi(t) = \exp\left[-(t/\tau)^{\beta_{KWW}}\right] \quad (2-7)$$

where  $\beta_{KWW}$  is the so-called stretching parameter.

**Fig. 7** shows the behavior of KWW functions of different  $\beta_{KWW}$  values and the corresponding peaks of the imaginary part of the susceptibility obtained by equation 2-4. The log-log scale shows clearly that the high-frequency wing of the susceptibility peaks decay approximately as  $\chi''(\omega) \propto \omega^{-\beta_{KWW}}$  while the low-frequency wing follows  $\chi''(\omega) \propto \omega^a$  with exponent  $a \sim 1$ . A rigorous examination of the relationship between the shape parameters of frequency and time relaxation functions can be found in reference [110]. The HN functions which would give the same high and low-frequency behavior are a good approximation of the stretched exponential transform. There are other empirical relaxation functions which may better reproduce some experimental data [107], usually at the cost of introducing more parameters.

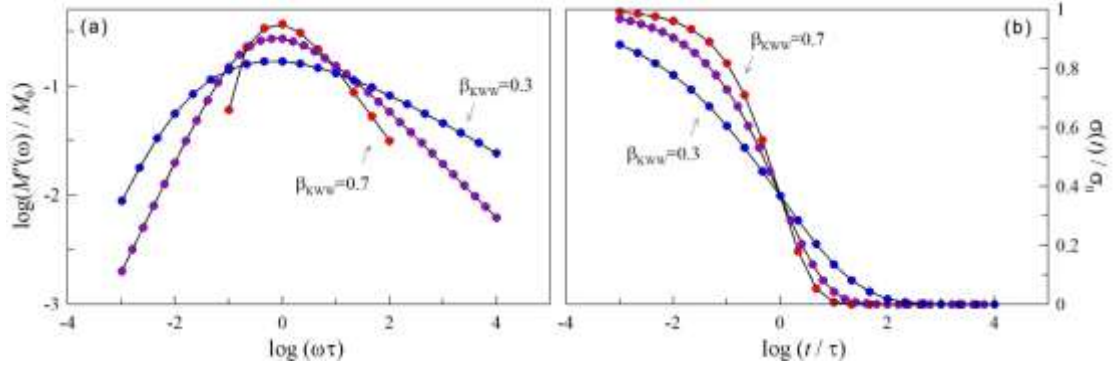


**Fig. 6.** Left: Relaxation peaks obtained by equation 2-4 from KWW correlation functions. The values of stretching exponent are  $\beta_{KWW} = 0.3$  (blue),  $\beta_{KWW} = 0.5$  (purple) and  $\beta_{KWW} = 0.7$  (red). Right: Corresponding KWW correlation functions.

At this point it is interesting to introduce the real shape of the  $\alpha$  peak in metallic glasses. **Fig. 8** shows experimental shear and Young's loss moduli obtained for several metallic glasses by Wang et al. [111], all metallic glasses showed a very similar behavior well described by an HN function. **Fig. 9**, according to Qiao and Pelletier in reference [112], shows that the direct transform of the KWW function with  $\beta_{KWW} \sim 0.5$  was also able to describe the universal behavior of the  $\alpha$  relaxation peak of amorphous alloys. It is important to recall that, in almost all studies, a common shape, with a high-frequency exponent of 0.4-0.5 is found for amorphous alloys [113-115].

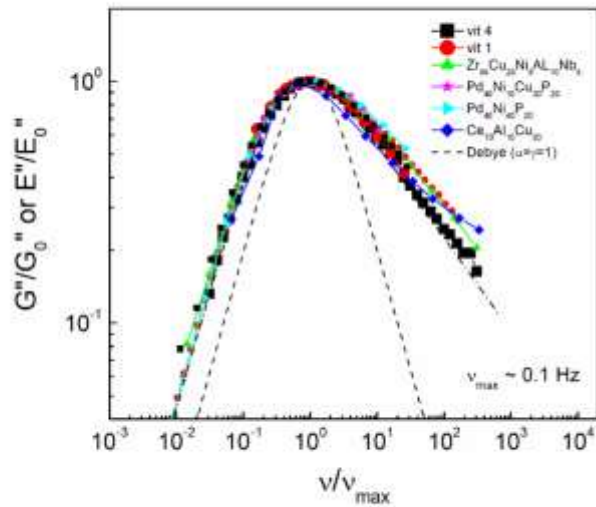


**Fig. 7.** Normalized loss modulus peak of amorphous alloys at a temperature were the peak maximum is near 0.1 Hz. Experimental data is compared to Debye and HN functions, the latter with parameters  $\alpha = 0.95$  and  $\gamma = 0.41$ . Reprinted from reference [111], with the permission of AIP Publishing.

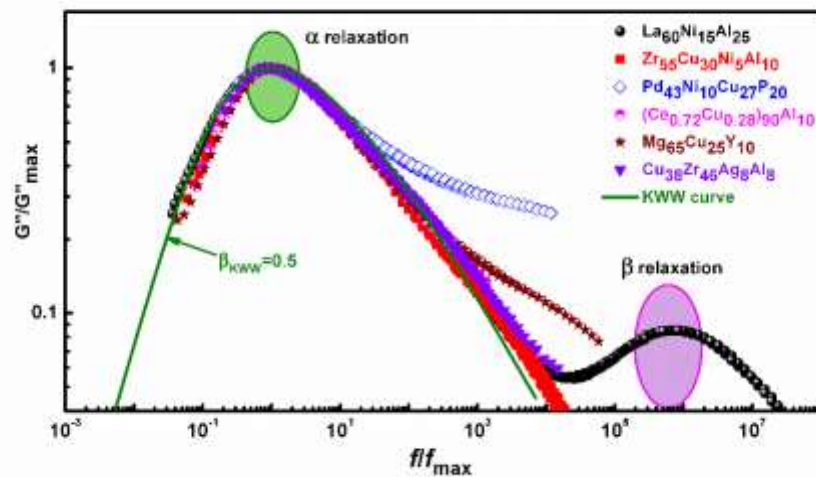


**Fig. 8.** Normalized loss modulus peak of amorphous alloys at a temperature were the peak maximum is near 0.1 Hz. Experimental data is compared to the transform of a KWW function with  $\beta_{KWW} = 0.5$  [112]. Reprinted from reference [112], copyright (2014), with permission from Elsevier.

Although the HN and KWW functions do not exactly coincide in the low-frequency side of the peak, the mechanical relaxation measurements are difficult to extend towards this low-frequency wing of the peak, as it requires long measurements in the supercooled liquid state. It is therefore difficult to correctly assess the behavior of the low frequency wing of the peak and diverse empirical functions may be used to characterize it. Generally, the use of asymmetric functions shows a good agreement if the low- and high-frequency exponents are adjusted. In ref. [116] (as shown in Fig.10), Yao et al. fitted various existing empirical  $\chi(\omega)$  functions to the experimental data obtained from an amorphous alloy. They found that the symmetric models, like the Debye and Cole-Cole functions, were not able to reproduce the experimental shape while the asymmetric models, like the Davidson-Cole, Havriliak-Negami and Jonscher functions, gave accurate descriptions of the data. As shown in Fig. 10, independent of the particular values obtained for the fitted parameters of each asymmetric model, all of them produced relaxation functions with similar low and high-frequency exponents. Interpreting this in terms of the underlying time spectrum, the  $\alpha$ -relaxation of metallic glasses must be characterized by a very similar relaxation time distribution in all systems, which contains a principal long time and a long tail of faster processes. Evidences of a discrete-like time spectrum have been given by Atzmon et al. [117, 118] and recently by Qiao et al. [119].

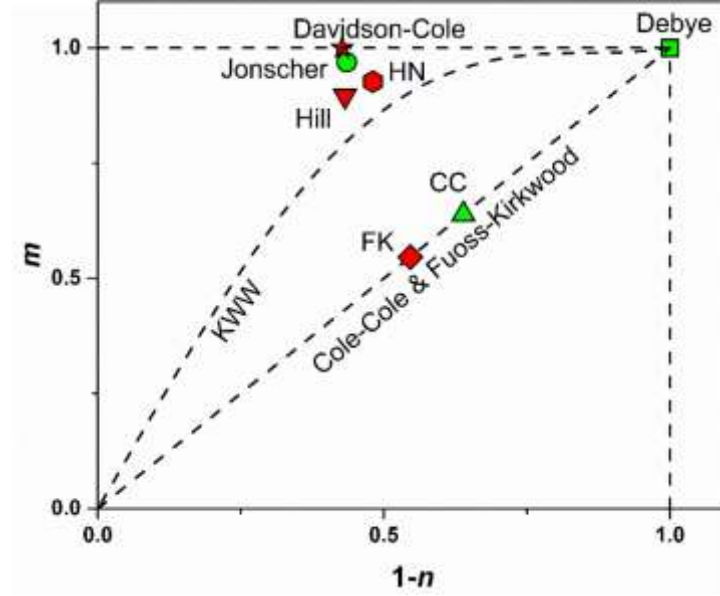


**Fig. 9.** Parameters of relaxation functions fitted to the mechanical relaxation data of  $Zr_{40}Ti_{25}Cu_8Be_{27}$  metallic glass.  $m$  and  $1-n$  correspond to the low and high-frequency slopes of the log-log plot of the loss modulus. From ref. [116]. Reprinted from reference [116]. Copyright (2017), with permission from Elsevier.

In spite of the particular relaxation model that better fits the experimental results, the dynamic relaxation behavior of a glassy material can be qualitatively described by the simple viscoelastic Maxwell equations or the ideal Debye behavior:

$$E' = E \frac{(\omega\tau)^2}{1+(\omega\tau)^2} \quad (2-8a)$$

and

$$E'' = E \frac{\omega\tau}{1+(\omega\tau)^2} \quad (2-8b)$$

Decreasing temperature causes the increase of relaxation time and such a correlation can be described by a temperature dependent shift factor  $\tau(T) = a_T \tau(T_{ref})$ . Representation of the relaxation functions on a horizontal logarithmic scale, where  $\ln\left(\frac{\omega}{a_T}\right) = \ln(\omega) - \ln(a_T)$ , allows us to determine  $a_T$  as the horizontal shift necessary

to generate a master curve by the superposition of the data obtained at different temperatures. In this way we can obtain information on the evolution of the relaxation time without imposing a particular relaxation empirical function. This is the so-called time-temperature-superposition (TTS) principle.

The average relaxation time  $\tau_\alpha$  obtained from mechanical relaxation shows two clear temperature behaviors below and above the glass transition region as shown in **Fig. 11** and **Fig. 12**, and reported in many other studies such as refs. [94, 120-125]. The apparent activation energy above  $T_g$  is related to the fragility of the melt as  $E_{\alpha,liquid}=mRT_g \ln 10$ , in metallic glasses  $E_{\alpha,liquid}$  takes values from  $50RT_g$  to  $170RT_g$  depending on the fragility [79], in absolute values  $E_{\alpha,liquid}$  is generally in the range 2-8 eV. In the out-of-equilibrium glass below  $T_g$ , the system is kinetically stuck in an unstable configuration. The long times characteristic of this temperature region complicate the experiments and the interpretation becomes more complex due to the presence of physical aging. When physical aging has a reduced contribution, the activation energy of  $\alpha$ -relaxation is found around  $25-50RT_g$  (1-2 eV) for most metallic glasses in the  $0.8T_g-T_g$  region. Below these temperatures, creep experiments give even lower activation energies of 0.5-1 eV [100].

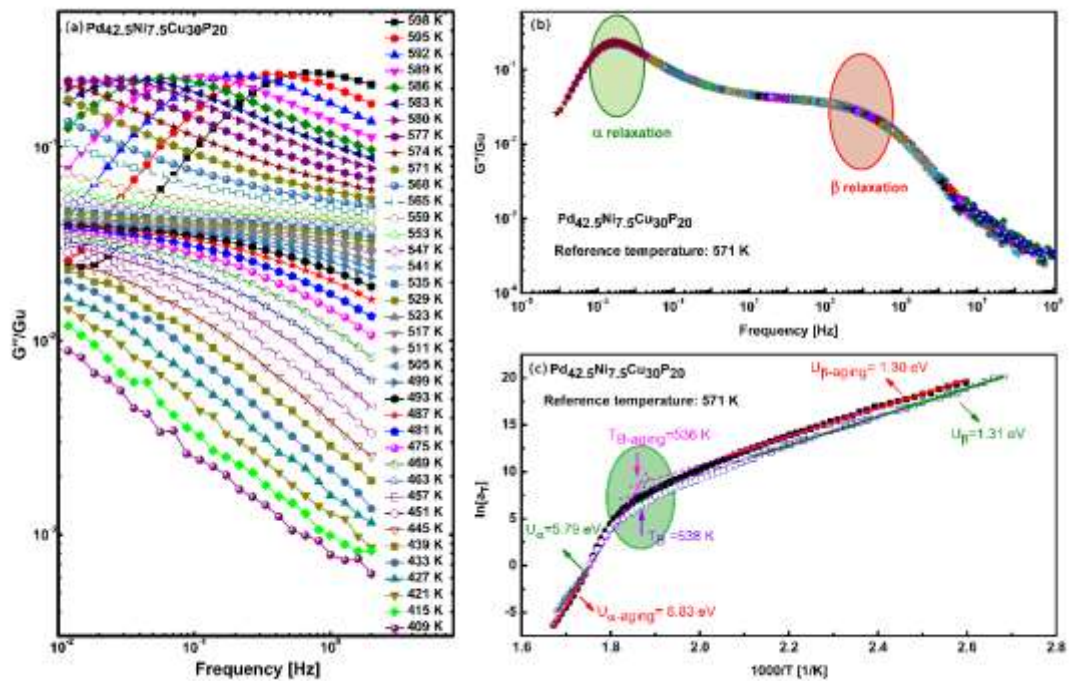


**Fig. 10.** (a) The normalized loss modulus spectra  $G''/G_u$  of  $\text{Pd}_{42.5}\text{Ni}_{7.5}\text{Cu}_{30}\text{P}_{20}$  amorphous alloy as a function of frequency at various temperatures. (b) Master curves for the loss modulus of  $\text{Pd}_{42.5}\text{Ni}_{7.5}\text{Cu}_{30}\text{P}_{20}$  amorphous alloy. (c) Master curves for the loss modulus of  $\text{Pd}_{42.5}\text{Ni}_{7.5}\text{Cu}_{30}\text{P}_{20}$  amorphous alloy at different states (as-cast and aging below  $T_g$ ). Reprinted with permission from reference[125]. Copyright (2014) American Chemical Society.

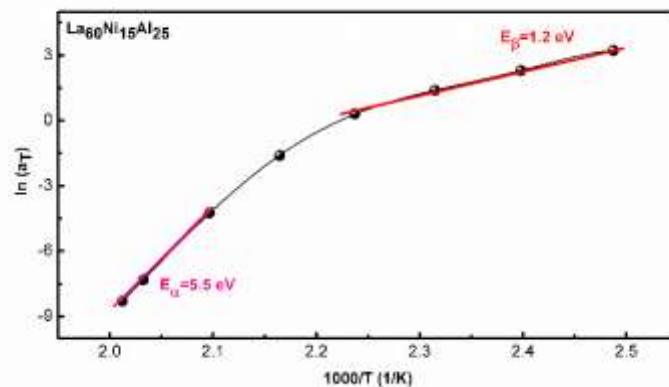


**Fig. 11.** Shift factor obtained by TTS principle for  $\text{La}_{60}\text{Ni}_{15}\text{Al}_{25}$  amorphous alloy. Reprinted from reference [94], with the permission of AIP Publishing.

Finally, the  $\alpha$  relaxation below the glass transition temperature  $T_g$  is dependent,

as all other properties, on the glass state. Structural relaxation towards more stable configurations increases both the time and activation energy of all processes, from diffusion to viscous flow [96, 126]. **Conceptually, physical aging is different from structural relaxation. The former corresponds to spontaneous relaxation of glass towards a lower energy state, while the latter to forced relaxation of glass subject to a designed thermal protocol [127, 128].** Differences of orders of magnitude of  $\tau_\alpha$  between as-quenched and annealed states are observed by mechanical relaxation [115], viscosity [104, 129] and X-ray Photon Correlation Spectroscopy (XPCS) results [130]. The dynamics of different iso-configurational states are difficult to assess, due to the influence of in situ aging during experiments of as-quenched samples [131]. As seen in **Fig. 13** the temperature behavior of  $\tau_\alpha$  can be interpreted as the system crossing various iso-configurational states; isothermal viscosity measurements of well annealed samples showed similar activation energy for the viscous flow of different iso-configurational states [104].

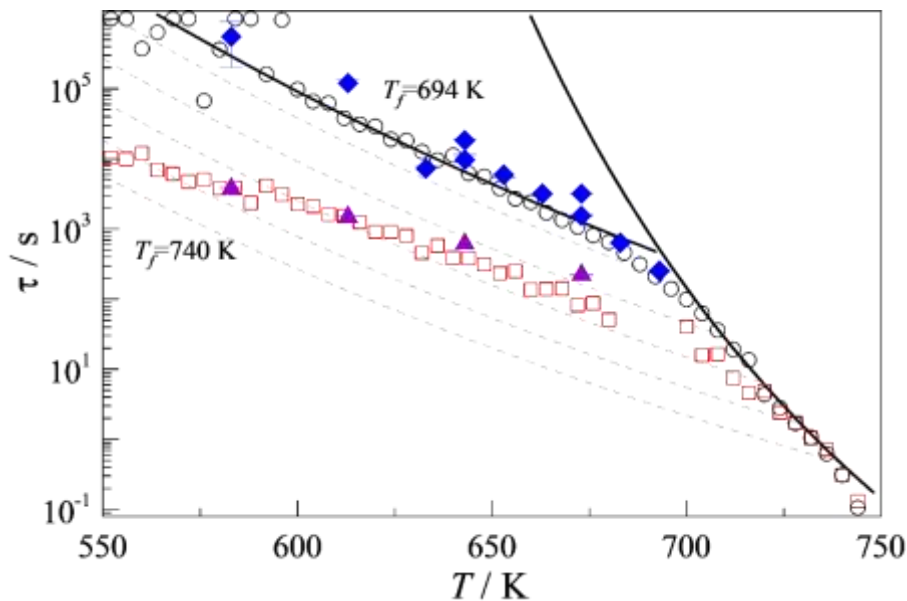


**Fig. 12.** Relaxation times obtained by dynamic (open circles) and quasi-static (full symbols) mechanical relaxation of as-quenched (red and purple symbols) and annealed (black and blue symbols)  $\text{Cu}_{46}\text{Zr}_{46}\text{Al}_8$  metallic glass. Reprinted From ref. [115] Copyright (2015), with permission from Elsevier.

Plastic deformation (irreversible deformation) can increase the disorder in glassy materials [132]. **Fig. 14** shows the evolution of loss factor  $\tan\delta$  with temperature at various states. The higher is the cold rolling ratio, the higher is the loss factor. Thus, the atomic mobility is increased by the cold-rolling treatment, which corresponds to an increase of the concentration in quasi-point defects based on the quasi-point defects (QPD) theory. This and other physical models will be detailed in section 4 below. Therefore, it is confirmed that the atomic mobility is increased by plastic deformation. According to the QPD model, the increment corresponds to increasing the concentration of quasi-point defects. Plastic deformation induces rejuvenation of the material. The concentration of “defects” is higher than the equilibrium value, so an evolution is expected when temperature is increased. These results in bulk metallic glass show good agreement compared with other glassy materials [132].

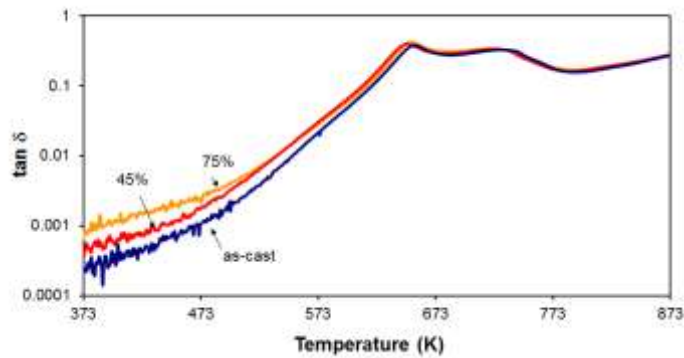


**Fig. 14.** Effect of the cold-rolling ratio ( $\varepsilon = 45\%$  and  $\varepsilon = 75\%$ ) on loss factor  $\tan\delta$  of  $\text{Ti}_{40}\text{Zr}_{25}\text{Ni}_8\text{Cu}_9\text{Be}_{18}$  amorphous alloy (The as-cast state is reference state) [133]. Reprinted From reference [133], copyright (2012), with permission from Elsevier.

**Fig. 15** shows the evolution of the internal friction with temperature in various structural states of the  $\text{Zr}_{56}\text{Co}_{28}\text{Al}_{16}$  bulk metallic glass. By selecting the as-cast state as reference state, annealing below the glass transition temperature  $T_g$  induces a slightly decrease compared to the reference state. Partial crystallization (heat treatment at 800 K) leads to a larger decrease than after annealing below the  $T_g$ . The

loss factor is almost negligible after complete crystallization. In contrast, the loss factor  $\tan \delta$  is higher than that of the reference state in the cold rolled sample.

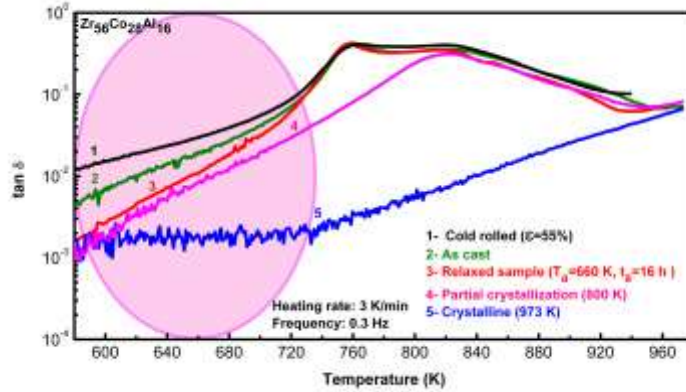


**Fig.15.** Evolution of the internal friction with the temperature in  $Zr_{56}Co_{28}Al_{16}$  amorphous alloy at different states [134]: (1) 55% thickness reduction after cold-rolling, (2) as-cast sample (3) after structural relaxation (annealing temperature is 660 K with annealing for 16 hours), (4) formation of partial crystallization (heating to 800 K with a heating rate of 3 K/min). Reprinted from reference [134], copyright (2014), with permission from Elsevier.

Cui et al. developed a dissipative nonaffine lattice dynamics theory for metallic glasses, with a bottom-up approach starting from a microscopic Hamiltonian for the motion of a tagged atom coupled to all other atoms in the material [135]. The theory leads to a generalized Langevin equation that is used in combination with non-affine dynamics to derive the dynamic viscoelastic moduli  $E'$  and  $E''$ . These moduli are functions of the vibrational density of states and of the emergent non-Markovian atomic-scale friction coefficient (memory kernel) that embodies the long-range coupling between atoms. The predictions of the viscoelastic theory compare very well with experimental data for uniaxial viscoelastic response of CuZr amorphous alloy, using the density of states from molecular dynamics simulations of the same system.

Importantly, no agreement can be found using either a density of states that does not feature excess of boson-peak modes at low frequency, or using the time-dependence of the non-Markovian friction in the equation of motion which

differs from a stretched-exponential function. This finding indicates strong memory effects at the atomic level, possibly due to the non-local electronic component of interaction. Here “non-local electron component” means the free-electron contribution to the atomic bonding. In metals, the free-electron contribution to bonding between two atoms can establish medium- and even long-range correlations in the atomic motions which involve several atoms. This is reflected in the many-body term used in embedded atom model (EAM) potential [136], for example. In turn, these correlations may give rise to memory-dependent effects in the atomic motion, which means that the velocity of a certain atom sees an effective damping at some point in time which may depend on the motion of the atom at earlier times due to the persistence of correlated medium or long-range interaction with other atoms. This should be contrasted with non-metallic materials where, instead, the bonding has less of many-body character. For example in silica glass, the atomic bonding is strongly localized (e.g. Si-O) [137], so memory effects may be less strong as there are less long-range correlations with other atoms. It is also shown that the  $\alpha$ -wing asymmetry in  $E''$  grows upon decreasing the temperature below  $T_g$ , which is linked to the growth of the characteristic time-scale of memory effect in the model. Hence, a link exists between the  $\alpha$  time and the characteristic time-scale over which atoms retain memory of their previous collision history (as shown in **Fig. 16**).

Hence, this analysis establishes that, in order to explain the mechanical  $\alpha$  relaxation and the  $\alpha$ -wing asymmetry in metallic glass, an excess of soft vibrational modes as well as strong memory effects in the dynamics due to non-local electronic coupling between many atoms, are necessary ingredients that cannot be neglected. Furthermore, the approach is directly applicable to a variety of glassy and partly-ordered systems that feature a boson peak, hence not only metallic glasses but also polymer glasses, silica glasses and even quartz, by suitably extending the theory to include bond-bending interactions, needed to describe covalent bonds. Hence, the framework opens up the way for a truly atomic-level predictive and quantitative

description of mechanical response and relaxation in disordered materials.

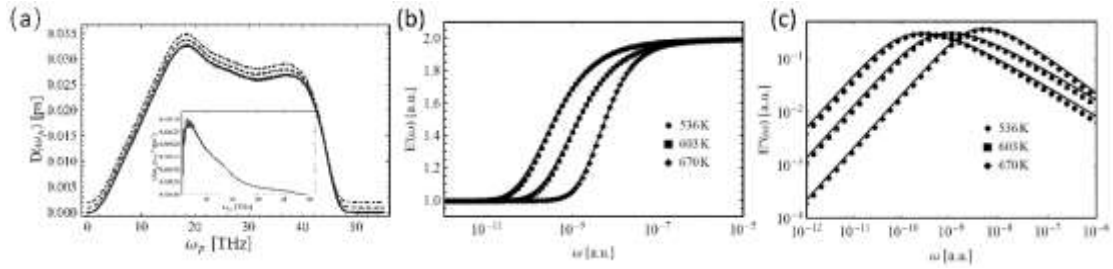


**Fig. 16.** The atomic-scale theory of viscoelasticity in metallic glasses. (a) Phonon density of states of a CuZr metallic glass. The inset shows the reduced states over Debye's model, which indicates the appearance of Boson peak at low frequency. The theoretically predicted storage modulus  $E'$  (b) and loss modulus  $E''$  (c) as a function of frequency, which are in fairly agreement with experimental data [135]. Reprinted figures with permission from reference [135], copyright (2017) by the American Physical Society.

### 2.1.2 Secondary relaxations

Johari and Goldstein suggested that secondary relaxation was a universal phenomenon of glassy materials and intrinsically linked to the  $\alpha$  relaxation [138]; this kind of secondary process is termed as slow  $\beta$  relaxation [93]. On the other hand, the presence of one or various internal friction secondary peaks in amorphous materials can be associated to different origins, some of them not directly related to the amorphous state as similar anelastic processes can be found in the crystalline counterparts. First reports of internal friction peaks date back to Berry et al. [139], who observed a relaxation process below room temperature in a sputtered film of  $\text{Nb}_3\text{Ge}$  metallic glass. With an activation energy of 0.52 eV the peak was interpreted as stress induced point defect relaxations, similar to the ones found in crystalline solids although not showing a Debye relaxation shape but an asymmetric distribution. The intensity of the peak decreased with aging. Yoon and Eisenberg [140] ascribed similar peaks, located around 250K with activation energies of  $E \sim 1.0$  eV, to the movement of B atoms in  $\text{Fe}_{40}\text{Ni}_{40}\text{P}_{14}\text{B}_6$  and  $\text{Fe}_{32}\text{Ni}_{36}\text{Cr}_{14}\text{P}_{12}\text{B}_6$  amorphous alloys.

Later work by Berry [141] suggested that this well-defined atomic-scale relaxation processes were linked to hydrogen absorption and its effect in the glassy structure. Kunzi et al. [142] found similar peaks in  $\text{Cu}_{50}\text{Zr}_{50}$ ,  $\text{Co}_{35}\text{Y}_{65}$  and  $\text{Co}_{35}\text{Dy}_{65}$  amorphous alloys and attributed them to intrinsic atomic-scale processes of the amorphous structure, independently of hydrogen or oxygen absorption. Khonik et al. [143] showed that both cold work and hydrogenation induced internal friction peaks with activation energies  $\sim 0.51$  eV. They argued that the dependence of the relaxation intensity on the amplitude of the oscillation indicated that the relaxation process is related to non-local “dislocation-like” defects introduced during inhomogeneous deformation. A more recent ultrasound spectroscopy study [144] interpreted a low temperature peak at 250 K in  $\text{Zr}_{55}\text{Cu}_{30}\text{Al}_{10}\text{Ni}_5$  amorphous alloy as originated by thermal relaxation of squeezed free-volume due to a transition in the electron-phonon coupling behavior. All these secondary relaxations mentioned above are observed at temperatures far below  $T_g$ , even below room temperature in many cases, and at frequencies within the 1-3000 Hz range. Therefore, they are not detected by mechanical spectroscopy near  $T_g$ . They correspond to very fast processes far from  $\alpha$ -relaxation, attributed to different origins but not directly related to the glass transition process. However, it is important to take these processes into consideration in order to have a complete general picture of the mechanical relaxation spectrum and to understand its relationship with the mechanical properties of amorphous alloys.

In the last decade, the study of secondary relaxations has been centered on processes detected at  $0.7-0.9T_g$  by mechanical spectroscopy in the frequency range of 0.01-100 Hz. It is generally assumed that these secondary relaxations correspond to the slow  $\beta$  or JG relaxation. In non-metallic glass formers both  $\alpha$  and slow  $\beta$  relaxations merge at high temperatures [62]. Although crystallization prevents to explore this temperature region in metallic glasses, the merge between the two relaxations has been inferred [145]. These relaxations can be observed as well separated secondary peaks, like in some La and other rare earth based amorphous

alloys [146, 147], as prominent high-frequency (or low-temperature) shoulders of the  $\alpha$  peak, like in some Pd-based glasses [148], or as high-frequency excess wings of the main  $\alpha$  relaxation [149]. The emergence of a well-defined secondary peak as function of the alloy composition can be observed in **Fig. 17** for La-based amorphous alloy [150]. More than two decades ago, Okumura et al. [151, 152] already showed the presence of a secondary peak in  $\text{La}_{55}\text{Al}_{25}\text{Ni}_{20}$  metallic glass. Wang's work on La-based metallic glasses [146] showed that both intensity and peak temperature of the  $\beta$ -relaxation were strongly influenced by the chemical composition. This was further examined by Yu et al. [62], they related the appearance of  $\beta$  relaxation in La- and Pd-based metallic glasses to similar negative values of enthalpy of mixing between all the elements of the alloy. Positive or large differences in enthalpy of mixing suppressed  $\beta$ -relaxation. Through systematically alloying different types of elements, Wang's group found that the pronounced  $\beta$  relaxation peaks near  $T_g$  always evolved hand in hand with the boson heat capacity peaks in La-based metallic glasses [153]. This phenomenon suggests the  $\beta$  relaxation arises from the regions which mainly contribute to the boson peak and provides the first experimental evidence for the connection between the slow and fast glassy dynamics.

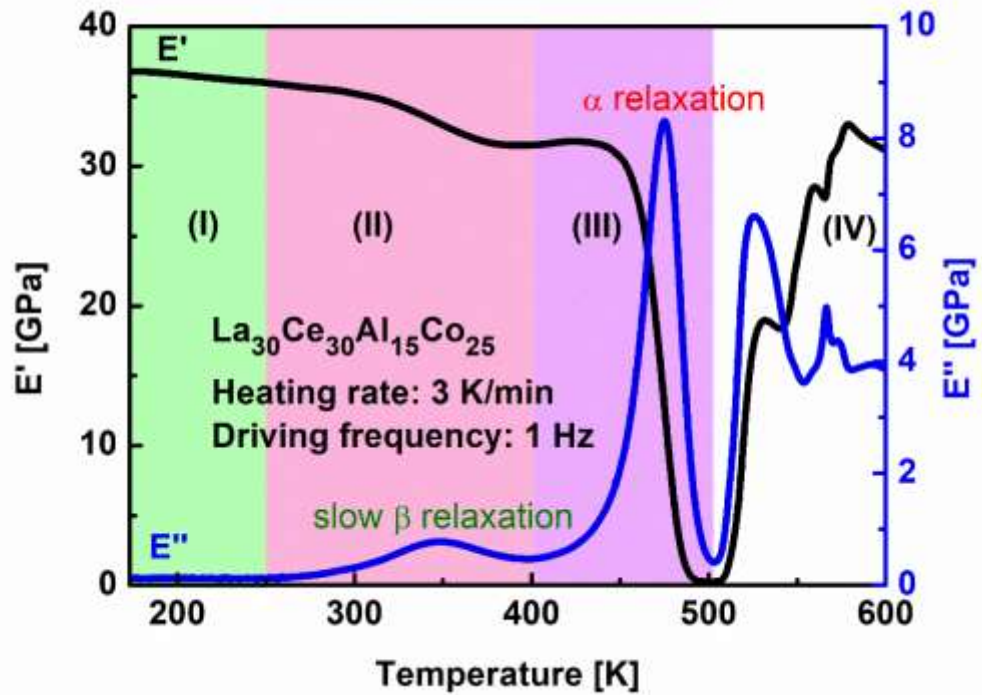


**Fig. 17.** The temperature dependence of the storage modulus  $E'$  and loss modulus  $E''$  with temperature in  $\text{La}_{30}\text{Ce}_{30}\text{Al}_{15}\text{Co}_{25}$  amorphous alloy. Reprinted from reference [150], copyright (2019), with permission from Elsevier.

An important point for discussing the origin of the  $\beta$  relaxation is its behavior upon structural relaxation or aging. Annealing below  $T_g$  drives the glass towards a more stable state. This is a structural relaxation process which induces a reduction of free volume with the associated enthalpy change. The magnitude of the enthalpy change can be revealed by subsequent measurement of the specific heat  $c_p$ . The formation energy of free volume between as-cast and relaxed states was estimated to be of 5.89 eV/atom in  $\text{Zr}_{55}\text{Cu}_{30}\text{Ni}_5\text{Al}_{10}$  [154] and 7.45 eV/atom in  $\text{Zr}_{55}\text{Cu}_{30}\text{Ni}_5\text{Al}_{10}$  [155]. These values are quite larger than the energy of vacancy creation in pure metals ( $\leq 2$  eV/atom), suggesting that the relaxation process involves notable structural rebuilding [156], which is reflected in an increase in the hardness and, eventually, the brittleness of the glass.

From the perspective of free volume, the structural relaxation process always implies a reduction of internal friction or loss modulus related to the release of free volume. **Fig. 18** shows the reduction of intensity and the evolution towards higher temperatures of the secondary relaxation shoulder for  $\text{Pd}_{42.5}\text{Ni}_{7.5}\text{Cu}_{30}\text{P}_{20}$  metallic glass. The constant loss modulus background at temperatures below the onset of the secondary peak is also reduced. The effect of aging on the mechanical relaxation of metallic glasses is reported in many works [107, 157-162]. In metallic glasses with prominent slow  $\beta$  relaxations, like some La [163] and Y-based alloys [164], the process of physical aging during annealing is not able to suppress the secondary peak and it is therefore a characteristic feature of the structural dynamics of well relaxed iso-configurational states. In other systems, the annealing may totally suppress the secondary relaxation. In this case it is difficult to assess if the presence of a secondary peak is not just the observation of the high-frequency tail of the  $\alpha$ -relaxation combined with in situ physical aging [114]. As already discussed by Chen [159], the sub- $T_g$  relaxation in amorphous alloys has some different features from the JG-relaxation in polymeric or molecular glasses. In this latter substances, the slow  $\beta$ -process shows a distinct peak at  $T < 0.6T_g$  (at a frequency of 1 Hz) and small effect due to annealing near  $T_g$ .

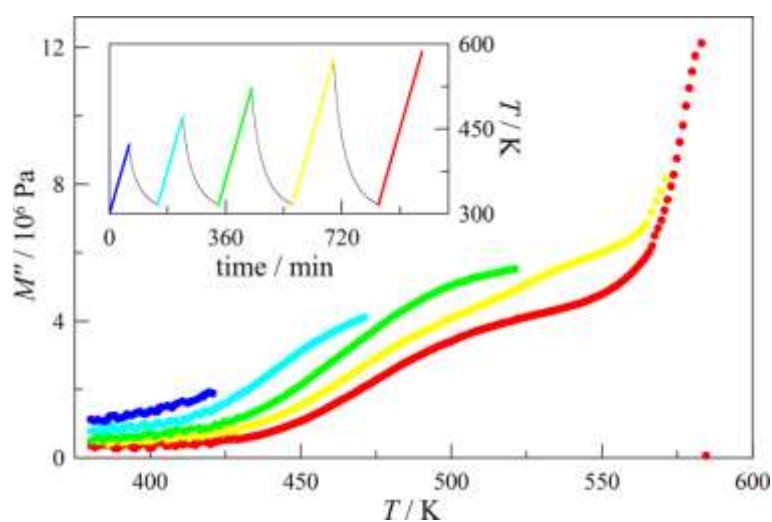


**Fig. 18.** Loss modulus of Pd<sub>42.5</sub>Ni<sub>7.5</sub>Cu<sub>30</sub>P<sub>20</sub> measured at a constant frequency of 1 Hz during consecutive heating runs. The applied thermal protocol is shown in the inset. Reprinted with permission from reference [165]. Copyright (2016) American Chemical Society.

The activation energy of the  $\beta$  relaxation is found  $E_{\beta} \sim 26RT_g$  (0.5-1.5 eV) in amorphous alloys [166, 167], which is similar to the activation energies extracted from aging, atomic diffusion and onset of plastic deformation, as will be discussed below. The microscopic origin has been widely debated. From atomistic simulations, the  $\beta$  process was attributed to cooperative movements of different nature than the  $\alpha$  relaxation, like string-like motions [168, 169]. Recent simulation works have demonstrated that, at least in the simulated systems, the string-like cooperative motions are the origin of the secondary relaxation peak detected by mechanical spectroscopy [170-172]. Although being cooperative,  $\beta$  relaxation involves only part of the atoms that could participate in stress relaxation. X-ray diffraction combined with the extended X-ray absorption fine structure (EXAFS) results showed that the relaxation originated from short range collective rearrangements of the large solvent atoms in a binary metallic glass [173]. In some metallic glasses, like in Zr<sub>55</sub>Cu<sub>30</sub>Al<sub>10</sub>Ni<sub>5</sub> [174] and La<sub>55</sub>Al<sub>25</sub>Ni<sub>20</sub> [175], there is evidence of a double glass transition related to phase separation or to double-stage unfreezing of the mobility of the different species during heating, thus resulting in a secondary peak or shoulder of the loss modulus.

The presence of slow  $\beta$  relaxations, their relationship to structural and/or chemical heterogeneities and their universality in the glass state have been discussed since the earliest works reporting such phenomena [176], and the debate on their microscopic origin remains open. What is certainly true is that, either if they are related to unrelaxed structures produced by rapid quenching or mechanical deformation or if they are intrinsic to certain metallic glass compositions, many authors propose that they are indicative of structural heterogeneity. Furthermore,

while the spectrum of the  $\alpha$  relaxation is very similar in all metallic glass-forming systems, secondary relaxations characterize the specificities of the distribution of relaxation times of each particular sample.

As aforementioned, some researchers proposed that the slow  $\beta$  relaxation is due to the presence of structural heterogeneities, however, compelling experimental evidence is lacking [177] and the debate on this point is still open [178]. In the case of fragile liquids (i.e. liquids with large steepness index  $m$  values), they usually have more pronounced  $\beta$  relaxations which manifest as distinct peaks or broad humps, while  $\beta$  relaxations are shown as an excess wing in strong liquids (i.e. liquids with small  $m$  values) [166, 179]. This overall correlation is not strictly followed in amorphous alloys or metallic glasses. For example, the family of La-based metallic glasses show the most distinct secondary  $\beta$  peaks even though they are generally considered as strong liquids relative to other metallic glasses.

Conceptually, physical aging is a process through which glassy materials evolve into a more stable state, which plays an important role in mechanical relaxation of structural glasses, such as amorphous alloys [148, 180]. **Fig. 19(a)** exhibits the effect of structural relaxation below the glass transition temperature  $T_g$  on the loss modulus of  $\text{La}_{60}\text{Ni}_{15}\text{Al}_{25}$  metallic glass (the aging temperature is 448 K and aging time is 16 hours, the glass transition temperature  $T_g$  of  $\text{La}_{60}\text{Ni}_{15}\text{Al}_{25}$  metallic glass is 461 K ) [181]. The intensity of the slow  $\beta$  relaxation of the  $\text{La}_{60}\text{Ni}_{15}\text{Al}_{25}$  metallic glass decreases by aging below  $T_g$ . In parallel, compared with the as-cast state, the peak maximum of the slow  $\beta$  relaxation shifts to higher temperature after aging below  $T_g$ , which is in accordance with the experimental results reported by Wang *et al.* [180]. As we discussed in the previous section, unlike for  $\text{La}_{60}\text{Ni}_{15}\text{Al}_{25}$  metallic glass, in Pd-, and Zr-based metallic glasses, the  $\beta$  process is not a resolved peak but it is manifested as a “shoulder” or “excess wing” on the curve of loss modulus versus temperature [62, 177, 182]. As shown in **Fig. 19(b)**, it is evident that after structural relaxation below  $T_g$  the “excess wing” becomes less evident [183]. However, one can see that the part

of the loss modulus versus temperature curve, which is linked to the  $\alpha$  relaxation, keeps almost unchanged [Fig. 19(b)], which is in good agreement with the results obtained from the La-based metallic glass [181]. Several investigations suggested that the slow  $\beta$  relaxation corresponds to inherent structural heterogeneities in metallic glasses, such as soft domains, liquid-like regions, local topological structure of loose packing regions as well as flow units [79, 94]. During physical aging below  $T_g$ , the thermal activation of atoms within those regions causes the evolution of the glassy structure towards a more stable state with a consequent reduction of structural heterogeneities. Thus, structural relaxation below  $T_g$  reduces the concentration of “defects” in metallic glasses. Wang *et al.* reported a similar phenomenon in the  $\text{La}_{60}\text{Ni}_{15}\text{Al}_{25}$  bulk metallic glass [180]. According to the non-isothermal dynamic mechanical experiments (in isochronal temperature scans) [180], the Poisson’s ratio decreases as the peak temperature of the slow  $\beta$  relaxation shifts to higher temperatures for a given frequency or as the  $\beta$  process moves to a lower frequency at a given temperature. Based on the Eshelby’s theory, Sun *et al.* recently developed a micromechanical model that relates the properties of the local elastic heterogeneities of metallic glasses to their overall elastic properties (i.e. shear/bulk modulus and Poisson’s ratio) [10]. During structural relaxation, the volume fraction of liquid-like regions is expected to gradually decrease.

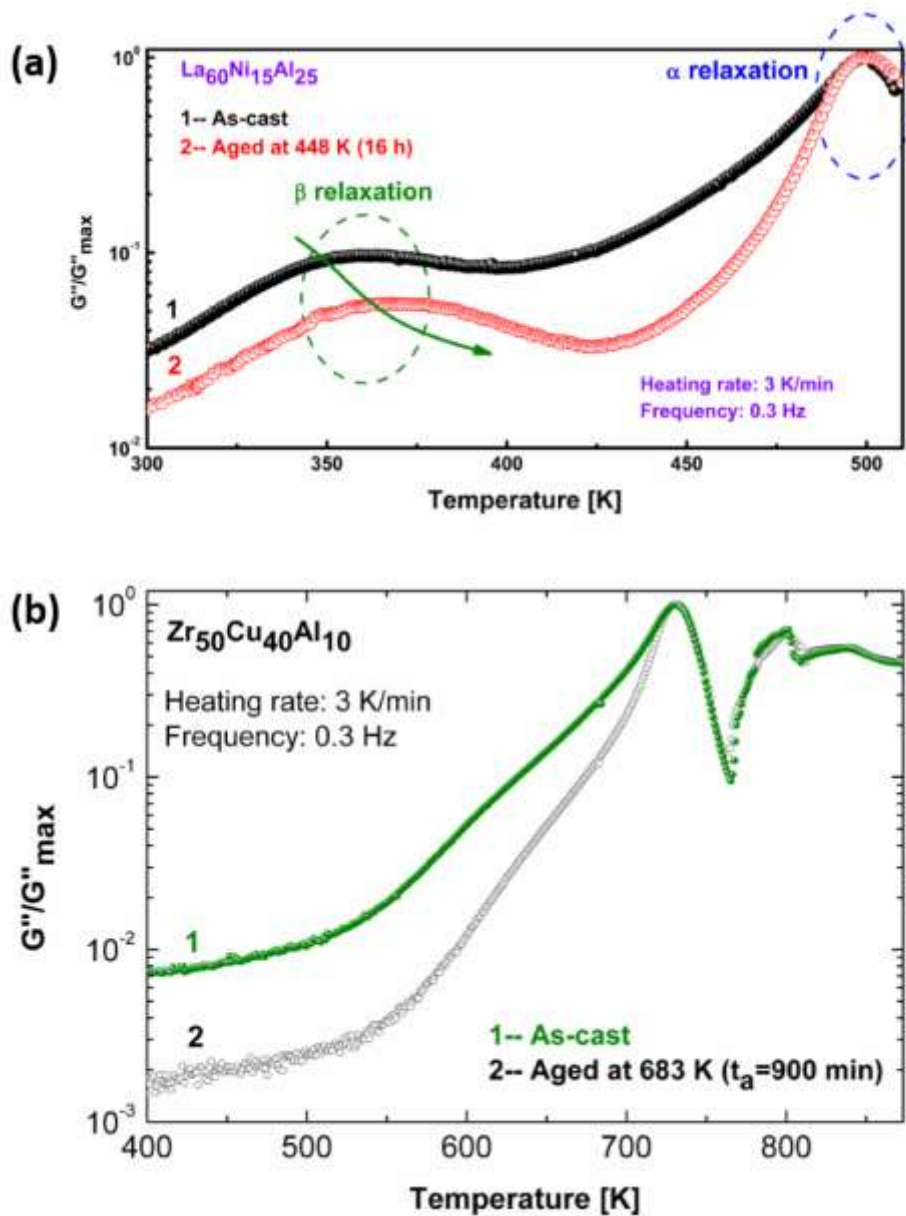


**Fig. 19.** (a) Temperature dependence of the normalized loss modulus of  $\text{La}_{60}\text{Ni}_{15}\text{Al}_{25}$  bulk metallic glass at as-cast state and annealed state (aging at 448 K with annealing time 16 hours) [181]; Reprinted from reference [181], copyright (2015), with permission from Elsevier. (b) Evolution of the loss modulus  $G''$  with the temperature of  $\text{Zr}_{50}\text{Cu}_{40}\text{Al}_{10}$  bulk metallic glass: (1) As-cast state and (2) after aged at 683 K with aging time is 900 min [183]. Reprinted from reference [183], copyright (2015), with permission from Elsevier.

Both the amplitude ( $\Delta G''$ ) and the relaxation time of the slow  $\beta$  relaxation ( $\tau_{\beta}$ ) were found to strongly depend on the physical aging below  $T_g$ . **Fig. 20** shows the

evolution of the slow  $\beta$  relaxation for different annealing times [184]. It is clear that the intensity of the slow  $\beta$  relaxation decreases with increasing aging time, while the peak of the slow  $\beta$  relaxation shifts to lower frequency with increasing annealing time. Theoretically, the shift of the slow  $\beta$  relaxation to a lower frequency indicates the increase of the relaxation time. In general, the increase of relaxation times corresponds to the increase of density, thereby in line with the effect of annealing. This phenomenon is closely connected to the densification process caused by structural relaxation in amorphous alloys. Similar observations were also shown in polymeric glasses [185, 186].

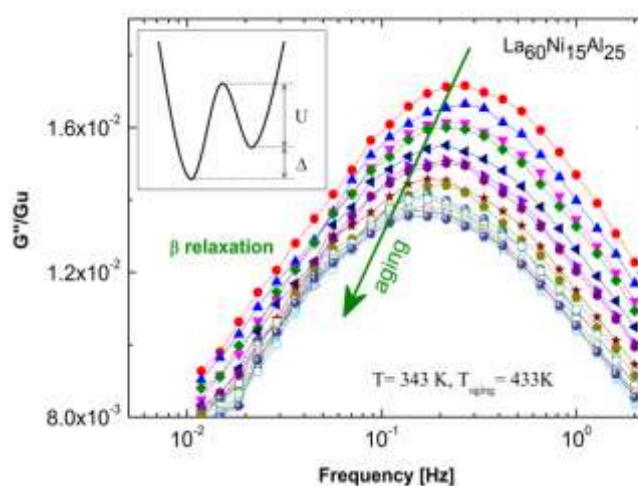


**Fig. 20.** Mechanical loss spectra of JG  $\beta$  relaxation in  $\text{La}_{60}\text{Ni}_{15}\text{Al}_{25}$  amorphous alloy aged at 433 K with different aging time (Testing temperature is 343 K). Insert is schematic of asymmetric double well potential (ADWP) model [184]. Reprinted from [184], with the permission of AIP Publishing.

In order to understand the effect of structural relaxation on the slow  $\beta$  relaxation in glass-forming liquids, Dyre and Olsen proposed the asymmetric double well potential model (ADWP) model in organic glass formers [187], they found that the correlation between the intensity and relaxation time of the slow  $\beta$  relaxation process depends on temperature. The ADWP model can be used to describe the behavior of the slow  $\beta$  relaxation in metallic glass during aging. In the framework of the ADWP

model, the relaxation time  $\tau_\beta$  and maximum of the mechanical loss  $G''_{max}$  are given as [187]:

$$\begin{aligned}\tau_\beta &= \tau_0 \exp\left(\frac{2U + \Delta}{2k_B T}\right) \cosh^{-1}\left(\frac{\Delta}{2k_B T}\right) \\ G''_{max} &= G''_0(T) \cosh^{-2}\left(\frac{\Delta}{2k_B T}\right)\end{aligned}\tag{2-9}$$

where  $\tau_0$  and  $G''_0$  are pre-factors;  $U$  and  $\Delta$  are the free energies as illustrated in the inset of **Fig. 20**.

Considering the linear correlation between  $\ln(\tau_\beta)$  and  $\ln(G''_{max})$  observed during the physical aging below  $T_g$ ,  $\ln(\tau_\beta) = b - a \ln(G''_{max})$  (as shown in **Fig. 21**), one can find that

$$\frac{2U + \Delta}{2kT} - \ln\left(\cosh\left(\frac{\Delta}{2kT}\right)\right) = 2a \ln\left(\cosh\left(\frac{\Delta}{2kT}\right)\right)\tag{2-10}$$

For  $\Delta \gg 2kT$ , Eq. (2-10) reduces to

$$\frac{2U + \Delta}{2kT} - \frac{\Delta}{kT} + \ln(2) = 2a \left(\frac{\Delta}{2kT} - \ln(2)\right)\tag{2-11}$$

from which one obtains

$$a = \frac{\frac{U}{kT} + \ln(2)}{\frac{\Delta}{kT} - 2\ln(2)}\tag{2-12}$$

Evidently, the ratio  $U/\Delta$  remains approximately constant ( $U/\Delta \sim a$ ) during structural relaxation. Notably, the constant coefficient  $a \sim 2$  was also found during physical aging

experiments for polymeric glasses [186] and molecular dynamics simulations (MDS). According to the data reported by Dyre and Olsen [187] a value of the coefficient  $a \sim 2$  was found in an equilibrium organic glass forming liquid, implying that a similar relaxation behavior could be extended to a liquid state.

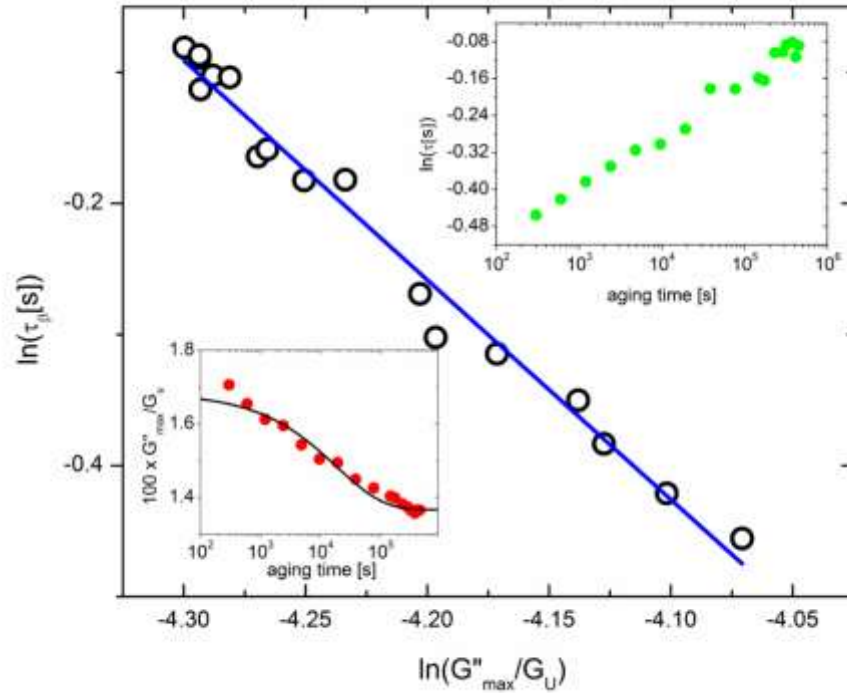


**Fig. 21.**  $\ln(\tau_\beta)$  vs  $\ln(G''_{\max}/G_U)$  for  $\text{La}_{60}\text{Ni}_{15}\text{Al}_{25}$  amorphous alloy aged at 433K with different aging times (the testing temperature is 343K) [184]. Reprinted from [184], with the permission of AIP Publishing.

Zhao et al. [188] studied the influence of the cooling rate on the mechanical relaxations in a La-based metallic glass. They reported that the intensity of the slow  $\beta$  relaxation of the metallic glass became more evident for a higher cooling rate. This behaviour is also consistent with the notion that the slow  $\beta$  relaxation is rooted in the concentration of loosely packed atoms, free volume or flow units (as shown in [Fig. 22](#)), which increases under a high cooling rate while decreases under structural

relaxation or physical aging, as discussed in the prior works [33, 173, 177, 189].

Based on the above discussions, now we may briefly summarize the main findings on the slow  $\beta$  relaxation in metallic glasses: (i) the intensity of the slow  $\beta$  relaxation is reduced by sub- $T_g$  structural relaxation; and (ii) the formation of nano-crystals during annealing above  $T_g$  causes a drastic reduction of the slow  $\beta$  relaxation amplitude. Both phenomena can be rationalized as a result of the decrease of structural heterogeneity or local atomic mobility in metallic glasses.

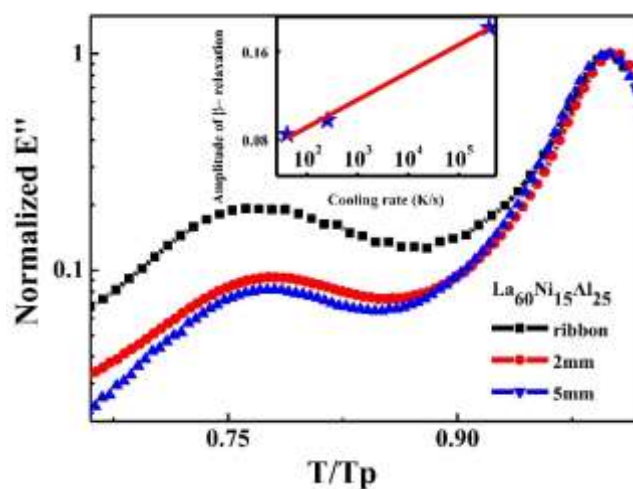


**Fig. 22.** The normalized loss modulus of the  $\text{La}_{60}\text{Ni}_{15}\text{Al}_{25}$  metallic glass for the ribbon and rod ( $T_p$  is the peak maximum of the slow  $\beta$  relaxation). The inset is the quenching rate dependent amplitudes of the slow  $\beta$  relaxation [188]. Reprinted from reference [188], copyright (2014), with permission from Elsevier.

More recently, another faster secondary relaxation was reported in metallic glasses [35, 61, 190]. This relaxation process is faster than the slow  $\beta$  relaxation discussed above, and we will call it fast  $\beta$  relaxation, although it should not be mistaken by the fast  $\beta$  relaxation predicted by the Mode Coupling Theory and observed in the liquid state within the GHz-THz range. On the basis of loss modulus, **Fig. 23(a)** shows a fast  $\beta$  relaxation process observed in the metallic glasses within the temperature range  $0.25\text{-}0.58 T_g$  [35]. Compared with the slow  $\beta$  relaxation, the fast  $\beta$  relaxation is ascribed to the rattling motion of loosely bonded atoms caged by

relatively tightly bonded atoms (as shown in [Fig. 23\(b\)](#)). As the rattling motion is activated with a low activation energy, which only shows small temperature dependence, fast  $\beta'$  relaxation is often treated as nearly a constant loss in a low-temperature region or high-frequency domain (as shown in [Fig. 23\(c\)](#)). Regarding the fast relaxation process, Barmatz *et al.* found that the activation energy of the fast  $\beta$  relaxation in Ni- and Fe-based metallic glasses was 0.03~0.05 eV, which is nearly the same value of the relaxation caused by the rattling motion of oxygen atoms in fused silica (~0.04 eV) [191]. In the case of Pd<sub>42.5</sub>Ni<sub>7.5</sub>Cu<sub>30</sub>P<sub>20</sub> metallic glass, Kato *et al.* [192] reported an activation energy of 0.25 eV obtained from the shift factor of the relaxation spectra, which is about 5 ~ 8 times larger than the findings of Barmatz *et al.* [193]. Assuming that the activation energy of fast  $\beta$  relaxation is 0.04 eV with a pre-exponential factor of  $10^{14}$ , Kato *et al.* estimated that the loss peak should be located near  $\omega_p = 10^{14} \exp\left(\frac{0.04}{548k}\right) \approx 2.7 \times 10^{14} \text{ rads}^{-1}$  at the reference temperature of 548 K. Thus, these authors proposed that they measured a larger activation energy region (low-frequency side) of the fast  $\beta$  relaxation [192]. Interestingly, Wang *et al.* [61] later found that the intensity of the activation energy for the fast  $\beta$  relaxation is around half of that for the slow  $\beta$  relaxation. As illustrated in [Fig. 23\(d\)](#), the fast  $\beta$  relaxation is associated with most mobile atoms that produce the individual localized inelasticity events, while the slow  $\beta$  relaxation with the local but collective atomic rearrangements that generates a typical local plastic flow event. The main  $\alpha$  relaxation then arises from the percolation of the local flow events through the elastic glass matrix.

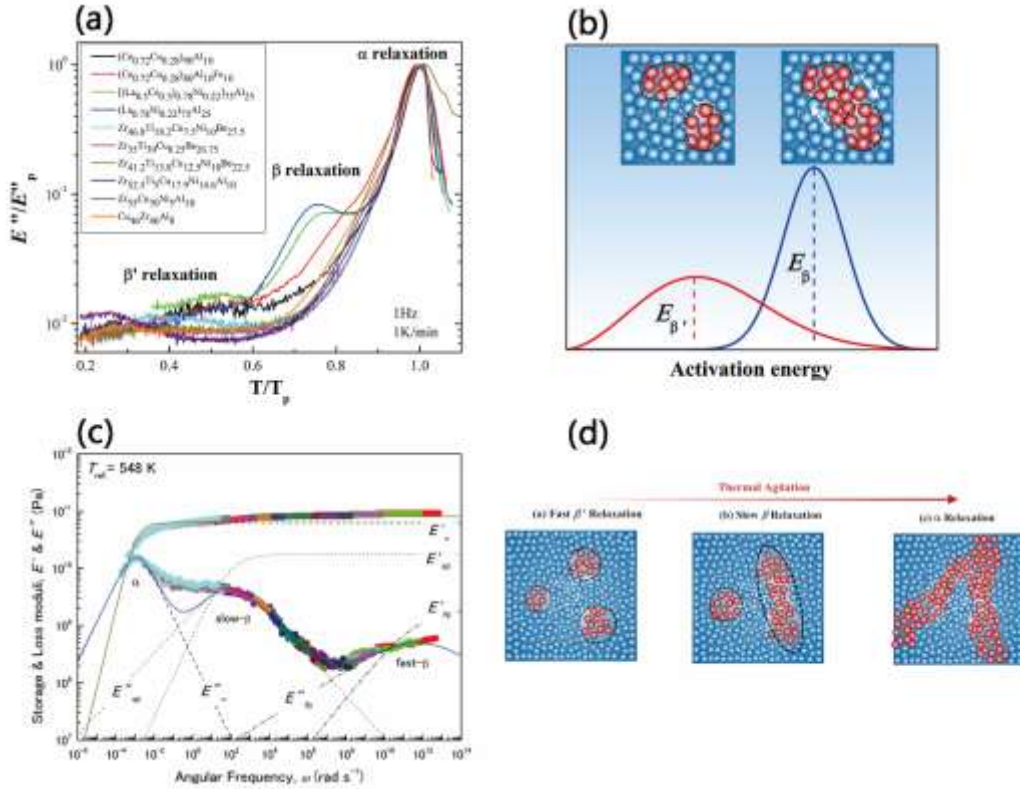


**Fig. 23** (a) Comparison of the temperature-dependent the normalized loss modulus of the typical amorphous alloys [35]. Reprinted from reference [35], copyright (2017), with permission from Elsevier. (b) Distribution of activation energy of fast  $\beta'$  and slow  $\beta$  relaxation in amorphous alloys [36]. Reprinted from reference [36], copyright (2018), by permission of Oxford University Press. (c) Master curves of storage modulus ( $E'$ ) and loss modulus ( $E''$ ) spectra for  $\text{Pd}_{42.5}\text{Ni}_{7.5}\text{Cu}_{30}\text{P}_{20}$  amorphous alloy (reference temperature  $T_r = 548$  K) and the observed triple relaxation modes ( $\alpha$  relaxation ( $\alpha$ ), slow  $\beta$ -relaxation ( $s\beta$ ) and fast  $\beta$  relaxation ( $f\beta$ )). The dotted line is the fitting curve with the relaxation equation Eq. (6) using the stretched exponent ( $\beta_{KWW}$ ); the solid line is the sum of the fitting curve of relaxation modes. At the high-frequency side of  $\alpha$  relaxation ( $\omega = 10^{-3}$ – $10^2$  rad  $s^{-1}$ ), owing to an irreversible structural relaxation that occurred during the measurements of the corresponding dynamic relaxation curve, the  $\alpha$  relaxation peak is considered to be asymmetrical [192]. Reprinted from reference [192], copyright (2013), with permission from Japan Society of Powder and Powder Metallurgy. (d) The illustrated mechanisms of dynamic mechanical relaxations in amorphous alloy [61]. Reprinted by permission from Macmillan Publishers Ltd: Nature Communications, reference[61], copyright (2015).

The presence of ‘faster’ secondary relaxations has been also recently detected by simulation in thin film metallic glasses, where the particle dynamics perpendicular to

the materials surface show a multistep relaxation, in this case related to the enhanced mobility of the atoms near the surface[194].

## **2.2 Mechanical relaxation behavior and physical properties of liquids and glasses.**

### **2.2.1 Structural relaxation, glass transition and crystallization**

**Fig. 24 (a)** shows the DSC curves of  $\text{La}_{55}\text{Al}_{25}\text{Ni}_{10}\text{Cu}_{10}$  bulk metallic glass after annealing for increasing times at 435 K, below the glass transition temperature  $T_g$ , showing the over-shoot over the DSC signal around  $T_g$  [195]. The magnitude of the over-shoot increases with annealing time, showing the differences in enthalpy of the different glass states obtained through structural relaxation by different annealing protocols. **Fig. 24 (b)** shows the kinetics of relaxation enthalpy as a function of the annealing time.

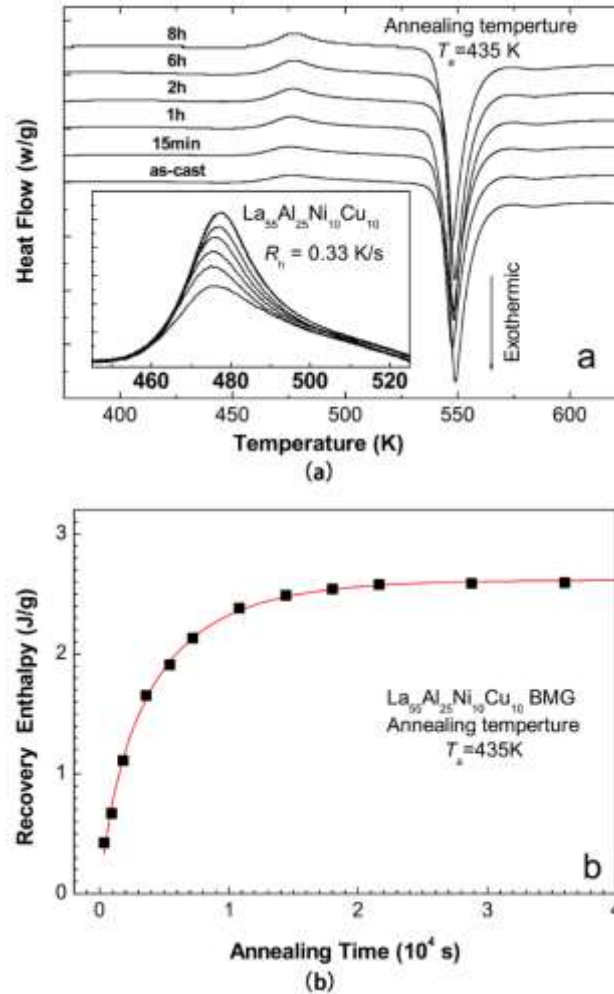


**Fig. 24.** (a) DSC curves of  $\text{La}_{55}\text{Al}_{25}\text{Ni}_{10}\text{Cu}_{10}$  amorphous alloy for different annealing times. (b) Recovery enthalpy obtained from the DSC experimental data. Reprinted by permission from [195], Springer, copyright (2008).

The kinetics of enthalpy relaxation below  $T_g$  are found to follow a stretched exponential (KWW) behavior, see **Fig. 25**, indicating the participation of a distribution of relaxation times similar to the observed in mechanical relaxation [196], and they have been attributed to the same processes generating the slow  $\beta$  relaxation [197]. Generally, the kinetics of structural relaxation or aging detected by calorimetry show activation energies of the order of 1-1.5 eV [197] and stretching exponents  $\beta_{\text{KWW}} < 0.5$ . On the other hand, the thermally activated processes of glass transition and crystallization, occurring in the supercooled liquid region, show higher apparent

activation energies in agreement with the  $\tau_\alpha$  and viscosity behaviors above  $T_g$  [124, 182, 198].

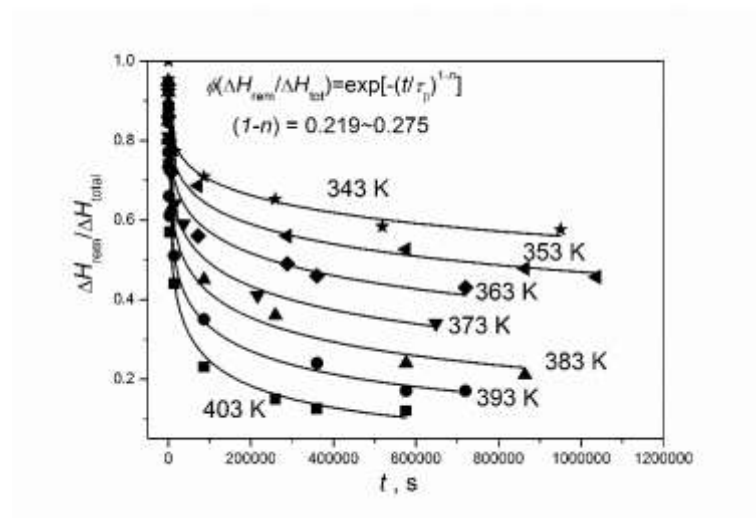


**Fig. 25.** Dependence of normalized remaining enthalpy on annealing time at temperatures below  $T_g$  for  $\text{La}_{55}\text{Al}_{25}\text{Ni}_{20}$  metallic glass. Reprinted with permission from reference [197]. Copyright (2016) American Chemical Society.

The recovery enthalpy experiments at different temperatures for given aging time in the  $\text{Zr}_{55}\text{Cu}_{30}\text{Ni}_5\text{Al}_{10}$  and  $\text{Cu}_{46}\text{Zr}_{45}\text{Al}_7\text{Y}_2$  metallic glasses are shown in **Fig. 26**. By increasing the annealing temperature, the value of recovery enthalpy in the metallic glasses reaches the maximum value. This is due to two opposite factors: the kinetics is accelerated when temperature increases, but the final magnitude decreases and hence the maximum value is observed. The position depends on the aging time. An increase of the annealing time will shift the maximum towards lower temperatures. A similar enthalpy relaxation behavior was reported for  $\text{La}_{50}\text{Al}_{25}\text{Ni}_{25}$  bulk metallic glass [195].

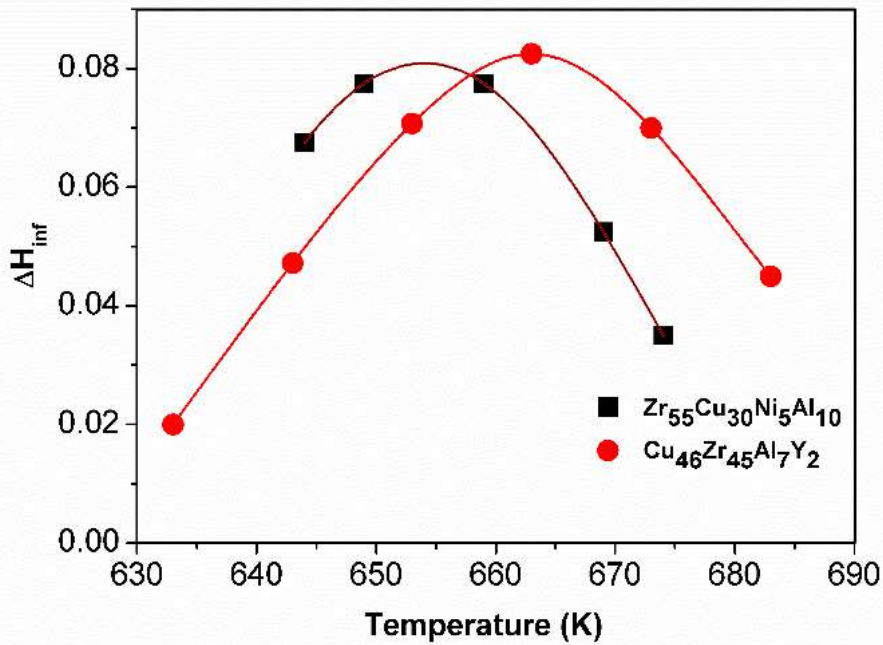


**Fig. 26.** Enthalpy relaxation in  $Zr_{55}Cu_{30}Al_{10}Ni_5$  and  $Cu_{46}Zr_{45}Al_7Y_2$  amorphous alloys after annealing at different temperatures [199]. Reprinted from reference [199], copyright (2011), with permission from Elsevier.

Let us consider here the annealing time and temperature dependence of the loss factor  $\tan \delta$ , shown in **Fig. 27**, which can be discussed in the framework of the quasi-point defects theory. Structural relaxation in bulk metallic glasses reduces the atomic mobility, due to a decrease in the defect concentration towards the equilibrium value at the annealing temperature. The value of  $\tan \delta$  increases by increasing the temperature of physical aging in metallic glasses, which ascribes to an increase in defect mobility with temperature.

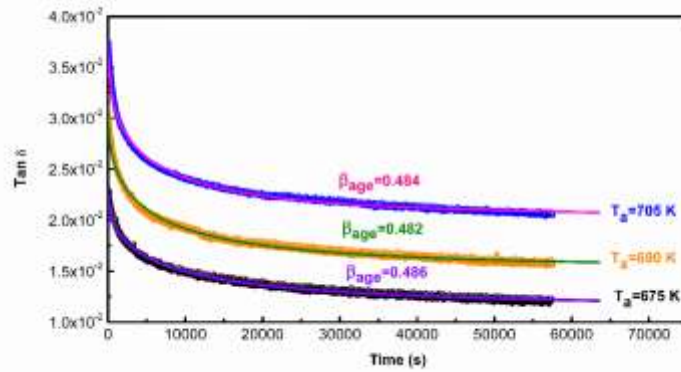


**Fig. 27.** Time dependence of the loss factor  $\tan \delta$  in  $Zr_{56}Co_{28}Al_{16}$  amorphous alloy during structural relaxation at various temperatures [134]. Reprinted from ref. [134], Copyright (2014), with permission from Elsevier.

Annealing protocols may induce also an increase in density and elastic moduli [11], as well as many other important physical properties. Recent studies have shown that metallic glasses may show two-step structural relaxation processes, attributed to  $\beta$  and  $\alpha$  relaxation [200]. A detailed understanding of the structural relaxation process gives a more precise control of the properties modification during annealing, permitting, for instance, the improvement of the magnetic behavior while avoiding significant deterioration of the mechanical properties [201]. However, annealing is highly restricted by the onset of crystallization. Bulk metallic glasses with high glass-forming ability show reduced glass transition temperatures  $T_{rg} = T_g/T_m < 0.7 - T_m$  being the melting temperature – [202], and have supercooled liquid regions of  $\sim 50$  K where their formability properties can be used for industrial purposes. Partial crystallization affects the relaxation processes in the glass state. The crystalline particles induce an increase in the bulk modulus and a reduction of the loss modulus, reflecting a decrease on the viscoelastic response and particularly a reduction in the intensity of the secondary relaxation. This is the anticipated behavior as the material is transforming into a glass/crystalline composite. Fully crystallized samples show eventually a large increase of their bulk modulus and a negligible loss modulus.

### 2.2.2 Diffusion and microscopic dynamics

The atomic dynamics in glasses, and in particular in amorphous alloys, is radically different from that of crystalline materials due to an essential fact: the metastable character of the glass configuration makes the system to be in a continuous evolution driven by the atomic motion. In the liquid state, microscopic dynamics allows an advective/diffusive description. In the glassy state, the description becomes vibrational/diffusive. In both cases, diffusion is an essential aspect of atomic dynamics. Diffusion in glasses and glass-forming liquids, and its relationship with relaxation processes is a subject of high interest [203]. At high temperatures the diffusion of the different components is coupled. However in most glass-forming liquids at temperatures below  $\sim 1.2T_g$ ,  $\eta$  (or  $\tau_\alpha$ ) and  $D$  become decoupled, as well as the diffusion of the different components. The origin of the breakdown of the Stokes-Einstein relation is a subject of intense research in the physics of glasses [203-205].

**Fig. 28** shows the behavior of diffusion of several atomic species in liquid  $\text{Pd}_{43}\text{Cu}_{27}\text{Ni}_{10}\text{P}_{20}$ , obtained by Bartsch *et al.* [206]. In the equilibrium melt and under small undercooling the diffusivities of the different elements are coupled and satisfy the Stokes-Einstein relation. However, below  $T_c$ , the critical temperature of the mode coupling theory, the diffusion of the different atoms decouples from that of the liquid. It is found that the diffusion coefficient increases as the radius of the considered species decreases, revealing that the diffusion process is mostly controlled by the atom size. Besides, over the whole temperature range the viscosity corresponding to Pd diffusion, the majority and slowest atom of the melt, coincides with that of the fluid. On this basis Bartsch suggested that the viscosity of the melt is ruled by the diffusion of the slowest element, which may form a slow subsystem actually driving the liquids dynamics, while smaller atoms can diffuse faster inside of the Pd subsystem.

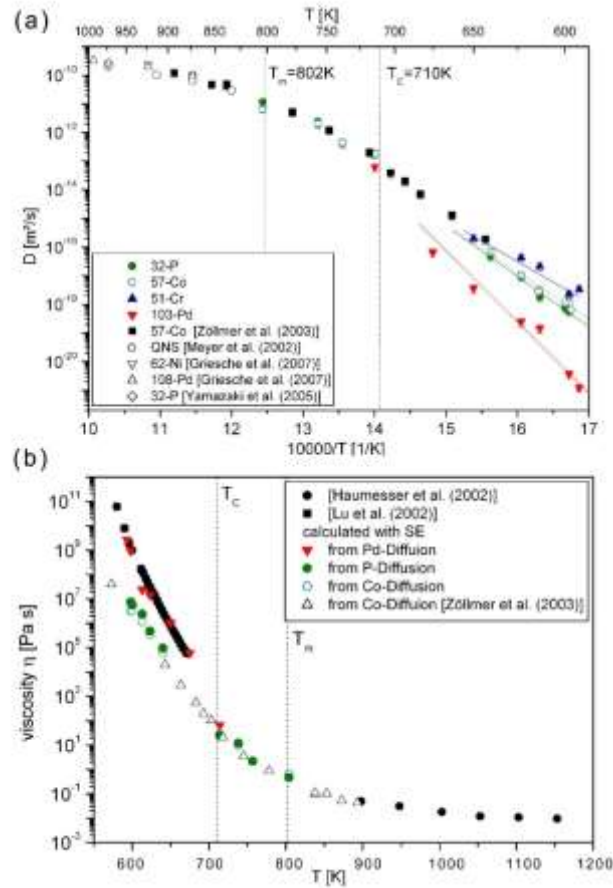


**Fig. 28.** (a) Arrhenius plot for diffusion of Pd, P, Co and Cr in liquid  $\text{Pd}_{43}\text{Cu}_{27}\text{Ni}_{10}\text{P}_{20}$  alloys.  $T_m$  and  $T_c$  are the melting and critical temperature of the mode coupling theory, respectively. (b) Diffusion-viscosities of Pd, Co, and P computed from the Stokes-Einstein relation compared to the liquid viscosity. Reprinted figures with permission from reference [206], copyright (2010) by the American Physical Society.

Diffusion in the glass state is mediated by the free volume [203]. Thus, it shows a two differentiated Arrhenius dependences in the glass and supercooled liquid regions. Diffusivities in the glass state are higher than those that correspond to the extrapolation of the supercooled region. The connection between atomic dynamics and structural relaxation can be revealed by dynamic mechanic analysis. DMA studies on  $\text{Ti}_{40}\text{Zr}_{25}\text{Ni}_8\text{Cu}_9\text{Be}_{18}$  amorphous alloy [133] showed that atomic mobility is reduced moderately by physical aging and drastically by crystallization, as it is expectable. Furthermore, plastic deformation induces glass rejuvenation, increasing the atomic

mobility. These findings are easily described in the framework of the free-volume model [207, 208] or the quasi-points defects model [209], as structural relaxation allows free volume / quasi-point defects reduction while plastic deformation has the opposite effect.

While the diffusion of larger atoms is connected to primary relaxation, fast diffusion of the smaller atoms has been found to have a direct correlation to the slow  $\beta$  relaxation. Yu *et al.* [169] found that the activation energies of the slow  $\beta$  relaxation and the diffusion of smaller atoms coincide within experimental error. Cohen *et al.* [168] proposed that  $\beta$  relaxation is due to a cooperative string-like mechanism, in which chains of particles oscillate in a caged dynamics. Further evidence [33] relates  $\beta$  relaxation to spatial heterogeneity, as it was observed that the intensity of  $\beta$  relaxation decreases as the spatial heterogeneity is reduced by annealing.

### **2.2.3 Mechanical behavior**

Deformation in metallic glasses is highly dependent on temperature and strain rate. At low temperatures and high strain rates strain is highly concentrated in thin spatial layers as small of 10-100 nm [77], so called shear bands. Shear bands may appear as a non-usual mechanism of deformation in solid state physics, but were previously observed in metals, glasses, granular systems and liquids [77]. On the contrary, homogeneous flow is observed at higher temperatures and in the supercooled liquid region. In these conditions, the flow rate determines if the flow is non-Newtonian or Newtonian [12].

The comprehension of the mechanic response of metallic glasses departs from an outstanding fact: the lack of long range order prevents the usual deformation mechanisms of metallic alloys, such as dislocations or grain boundary sliding. However, being this a prominent property, eventually another phenomenon, such as local heterogeneity, is being highlighted as the key dominant feature controlling the mechanical behavior.

Metallic glasses show compositional, elastic and dynamic heterogeneities. This fact has been widely observed both numerically and experimentally [13, 210-214], and gives a basis for the comprehension of their mechanical behavior. The successive theoretical models developed to understand the mechanical behavior, namely free volume, shear transformation zones or flow units, introduce heterogeneity as a dominant aspect. The different local environments in the glass have a distribution of densities, elastic modulus and dissipation rates. Although there is a continuum of values of these features, a simple picture distinguishes between solid-like environments when the atomic packing is dense and liquid-like in the opposite case. This description easily evokes the expected mechanical behavior of the different locations in the glass.

The response of the alloy to mechanical stress is then a stochastic coupling of the response of the individual heterogeneous regions. Furthermore, the process must be understood as a cascade of individual events which, in turn, redefine the topology of the glass. **In general, the resultant deformation field in the glass is characterized by both affine and non-affine deformation. In principle, the affine deformation conforms to an affine transformation and usually manifests as homogeneous deformation. By comparison, the non-affine deformation results from the departure of the deformation field from the affine deformation. In the early work of Falk and Langer [215], a computational scheme was developed to quantify the non-affine deformation in amorphous alloys.** Before yielding, solid-like regions experience affine deformations while STZ or more generally liquid-like regions/flow units experience non-affine deformations which accommodate preferentially the plastic deformation; and, at the same time they generate new defects in their environment which, in turn, induce the creation or annihilation of other flow units [207, 216]. This is an anelastic process which involves local dilation of the glass: shearing distorts the atomic environment, thus generating new free volume. The global response of the glass to this phenomenon is largely temperature dependent; at low temperatures, this dynamically created excess

of free volume may remain over large time scales, thus decreasing the deformation resistance and resulting in strong shear localization. Close to the glass transition, structural relaxation during deformation induces also a continuous redistribution of free volume. Positron lifetime measurements show that the free volume increase is associated to an increase of the concentration of flow defects, rather than to an increase in their size [217]. Homogeneous flow may be thus understood as the response of a highly viscous liquid with suspended solid-like particles, whose concentration decreases as the material approaches the glass transition. **Here, it may be worth noting that, conceptually, affine and non-affine deformation is related to the topology of a deformation field, whether they conform to an affine transformation or not, while anelastic and inelastic deformation is related to the reversibility of a deformation field. If deformation shows time dependent reversibility, we call this deformation anelastic; otherwise, we call it “inelastic” if the deformation is not reversible. In general, non-affine (or affine) deformation could either inelastic or anelastic.**

The connection between the atomic processes developing in the material and the macroscopic properties is not easy. If we consider, for example, the elastic moduli, it is known that in solids it depends on both the bond strength and the relaxation spectra. At low temperatures the elastic moduli of crystalline materials are mainly dependent on the bond strength, the relaxation spectrum playing a role only for periodic excitations. However, in glasses structural relaxation plays an important role in quasi-static deformation even at low temperatures [218]. And the two main relaxation processes, primary and secondary, play noticeable different roles.

Annealing below  $T_g$  induces local evolution to better packed atomic structures, resulting in shorter interatomic distances and a consequent reduction in free volume. This irreversible relaxation process relaxation towards a denser glassy state changes the short range order (SRO) and increases the elastic modulus accordingly [219]. After full relaxation the glass properties become only dependent on the annealing

temperature, and further annealing at different temperatures induces only reversible changes [114, 165].

Xu *et al.* [220] show that structural, primary relaxation has a central role in the fracture behavior of metallic glasses. To begin with, structural relaxation often induces a ductile to brittle transition. Even when keeping a ductile behavior, the reduction of free space associated to structural relaxation often reduces the toughness of the material. Pan *et al.* [221] report that structural relaxation decreases the activation volume, which is in corroboration of relaxation-induced embrittlement behavior.

Contrarily, plastic deformation – such as cold work and shot-peening – induces glass rejuvenation, by increasing the free volume of glass [219, 222]. Interestingly, elastostatic tensile loading – well below the yield strength – and thermal cycling have a similar effect [222]. While in the former case the density reduction associated to rejuvenation is attributed to the non-affine strains at atomic level, in the latter it is attributed to spatially inhomogeneous coefficients of thermal expansion (CTE) which may induce anisotropic strains homogeneously distributed in the whole volume. In both cases, the heterogeneous structure of the glass has a macroscopic effect.

While the connection between structural relaxation and the mechanical response of glass could be anticipated, the role of secondary relaxation is more subtle and was recognized only recently. The activation energy of  $\beta$  relaxation was found to be of the same order of that of the activation of STZ. Johnson and Samwer proposed a cooperative shearing model (CSM) [223-225] which models the onset of plastic flow on the basis of the Frenkel assumption [226]. According to the CSM model, the activation energy of STZ is given by

$$W_{STZ} = (8/\pi^2)G\gamma_c^2\zeta\Omega \quad (2-13)$$

where  $\Omega$  is the average volume of a STZ,  $G$  is the shear modulus,  $\gamma_c$  the average elastic limit and  $\zeta$  a factor due to the matrix confinement of a STZ. This model

describes many aspects of the temperature dependence of the mechanical response of metallic glasses. Later, Harmon et al. [224] suggested that isolated STZ events are related to  $\beta$  relaxations, while percolation of them is associated to primary relaxation which eventually induces the collapse of the matrix and the breakdown of elasticity. Experimental evidence confirmed the link between the energy of the slow  $\beta$  relaxations and the potential energy barriers of STZ:  $U_\beta \approx 26 (\pm 2) RT_g \approx W_{STZ}$  [167]. Thus, taking STZ as the predominant mechanism for plastic deformation, metallic glasses showing a prominent slow  $\beta$  relaxation are expected to show a ductile behavior, as observed for example in the La-based amorphous alloys [227].

Inspired by the reported experimental evidence, a possible link between  $\beta$  relaxation and glass ductility was searched for. Initially, some empirical correlations between the mechanical properties of metallic glasses were discovered. In particular, it was found that ductile metallic glasses mostly have high Poisson ratios –  $\nu > 0.31 - 0.32$  – and low ratios of elastic shear modulus  $\mu$  to bulk modulus  $B$  –  $\mu/B < 0.41 - 0.43$  – [90, 228, 229]. The microscopic origin of these correlations was subsequently investigated. Firstly, it was noted that the onset of local shearing appears when the effective potential energy barriers opposing shear band formation are tilted by the applied forces. Experimental data showed that ductile glasses tend to have lower potential energy barriers [223]. More recently, the link between the microscopic dynamics of the secondary relaxation and the ductility of the glass was established by mechanical spectroscopy [180, 230]. The nearly constant loss (NCL) in the mechanical susceptibility reflects the caged dynamics and is directly related to the effective Debye-Waller factor  $f_0$ . Upon annealing below the glass transition, the intensity of the NCL, the Poisson ratio and the intensity of the secondary  $\beta$  relaxation decrease, and the material becomes brittle. An even closer link between  $\beta$  relaxation and the caged dynamics was recently revealed, as the temperature dependence of the NCL changes at the onset of  $\beta$  relaxation [231]. These results indicate that, on the one

hand, secondary relaxation acts as a precursor of primary relaxation and, on the other hand, secondary relaxation controls the mechanical response of the glass in the region well below the glass transition. However, there still lacks a comprehensive theory relating  $\beta$  relaxation and compressive plasticity in amorphous alloys. Experimental data for various amorphous alloys are sometimes contradictory to each other [232]. Although important mechanisms of room temperature ductility like shear-band arrest or shear-band deflection seem to be related to structural inhomogeneity, the connection between secondary relaxation and these processes is not clear. Besides, plasticity and toughness of glass may be highly deteriorated by oxidation [233].

It has been also claimed that  $\beta$  relaxation is present in creep and stress relaxation. Analysis of elastostatic (i.e. compressive creep at low stress level) experiments on metallic glasses showed an increase in subsequent compressive plasticity [234], which was attributed to the generation of more disorder. Later, Sandor *et al.* reported that creep can induce local atomic reordering in LaNiAl metallic glasses [235], in a process of which the activation energy is of the same order as the slow  $\beta$  relaxation. More recently, Greer and Sun revealed a notable increase on the amplitude of  $\beta$  relaxation after an elastostatic processing [222]. This result indicates that, on the one side, low intensity creep induces glass rejuvenation and, on the other side, that glass rejuvenation is associated not only to primary relaxation but also to  $\beta$  relaxation. Furthermore, it is a new clue on the link between glass plasticity and  $\beta$  relaxation which needs further analysis. As for stress relaxation experiments, a change in the relaxation behavior in the elastic regime below  $T_g$  of  $Zr_{52.5}Ti_5Cu_{17.9}Ni_{14.6}Al_{10}$  amorphous alloys was also associated to a crossover between primary and secondary relaxation [236].

As indicated above, at low temperatures and high strain rates, excessive mechanical straining eventually induces the creation of shear bands. Given the possible connections between  $\beta$  relaxation and the mechanical properties of glass, it is expectable that  $\beta$  relaxation be also connected with the process of shear band creation.

However, the link is yet to be explored in depth. The transition between inhomogeneous and homogeneous flow regimes was found to follow an Arrhenius dependence with an activation energy  $\Delta E_s \sim 0.3 - 0.5$  eV for Pd-, Zr- and Fe-based amorphous alloys [237]. These values is about 1/4 to 1/2 of the activation energy of STZ, namely  $\Delta E_s/W_{STZ} \sim 0.25 - 0.5$ , which may be explained in the CSM framework by considering that the height of the potential energy barrier  $W_{STZ}$  decreases with increasing shear stress [62].

The search of the elementary excitation process in amorphous alloys is often based on the study of their stress relaxation behaviors. This could be done via creep experiments [238], stress relaxation experiments [239, 240] or dynamic mechanical analyses [61, 241]. In principle, plasticity in metallic glasses at a finite temperature is thermally activated and stress assisted. Therefore, local plasticity is inherently related with local stress relaxations. According to Yu *et al.* [38], who suggested that the activation energy of the slow  $\beta$  relaxation  $E_\beta$  in metallic glasses is proximately equivalent with the potential energy barriers of STZs,  $W_{STZ}$ , that is  $W_{STZ} = E_\beta$ . This result implies an intrinsic correlation among activation of potential STZs, the slow  $\beta$  relaxation, and the inhomogeneous atomic structure of metallic glasses. In many polymer glasses the transition from ductile to brittle occurs at the characteristic temperature of the slow  $\beta$  relaxations, and transitions of impact toughness, yield strength and failure modes were also often correlated with the  $\beta$  relaxations. In addition, polymers with the pronounced  $\beta$  relaxations usually possess good ductility and *vice versa*.

In order to correlate the fast  $\beta$  relaxation with the plasticity of the amorphous alloy,  $E_\beta$  and  $E_{\beta'}$  values of different amorphous alloys are shown in **Fig. 29(b)**. From **Fig. 29 (a)**, in the vicinity of the peak temperature of the fast  $\beta'$  relaxation process, a brittle-to-ductile transition is observed. Based on the **Fig. 29(b)**, for the brittle amorphous alloys, such as the Ce-, Mg- and La-based metallic glasses, it is found that the ratio of  $E_{\beta'}/E_\beta \sim 0.50$ . On the other hand, for the ductile amorphous alloys, such as the Zr-, Cu- and Pd-based amorphous alloys, the ratio is found  $E_{\beta'}/E_\beta \sim 0.30$ . In this viewpoint, the smaller the ratio  $E_{\beta'}/E_\beta$  is, the metallic glasses present better plasticity

during the deformation. Ductile amorphous alloys show smaller ratios of  $E_{\beta'}/E_{\beta}$ , which corresponds to low activation energy. Compared with the brittle amorphous alloys, the STZs in ductile amorphous alloys are much easily activated.

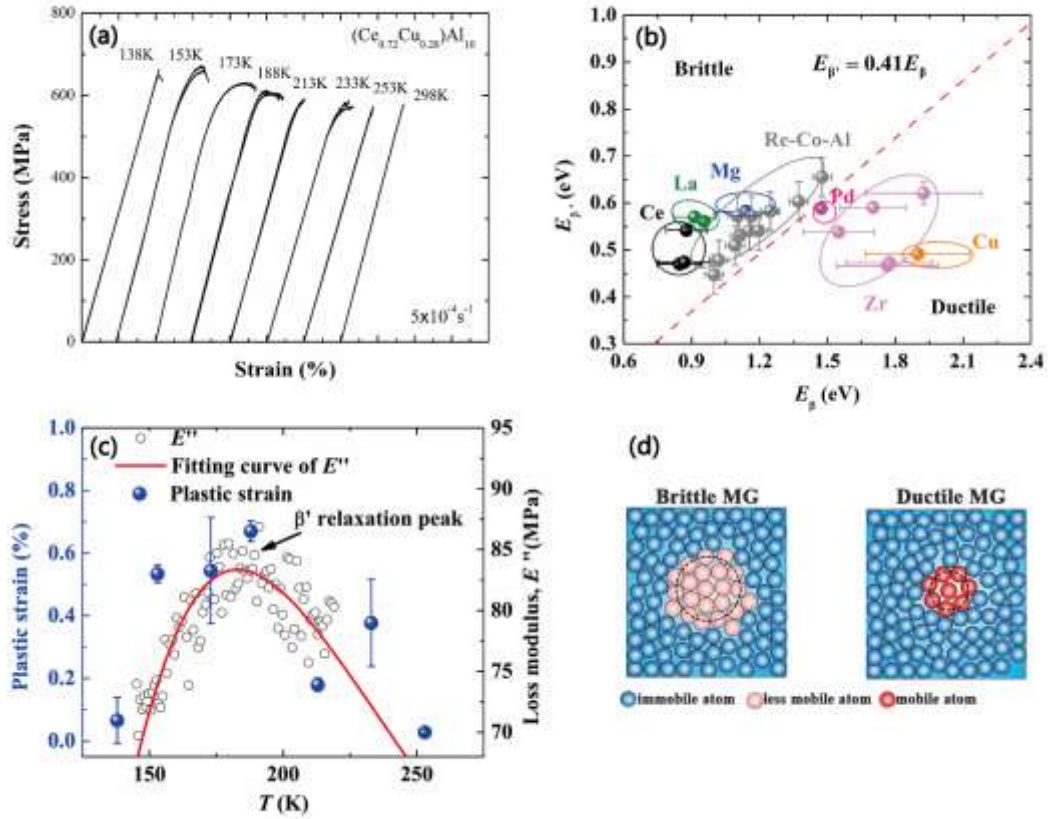


**Fig. 29.** (a) The compressive stress-strain curves with wide temperature range from 138K~298K, showing significant plasticity achieved in the temperature domain where the fast  $\beta'$  is pronounced. Reprinted from reference [35], copyright (2017), with permission from Elsevier. (b) Variation of  $E_{\beta}$  with  $E_{\beta'}$  across various amorphous alloys [35, 36]. Reprinted from reference [36], copyright (2018), by permission of Oxford University Press. (c) Relation between brittle-to-ductile transition and the fast  $\beta'$  relaxation in amorphous alloys [35]. Reprinted from reference [35], copyright (2017), with permission from Elsevier. (d) Schematic illustration of atomic structure for brittle and ductile amorphous alloys[35]. Reprinted from reference [35], copyright (2017), with permission from Elsevier.

**Fig. 29 (c)** shows the brittle-to-ductile transition in Ce-based amorphous alloy. Obviously, the plasticity of Ce-based metallic glass is closely connected to the fast  $\beta'$  relaxation. The phenomenon suggests the fast  $\beta'$  relaxation triggers the plasticity in metallic glasses. **Fig. 29 (d)** displays schematic illustration of the atomic structure for

the brittle and ductile metallic glasses. For the ductile amorphous alloys, the “softer” spots have a clear distinction in atomic mobility compared with glassy matrix. On the contrary, the atomic distribution of the brittle amorphous alloy tends to be less mobile. These results suggest the mechanisms of the fast  $\beta$  relaxation process of amorphous alloys and mechanisms of plastic deformations are correlated. This means the mechanisms of plastic deformation of amorphous alloys could be understood from the perspective of the fast  $\beta$  relaxation process. It is well documented that various relaxation modes observed during thermal activation processes have a close relationship with the mechanical deformation behavior of amorphous alloys at room temperature. Nanoscale STZs having lower activation energy than their surrounding regions are distributed inside the metallic glass, and anelasticity is interpreted by the local plastic deformation within these zones. It was shown that the activation energy for STZ during deformation is equivalent to the activation energy for slow  $\beta$  relaxation [167]. On the other hand, the activation energy for steady-state viscous flow in metallic glass is equivalent to the activation energy of  $\alpha$  relaxation [79, 242]. This means that weakly bonded regions in metallic glass behave as STZs in the stress-induced case or as islands of mobility for slow  $\beta$ -relaxation in the thermal activation case. In contrast, relaxation in strongly bonded regions leads to yielding for the stress-induced case and to  $\alpha$  relaxation (glass transition) for the thermal activation case.

On the basis of these findings described above, it is evident that the fast secondary relaxation is an important phenomenon and more research in this area would be beneficial to gather a deeper understanding of the deformation physics of metallic glasses [35, 243]. Whether this fact is essential or not, it is proved that  $\beta$  relaxation correlates to structural heterogeneity or, in other words, to the existence of “soft” regions in amorphous alloys [94, 146, 227]. In these loose packed regions, atomic movement is easier and consequently the activation of STZs is enhanced. In addition, nucleation of multiple shear bands in these “soft” domains is responsible for the plasticity of amorphous alloys. On the other hand, the resistance in “hard” domains impedes propagation of shear bands during the deformation process [212].

Though the question is far to be solved, the present knowledge on the features of secondary relaxation confirms its central role in the study of the mechanical behavior of amorphous alloys.

### **3. Characterization of structural heterogeneity in amorphous alloys**

In the previous section, we presented a review of the macroscopic features correlated to structural heterogeneity in amorphous alloys. In this section, our attention will be shifted to the experimental and simulation approaches by which structural heterogeneity and its correlation with the properties of amorphous alloys can be characterized.

To gain holistic understanding of the structure-property relation of amorphous materials, as suggested in the recent experiments and simulations [23, 244-246], one must take into account both the static and dynamic aspects of their disordered atomic structures. In other words, not only the static atomic packing features such as the short- or medium- range ordering (SRO or MRO) associated with icosahedral or crystal-like atomic clusters but also the relaxation spectra of metallic glasses should be considered to understand their different behaviors and properties [61, 177, 247-251]. Over the past decades, a great deal of efforts have been devoted to finding direct experimental evidence of dynamical/structural heterogeneity in metallic glasses [210, 218, 252-261]. As suggested in a number of prior works [13, 69, 219, 253, 259, 262, 263], the amorphous structure of metallic glasses is composed of “solid-like” and “liquid-like” regions, similar to a nano-scale composite (as illustrated in [Fig. 30](#)). When perturbed by an external stimulus, the “liquid-like” ones respond inelastically whereas the “solid-like” atoms respond elastically within a given time [219, 253, 259, 263-266]. In view of this, the local heterogeneity and its evolution during the thermal annealing or plastic deformation in metallic glasses can be therefore characterized experimentally by approaches such as the X-ray diffraction method [265], high-rate nanoindentation [218, 245, 253], dynamic atomic force microscopy (DAFM) [255,

259, 264, 267, 268] and atomistic simulations [251, 263, 269-272].

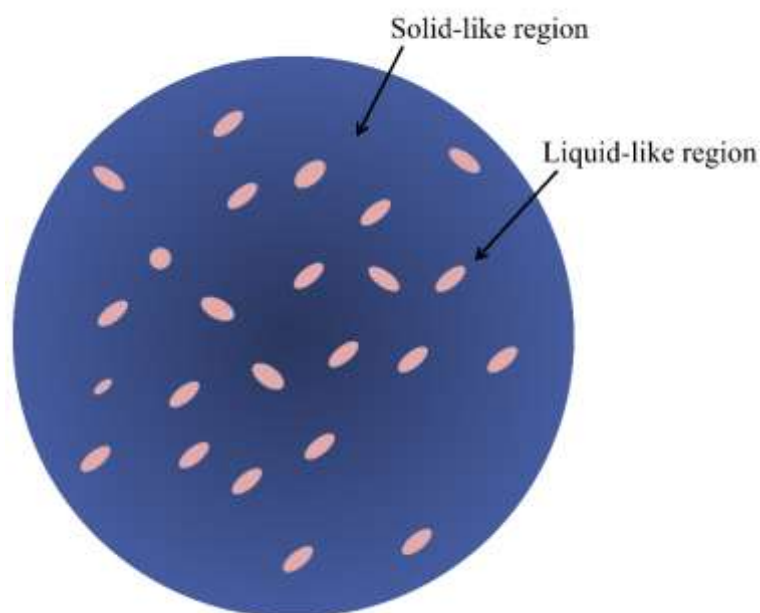


**Fig. 30.** The schematics of the amorphous structure of amorphous alloys.

### 3.1. High-energy X-ray diffraction method

The mechanical properties of glasses are known to be related to their atomic level elastic heterogeneity [255, 269, 273-276]. Moreover, the elastic response of glasses at the atomic level, being anelastic and highly inhomogeneous, strongly reflects their intrinsic structural heterogeneity [277, 278]. In light of earlier studies on the atomic pair-density function (PDF) of glasses [279-283], the apparent strain is found to be inhomogeneous at the atomic scale. Nevertheless, direct experimental evidence of elastic heterogeneity in metallic glasses is still scarce. Only recently did Dmowski et al [265], using the quantitative X-ray diffraction analysis, demonstrate that only about 3/4 in volume fraction of metallic glasses deforms elastically while the rest deforms in an anelastic manner showing no resistance to external loading within the experimental time scale.

According to Poulsen et al. [279], the local strain in amorphous alloys can be measured by tracking shifts in the first diffraction peak in the structure function,  $S(Q)$  where  $Q = 4\pi\sin\theta/\lambda$  is the diffraction vector,  $\theta$  the diffraction angle and  $\lambda$  the wavelength of the probe, or, alternatively, by determining the shift in the atomic pair-density function (PDF), which can be obtained by Fourier-transforming of  $S(Q)$ ,

$$g(r) = 1 + \frac{1}{2\pi^2 r \rho_0} \int [S(Q) - 1] \sin Qr Q dQ, \quad (3-1)$$

where  $\rho_0$  is the number density of atoms, with  $Q$  either parallel or perpendicular to the stress axis. To characterize the anisotropic atomic response in the mechanically deformed metallic glasses, Dmowski et al [265] employed the modified PDF through the spherical Bessel transformation,

$$g_l^m(r) = \frac{(i)^l}{2\pi^2 \rho_0} \int S_l^m(Q) J_l(Qr) Q^2 dQ, \quad (3-2)$$

where  $J_l(x)$  is the spherical Bessel function. Note that  $J_0(x) = \sin x/x$  is only for the isotropic component ( $l=0$ ) and for axial symmetry the terms with  $l=2$  and  $m=0$  need to be evaluated. Taking advantage of the 1-ID/XOR beam line of the Advanced Photon Source, Argonne National Laboratory, Dmowski et al [265] carried out X-ray diffraction measurements on a  $Zr_{52.5}Cu_{17.9}Ni_{14.6}Al_{10}Ti_5$  amorphous alloy, which was creep deformed at the stress of 1.2 GPa and the temperature of  $T = 573$  K for 30 minutes. The anisotropic PDF due to anelastic strain was evaluated with  $l=2$  PDF in the specimen. It is worth noting that for axial elongation along  $z$ , the elliptical PDF due to affine deformation,  $g_{2,aff}^0(r)$  can be expressed in terms of the derivative of the isotropic PDF,  $g_0^0(r)$ ,

$$g_{2,aff}^0(r) = \varepsilon_{zz,aff} \bar{g}_{2,aff}^0(r) = -\varepsilon_{zz,aff} \left(\frac{1}{5}\right)^{1/2} \frac{2(1+\nu)}{3} r \frac{d}{dr} g_0^0(r) \quad (3-3)$$

whereas the total PDF is fitted by

$$g_{2,total}^0(r) = \varepsilon_{zz,anel} \bar{g}_{2,anel}^0(r) + (\varepsilon_{app} - \varepsilon_{zz,anel}) \bar{g}_{2,aff}^0(r) \quad (3-4)$$

where  $\varepsilon_{zz,anel}$  is the anelastic strain, and  $\varepsilon_{zz,aff} = \varepsilon_{app} - \varepsilon_{zz,anel}$  is the affine (elastic) strain.

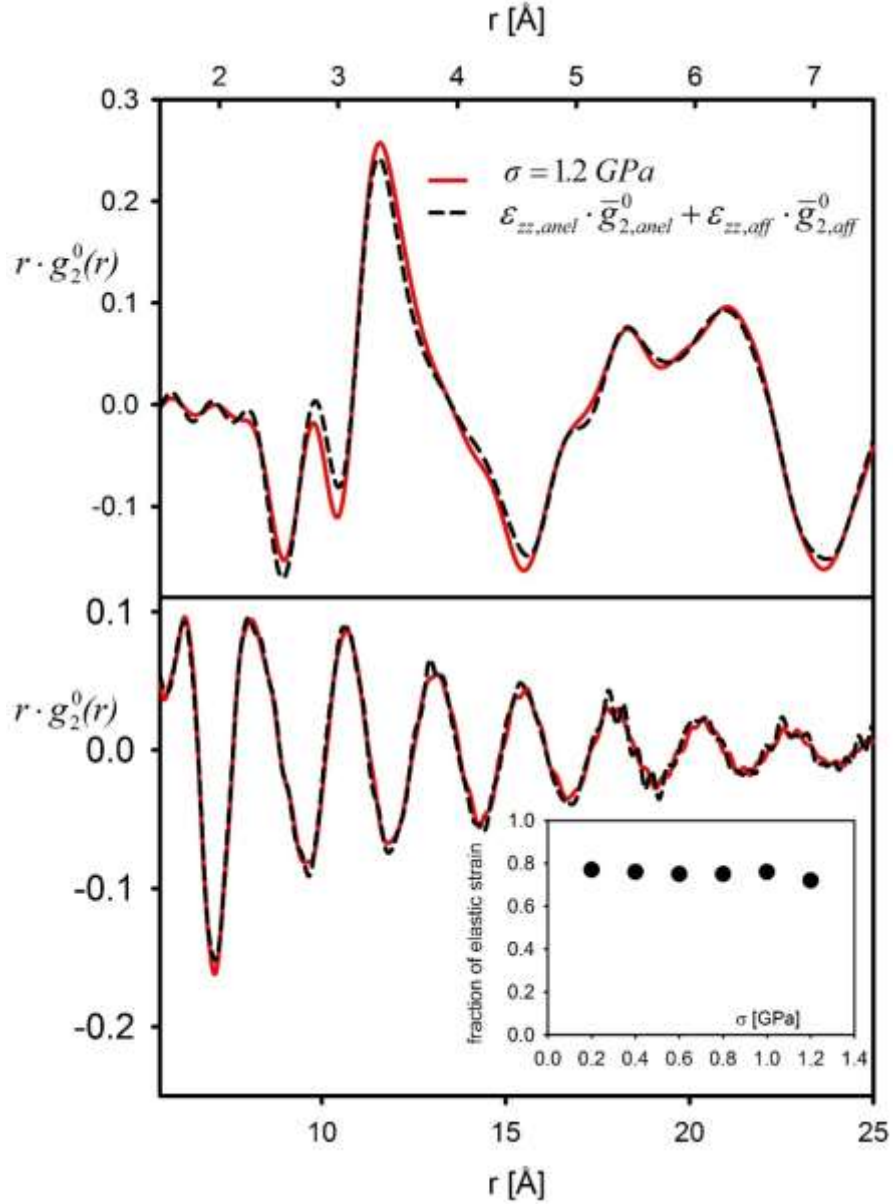


**Fig. 31.** The  $l=2$  component of the PDF,  $g_2^0(r)$ , at 1.2 GPa, fitted to the combined PDF for affine and creep(anelastic) deformation, Eq. (4). The inset shows the fraction of elastic strain compared to the total apparent strain. It appears constant of applied external stress up to 1 GPa, and on average it is about 76%. The rest, 24%, is the

anelastic strain. From reference [265]. Reprinted figures with permission from reference [265], copyright (2011) by the American Physical Society.

As a consequence, X-ray scattering and anisotropic PDF analysis can be used to evaluate the elastic and anelastic contribution, respectively, in the deformed metallic glass. As demonstrated in Fig. 31, the  $g_{2,total}^0(r)$  is in excellent agreement with the observed  $g_{2,obs}^0(r)$  at  $\sigma=1.2\text{GPa}$ , confirming that the strain in this metallic glass included both the anelastic as well as elastic or affine components. The inset of this figure shows the fraction of the affine strain to the total strain,  $z = \varepsilon_{zz,aff}/\varepsilon_{app}$ , as a function of the applied stress. It is interesting to note that the value of  $z$  is almost independent of the applied stress and an average 24% of the total strain is anelastic. This agrees with the simulation suggesting that about 20% of the apparent elastic strain is actually anelastic [278].

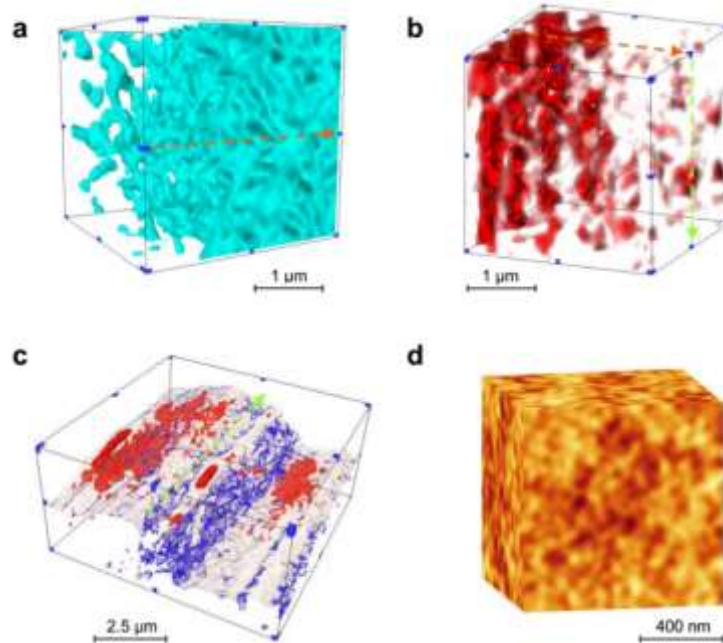


**Fig. 32.** Hierarchical microstructure of as-quenched metallic glasses [29]. (a) The low-density regions in  $\text{Pd}_{40}\text{Ni}_{10}\text{Cu}_{30}\text{P}_{20}$  metallic glass. (b) The high-density regions in  $\text{Zr}_{52.5}\text{Ti}_5\text{Cu}_{17.9}\text{Ni}_{14.6}\text{Al}_{10}$  metallic glass. (c), The high-density regions (marked by red color) and low-density regions (marked by blue color) in  $\text{Zr}_{64.13}\text{Cu}_{15.75}\text{Ni}_{10.12}\text{Al}_{10}$  metallic glass. (d) The 3D fine structure reconstructed by nano-CT for

Zr<sub>41.2</sub>Ti<sub>13.8</sub>Cu<sub>12.5</sub>Ni<sub>10</sub>Be<sub>22.5</sub> metallic glass. The local region with a larger density is marked by darker color. The dashed orange arrow points to the center of the metallic glass in (a) and (b). The dashed green arrow is in the direction of tensile stress in (b) and (c). Reprinted from reference [29], copyright (2018), with permission from Elsevier.

Aside from the aforementioned indirect evidence for the structural heterogeneity in metallic glasses, the complex microstructures of different types of metallic glasses with different thermomechanical histories were directly detected with the synchrotron X-ray nano-computed tomography (nano-CT) by Huang *et al.* [29]. The detected gray value  $g$  in the nano-CT experiment is roughly proportional to the local density. Different 3D density fluctuations spanning from nano- to micrometer scale, which decouple with the chemical homogeneity are reported in all these metallic glasses. Fragile metallic glasses, like Pd<sub>40</sub>Ni<sub>10</sub>Cu<sub>30</sub>P<sub>20</sub> amorphous alloy, are more heterogeneous and exhibit a gradient microstructure with more low-density regions (or less high-density regions) near the central parts of the glasses (see the orange arrows in **Fig. 32(a)** and **Fig. 32(b)**). Homogeneous deformation at high temperatures near  $T_g$  elongates the high- and low- density regions along the direction of tensile stress (see the green arrows in **Fig. 32(b)** and **Fig. 32(c)**). At a high resolution close to 30 nm, it can be seen that the submicron high- or low-density regions are composed of smaller high- or low-density regions of tens of nanometers (see the green arrows in **Fig. 32(d)**).

Inhomogeneous deformation at the low temperature far below  $T_g$  rejuvenates the structure of Zr<sub>64.13</sub>Cu<sub>15.75</sub>Ni<sub>10.12</sub>Al<sub>10</sub> amorphous alloy by creating a large amount of low-density regions (**Fig. 33(a)**). Nanoscale quadrupolar high-density regions and shear-band-like low-density regions can be also observed in the direction of the maximum shear stress, which signal shear localization [284, 285] (**Figs. 33(b)** and **(c)**). From **Fig. 33(d)**, it can be seen that the overall density of the deformed Zr<sub>64.13</sub>Cu<sub>15.75</sub>Ni<sub>10.12</sub>Al<sub>10</sub> amorphous alloy decreases compared to that of the as-quenched one. The densities of the shear-band-like regions in **Fig. 33(c)** lie in the

low-density part of the density distribution of the deformed amorphous alloy. Furthermore, with the 3D box-counting method, it was found that the hierarchical microstructures of the as-quenched and deformed amorphous alloys are self-similar and fractal-like (see the microstructures in Fig. 32, Figs. 33(a) and (c)).

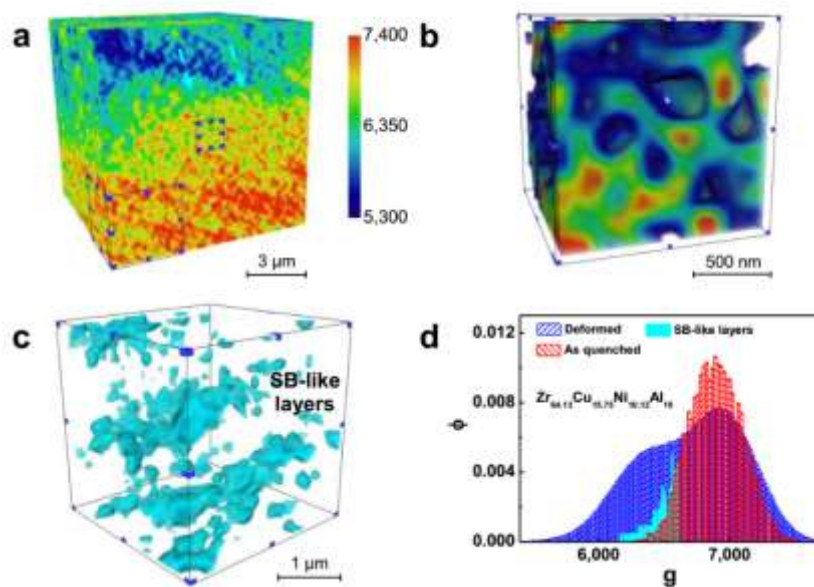


**Fig. 33.** Rejuvenated microstructure of inhomogeneous deformed amorphous alloy [29]. (a) The 3D microstructure reconstructed by nano-CT for severely deformed  $Zr_{64.13}Cu_{15.75}Ni_{10.12}Al_{10}$  amorphous alloy. The cyan dashed arrows point to the direction of in-plane principal stress in the deformation process. The high-density regions in the frame of the middle part and the low-density regions in the frame of the bottom-left part are enlarged in (b) and (c), respectively. (b) The quadrupolar high-density regions in deformed  $Zr_{64.13}Cu_{15.75}Ni_{10.12}Al_{10}$  amorphous alloys. (c) The low-density layers in deformed  $Zr_{64.13}Cu_{15.75}Ni_{10.12}Al_{10}$  amorphous alloy. (d) The  $g$  distributions of as-quenched, deformed  $Zr_{64.13}Cu_{15.75}Ni_{10.12}Al_{10}$  amorphous alloys and low-density layers in deformed  $Zr_{64.13}Cu_{15.75}Ni_{10.12}Al_{10}$  amorphous alloy. Reprinted from reference [29], copyright (2018), with permission from Elsevier.

The formation of the fractal heterogeneous microstructures of different metallic glasses could be rationalized by the percolation of high-density regions during glass transition or by the percolation of low-density regions during plastic deformation [29, 286, 287]. If the concentration of the pre-defined low-density regions  $p = 1$ , the dimension of the glass microstructure  $D_f = 3$ . With the decrease of  $p$ , the dimension of

the glass microstructure decreases below 3 and the low-density regions appear “fractal-like”, which exhibit a correlation length  $\zeta$  that increases with  $p$ . When  $p$  reaches a critical value  $p_c$ ,  $\zeta$  becomes infinite. When  $p < p_c$ , the low-density regions are made up of finite clusters. Notably, the fractal-like microstructure in the metallic glasses is different from those formed by a diffusion-limited aggregation process (DLA) due to the combined effect of temperature and stress during the formation and deformation of glasses [286]. Interestingly, given a similar temperature difference from the surface to the center of a sample, a more gradient microstructure is formed in the more fragile amorphous alloy, which could be attributed to its large temperature sensitivity of viscosity or free volume [207, 288]. According to the STZ theory, under a large shear stress, the growth rate of the density  $\Lambda$  of STZs  $\dot{\Lambda} \propto \Lambda / (1 + \Lambda)$  [289]. Therefore,  $\Lambda$  increases more rapidly in the local fertile low-density regions where  $\Lambda$  is already large, and grows slowly in the high-density regions where  $\Lambda$  is small. Thus, the heterogeneous microstructure of metallic glasses can be severely changed by inhomogeneous plastic deformation at low temperatures. According to the 3D box-counting method, it is found that the fractal dimension  $D_f$  derived from the size distribution of the low-density regions is around 2.5 in all the as-quenched and deformed metallic glasses (**Fig. 34(a)**), while the fractal dimension  $D_f$  of the shear-band-like regions in **Fig. 33(c)** is  $\sim 2.2$  (**Fig. 34(a)**). Moreover, the correlation length  $\zeta$  of the fractals in the more fragile or inhomogeneously deformed metallic glasses is longer than that in the as quenched metallic glasses. This is consistent with the combined effect of temperature and stress on structural heterogeneity in metallic glasses (**Fig. 34(b)**) [29].

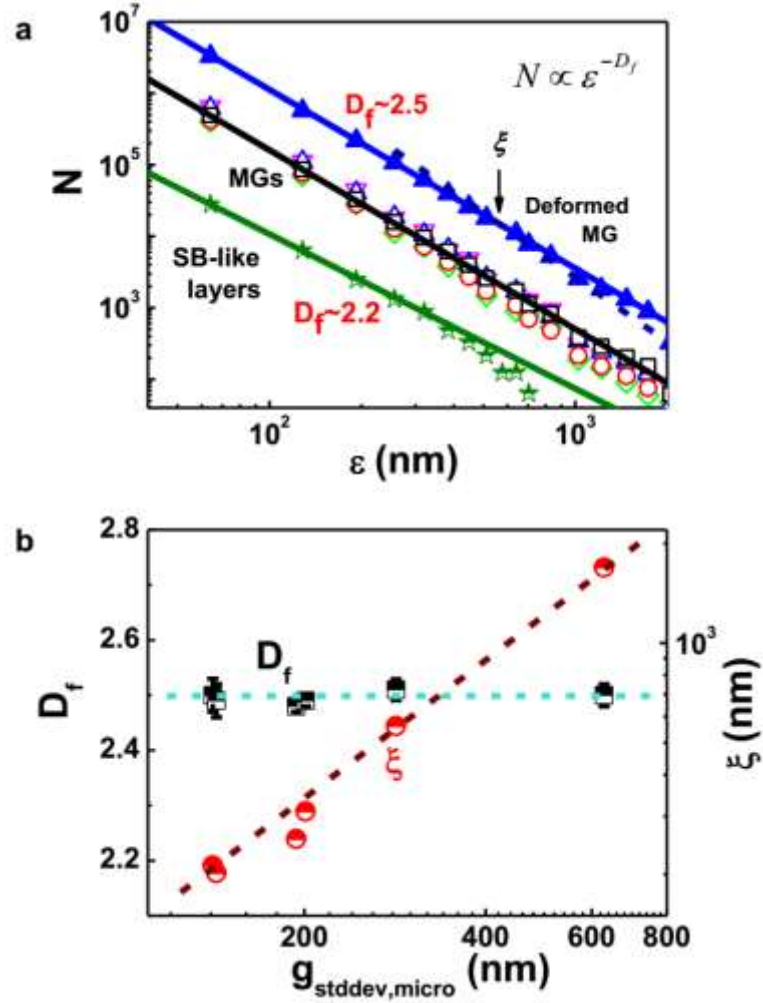


**Fig. 34.** Fractal order and microstructural heterogeneity in metallic glasses [29]. (a) The  $\varepsilon$ -dependent  $N$  in a double logarithmic coordinate for the low-density regions in metallic glasses at  $D_f$  of  $\sim 2.5$  (the open squares, circles, up-triangles, down-triangles, diamonds and solid up-triangles are for  $\text{Pd}_{40}\text{Ni}_{10}\text{Cu}_{30}\text{P}_{20}$ ,  $\text{Zr}_{52.5}\text{Ti}_5\text{Cu}_{17.9}\text{Ni}_{14.6}\text{Al}_{10}$ ,  $\text{Zr}_{64.13}\text{Cu}_{15.75}\text{Ni}_{10.12}\text{Al}_{10}$ ,  $\text{Zr}_{41.2}\text{Ti}_{13.8}\text{Cu}_{12.5}\text{Ni}_{10}\text{Be}_{22.5}$ ,  $\text{Mg}_{60}\text{Cu}_{30}\text{Gd}_{10}$  and deformed  $\text{Zr}_{64.13}\text{Cu}_{15.75}\text{Ni}_{10.12}\text{Al}_{10}$  amorphous alloys, respectively), and the low-density layers in deformed  $\text{Zr}_{64.13}\text{Cu}_{15.75}\text{Ni}_{10.12}\text{Al}_{10}$  metallic glass with  $D_f$  of  $\sim 2.2$  (the half-open pentagons). The black, blue, navy and olive lines are the fitting lines of  $N(\varepsilon) = N_0\varepsilon^{-D_f}$  with  $D_f$  as 2.5, 2.5, 3 and 2.16, respectively. (b) The  $g_{\text{stddev,micro}}$ -dependent  $D_f$  and  $\xi$  for different metallic glasses.  $g_{\text{stddev,micro}}$  is the standard deviation of the  $g$  distribution for different metallic glasses at the micrometer scale. The dashed lines are the guide lines for the eyes [29]. Reprinted from reference [29], copyright (2018), with permission from Elsevier.

### 3.2. High-rate Nanoindentation method

According to Yang et al.[265, 268], that metallic glasses as a whole deform in an anelastic fashion can be considered as a reflection of the underlying structural heterogeneity. In other words, nano-scale anelasticity provides another effective metric to characterize the dynamic structural heterogeneity in metallic glasses. To this end, they devised a nanoindentation scanning experiment for a Zr based metallic glass, as illustrated in **Fig. 35** (a)-(d) [245].

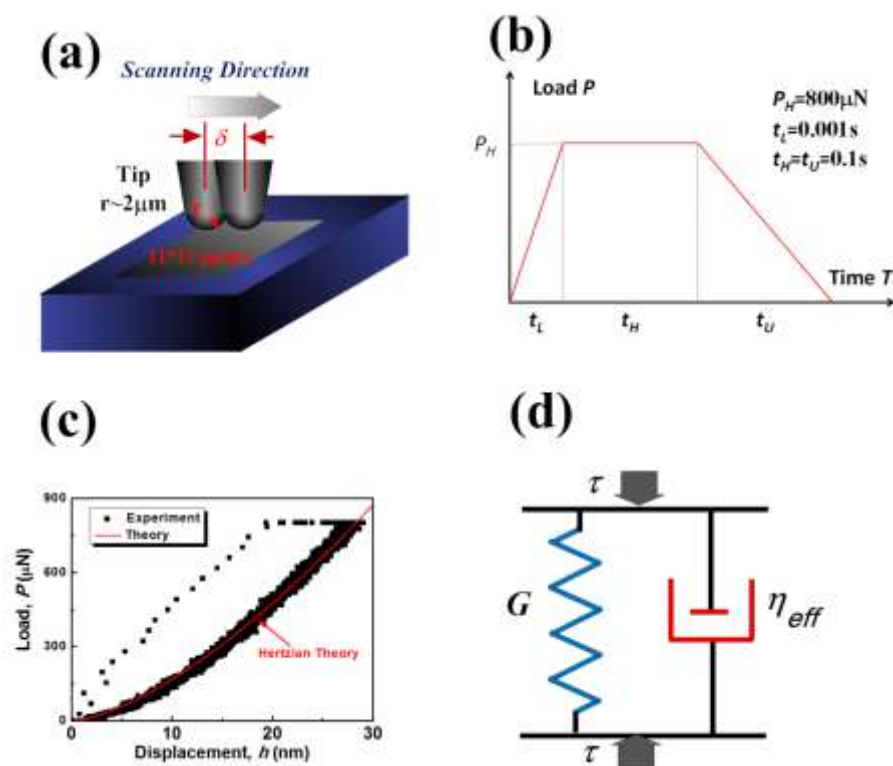


**Fig. 35.** (a) Schematic illustration of the scanning nanoindentation test to map out the structural heterogeneity in a bulk metallic glass, (b) the sketch of the indentation load function, (c) the representative nanoindentation  $P$ - $h$  curves obtained at  $P_H = 800$  mN, showing the anelastic deformation in the Vit105 bulk metallic glass. The Hertzian curve (red line) corresponds to the indenter tip radius of 2 mm, shear modulus of 30 GPa and Poisson's ratio of 0.363 for Vit105, (d) the sketch of the effective Kelvin model [245]. Reprinted From reference [245], copyright (2014), with permission from Elsevier.

To probe local anelasticity, a load function featured with an asymmetric loading-holding-unloading profile can be applied at each indentation spot (**Fig. 35(b)**). The unusually high loading rates could be achieved by virtue of the ultrafast data acquisition capability (with a maximum of 30,000 points per second) of the state-of-art nanoindentation system [265]. For metallic glasses, the loading time  $t_L$ , the holding time  $t_H$  and unloading time  $t_U$ , can be fixed at 0.001 s, 0.1 s and 0.1 s, respectively. The holding time is sufficiently large to ensure the full recovery of the anelastic deformation caused by the fast loading.

In theory, the total mechanical strain,  $\gamma$ , occurring to metallic glasses in the nanoindentation experiment can be related to the external shear stress,  $\tau$ , according to the anelastic model developed on the notion of structural heterogeneity[218, 253, 267],

$$\dot{\gamma} + 2\omega e^{-\frac{\Delta G}{kT}}\gamma = \frac{\dot{\tau}}{\mu} + 2\omega e^{-\frac{\Delta G}{kT}}\left(\frac{\beta\Omega}{kT} + \frac{1}{\mu}\right)\tau \quad (3-5)$$

where  $\omega$  is the attempt frequency of the liquid-like atoms,  $\Delta G$  the energy barrier against the activation,  $t$  the time,  $k$  the Boltzmann constant,  $T$  the ambient temperature, and  $\Omega$  the activation volume. Referring to the standard linear solid (SLS) model in rheology, which is composed of two springs and one dashpot, the physical parameters mentioned above can be translated into the spring moduli,  $G_I$  and  $G_{II}$  and dashpot viscosity  $\eta$ . Furthermore, taking into account that in a load controlled nanoindentation experiment the stress rate  $\dot{\tau}$  can be approximated as zero at small indentation loads, since the time spent for a load increment in the nanoindentation is longer than the relaxation time of the liquid-like region, Eq. (3-5) could be simplified to a Kelvin model (**Fig. 35(d)**):

$$\dot{\gamma} + \frac{G_I G_{II}}{\eta(G_I + G_{II})}\gamma = \frac{G_{II}}{\eta(G_I + G_{II})}\tau \quad (3-6)$$

Or simply

$$\dot{\gamma} + \frac{G}{\eta_{eff}} \gamma = \frac{\tau}{\eta_{eff}} \quad (3-7)$$

where  $G = G_I$  and the effective viscosity  $\eta_{eff} = \eta(1 + G_I/G_{II}) = \eta(1 + 1/\alpha)$ .

Based on the above modeling, one can obtain these physical parameters including local shear modulus  $G$ , the local relaxation time  $t_c$  and the local viscosity  $\eta_{eff}$  all from a single indentation experiment. For an elastic Hertzian contact, the load-displacement relation can be expressed as

$$h(t)^{3/2} = 3P(1 - \nu)/8G\sqrt{R} \quad (3-8)$$

where  $h$  is the indent depth;  $P$  is the indentation load,  $\nu$  is the material's Poisson's ratio;  $G$  is the material's shear modulus; and  $R$  is the indenter tip radius. For an anelastic solid as shown in **Fig. 35 (c)**, the loading curve can be derived from the Hertzian solution using the integral transform method[38]

$$h(t)^{3/2} = h_0(t)^{3/2} - \frac{(1-\nu)3\dot{P}t_c}{8\sqrt{R}G} \left[ 1 - \exp\left(-\frac{t}{t_c}\right) \right] \quad (3-9)$$

where  $\dot{P}$  is the loading rate;  $t_c = \eta/G$  is the relaxation time of the liquid-like region; and  $h_0$  is the Hertzian solution  $h_0(t)^{3/2} = 3P(t)(1 - \nu)/8G\sqrt{R}$ . By fitting the experimental data to Eqs. (3-8) and (3-9), one can obtain the shear modulus  $G$  and the relaxation time  $t_c$  point by point. After that, the local viscosity  $\eta_{eff}$  can be also computed from  $t_c = \eta_{eff}/G$ .

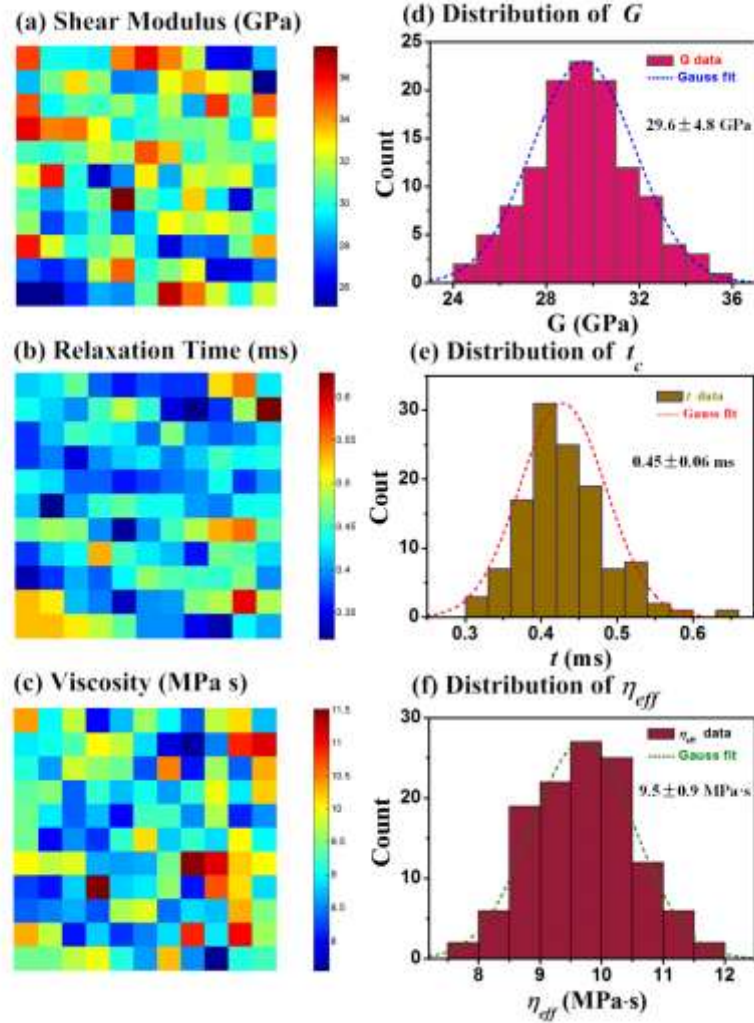


**Fig. 36.** Mapping of (a) local shear modulus, (b) local relaxation time and (c) local viscosity of the Zr-based amorphous alloy at the indentation load of 800 mN and the scanning space of 100 nm. On the right are the corresponding statistical distribution of (d) local shear modulus, (e) local relaxation time and (f) local viscosity. The dashed lines are the Gaussian fitting to the experimental data [245]. Reprinted from reference [245], copyright (2014), with permission from Elsevier.

Following the above method, the ultra-fast spherical nanoindentation scanning of 11 x 11 points in a square lattice with spacing of 100 nm was performed on a Zr based metallic glass, mapping the local shear modulus, the local relaxation time and the local viscosity. As seen in (Fig. 36(a)-(c)), the tested amorphous structure exhibits the variations in not only the local static property, such as the shear modulus, but also the local dynamic properties, such as the local viscosity or relaxation time. Moreover, the

statistical distributions of  $G$ ,  $t_c$  and  $\eta_{eff}$ , can be fitted to a Gaussian curve (Fig. 36(d)-(f)), which agrees with the previous findings with respect to the distribution of local properties in metallic glasses [13].

### 3.3. Atomic Force Microscopy (AFM)

#### 3.3.1. Dynamic atomic force microscopy (DAFM) and nano-scale energy dissipation: theoretical analysis

Aside from nanoindentation, dynamic atomic force microscopy (DAFM) with amplitude-modulation, also known as tapping mode AFM, is an effective tool to characterize heterogeneous structure and properties of a variety of materials [290-294]. In DAFM, a vibrating AFM probe (tip) is engaged with a sample surface at a pre-defined set-point amplitude and vibration frequency. The tip-surface interaction force usually leads to a reduction of the oscillation amplitude from its initial value. The resultant phase lag of the tip vibration with respect to the external excitation reflects the dissipation of energy, which varies with the site-specific material structure and some other factors, such as surface capillary forces and roughness [253, 257-260]. Regardless of the nano-scale energy dissipation mechanisms, the energy dissipated,  $E_{dis}$ , resulting in the phase shift,  $\phi$ , during tip sample interactions can be expressed as:

$$E_{dis} = \left( \sin \phi - \frac{\omega}{\omega_0} \frac{A}{A_0} \right) \frac{\pi k A A_0}{Q} \quad (3-10),$$

where  $\omega$  is the drive frequency,  $\omega_0$  is the resonant frequency of cantilever,  $A$  is the vibration amplitude during testing,  $A_0$  is the free amplitude without tip-sample interaction,  $k$  is the spring constant of cantilever, and  $Q$  is the quality factor [13, 210, 219, 261-263]. It is noted that, for a high  $Q$  value ( $>200$ ), the quality factor ( $Q$ ) can be simply calculated as the ratio of the peak frequency  $\omega_0$  to the width-at-half-maximum

$\gamma$  of the peak. Meanwhile, the time-average elastic force ( $F_{ts}$ ) exerted on the sample surface can be also derive as  $F_{ts} = F_0/2\cos\left(\frac{\pi}{2} - \Delta\varphi\right)$ , where  $F_0 = kA_0/Q$ .

To identify the mechanism of nano-scale energy dissipation in the DAFM, Garcia et al. [292] provides a convenient way by examining the shape of the curve of  $\delta E_{dis}/\delta(A_{sp}/A_0)$  versus  $A_{sp}/A_0$ . As demonstrated in Fig. 37, three different dissipation mechanisms including long-range surface attraction, surface energy hysteresis and sample viscoelasticity (or anelasticity for metals) are keyed to the three distinctive curves of  $\delta E_{dis}/\delta(A_{sp}/A_0)$  with  $A_{sp}/A_0$ , respectively.

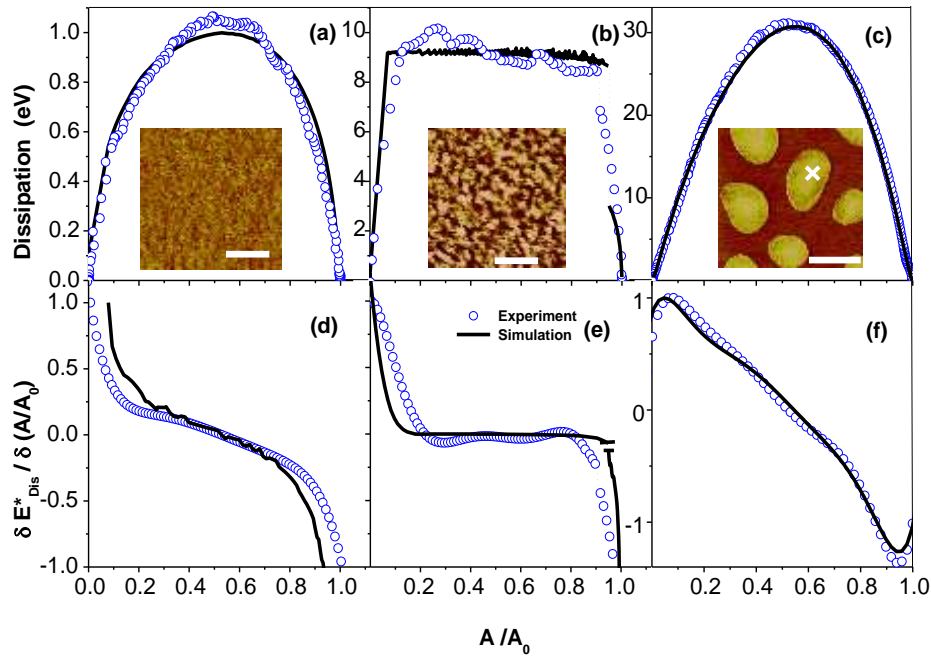


**Fig. 37.** (a)-(c) The measured and simulated dynamic dissipation curves  $E_{dis}$  as a function of the amplitude ratio  $A/A_0$  and (d)-(f) the corresponding derivatives. Note that (a) and (d) are obtained on a silicon surface with  $A_0=6.6$  nm and  $k=2$  N/m, (b) and (e) on a silicon with  $A_0=32.5$  nm and  $k=2$  N/m, and (c) and (f) on a PS region in the blend of a PS/PB polymer with  $A_0=15$  nm. Note that the images are taken from reference [292]. Reprinted figures with permission from reference [292], copyright (2011) by the American Physical Society.

### 3.3.2. DAFM analysis of dynamical structural heterogeneity in metallic glasses

Owing to its unique ability to detect a wide variety of dynamical processes with

unprecedented temporal and spatial resolution, DAFM has been recently employed to study the dynamic structural heterogeneity at nanoscale and its evolution in metallic glasses during plastic deformation or thermal annealing [255, 259, 264, 267, 268]. According to Lu et al [264], by tapping the surface of a metallic glass with a vibrating AFM tip, mechanical energies are transferred from the tip to metallic glass surface layers. If the structure of a metallic glass is homogenous and the tip-surface interaction remains elastic, the transferred energy should be stored as elastic strain energy and fully released upon tip retraction (Fig. 38(a)), thereby resulting in no structural contrast in the AFM phase image. However, if the structure of a metallic glass is dynamically heterogeneous, a portion of the transferred energy would be dissipated away by the local “liquid-like” regions in a similar way as by a viscous liquid. As a result, viscoelasticity takes place as a manifestation of this local dynamic heterogeneity (Fig. 38(b)), hence giving rise to the structural contrast in the AFM phase images.

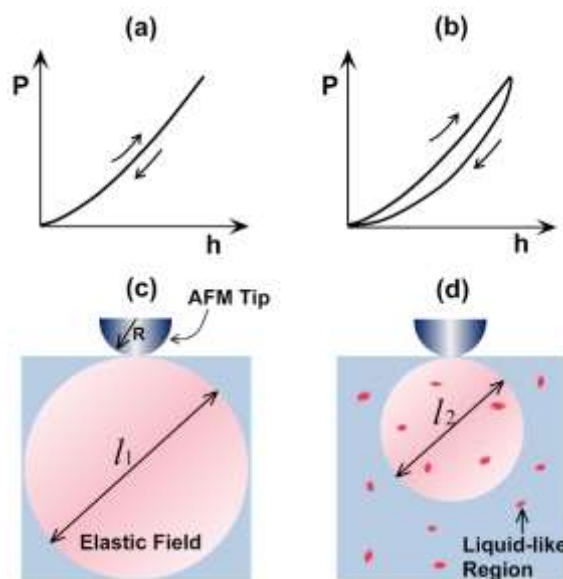


**Fig. 38.** The schematic illustrations of the mechanical response for elastic and viscoelastic material under AFM tip tapping [264]. Reprinted by permission from Macmillan Publishers Ltd: Scientific Reports, reference[264], copyright (2016). The typical load-displacement ( $P$ - $h$ ) curve for (a) elastic and (b) viscoelastic material; (c) the elastic interaction volume within an elastic material with its size  $l_1$  correlated with

the elastic properties and AFM tip radius; and (d) the elastic interaction volume within a viscoelastic material with its size  $l_2$  correlated with the viscoelastic properties and AFM tip radius. Note that, if all conditions remain identical except the presence of liquid-like regions,  $l_2$  should be smaller than  $l_1$  because of the energy dissipation [295].

Taking the advantage of DAFM, Liu et al. [259] firstly characterized the nanoscale mechanical heterogeneity of a deposited  $Zr_{55}Cu_{30}Ni_5Al_{10}$  metallic glass thin film with an atomic flat and damage-free sample surface. **Fig. 39(a-b)** presents the surface topography, phase shift, and amplitude images recorded simultaneously in DAFM. After ruling out the effect of the roughness, oxidation and residual stress, they obtained the nanoscale phase shift image (**Fig. 39(b)**), of which the contrast reflects the nanoscale variation in the phase shift for the studied Zr based amorphous alloy. It is worthy to note that referring to the previous work [292], the nano-scale energy dissipation,  $E_{dis}$ , spectrum obtained from the Zr-based thin film metallic glass is consistent with that of anelasticity (**Fig. 39(c-e)**). A variation of  $\sim 12\%$  for the apparent energy dissipation, can be attributed to non-uniform distribution of local viscoelasticity.

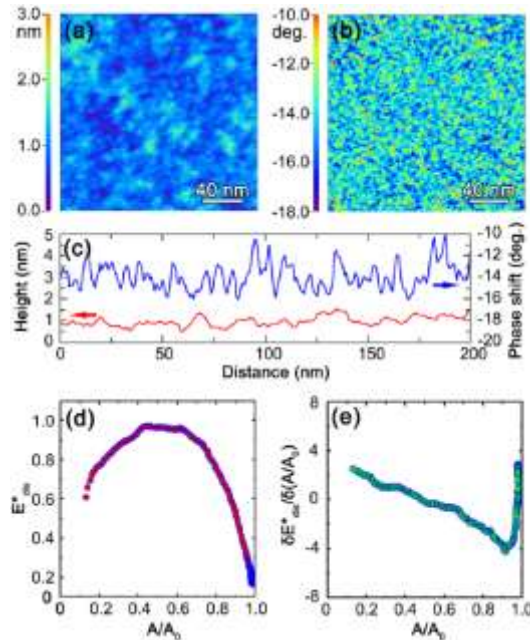


**Fig. 39.** (a) The height image with rms roughness of  $\sim 0.3$  nm, (b) the phase shift

image, (c) height and phase shift profiles taken from the same region, (d) the normalized energy dissipation ( $E^*_{dis}$ ) spectrum and (e) its derivative as a function of the amplitude ratio  $A/A_0$  for the  $Zr_{55}Cu_{30}Ni_5Al_{10}$  thin film metallic glass. From ref. [259]. Reprinted figures with permission from reference [259], copyright (2011) by the American Physical Society.

Moreover, the characteristic length of the viscoelastic heterogeneity can be evaluated by the correlation functions  $P(r) = 2\sigma^2 \left[ 1 - \exp\left(-\left(r/\xi\right)^{2\alpha}\right) \right]$ , where  $P(r) = \langle P(r) - P(0) \rangle^2$ , in which  $P(r)$  and  $P(0)$  are the phase shift at the coordinate  $(x,y)$  and the reference position  $(x_0,y_0)$ , respectively, and  $\sigma$  is the root mean square roughness or phase shift,  $\alpha$  is the roughness (or phase shift) exponent, and the lateral correlation length  $\xi$  defines the distance between two correlated points [61]. Based on the data fitting, the correlation length for the phase shift is found to be  $\sim 2.5$  nm, which is consistent with the characteristic length of secondary relaxation in MGs or the dimension of shear transformation zones for plastic flow. It was the first time to provide experimental evidence of the nanoscale viscoelastic heterogeneity in MGs. Subsequently, Yang et al [267] reported an average radius of  $\sim 2$  nm for defined loose-packing phases in the DAFM image, which, in order of magnitude, is consistent with both the theoretical estimation [296] and experimental measurement [297] of the average size of STZs ( $\sim 2$  nm).

### **3.3.3. The thermal annealing-induced evolution of nanoscale dynamical heterogeneity in metallic glasses**

In the work by Liu et al [259], EXASf and XRD were used to study the structural evolution in MG thin film upon annealing, showing that the excess quench-in defects can be annihilated out, thus resulting in the relaxation of the metallic glass film towards equilibrium with a very similar structure to a bulk sample. Subsequently, their DAFM measurements on the annealed film show the reduced variation of phase shift of  $\sim 8\%$  and the increased correlation length of  $\sim 4.2$  nm that is close to the upper size limit of the STZs in Zr-based bulk metallic glasses [297]. Such

an increase in the correlation length agrees very well with the recent atomistic simulations [257, 298] which showed that glasses obtained by slow quenching are more densely packed with enhanced short range order.

A more comprehensive study on the effect of thermal annealing on the nanoscale structural heterogeneity in metallic glasses was presented by Yang et al [267]. In their work, high-resolution DAFM images were firstly obtained by correcting the surface adhesion and topography effects, revealing the nanoscale structural heterogeneity in a Zr-Ni metallic glass film. Following the atomic stress theory [71], the authors set a boundary-defining criterion to perform a quantitative analysis of the metallic glass structure. Consequently, the loose-packing “phase” was defined as the region taking the top  $P_c$  percent of the total energy dissipation, where  $P_c$  refers to the area under the curve of the energy dissipation distribution, as demonstrated in the [Fig. 40\(a-b\)](#) [267]. As a result, it could be shown that the inclination angle  $\phi$  of the isolated loose-packing phases has a uniform distribution in  $[-180^\circ, 180^\circ]$  ([Fig. 40\(c\)](#)), indicative of the random orientation of the loose-packing phases. By comparing the averaged maximum ( $D_{max}$ ) and minimum ( $D_{min}$ ) bounding lengths of the loose-packing phases ([Fig. 40\(d\)](#) and [Fig. 40\(e\)](#)), one can find that their shape is close to an ellipse with an aspect ratio close to 2. This ratio agrees well with what was observed from the atomistic simulations [299], in which similar shape anisotropy, with an aspect ratio of 1.5 ~ 2.0, was found for shear-intensified regions in a metallic glass. Moreover, assuming that these loose-packing phases take on a circular shape, their average radius could be estimated as ~2nm, which is consistent with of the average size of STZs (~2 nm) [296, 297] and also agrees with that obtained by Liu et al [259] through DAFM of Zr-based amorphous alloys. Therefore, as the authors [267] pointed out, the obtained DAFM results show that the loose-packing phases possess similar geometric features to those already known for STZ sites [13, 299].

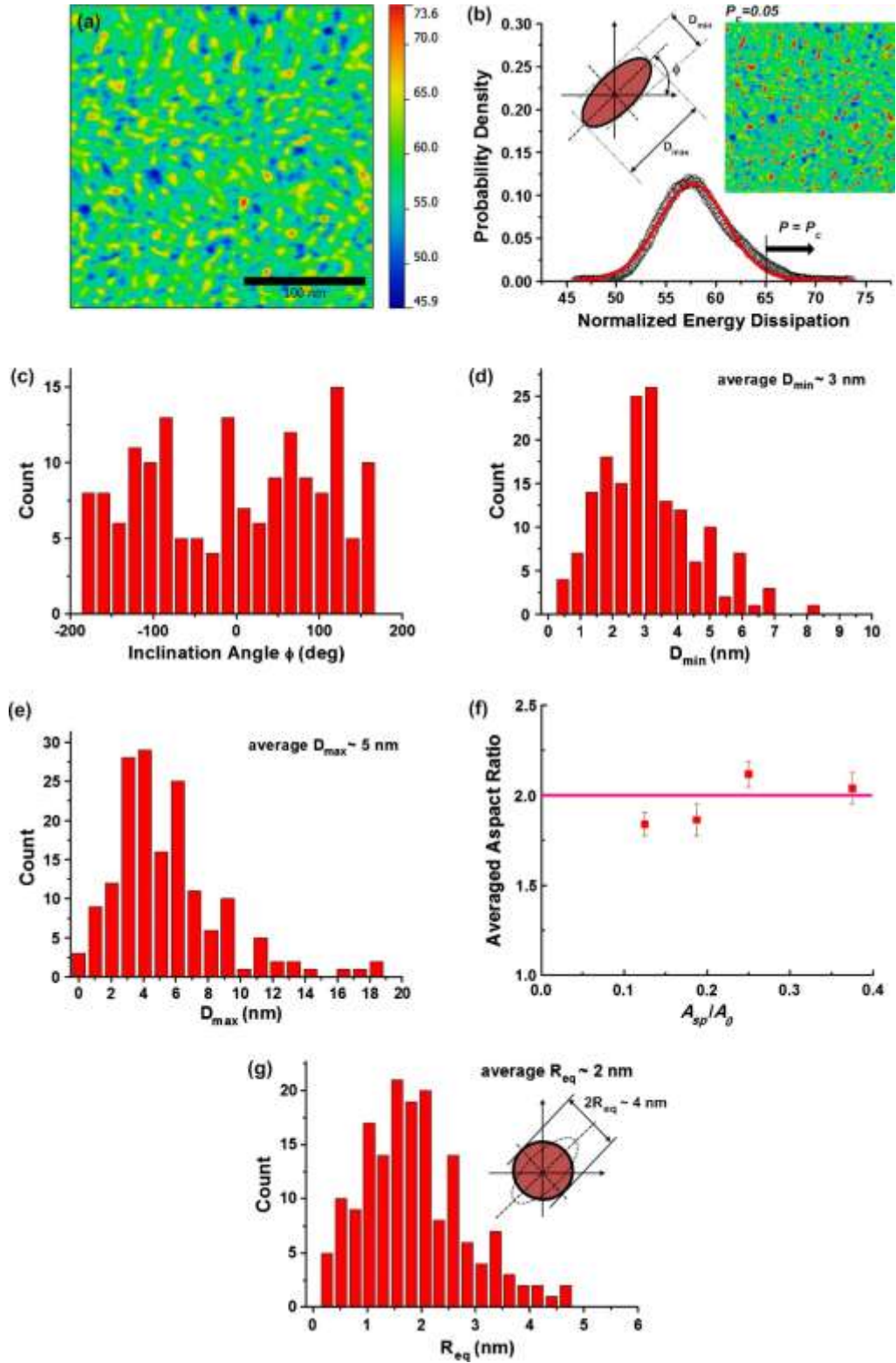


**Fig. 40.** (a) The structural contrast formed through the normalized energy dissipation at  $A_{sp}/A_0 = 0.15$ . (Note that the numbers next to the color bar here after refer to the percentages of the normalized energy dissipation.) (b) The Gaussian-type density

distribution of the normalized energy dissipation. Insets: (left) sketch illustrating the different geometric parameters defined for an elliptical loose-packing region; (right) sketch highlighting (in red) the loose-packing phases in (a). Histograms of (c) the inclination angle  $u$  of the loose-packing phases, and the lengths of (d) the short axis,  $D_{\min}$ , and (e) the long axis,  $D_{\max}$ . The sketch in the inset of (e) demonstrates the definition of  $R_{eq}$ . (f) The variation in the averaged aspect ratio of the loose-packing phases with the  $A_{sp}/A_0$  ratio, and (g) the equivalent disk radius,  $R_{eq}$ , of the loose-packing phases [267]. Reprinted from reference [267], copyright (2012), with permission from Elsevier.

In the same study [267] the nanoscale structural evolution associated with the loose- and dense-packing phases in the Zr-Ni metallic glass film was explored. As shown in Ref. [267], the size and number of the loose-packing phases, which are randomly dispersed in the thin film, diminish rapidly as a result of the densification in those places after thermal annealing. Moreover, densification in the dense-packing regions becomes more prevalent than that in the loose-packing regions during thermal annealing. For a pre-defined cut-off value  $\bar{R}$ , the number of the dense-packing-phase clusters with a size greater than  $\bar{R}$  can be computed through  $N(\bar{R}) = \sum_{R \geq \bar{R}} n(R_{eq})$ , in which  $R_{eq}$  refers to the radius of a circle that has the same area as the interconnected dense-packing phases rather than the physical size of the individual dense packing phases, and  $n$  is the number of the cluster of the dense-packing phases with the size of  $R_{eq}$ . As demonstrated in **Fig. 41** [267], by examining the trend line of the double-logarithmic plot of  $N$  vs.  $\bar{R}$ , it is found that the Gaussian-type size distribution becomes stretched after annealing and ultimately transforms to a power-law scaling,  $N(\bar{R}) \sim \bar{R}^{-(\alpha-1)}$ , where  $\alpha$  is defined as a “cluster fractal dimension” (**Fig. 41(c)**). These results indicate that the clusters of dense-packing phases continue to grow while newly formed dense-packing phases of a smaller size emerge. Interestingly, regardless of the selected cut-off energy, the value of fractal dimension  $\alpha$  for the growth of the dense packing phases is estimated to be  $\sim 1.7$ , similar to that of  $1.63 - 1.7$  found in many other 2-D patterns generated in a variety of physical processes, such as dielectric breakdown [245] and metal leaf growth [267]. According to references [264,

265], the power-law scaling signals the formation of a fractal-dimensional supercluster, which can have a divergent and sample-spanning size. Consequently, it was suggested that despite being driven by different growth mechanisms, the formation of such fractal-dimensional superclusters might share a common kinetic origin [265].

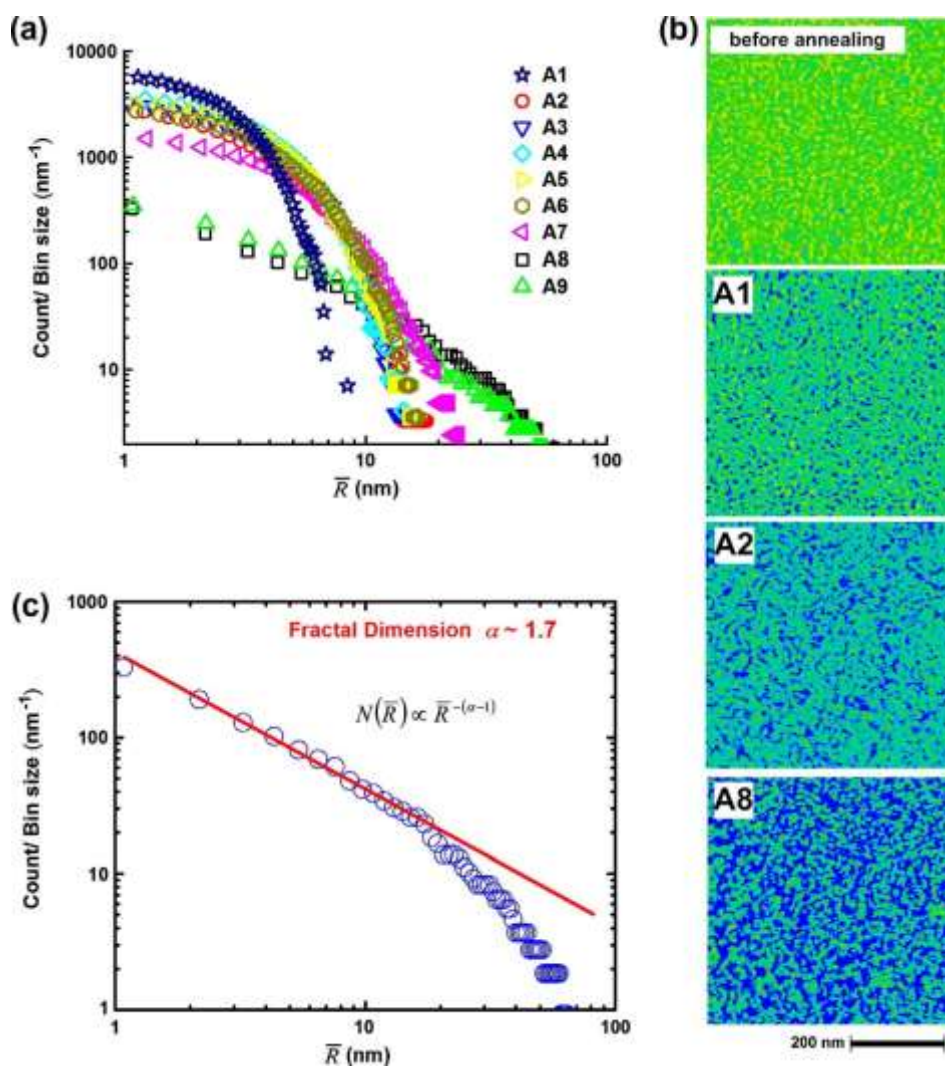


**Fig. 41.** The annealing-induced formation of a fractal-like network of the dense-packing phases characterized by  $E_{\text{dis}}Q/\pi k A_{\text{sp}} A_0 \leq 45\%$ . (a) The accumulated size distributions of the dense-packing regions (note that the designations of the curves (A1-A9) are in ascending order of annealing); (b) the structural images rendered with the same color bar, vividly showing the emergence of a fractal-like supercluster (note that the dense-packing regions are highlighted in blue for clarity);

and (c) the power-law size scaling for the accumulated size distribution of the dense-packing regions with an exponential cut-off. Note that the counts shown in (a) and (c) are normalized by the bin size to remove the statistical bias for data comparison [267] Reprinted from reference [267], copyright (2012), with permission from Elsevier.

### 3.3.4. Plasticity-induced evolution of nanoscale dynamical heterogeneity in metallic glasses

Over the past decades, tremendous research efforts have been made to elucidate the possible structural mechanisms that may give rise to the attractive mechanical properties of metallic glasses. Through the recent development in theories [71, 208, 215, 296, 300] and atomistic simulations [77, 270, 299], as well as in experiments [218, 253, 254], it is now widely accepted that the local structural heterogeneity plays a vital role in the room-temperature plastic deformation of amorphous alloys. However, the experimental data directly uncovering the nanoscale structural heterogeneity and its subtle change caused by plasticity are still scarce. Only until recently did Lu et al [264] show that DAFM can be employed to study the effect of plasticity on structural heterogeneity in amorphous alloys due to its high spatial and temporal resolution in detecting a variety of dynamical process in materials [259, 268, 290-292, 294, 301].

Through the DAFM technique, Lu et al [264] investigated the plasticity-induced structural evolution in the  $Zr_{70}Ni_{30}$  thin film metallic glass which is otherwise hidden in conventional mechanical tests. It was clearly displayed that the distributed plastic flow leads to a spatial amplification of the nano-scale structural heterogeneity, which can be linked to the limited growth, reorientation and agglomeration of some nano-scale energy-absorbing regions. **Fig. 42(a-c)** display the typical energy dissipation images obtained at indentation loads of 0 N, 40 mN, and 3 N respectively. It is evident that plasticity causes an overall increase in the viscoelastic energy dissipation. When compared to an initial random homogeneous distribution of the high-dissipation regions (HDRs)(**Fig. 42(a)**), some kind of plasticity-induced

structural polarization, as manifested by the coalescence of the HDR, can be noticed (Fig. 42(b-c)). At a higher indentation load of 3N, the structural polarization becomes more significant with the HDR localized into the patterns of a quadrupolar symmetry. This indicates that the observed structural polarization or localization is mainly driven by the maximum shear stress.

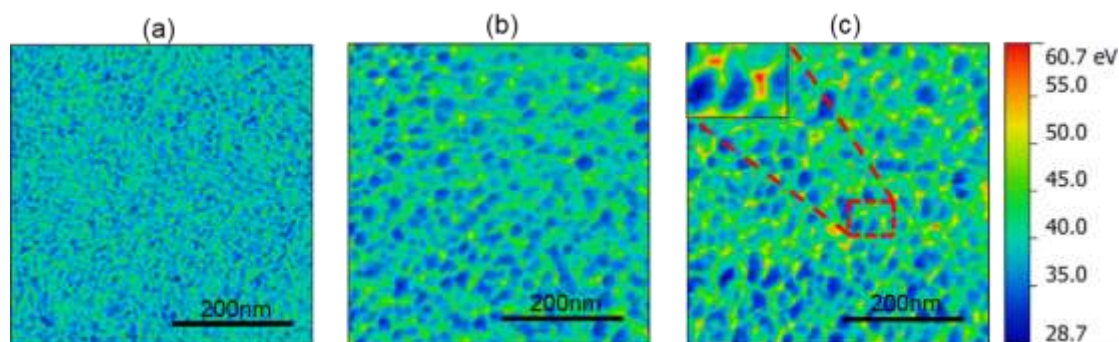


**Fig. 42.** Energy dissipation images of  $Zr_{70}Ni_{30}$  TFMG and the corresponding 2D FFT patterns [264]. (a-c) Are energy dissipation images obtained at the as-deposited state, at the indentation area with the load of 40 mN and 3 N, respectively. The zoom-in image of the area boxed in red in (c) clearly shows the quadrupolar characteristics of HDR. Reprinted by permission from Macmillan Publishers Ltd: Scientific Reports, reference[264], copyright (2016).

To further understand the plasticity-induced structural evolution in the thin film metallic glass, Lu et al [264] performed a thorough statistical and geometrical analysis of the AFM images obtained. Fig. 43(a) shows the typical distribution spectra of the viscoelastic energy dissipation before and after the occurrence of plasticity [264]. As indicated in Fig. 43(a), on a statistic average, the loss-dissipation regions (LDR) can be viewed as being almost “intact” during the plastic flow considering the overlap of the energy distributions in the low dissipation tail; however, the energy distribution obtained after the occurrence of plasticity becomes broadened and skewed to the high energy tail. This indicates that plasticity not only causes structural polarization as seen in Fig. 42(b-c) but also produces more HDR. Furthermore, by following the method in Ref. [267] and taking the HDR as those above a cut-off value selected on the

energy dissipation distribution, such as the top 5%, Lu et al [264] also characterized the shape and orientation of these HDR. It was observed that the aspect ratio of these HDR regions increases from  $\sim 1.9$  to  $\sim 2.4$  or their shape becomes slender after plasticity occurs. This trend of shape change implies a higher stress concentration when the HDR are activated. Meanwhile, the average equivalent radius of these HDR, by assuming the shape of HDR to be a circular, increases from  $\sim 3$  nm to  $\sim 6$  nm with increasing applied stress, which confirms the growth of the HDRs. In addition, an energy barrier of 0.3–0.5 eV is deduced for these nano-scale regions, which possess an energy barrier of 0.3–0.5 eV, about half of that for a typical shear transformation event that usually occurs at the onset of plasticity [218]. Therefore, the plasticity-induced structural evolution in the  $Zr_{70}Ni_{30}$  thin film metallic glass was revealed in this work through the dynamic AFM technique which functions as a result of the viscoelastic heterogeneity intrinsic to the TFMG.

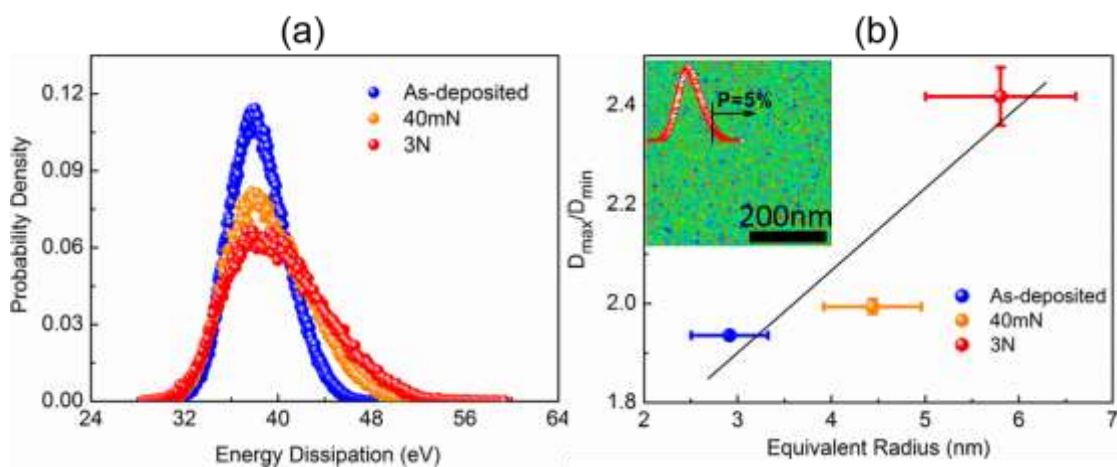


**Fig. 43.** The energy dissipation spectra of  $Zr_{70}Ni_{30}$  thin film metallic glass (TFMG) and characteristics of the HDR in  $Zr_{70}Ni_{30}$  TFMG [264]. (a) The spectra are obtained at the as-deposited state and at the indentation area with the load of 40 mN and 3 N. For each state, ten different sites of a  $500 \text{ nm} \times 500 \text{ nm}$  size were scanned. (b) The averaged aspect ratio versus the equivalent disk radius of HDR in  $Zr_{70}Ni_{30}$  TFMG. Insets: normalized energy dissipation image (shown in Fig. 38(c)) and the corresponding energy spectrum (red curve). The top 5% of the total energy is defined as the HDR, which is highlighted in red in the image.  $D_{max}$  and  $D_{min}$  are the averaged

maximum and minimum bounding lengths of the elliptical HDR, respectively.  $Req$  is the average size (radius) of these HDR by assuming that they take on a circular shape. The black line is drawn for eye guides. Reprinted by permission from Macmillan Publishers Ltd: Scientific Reports, reference[264], copyright (2016).

### **3.3.5. Atomic force acoustic microscopy (AFAM) and local elastic properties of metallic glasses**

AFAM is a contact resonance indentation technique, which can be used to measure the indentation modulus, an elastic constant which accounts for both the compressive and shear deformations in the contact zone between isotropic or anisotropic materials [302]. In this technique, the resonances of atomic force cantilevers with the tip contacting the specimen surface are measured. From such a measurement, the local indentation modulus can be derived from the tip-sample contact stiffness  $k^*$ , by using Hertzian contact mechanics and calibration procedures with materials for which the elastic properties are well known [255, 302].

According to the theory [303], a scale-dependent distribution of elastic constants in space is intrinsic to the amorphous materials because of the significant variations of the local potential energy of a cluster of atoms or molecules. Different configurations of an ensemble of atoms or molecules can be considered as the origin of dynamical heterogeneity often observed in studies of relaxation modes [255]. By using AFAM, Wagner et al [255] measured the local so-called indentation modulus in amorphous Pd-Cu-Si alloy, which exhibits a 10-30 times wider distribution on a scale below 10nm when compared to its crystalline counterpart. It is worthy to note that, from the dynamic mechanical response of the tip-sample contact, the imaginary part of  $k^*$ , which is related to damping phenomena, is also obtained in addition to its real part [304, 305]. Nevertheless, in contrast to DFAM, the imaginary part of AFAM for the studied metallic glass can be neglected since it was much smaller than the real part [255].

### **3.4. Computational simulation of nanoscale structural heterogeneity in metallic glasses**

Based on the experimental results obtained by the state-of-art techniques, such as high-energy synchrotron X-ray diffraction, dynamic atomic force microscopy, and high-rate nanoindentation, the structural heterogeneity with a dynamical nature can be confirmed for metallic glasses. However, a thorough understanding of the dynamical heterogeneity at the atomic scale still remains challenging. To address the issue, computational or atomistic simulations have been carried over the past years to uncover the atomic-scale structural heterogeneity and to establish a causal link between the local structure and macroscopic properties of amorphous alloys[69, 251, 270].

According to the previous atomistic simulations [13, 247-249], there exists ordered atomic packing, such as icosahedra or crystal-like atomic packing in the amorphous structure of amorphous alloys in spite of the lack of any long-range translational symmetry. These local “motifs”, often known as short range order or medium range order (SRO or MRO) are commonly referred to as the building blocks of metallic glasses [13, 247-249, 306]. From the atomic packing perspective, the internal structure of amorphous alloy is inherently inhomogeneous, and it is the different types and degrees of structural order developed and distributed in the amorphous structure that lead to the structural inhomogeneity and thus property variability [69, 251, 271, 272]. In other words, there is a spectrum of the local topology and order across the whole range of atomic configurations in metallic glasses, which plays a key role in determining their properties. **Fig. 44(a)** schematically shows such a local structural distribution across a range of SROs, ordered to varying degrees, for a metallic glass. As seen in **Fig. 44(b)**, this is in accordance with simulation results for a Cu-Zr amorphous alloys [69, 251]. After revisiting the data obtained by Ding et al [69] for a variety of Cu-Zr amorphous alloys produced via molecular dynamics simulations, Ma further pointed out [251] that tuning the structural inhomogeneity in a controllable manner provides a possible route to improve the properties of amorphous alloys, such as their deformability or stability.

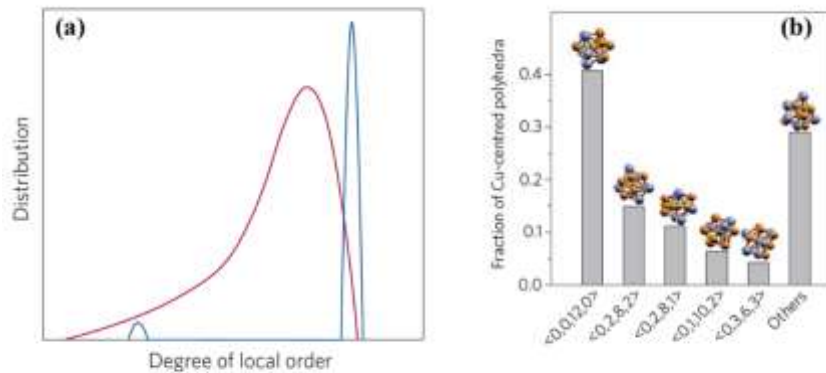


**Fig. 44.** (a) Schematic illustration contrasting the distribution of local order in metallic glasses (red curve) with conventional crystalline metals (blue curve); the amorphous alloys structure features varying degrees of short-to-medium-range order. The crystal however has bifurcated local environments composed of a near-perfect lattice (well-defined spike), plus discrete defects such as dislocations and vacancies (small peak)[251]. (b) Coordination polyhedra distribution in an amorphous alloy. Fractions of various Voronoi polyhedra around Cu atoms in a 32,000-atom molecular dynamics simulation of a  $\text{Cu}_{64}\text{Zr}_{36}$  amorphous alloy model prepared by quenching at  $1 \times 10^9 \text{ K s}^{-1}$  from liquid to 300 K. Figure (b) is constructed by Ma [251] based on data in reference[307]. Reprinted by permission from Nature [251] copyright (2014).

From the recent experiments and simulations, it was found that the local structural spectrum of metallic glasses contains both chemically and topologically favorable local configurations [13, 247, 248, 308] and geometrically unfavored motifs (GUMs) [251]. The interpenetrating quasi-equivalent clusters (coordination polyhedra) [13, 248] can be viewed as the locally favored structures, which constitute the building blocks and form the structural “backbone” of amorphous alloys through interconnection [251]. These local motifs are believed to be responsible for the stability of amorphous alloys and significantly impact their properties such as specific heat, crystallization activation energy, relaxation dynamics, and local elastic moduli and its nanoscale heterogeneity, etc.[13, 251]. Particularly, GUMs with most disordered (unfavoured) local environments are relatively unstable and hence more

conducive to reconfiguring via thermal- or stress-induced relaxation [251, 270]. From the structural perspective of atomic packing, the GUMs are naturally linked to liquid-like regions, which have not been clearly and physically defined as to how liquid-like they are rheologically, and their population, location, length scale and geometric arrangements [69, 251, 309]. Under external stimuli, local regions with a high content of GUMs are more flexible to enable reconfiguration to reduce energy and behave more liquid-like [251]. According to Ding et al [69], the residual “elastic strain” (originated from bond orientation or structural anisotropy) normalized by the total strain was considered as an indicator of solidity. Moreover, as demonstrated in **Fig. 45**, the GUMs are inhomogeneously distributed in a metallic glass system. The formation of nanoscale ‘soft spots’ can be correlated with the mechanical (elastic and plastic) heterogeneity: the highest deformation propensity appears to arise from GUM environments where atoms with the lowest packing order reside [251, 270].

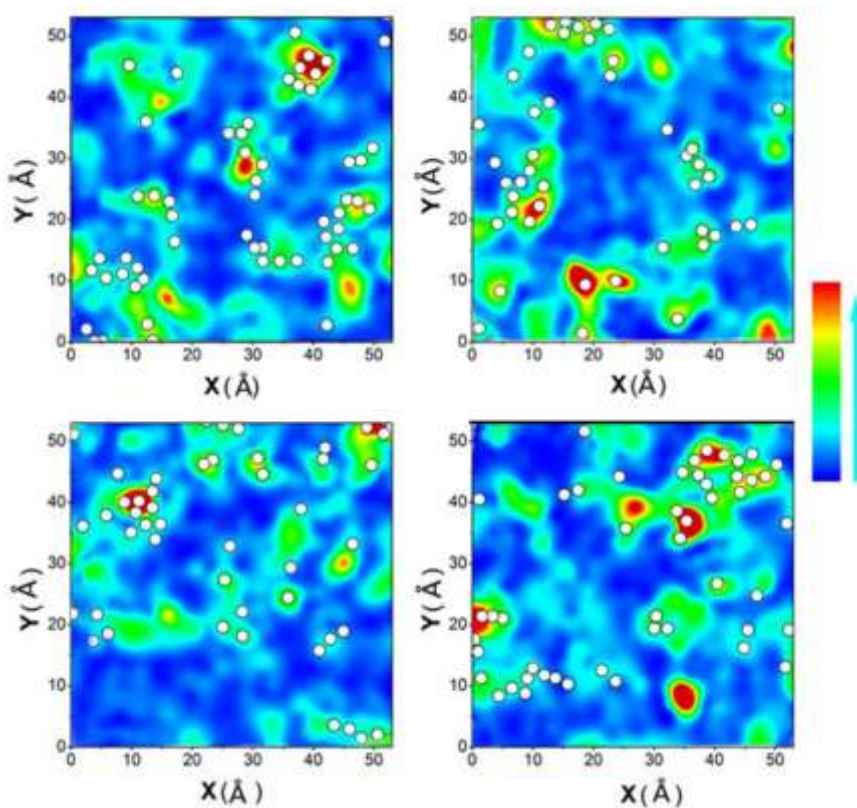


**Fig. 45.** Contour maps showing the heterogeneous spatial distribution of Cu and Zr atoms that participate the most in soft modes, correlated with those that contribute the most to deformation strain [251]. Reprinted by permission from Nature [251], copyright (2014). The  $\text{Cu}_{64}\text{Zr}_{36}$  metallic glass model was prepared via cooling at  $1 \times 10^9 \text{ K} \cdot \text{s}^{-1}$  in a molecular dynamics simulation. (a)–(d), The four sampled representative thin slabs each has a thickness of 2.5 Å. The colors indicate the different degrees of participation (increasing along the arrow in the color scale bar) in soft vibrational modes. The white circles mark the locations of the top 10% of the local motifs that have experienced the most accumulative non-affine strains, on athermal quasistatic shear of the simulation box to a global strain of 5%. Constructed from data reported in reference [270].

To explore the atomic-level structural heterogeneous features and its correlation with elastic heterogeneity in amorphous alloys, Fan et al [269] employed the activation and relaxation technique (ART) [310, 311] in their computer simulation on a model amorphous Zr-Cu alloy. In ART, the initial perturbations are introduced to a small group of atoms with local connectivity, which can provide important information for the local excitation in the amorphous system in terms of the concept of potential landscape energy [83]. Specifically, they select an atom as the central atom, and then randomly displace this atom and its first nearest neighbors, defined by the cutoff between the first and second peaks in the PDF. The magnitude of displacement is typically fixed at a constant value, e. g. 0.5 Å, while the direction is randomly chosen.

In the work of Fan et al [269], two starting model, system I and II are prepared. System I is the inherent structure of a liquid at 2000 K, which is far above the glass transition temperature ( $\sim 700 \text{ K}$ ). System II represents a relatively more stable glass. The system is first annealed at 1000 K, and then quenched to zero temperature with a cooling rate of  $10^{12} \text{ K/s}$ . The potential energy of system II is about 0.015 eV per atom ( $\sim 0.3\%$ ) lower than system I. Through the simulation on the model amorphous systems, they showed that the distribution of activation energy reflects its inherent structure more clearly than the structure, for instance, described by the atomic pair density function (PDF). Interestingly, the less stable amorphous system with higher

potential energy and larger fraction of low-energy reactions has stronger peaks in the PDF among the subgroup of atoms with shear modulus in the lowest 5% (see [Fig. 46](#)). This clearly reflects clustering of soft atoms in system I but a more homogenous distribution in system II.

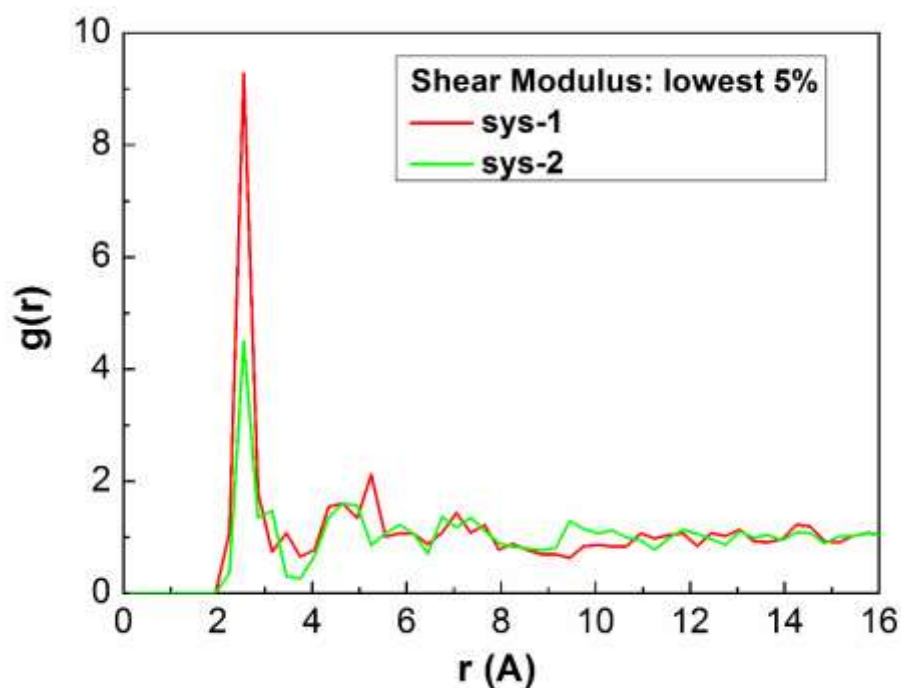


**Fig. 46.** The PDF of a subset group of atoms with lowest 5% shear modulus in two systems [269]. Red curves are for system I, green curves are for system II. Reprinted figures with permission from reference [269], copyright (2014) by the American Physical Society.

Furthermore, when showing the positions of soft atoms as shown in [Fig. 47](#), they did find that the distribution of soft atoms in the less stable amorphous system is more heterogeneous than in the relatively stable one.

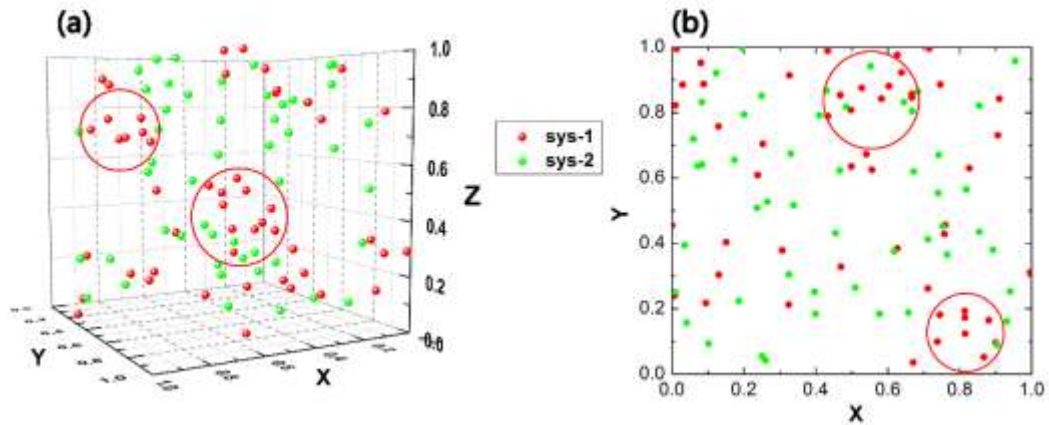


**Fig. 47.** The positions of the atoms with the lowest 2.5% shear modulus [269], in 3D display (a), and 2D projection in  $X$ - $Y$  plane (b). Atoms in red are for system I, and atoms in green are for system II. Reprinted figures with permission from reference [269], copyright (2014) by the American Physical Society.

According to Fan et al., this leads to the quite different distribution of local coarse grained shear modulus other than that of the single atom shear modulus in the amorphous systems (see **Fig. 48**). In other words, the results in **Fig. 46-48** indicate that the evolution of atomic-level elastic modulus in amorphous systems is intrinsically related to the heterogeneous distribution of their soft atoms.

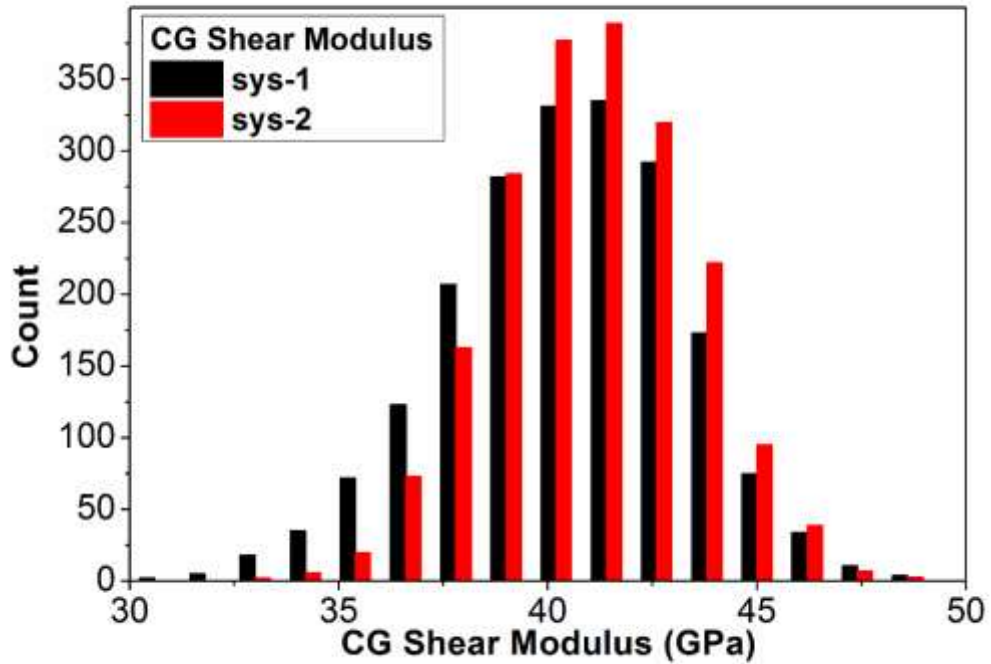


**Fig. 48.** The distribution of the first nearest neighbor coarse-grained (CG) shear modulus, in both systems [269]. Black bars are for system I, and red bars represent system II. Reprinted figures with permission from reference [269], copyright (2014) by the American Physical Society.

By using computational simulation combined with X-ray diffraction experiment, Li et al. [260] generated realistic three-dimensional atomistic structures of Zr-Cu metallic glasses. From the analysis of the medium-range order in amorphous systems with a cluster correlation method, they found that the glass systems consist of a string-like backbone icosahedral network and a liquid-like structure filling in the remaining space. A clear picture of the structural heterogeneity is thus presented for metallic glasses, which is associated with the strong and string-like correlations between the icosahedral  $\langle 0,0,12,0 \rangle$  clusters in the metallic glasses.

Peng et al [258] reported the structural geometry feature and size distribution of the local atomic rearrangements with external shear stress by molecular dynamics (MD) simulation for two-dimensional (2D) and three dimensional (3D) Lenard-Jones

(LJ) binary mixtures and 3D CuZr metallic glass in shear deformation. It was shown that the local atomic rearrangements are self-organized during shear deformation, taking into account that the structural geometry of the local atomic rearrangement exhibits fractal feature. Moreover, a universal scaling of size distribution of local atomic rearrangements is found to be in the form of the power-law distribution. Interestingly, however, it is generic and independent of the atomic potential or system size. In view of this, amorphous solids possess structural heterogeneity in nature.

Fujita et al [261] further employed a quantitative computational method as well as dynamic mechanical analysis (DMA) to investigate the cyclic shear deformation of a chemically heterogeneous  $\text{Cu}_{45}\text{Zr}_{45}\text{Ag}_{10}$  metallic glass. They found that cyclic deformation leads to the formation of irreversible STZs and a permanent uniform strain. The atomic heterogeneity of the metallic glass plays vital role in the initiation of STZs and the accumulated permanent strain has a linear relation with the number of STZs, as shown in **Fig. 49(a)** and **(b)**.

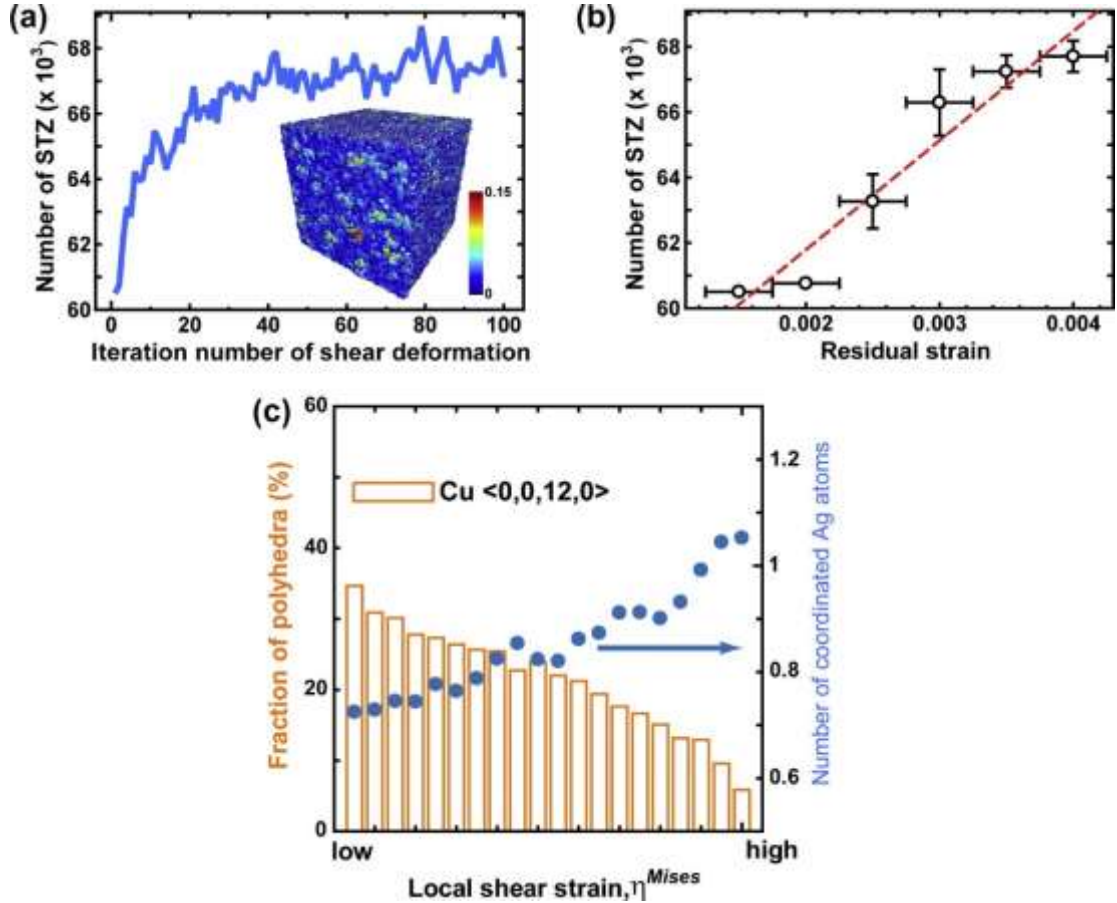


**Fig. 49.** (a) A plot of STZ number vs. the number of iteration cycles. (Inset) Three-dimensional map of local shear strain,  $\eta_{\text{von Mises}}$  after the one hundredth iteration. The local strain is indicated using the colored scale bar. (b) The relation between STZ number and residual strain. The dotted line represents a least squares fitting. (c) A local strain diagram of Cu atoms after the one hundredth iteration. The fraction of the icosahedral cluster and the average number of coordinated Ag atoms for Cu atoms are counted in 20 groups with different stains. From ref. [261]. Reprinted from reference [261], copyright (2012), with permission from Elsevier.

The authors examined the correlation between local strain and the inherent atomic structure of Cu-centered polyhedra coordinated with Ag atoms, i.e. full icosahedra with Voronoi index  $\langle 0, 0, 12, 0 \rangle$  (see Fig. 49(c)). It was therefore revealed that the Ag-depleted regions have stronger shear resistance, whereas the Ag-rich regions yield larger local strains. These results indicate that the heterogeneous Ag distribution intrinsically affects the formation of STZs: Ag-rich regions with looser atomic packing have weaker shear resistance to the initiation of STZs.

On the other hand, it is also recognized that dynamical heterogeneity, being intrinsic to metallic glasses, is definitely a nontrivial factor for the establishment of their sophisticated structure-property relations. In a recent extensive molecular dynamics simulation work by Hu et al [210], a combination of isoconfigurational ensemble and atomic pinning methods is applied to distinguish and characterize the heterogeneity at the atomic level in metallic glasses. According to the distinctive atomic-level responsiveness and mechanical performance, they well distinguished flow units from the elastic matrix in metallic glasses. As demonstrated in **Fig. 50**, after yielding, there is a significant variability in the spatial distribution of the non-affine deformation regions in the studied Cu-Zr metallic glasses when compared to their initial configuration. This indicates that the emergence of the non-affine deformation regions in the elastic regime is an intrinsic response in metallic glasses. Through a more detailed analysis of atomic position, they further revealed the microscopic features of the flow units, such as the shape, spatial distribution dimensionality, and correlation length.

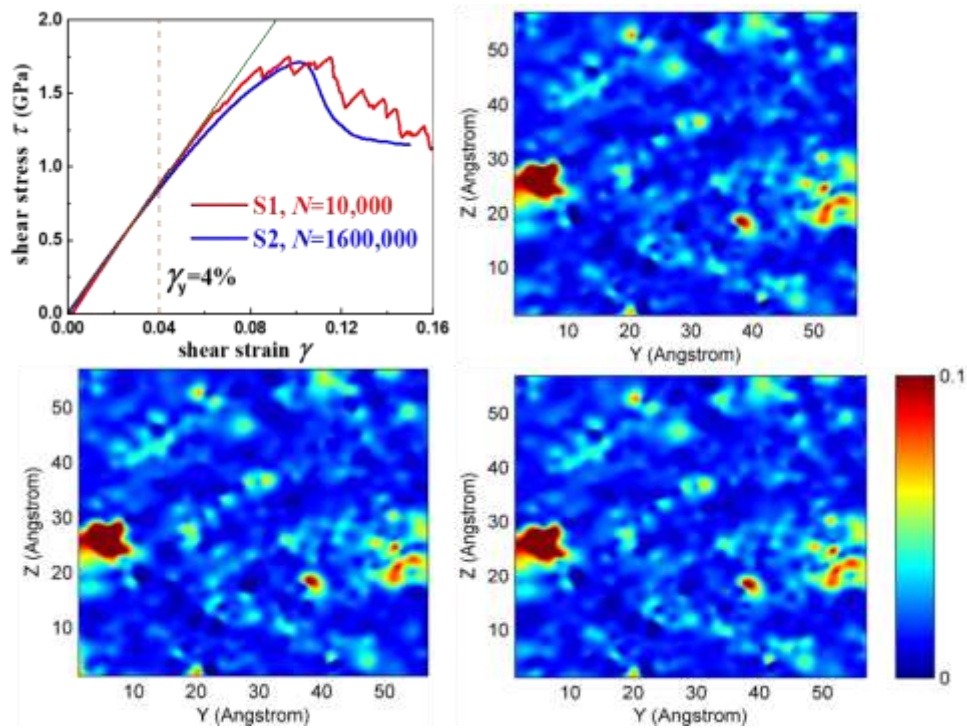


**Fig. 50.** (a) Shear stress-strain curves of  $\text{Cu}_{50}\text{Zr}_{50}$  amorphous alloy for S1 and S2 at 1 K with strain rate  $1.0 \times 10^8 \text{ s}^{-1}$  [210]. The yielding strain is about 4%. (b)–(d) Contour maps of the same slice ( $5^\circ\text{A}, \sim 2d\text{Cu}$ ) from three independent shear runs to the yielding point (4%) in S1. The color scale represents the atomic non-affine displacement. Reprinted figures with permission from reference [210], copyright (2016) by the American Physical Society.

Using molecular dynamics simulation, Sun et al [256] investigated the correlation of dynamic properties of amorphous solids to their dynamical heterogeneity. They reported that atomic interaction stiffness plays an effective role on low- $T$  relaxation in amorphous solids. As the atomic interaction stiffness increases, amorphous solids including metallic glasses exhibit more pronounced low- $T$  relaxations due to the enhancement of both atomic mobility and dynamical heterogeneity (see **Fig. 51**).

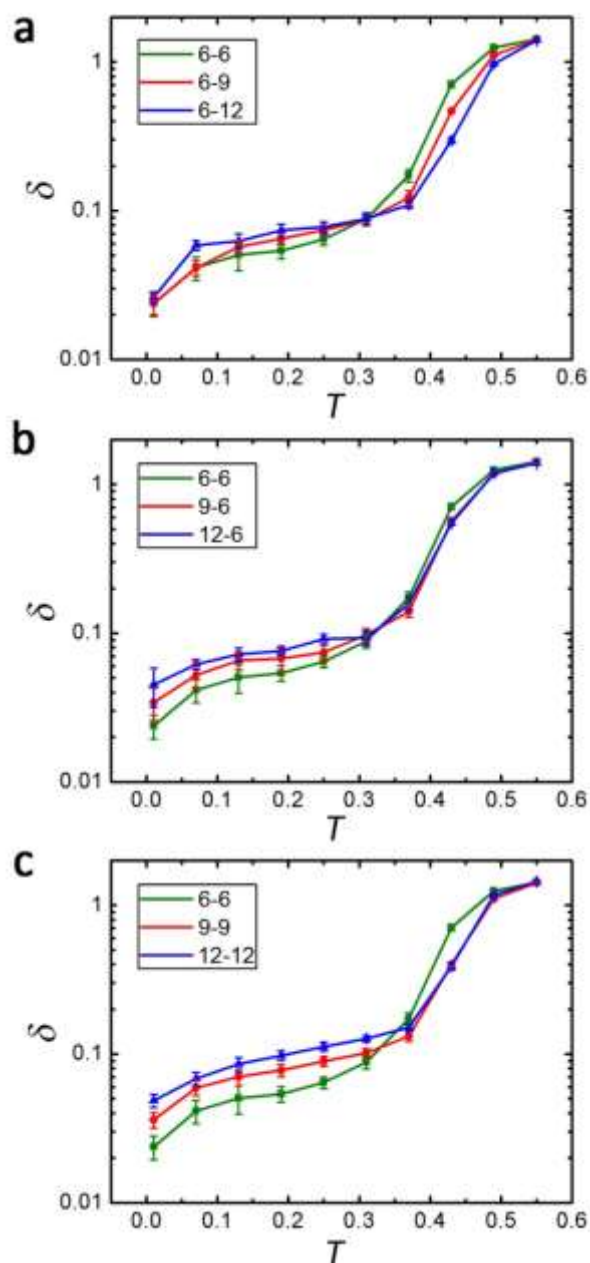


**Fig. 51.** The internal friction measured by MD-DMA [256]. (a)-(c) The internal frictions for models with different attractive interactions, repulsive interactions and both attractive and repulsive interactions, respectively. Low-temperature relaxation dynamics is enhanced with the increase of interaction stiffness. Published with permission of Royal Society of Chemistry, from reference [256], copyright (2016). Permission conveyed through Copyright Clearance Center, Inc.

In addition, Fujita et al [312] performed extensive dynamical molecular

simulations with embedded atom method (EAM) and found an intrinsic correlation between the dynamical heterogeneity, atomic structure and chemistry in a  $\text{Cu}_{45}\text{Zr}_{45}\text{Ag}_{10}$  bulk glass forming supercooled metallic liquid. They observed a strong coupling between dynamic heterogeneities and chemical short range order. The intrinsic correlation between the dynamics, atomic structure and chemistry for the  $\text{Cu}_{45}\text{Zr}_{45}\text{Ag}_{10}$  amorphous alloy is found to be associated with significant spatial partitioning and dynamic isolation between Cu-rich slow-dynamics regions and Ag-rich fast-dynamics regions.

As can be seen in **Fig. 52(a)**, a three-dimensional (3D) displacement map with dimensions of  $53 \times 53 \times 53 \text{ \AA}^3$  visualizes the isosurfaces of slow-dynamic regions with  $\Delta r^2$  being less than  $25 \text{ \AA}^2$  and fast-dynamics regions with  $\Delta r^2$  being greater than  $80 \text{ \AA}^2$ . The slow- and fast-dynamics regions, corresponding to Ag-poor and Ag-rich regions, respectively, appear to be partitioned from each other. **Fig. 52 (b)** illustrates both isosurfaces of slow dynamics regions and Ag atoms, which further confirms the correlation between dynamic heterogeneity and chemical inhomogeneity. Furthermore, this can be used to explain the improved glass-forming ability with Ag addition by retarding crystallization kinetics. It is suggested that since both slow- and fast-dynamics regions are much smaller than the critical size of crystallites, the spatial partitioning and dynamic isolation caused by the coupling may significantly retard the kinetics of crystallization of the supercooled liquid and leads to improved glass forming ability.

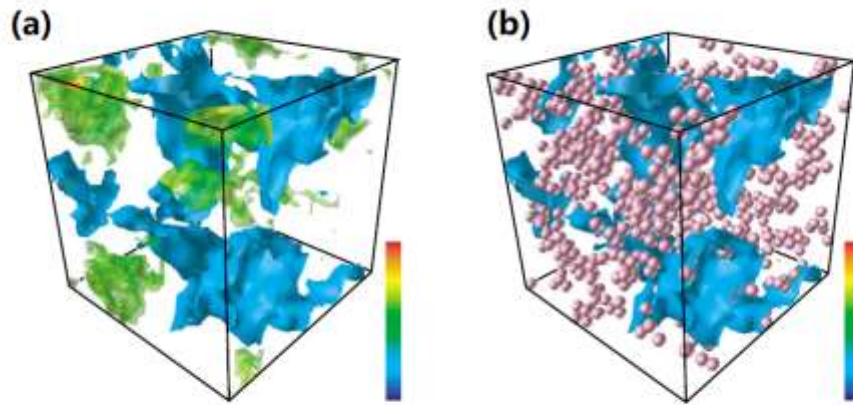


**Fig. 52.** Correlation between atomic mobility of Cu atoms and their local structural environments in  $\text{Cu}_{45}\text{Zr}_{45}\text{Ag}_{10}$  amorphous alloy at 800K [312]. The Cu atoms are sorted into 20 groups in the increasing order of their displacement. In each group, the percentage of  $\langle 0,0,12,0 \rangle$  polyhedra and the number of coordinated Ag atoms are plotted with **(a)** 3D mean-square displacement map of all atoms based on propensity motion for a long time interval of  $1.5t_\alpha$ . The isosurfaces indicate the slow- and fast-dynamics regions where  $\Delta r^2$  is less than  $25 \text{ \AA}^2$  (blue regions) and more than  $80 \text{ \AA}^2$  (green to red regions), respectively. **(b)** 3D map showing both isosurfaces of slow-dynamics regions and distribution of Ag atoms (balls). The slow-dynamics regions are apparently Ag-poor regions. The cube has the dimensions of  $53 \times 53 \times 53 \text{ \AA}^3$ ; the color bars shown in **(a)** and **(b)** show the range from fast (top) to slow (bottom) dynamics. Reprinted figures with permission from reference [312], copyright (2010) by the American Physical Society.

## 4. Theoretical understanding of structural heterogeneity and relaxation dynamics in amorphous alloys

### 4.1. Physical origin of structural heterogeneity

Over the past decades, the concept of structural heterogeneity has been playing a key role in different theories attempting to understand the origin of relaxation dynamics and glass transition in various glass-forming liquids [313, 314]. Notably, some of these theories and models, including the random first order transition theory (RFOT) [314], the twinkling fractal theory [49], the two-order parameter theory [47, 58, 315] and some others [11, 39, 316-318], were further extended to understand the physical and mechanical properties of the corresponding glasses [319-321]. In general, structural heterogeneity is conceived to be the characteristics of a supercooled liquid and also to be the origin for the dramatic slow-down of liquid dynamics and thus glass transition. The evolution of structural heterogeneities then gives rise to the transition of the relaxation time of a supercooled liquid from an exponential to a stretched exponential function or the well-known Vogel-Fulcher-Tammann function (VFT) [322]. Because of rapid quenching, the heterogeneous structure in glass then appears as a frozen-in structural feature inherited mainly from an equilibrium liquid at a high temperature. In this section, we would like to have a brief overview of some of these theories, particularly the RFOT theory [41, 44] and the two-order parameter theory [46, 315], in the context of amorphous metals.

In the same spirit of the Adam Gibbs theory [40], it is considered in the RFOT theory that a liquid is inherently heterogeneous because of the thermodynamic gain brought about by the increase of the configurational entropy of the whole system [44]. Compared to a homogeneous liquid as seen in [Fig. 53\(a\)](#), the addition of a liquid droplet configurationally different from the previous homogeneous liquid results in an increase of the system configurational entropy,  $TS_c$ , where  $T$  stands for the temperature while  $S_c$  the average configurational entropy gain. However, the presence

of a liquid droplet also raises the energy because of the surface energy  $\sigma_{\text{surf}}$ . Minimizing the free energy of the heterogeneous liquid gives a critical length scale  $\xi = \left(\frac{\sigma_{\text{surf}}}{TS_c}\right)^{\frac{1}{d-\theta}}$  [44], where  $d$  = the regular dimension with 2 for a plane and 3 for a space and  $\theta$  = the surface fractal dimension of the liquid droplet. In sharp contrast to the conventional first order transition theory, the liquid droplet cannot grow above  $\xi$  in size but appears and disappears randomly in a manner akin to thermal fluctuation [44]. With the decreasing temperature and hence the increasing length scale  $\xi$ , the liquid droplets start to populate the heterogeneous liquid, thereby forming a “mosaic” as illustrated in Fig. 53(b).

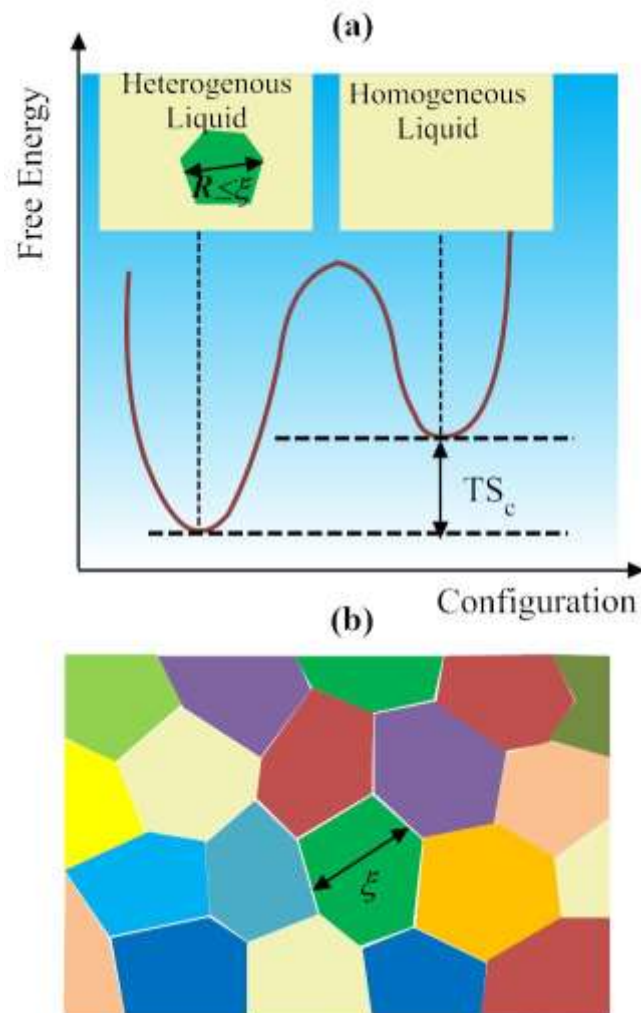


**Fig. 53.** The schematics of (a) the free energy of homogenous liquid versus

heterogeneous liquid containing a liquid droplet with size  $R$  and (b) the mosaic composed of numerous liquid droplets.

From the perspective of relaxation dynamics, this liquid droplet behaves like the cooperative rearranging region (CRR) in the Adam Gibbs theory [40]. Moreover, it was estimated that the size of the liquid droplet be roughly 100 atoms or molecules at the conventionally defined glass transition temperature according to the RFOT theory [41-43]. Interestingly, this is somewhat consistent with the estimated size of shear transformation events in the cooperative shear model (CSM) developed by Johnson and Samwer for amorphous metals [323]. Based on the “mosaic” picture, the RFOT theory was further developed and used to study glass transition, stress relaxation, fragility, yielding in supercooled liquids and glass [41, 43]. Recently, through extensive atomistic simulations and theoretical analyses, Hu et al.[82] demonstrated that the dramatic slow-down of the dynamics in a  $Zr_{50}Cu_{50}$  metallic liquid is due to the growth of local iso-configurational regions, conforming to the picture of a heterogeneous supercooled liquid in the RFOT theory. Here, it is worth mentioning that the structural heterogeneity in metallic liquids is not only predicted through theories and simulations but also observed in the recent experiments[324]. As seen in **Fig. 54** [324], Zhang et al. reported the direct experimental visualization of the spatially heterogeneous dynamics in the Pt-based supercooled metallic liquid using electron correlation microscopy. The dynamics can be characterized by a growing length and time scale as the liquid cools toward the glass transition, which is consistent with the thermodynamic theory of glass transition.

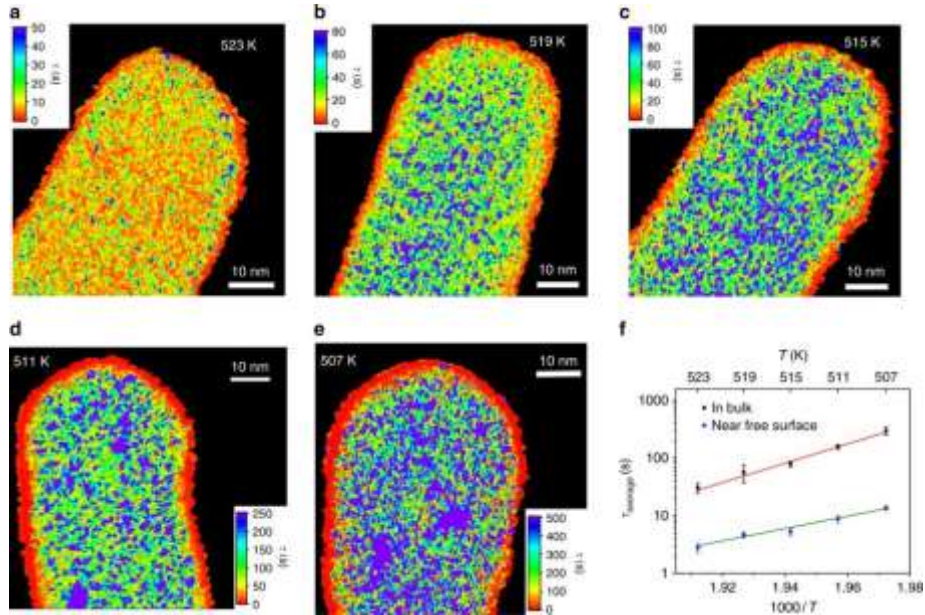


**Fig. 54.** Spatial maps of structural relaxation time on the nanowire in the supercooled liquid regime[324]. (a)  $T=523$  K, (b)  $T=519$  K, (c)  $T=515$  K, (d)  $T=511$  K, (e)  $T=507$  K. The maps show domains with varying relaxation time at the nanometer scale. With decreasing temperature, slow domains appear larger and occupy a greater fraction of the map, especially very close to  $T_g = 507$  K. There is a region  $\sim 1$  nm thick with  $\sim 20$  times shorter relaxation time near the surface of every wire. (f) The mean structural relaxation time for the nanowire interior (bulk) and the near-surface layer. The error bars are the standard deviation of the mean of four measurements on different nanowires. Fitting to the Arrhenius form yields activation energies of  $3.7 \pm 0.3$  eV for the bulk and  $1.7 \pm 0.3$  eV for the near-surface. Reprinted by permission from Macmillan Publishers Ltd: Nature Communications, reference[324], copyright (2018).

On the other hand, the two-order-parameter model proposed by Tanaka[315] pictures a supercooled liquid as a dynamically heterogeneous state composed of metastable solid-like islands below a transition temperature. Supercooling causes the liquid to transit from an ordinary liquid to a frustrated metastable liquid, which is populated with localized domains exchanging with each other dynamically at the rate of the structural ( $\alpha$ ) relaxation time. From the microstructural viewpoint, the formation of such a frustrated metastable liquid state can be attributed to the result of the competition between a long-range density (crystal-like) order and a short-range orientational order, which alternate and form a heterogeneous liquid structure, as

schematically depicted in **Fig. 55**. Such an alternating heterogeneous structure was observed recently in the  $Zr_{53}Cu_{36}Al_{11}$  amorphous alloy by Zhu et al. [20].

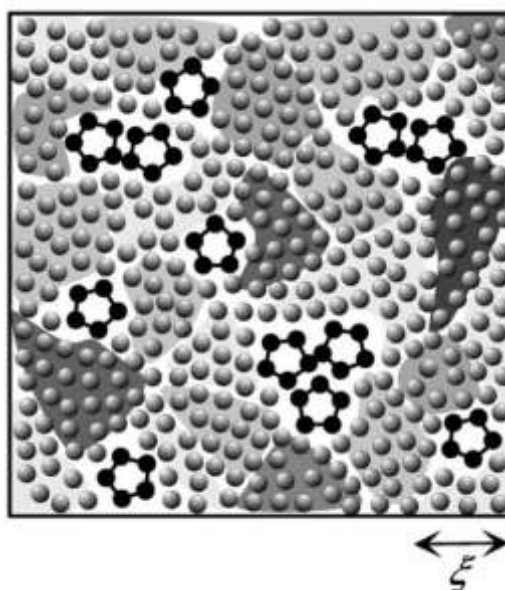


**Fig. 55.** Schematic figure of a supercooled liquid state. The black pentagons represent locally favored structures. Molecules belonging to normal-liquid structures are represented by gray spheres. A shaded region represents a metastable island with various degrees of crystal-like order, whose characteristic coherence length is  $n$ . The darker the color is, the higher the crystal-like order is and the higher the local density is. Note that the lifetime of metastable islands determines the structural relaxation [315]. From ref. [315]. Reprinted from reference [315], copyright (2017), with permission from Elsevier.

#### 4.2. Understanding relaxation dynamics from the perspective of defects

As we discussed in the chapter 2, the main relaxation mode in glasses is  $\beta$  relaxation [177, 325, 326], which is related to localized motions of some cooperative nature [83] and could be universal among all kinds of glasses. Since  $\beta$  relaxation is present in both a supercooled liquid and glass state, it affects the mechanical properties of glassy materials [13]. In general,  $\beta$  relaxation in glasses (i.e. amorphous polymers, oxide and metallic glasses) is dependent on cooling rate [188], chemical composition [177, 327, 328], pressure [329] and physical aging [180, 184],

which can be theoretically related to structural heterogeneity according to the RFOT theory [41, 42, 314] and two order-parameter theory [31, 315].

A non-crystalline structure is characterized by the excess Gibbs free energy as compared with the crystalline ground state. This excess energy quantifies the driving force for spontaneous atomic rearrangements, usually referred to as physical aging. Based on different theoretical models, physical aging below the glass transition temperature  $T_g$  induces a reduction of the “defects”, i.e. excess free volume [330], flow units [55], quasi-point defects [209], interstitial defects [331].

In general, one may argue that physical aging reduces the energy of low density atomic configurations by improving their local atomic packing. Or structural relaxation reduces the excess “free volume” and, in this way, may alter the structural heterogeneity of the glass. The quantitative analysis was carried out for polymers in Ref. [332], where it was proposed that  $\eta=A\exp[(BV_0)/V_f]$ , where  $V_f$  is the “free volume” per unit mass and  $V_0$  is the volume per unit mass. This idea conforms to the “free volume model” by Spaepen et al. [207]. By combining the classic free volume model and the notion of structural heterogeneity, which can lead to a generalized Maxwell model, the free volume model was further developed by Huang et al. [153] to reveal the connection of the boson peak and  $\beta$  relaxation near  $T_g$  in the La-based metallic glass. The  $\beta$  relaxation was therefore regarded as a series of localized flows in soft regions with different amount of free volume, being dispersed in an elastic amorphous matrix [153, 333].

Different from free volume, flow units can be regarded as nanoscale regions which correspond to pseudo “defects” in metallic glasses. The nanoscale flow units have lower elastic moduli, higher energy state, and lower hardness than the homogenous elastic matrix[334]. The flow unit model was built based on the concept of structural heterogeneity and the concentration of flow units can be correlated with various overall properties of metallic glass, such as density, elastic constants, recovered enthalpy and fictive temperature. In addition, the evolution of flow units,

which is linked to the structural heterogeneity of metallic glass, can be described by the density change during thermal annealing below the glass transition temperature  $T_g$  [155, 335, 336]. On the basis of the flow unit model, an empirical function for the time dependence of the physical properties of annealed metallic glass is given as follows [335-338] (as seen in **Fig. 56**):

$$M(t) = \frac{M_\infty}{1+c} \quad (4-1)$$

where  $t$  is the aging time, and  $M(t)$  is either enthalpy [338], density [155, 335, 336], shear modulus [337, 339], Young's modulus [337], plastic deformation strain [340] or hardness [337] and  $M_\infty$  is its asymptotic value which corresponds to the property of an "ideal" metallic glass [334]. The parameter  $c = [a/(b + t)]^{\beta_{KWW}}$  is related to the concentration of flow units, in which  $a$  and  $b$  are both constants at a given aging temperature. It was found that when  $t = 0$ ,  $c = [a/b]^{\beta_{KWW}}$ , which corresponds to the initial concentration of flow units in the as-cast state [336].

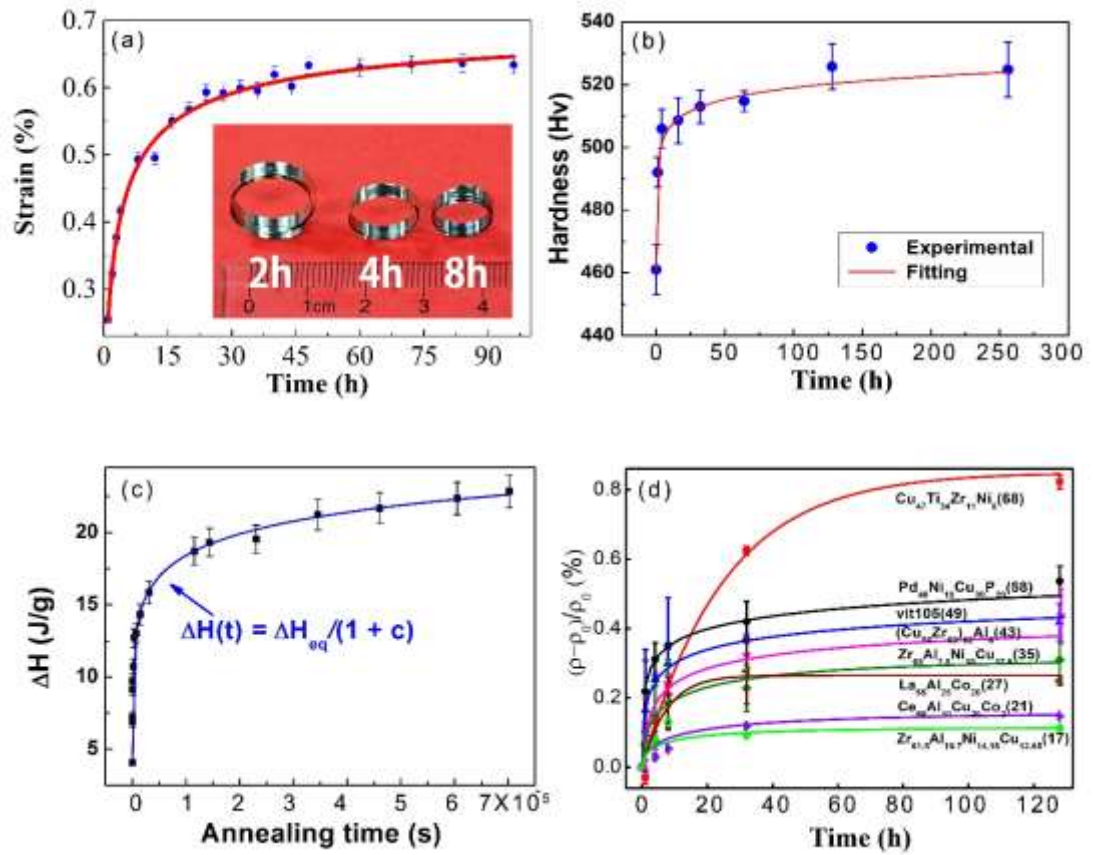


**Fig. 56.** Variation of the structural heterogeneity of metallic glasses with aging time based on the flow units model. **(a)** Change of  $\text{La}_{75}\text{Ni}_{7.5}\text{Al}_{16}\text{Co}_{1.5}$  amorphous alloy was found and held for different time [340]. Reprinted figures with permission from reference[340], copyright (2014) by the American Physical Society. **(b)** Change of Vickers micro-hardness of  $\text{Zr}_{52.5}\text{Cu}_{17.9}\text{Ni}_{14.6}\text{Al}_{10}\text{Ti}_5$  amorphous alloy with annealing time at 600 K [337]. Reprinted from reference [337], with the permission of AIP Publishing. **(c)** Enthalpy change after isothermal annealing of  $\text{Zr}_{52.5}\text{Cu}_{17.9}\text{Ni}_{14.6}\text{Al}_{10}\text{Ti}_5$  amorphous alloy at 600 K [338]. Reprinted from reference [338], with the permission of AIP Publishing. **(d)** Relative density variation of metallic glasses [336]. Reprinted from ref. [336], copyright (2017), with permission from Elsevier.

**Fig.57** shows the stretching exponent  $\beta_{KWW}$  as a function of temperature in a typical  $\text{La}_{60}\text{Ni}_{15}\text{Al}_{25}$  metallic glass, obtained by fitting stress relaxation experiments [341]. It should be noted that, with the increasing annealing temperature  $T_a$ , the parameter  $\beta_{KWW}$  value increases, indicating a more homogeneous structure at higher temperature. The Kohlrausch exponent  $\beta_{KWW}$  lower than 1 reflects a broad

distribution of relaxation time instead of a single Debye relaxation time. Hodge [342] interpreted the nonexponentiality to be a consequence of cooperativity of the rearranged structural units. Böhmer et al. [85] reviewed the non-exponential relaxations in around 70 strong and fragile glass formers. Several of experimental methods were employed to determine the Kohlrausch exponent  $\beta_{KWW}$ . The adopted methods include dielectric and specific heat spectroscopy [343, 344], viscoelastic modulus measurements in the shear and tensile modes as well as shear compliance investigations [345], quasi-elastic light scattering experiments [346], mechanical spectroscopy [134, 148, 189] and stress relaxation [95, 119, 181, 347-349].

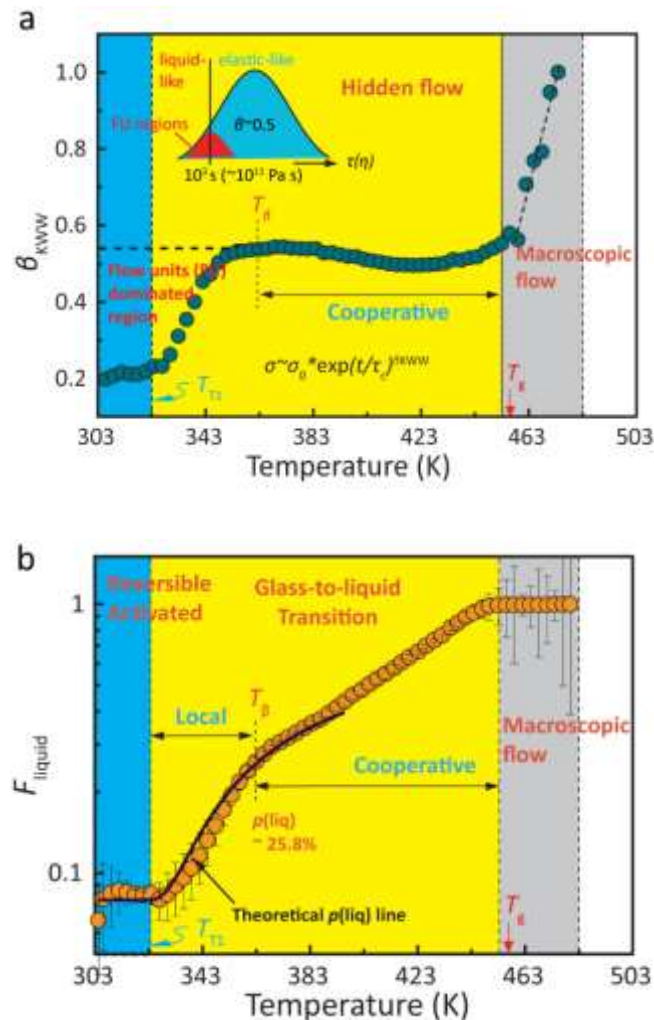


**Fig. 57.** (a) Evolution of  $\beta_{KWW}$  values (dark green circles) of  $\text{La}_{60}\text{Ni}_{15}\text{Al}_{25}$  metallic glass based on fitting from stress relaxation experiments at different temperatures [95].

(b) Evolution path of fraction of liquid-like zones  $F_{liquid}$  (orange circles) with increasing temperature [95]. Reprinted by permission from Nature Communications [95], copyright (2014).

It is well documented that the parameter  $\beta_{KWW}$  is connected with the dynamic heterogeneity: the lower the Kohlrausch exponent  $\beta_{KWW}$ , the wider the dynamic heterogeneity distribution of the glassy materials. Based on the stress relaxation of typical  $\text{La}_{60}\text{Ni}_{15}\text{Al}_{25}$  amorphous alloy (as shown in Fig. 57(a)), Wang et al. [95] reported that there are three different stages on the evolution of the Kohlrausch exponent  $\beta_{KWW}$ : (1) the parameter  $\beta_{KWW}$  remains around 0.2, which corresponds to the heterogeneous activation of flow units during the deformation process. (2) When the temperature surpasses the  $\beta$  relaxation temperature and below the glass transition temperature  $T_g$ , the parameter  $\beta_{KWW}$  keeps to be around 0.5. It is suggested that many flow units start to move in a cooperative mode at this stage. (3) When the temperature is above  $T_g$ , the amorphous alloy enters a homogeneous deformation process and behaves as a Newtonian viscous flow which is associated with the cooperative motions of atoms. In this temperature domain, the Kohlrausch exponent  $\beta_{KWW}$  increases dramatically. The evolution of the fraction of liquid-like zones  $F_{liquid}$  with temperature exhibits a similar tendency to the Kohlrausch exponent  $\beta_{KWW}$  (as shown in Fig. 57(b)).

The parameter  $\beta_{KWW}$  in the KWW equation is also associated with the fragility of the amorphous materials. The value of  $\beta_{KWW}$  close to 1 indicates that the system is likely to be a strong glass former; if the value is less than 0.5, it means that the glass could be fragile [350, 351]. Although the KWW exponent is generally perceived to be linked with fragility [350, 351], however, similar values (~0.5) of the KWW exponent were reported for amorphous alloys with different fragility. Therefore, it is still an open issue for the correlation of structural heterogeneity and the KWW exponent of amorphous alloys. The stretching parameter  $\beta_{KWW}$  can be dependent on or independent of the temperature of metallic glasses [155, 195, 352, 353]. A

computational simulation on the  $\text{Cu}_{50}\text{Ti}_{50}$  metallic glass indicates that the Kohlrausch exponent  $\beta_{KWW}$  is close to 0.50 around the glass transition temperature  $T_g$  [271]. Researchers proposed that  $\beta_{KWW}$  is almost independent of the temperature with a given distribution of the local relaxation times. In the same spirit of a flow defect model, the interstitialcy theory was originally proposed by Granato in 1992 [51] and more recently modified [354]. The only point defects available by thermal activation in simple crystals are vacancies and interstitials. While the structure and properties of vacancies are relatively straightforward, it is not the case for interstitials. Before the 1970-s, it was envisioned that interstitials occupy the octahedral cavity in the FCC structure. Currently, it is widely accepted that interstitials reside in a split configuration and sharing a lattice site with another atom. Examples of these split (or dumbbell) interstitials, termed also interstitialcies, are given in **Fig. 58(a-c)** for different crystalline lattices.

The dumbbell structure of dumbbell interstitials has far-reaching consequences. These defects are sensible to the applied shear stress, which brings string-like motions of 10-20 atoms near the defect nuclei, as exemplified by **Fig. 58(d)**. This motion leads to a strong inelastic decrease of the shear modulus, as shown by Granato and co-workers experimentally in the middle of the 70s. They studied the effect of copper to the ppm defect concentration range and noticed that if the shear softening is extrapolated towards large concentrations, an interstitial concentration of 2~3 % should lead to zero shear modulus. Meanwhile, vanishing shear modulus is a signature of liquids. Thus, Granato came to a hypothesis that melting can be related to the generation of dumbbell interstitials. Vacancies do not produce such a big shear softening effect.

The second major feature of dumbbell interstitials is the presence of low frequency modes (several times smaller than the Debye frequency) in their vibration spectrum, as found theoretically and confirmed by experiments. These low frequency modes are related to the aforementioned string-like atomic motion (**Fig. 58(d)**) and

lead to a large interstitial formation entropy  $S_i$  (about 10-20 in the units of the Boltzmann constant  $k_B$ ), which is by an order of magnitude higher than the formation entropy of vacancies. Granato showed that if melting occurs through the generation of interstitials for a few percents, the interstitial formation entropy can explain the observed heat of melting. This is not the case for vacancies.

The facts and ideas sketched above led to the interstitialcy theory [51]. He assumed that the change of internal energy  $U$  of a crystal upon an increase of interstitial defect concentration by  $dc_i$  can be written as:

$$\frac{dU}{dc_i} = \alpha_1 G(c_i) \Omega + \alpha_2 B \Omega \quad (4-2)$$

where  $G$  is the unrelaxed (instantaneous) shear modulus dependent on the defect concentration  $c_i$ ,  $B$  is the bulk modulus (largely insensitive to  $c_i$ ),  $\alpha_1$  and  $\alpha_2$  are dimensionless constants and  $\Omega$  is the volume per atom. Granato showed that  $\alpha_1 \approx 1 \gg \alpha_2$ , therefore the shear energy  $\alpha_1 G \Omega$  in Eq. (4-2) is much bigger than the dilatation energy  $\alpha_2 B \Omega$  [72]. Based on Eq. (4-2), the formation enthalpy for a single interstitialcy becomes:

$$H = \alpha G \Omega \quad (4-3)$$

where  $\alpha = \alpha_1$ . On the other hand, the concentration-dependent shear modulus can be derived as:

$$G = G_0 \exp(-\alpha \beta c_i), \quad (4-4)$$

where  $\alpha = \frac{1}{G \Omega} \frac{dU}{dc_i}$  is the same as in Eq.(4-3),  $G_0$  is the shear modulus of the

defectless crystal (i.e. corresponding to  $c_i = 0$ ) and the dimensionless shear susceptibility  $\beta = -\frac{1}{4G} \frac{\partial^2 G}{\partial \varepsilon^2}$  ( $\varepsilon$  is the applied shear strain) is directly related to the anharmonicity of the interatomic potential.

Depending on the temperature and defect concentration, the interstitialcy theory predicts equilibrium and metastable crystalline and liquid states. Although “interstitialcy defects” in the liquid do not have any clear topological pattern, they nonetheless remain identifiable structural units retaining the properties of dumbbell interstitials in the maternal crystal [355]. An important role of split interstitials in melting was mentioned in the literature [356, 357]. Recently rapid interstitialcy multiplication upon approaching  $T_m$  was supported by precise measurements of the shear modulus of pure aluminium and indium [358]. On the other hand, a large  $c_i$  near  $T_m$  should provide an additional contribution to the heat capacity  $C_p$ . It was recently shown [359] that this contribution in Al is observed as non-linear  $C_p$ -growth, which is common in metals but remains unexplained so far.

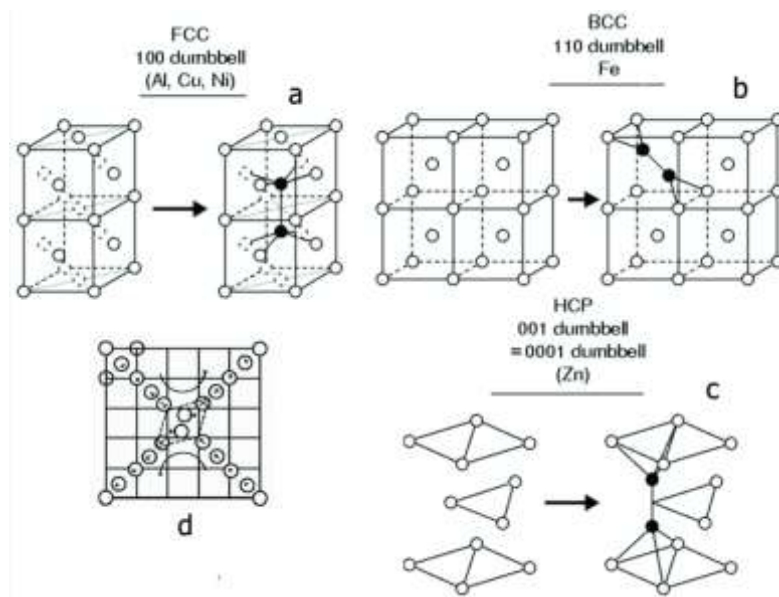


**Fig. 58.** Dumbbell (split) interstitials (interstitialcies) in different crystalline structures (a)–(c). (d) Schematic representation of string-like motion around the interstitialcy [360]. Reprinted From reference [360], Copyright © the Chinese Physical Society (2017), with permission from the Chinese Physical Society.

The interstitialcy theory provides quantitative explanations for quite a few important properties of equilibrium and supercooled liquids. First of all, the high formation entropy of interstitialcy defects explains the entropy of melting [361], which is known to be  $\approx 1.2k_B$  for all the elemental substances over the periodic table with only a few exceptions (so-called Richards rule). The interstitialcy theory allows derivation of the empirical Lindemann melting rule ( $\alpha T_m = \text{const}$ , where  $\alpha$  is the crystal thermal expansion coefficient), as well as the correlation between the melting temperature and shear modulus for elemental substances [51, 362]. The interstitialcy theory assumes that the liquid contains a few percent of interstitialcy defects. It provides interpretation of heat capacities of supercooled and equilibrium liquids [363], Vogel–Fulcher–Tammann (VFT) relation for the viscosity of supercooled liquids [364] as well as the fragility of liquid and its relation to the heat capacity jump at the glass transition [361, 363].

If “interstitialcy defects” remain to be identifiable structural units in the liquid state, it is reasonable to assume that they become frozen in the solid glass produced by melt quenching. Computational modelling shows that these “defects”, like in the liquid, do not have clear geometrical pattern but display the characteristic of dumbbell interstitials in crystalline metals, i.e. strong sensitivity to the external shear stress, distinctive local shear strain fields and characteristic low- and high-frequency modes in the vibration spectra of atoms [365]. Structural relaxation of glass can then be regarded as a change of concentration of these interstitialcy-type “defects”, which inherit the properties of maternal crystal. Eq.(4-4) should be then rewritten as:

$$G = \mu \exp(-\alpha\beta c) \quad (4-5)$$

where  $G$  is the unrelaxed shear modulus of glass,  $\mu$  is the shear modulus of the maternal crystal, which contain no interstitialcy-type “defects” (interstitialcy defects thereafter),  $c$  is the defect concentration,  $\beta$  represents the shear susceptibility and the dimensionless  $\alpha \approx 1$  is related to the strain field created by the defect. The defect formation enthalpy retains the form given by Eq. (4-3). Eqs. (4-3) and (4-5) constitute the basic assumptions of the interstitialcy theory for the glassy state. These equations provide explanations for some important phenomena in amorphous alloys occurring upon structural relaxation and crystallization.

The shear modulus  $G$  of as-cast metallic glass is reduced by 20% to 40 % with respect to the shear modulus  $\mu$  of the maternal crystal. Thus, by using Eq. (4-5) with a typical  $\beta = 20$  and accepting  $\alpha \sim 1$ , the concentration of frozen-in interstitialcy defects is 1.1% to 2.6%.

Isothermal structural relaxation of metallic glasses in the initial state leads to an increase of the shear modulus, and results from a decrease of the defect concentration, according to Eq. (4-5). The calculation gives a logarithmic increase of  $G$  with time [366], which is known as the “ln-time” kinetics for different properties of metallic glasses. By comparison, non-isothermal heat treatment of metallic glasses can lead to a change of the shear modulus depending on the applied thermal protocol. The relaxation kinetics can be reasonably reproduced within the framework of the interstitialcy theory [367]. Measurements of the shear modulus together with differential scanning calorimetry allow independent reconstruction of the underlying activation energy spectrum of structural relaxation. An example of such reconstruction is given in **Fig. 59**, which shows activation energy spectra for a Zr-based metallic glass recovered from independent measurements of the shear modulus and calorimetry [368]. It is noted that both methods give practically the same result. Integration of the spectra over the activation energy causes a change of the

absolute defect concentration upon structural relaxation,  $\Delta c = \int n_0(E_0) dE_0$ . For the data shown in **Fig. 59**,  $\Delta c \approx 0.0023$ , other metallic glasses show a similar trend [368]. Thus, only about one tenth of frozen-in defects can be annealed out during structural relaxation. Further decrease of  $c$  down to zero is related to crystallization.

Any change of the interstitialcy defect concentration will lead to corresponding change of the shear modulus  $G$  in Eq. (4-5). On the other hand, a change of  $G$  varies the enthalpy of defect formation according to Eq. (4-3) and consequently changes the whole heat content of glass. It should be noted that all relaxation phenomena in glass are intrinsically related to heat release or heat absorption, depending on the sign of defect concentration change. This relation can be quantified using Eqs. (4-3) and (4-5), and an expression for the heat flow per unit mass can be obtained [369]:

$$W = \frac{\dot{T}}{\beta\rho} \left[ \frac{G}{\mu} \frac{d\mu}{dT} - \frac{dG}{dT} \right] \quad (4-6)$$

where  $\dot{T}$  is the heating rate,  $\rho$  is the density and other quantities are the same as above.

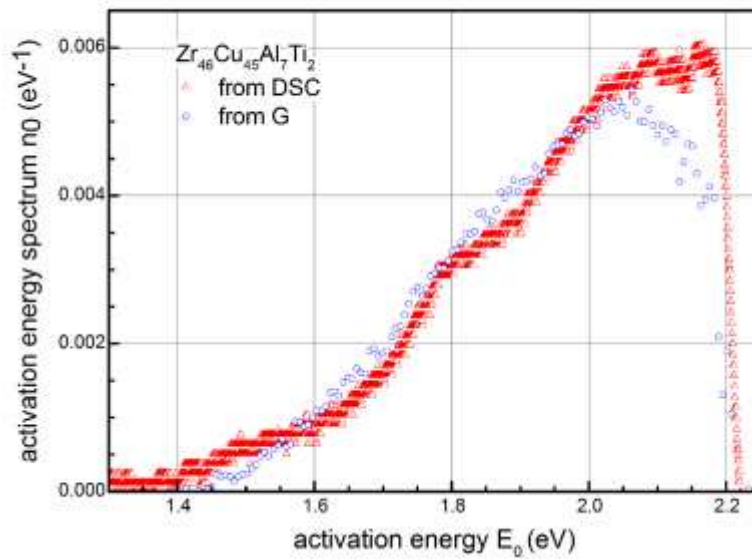


**Fig. 59.** Activation energy spectra of structural relaxation reconstructed from independent shear modulus and calorimetry data [368]. Reprinted from reference [368], copyright (2016), with permission from Elsevier.

Equation (4-6) shows that the heat flow depends on the shear moduli of glass and maternal crystal, which was benchmarked upon different metallic glasses. A representative example is given in **Fig. 60**, which shows differential scanning calorimetry trace taken on a Zr-based bulk glass together with calculation of the heat flow using Eq. (4-6) [370]. A good agreement between the theoretical predictions and experimental results is obtained. Eq. (4-6) not only describes exo- and endo-thermal heat flow in the glassy state but also precisely reproduces the heat release occurring upon crystallization. The latter fact leads to the assumption that the change of internal energy of glass upon crystallization is also controlled by the elastic energy of interstitialcy defects upon glass production. Since these defects disappear upon crystallization, their elastic energy is released with the heat of crystallization.

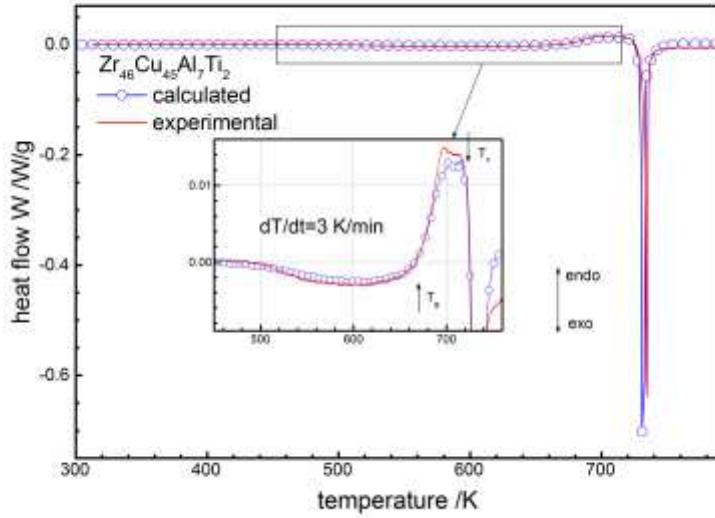


**Fig. 60.** Experimental DSC traces for  $Zr_{46}Cu_{45}Al_7Ti_2$  amorphous alloys and the heat flow calculated with Eq. (4-5) [370]. Reprinted by permission from Macmillan Publishers Ltd: Scientific Reports, reference[370], copyright (2016).

To verify the hypothesis, the difference between internal energies per unit mass of glass and maternal crystal within the framework can be defined as [371]:

$$\rho\Delta U = \frac{\mu}{\beta} \left[ 1 - \frac{G}{\mu} \right], \quad (4-7)$$

It is noted that the difference is governed by the shear moduli of glass and maternal crystal. Considering the shear modulus of glass just before and after crystallization, the change of internal energy should be equal to the heat of crystallization  $\rho Q_{cr}$ . The corresponding experiment was presented in ref. [371] and its main result is reproduced in **Fig. 61**, which shows  $\rho\Delta U$  calculated by using Eq. (4-7) as a function of  $\rho Q_{cr}$  for a number of Zr- and Pd-based glasses. The result falls on a straight line with the unity slope, which represents that the elastic energy of interstitialcy defects released upon crystallization is equal to the crystallization heat.

Thus, the heat content of glass with respect to the maternal crystal is mainly related to the elastic energy of frozen-in interstitialcy defects.

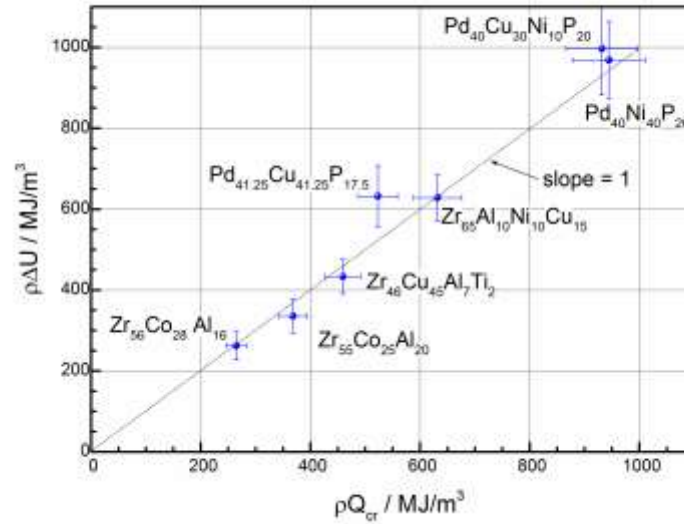


**Fig. 61.** Crystallization-induced change of the internal energy per unit volume  $\rho\Delta U$  as a function of the crystallization heat per unit volume  $\rho Q_{cr}$  for Pd- and Zr-based metallic glasses [371]. Reprinted from reference [371], copyright (2016), with permission from Elsevier.

The expected volume change  $\Delta V$  upon creation of an interstitialcy defect can be defined as  $\Delta V/\Omega = -1 + \alpha_i$ , where “-1” corresponds to the insertion of an interstitialcy defect,  $\alpha_i$  is the so-called relaxation volume, which reflects the relaxation of structure after defect creation and  $\Omega$  is the volume per atom [372]. If a defect concentration  $c$  is created, the volume increases by  $\Delta V$  and the relative volume change becomes  $\Delta V/V = (\alpha_i - 1)c$ . The defect concentration can be expressed by using Eq. (4-8), by assuming  $\Delta\rho/\rho = -\Delta V/V$ , the density change upon structural relaxation of glass is [373]:

$$\frac{\Delta\rho}{\rho} = \frac{\alpha_i - 1}{\alpha\beta} \ln \frac{G}{G_0} \quad (4-8)$$

where  $\alpha$  and  $\beta$  are the same as in Eq.(4-5),  $G_0$  and  $G$  are the shear moduli at the beginning and end of the relaxation, respectively. **Fig. 62** shows relative density change of a Pd-based glass as a function of  $\ln(G/G_0)$ . It is seen that the experimental points can be approximated by a straight line in agreement with Eq. (4-8). The angle coefficient of this dependence is found to be 0.037. Meanwhile, accepting the relaxation volume  $\alpha_i$  is equal to the averaged relaxation volume for split interstitials in crystalline FCC metals ( $\alpha_i \approx 1.6$ ), the shear susceptibility for this glass  $\beta = 17$  and  $\alpha \approx 1$ , Equation (4-19) gives the angle coefficient  $\frac{\alpha_i - 1}{\alpha\beta} = 0.035$ , which is practically equal to the experimental slope. Similar consideration can be applied to calculate the heat release upon structural relaxation-induced densification, which is consistent with the experimental observations [374].

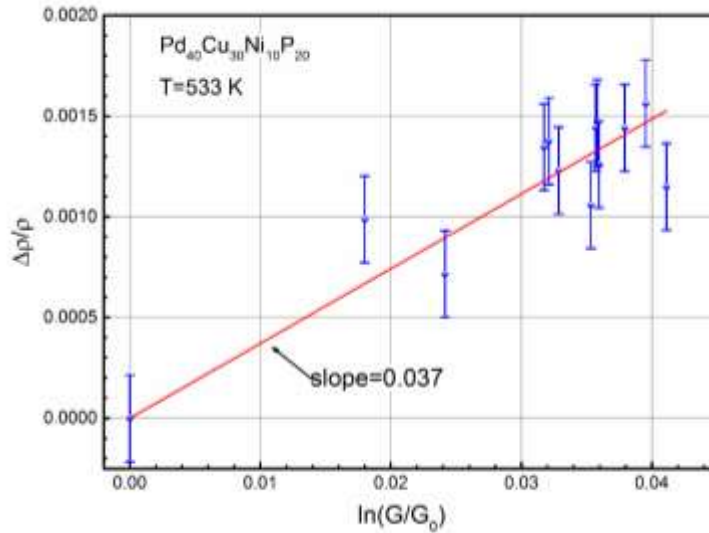


**Fig. 62.** Relative density change upon structural relaxation of the  $\text{Pd}_{40}\text{Cu}_{30}\text{Ni}_{10}\text{P}_{20}$

amorphous alloy as a function of  $\ln(G/G_0)$  [373]. Reprinted from reference [373], copyright (2017), with permission from Elsevier.

It should be noted that the effect of shear softening of glass (Eq. (4-5)), kinetics of heat release/absorption (Eq. (4-6)), the excess of the internal energy of glass (Eq. (4-7)), density change upon relaxation (Eq.(4-8)) and some other effects are strongly dependent on the shear susceptibility  $\beta$ . The definition of quantity (see the explanation for Eq.(4-16)) implies that  $\beta \neq 0$  only for the anharmonic interatomic potential since  $\partial^2 G / \partial \varepsilon^2 = 0$  for any harmonic potential. Therefore, all the aforementioned effects are intrinsically related to the anharmonicity of the interatomic potential and this is a major feature of glass. Meanwhile, the shear susceptibility is weakly dependent on glass chemical composition and varies in the range of  $15 \leq \beta \leq 21$  [375]. It appears that this quantity constitutes a universal integral parameter relating different physical phenomena including shear softening, heat effects and anharmonicity of interatomic interaction with the defect structure of metallic glasses [375]. Some other features of the interstitialcy theory and its applications to the interpretation of experimental data are reviewed in references [331, 360]. As discussed above this theory constitutes a comprehensive, internally consistent, verifiable and promising approach for understanding the defect structure or hence structural heterogeneity of metallic glasses.

In order to describe mechanical properties of amorphous materials with respect to its microstructure, Perez et al. proposed the quasi-point defect theory [209, 376, 377]. This theory assumes that glassy materials contain quasi-point defects, which correspond to fluctuations of enthalpy or entropy. The existence of quasi-point defects in the amorphous polymers has been confirmed by small angle X-ray scattering [378]. **Fig. 63(a)** shows the “defects” in an elementary volume of amorphous material. When an external mechanical stress is imposed on the structure, the stress resulting in the

maximum shear plane causes activation of these defects, which become polarized and bring the basic movements (as shown in Fig. 63(b)). The nucleation and growth from these sheared micro-domains (SMD) correspond to the onset of the inelastic response of the material (as seen in Fig. 63(c)). When this stress is applied for a longer time, new sheared micro-domains are nucleated (as shown in Fig. 63(d)). The plastic deformation is caused by coalescence of these SMD.

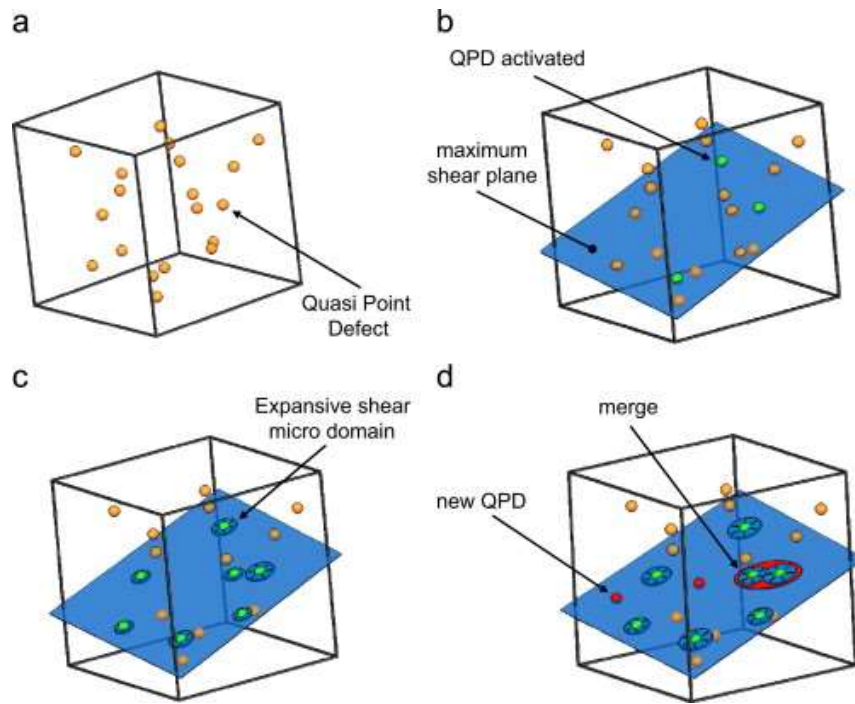


**Fig. 63.** Schemes corresponding to the quasi-point defect model (a) Quasi-point defects in amorphous materials (b), (c) and (d) activation of these QPD and growth of sheared micro-domains (SMD) induced by application of a stress [379]. Reprinted from ref. [379], copyright (2011), with permission from Elsevier.

Due to these quasi-point defects, the atoms or molecules of glass-forming liquids can perform relative motions, which results in dynamic relaxation behavior at macroscopic scale. According to the quasi-point defects model, the global characteristic relaxation time  $\tau_{relax}$  that describes the mobility of atoms or molecules of the glassy material can be defined as:

$$\tau_{relax} = t_0 \left( \frac{\tau_\beta}{t_0} \right)^{1/\chi} \quad (4-9)$$

where  $\tau_\beta$  is the mean time of the thermally activated jump of a structural unit and follows the Arrhenius law,  $t_0$  is a time scale parameter,  $\chi$  is a correlation factor related to the quasi-point defect concentration  $C_d$ ,  $\chi$  ranges from 0 (full order—perfect crystal) to 1 (full disorder—perfect gas).

In the framework of QPD model, the loss factor  $\tan\delta$  of the glassy materials can be expressed as:

$$\ln(\tan\delta) = -\frac{U_\beta}{kT} - \chi \ln\omega - \chi \ln(\tau^*) + \ln K_0 \quad (4-10)$$

where  $\tau^* = t_0 \left( \frac{\tau_\beta}{t_0} \right)^{1/\chi}$ ,  $U_\beta$  represents the activation energy for the structural unit movement for atoms or molecules, which is linked to the  $\beta$  relaxation,  $k$  is the Boltzmann constant.

According to Eq. (4-10), the  $\ln(\tan\delta)$  and  $\ln\omega$  are in linear relationship at a given temperature, the correlation factor  $\chi$  can be determined by:

$$\chi(T) = - \left\{ \frac{d\ln(\tan\delta)}{d\ln(\omega)} \right\}_T \quad (4-11)$$

**Fig. 64(a)** shows the variation of  $\ln(\tan\delta)$  versus frequency of the  $\text{Cu}_{46}\text{Zr}_{46}\text{Al}_8$  bulk metallic glass at different temperatures. According to prediction of the QPD model, glassy materials remain in an iso-configurational state when the temperature is below the glass transition temperature  $T_g$ . Thus, the correlation factor  $\chi$  is almost a constant. On the other hand, when the temperature rises above the glass transition temperature  $T_g$ , a metastable thermodynamic equilibrium is reached and then concentration of the quasi-point defects increases with temperature. Thus, the correlation factor  $\chi$  is strongly dependent on temperature.

**Fig. 64(b)** shows evolution of the correlation factor  $\chi$  with temperature in the  $\text{Cu}_{46}\text{Zr}_{46}\text{Al}_8$  bulk metallic glass for both as-cast state and annealed state [380]. It is

evident from Fig. 64(b) that the concentration of “defects” is almost constant when temperature is below the glass transition temperature  $T_g$ , therefore the correlation factor  $\chi$  remains nearly constant. When the temperature increases above  $T_g$ , the correlation factor  $\chi$  increases. The current experimental results are in good accordance with the prediction of the quasi-point defects model. At the same time, it should be mentioned that the correlation parameter  $\chi$  of the annealed state is slightly lower than that of as-cast state. Many investigations have demonstrated that physical aging below  $T_g$  reduces the concentration of defects, which induces a reduction of the atomic mobility in metallic glasses.

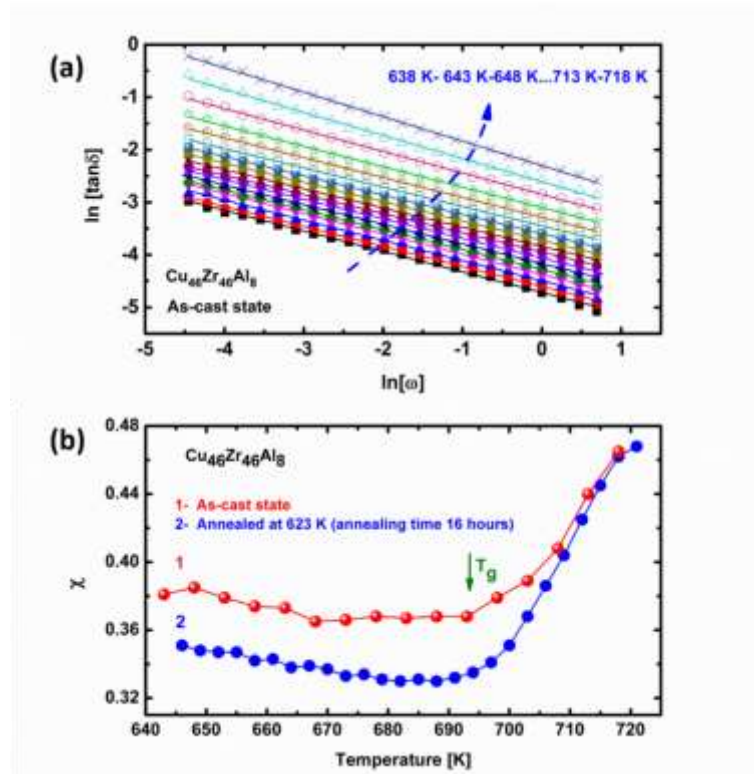


**Fig. 64.** (a) Influence of the driving frequency on the loss factor at different temperatures in the  $\text{Cu}_{46}\text{Zr}_{46}\text{Al}_8$  bulk metallic glass (the isothermal temperature ranges from 638 to 718 K with an interval of 5 K). Solid lines are fitted by Eq. (5-9) [380]. (b) Evolution of the correlation factor  $\chi$  with temperature for  $\text{Cu}_{46}\text{Zr}_{46}\text{Al}_8$  bulk metallic glass [380]. Reprinted from ref. [380], copyright (2017), with permission from Elsevier.

On the basis of the QPD theory, **Fig. 65** shows the evolution of the correlation factor  $\chi$  with temperature in  $Zr_{56}Co_{28}Al_{16}$  bulk metallic glass at various states. It is evident from **Fig. 65** that: (i) The correlation factor  $\chi$  increases after the cold-rolling deformation. The increment is attributed to an increase in the “defect” concentration and therefore to an increase in disorder and atomic mobility. Generally, the pre-plastic deformation is an effective route to improve the plasticity of metallic glasses either in tensile mode or in compressive route at room temperature [381]. (ii) The value of correlation factor  $\chi$  after structural relaxation is smaller than that of as-cast. (iii) Crystallization leads to a notable decrease of the correlation factor  $\chi$ . In line with the predication of the theoretical model, it is reasonable to conclude that in amorphous alloys, the higher the concentration of quasi-point defects reflected by the correlation factor  $\chi$ , the lower the atomic mobility, and *vice versa*.

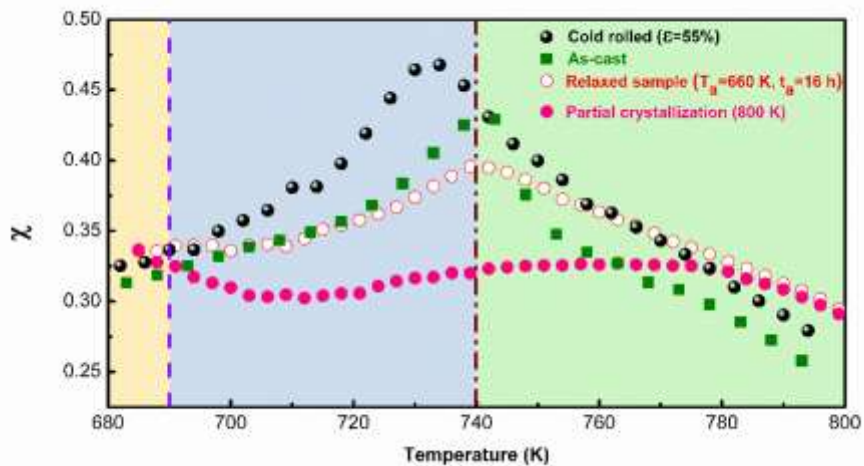


**Fig. 65.** Evolution of the correlation factor  $\chi$  with temperature in  $Zr_{56}Co_{28}Al_{16}$  bulk metallic glass at different states [134]. Reprinted from reference [134], copyright (2014), with permission from Elsevier.

The  $\beta$  relaxation is associated with the local structural heterogeneity of metallic glasses. For instance, **Fig. 66(a)** shows  $\ln(\tan \delta)$  vs  $\ln \omega$  at different temperatures obtained for the  $Pd_{43}Ni_{10}Cu_{27}P_{20}$  metallic glass. **Fig. 66(b)** presents the temperature

dependence of the correlation factor  $\chi$  and the loss factor  $\tan \delta$ . Based on these data, it is expected that the correlated factor  $\chi$  is closely associated with a mechanical relaxation process.

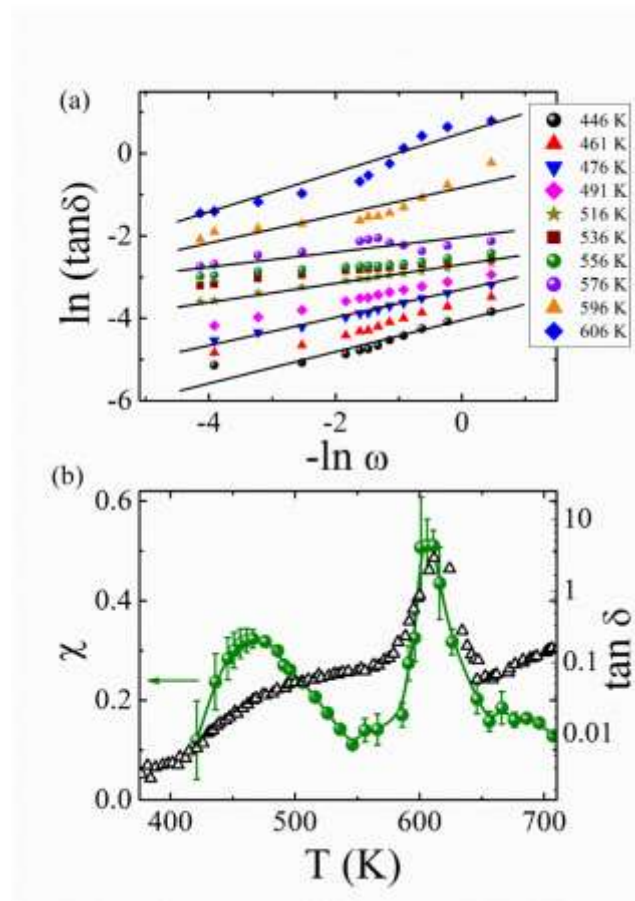


**Fig. 66.** (a) Variation of  $\ln(\tan \delta)$  vs  $\ln \omega$  at different temperatures of  $\text{Pd}_{43}\text{Ni}_{10}\text{Cu}_{27}\text{P}_{20}$  amorphous alloy; (b) Temperature dependence of the correlation factor  $\chi$  and the loss factor  $\tan \delta$ . Adapted with permission from reference [382]. Reprinted from reference [382], with the permission of AIP Publishing.

Based on the above discussion, it is proven that the atomic mobility of metallic glasses is closely related to the local atomic arrangements. With regard to the influence of plastic deformation on the concentration of “defects”, it has been shown that crystallization activation energy decreases after cold-rolling compared to the as-cast state. In addition, creation of free volume or augmentation of concentration of

the quasi-point defects is induced by plastic deformation. As a consequence, larger concentration of the quasi-point defects leads to higher atomic mobility and diffusivity [271]. Chen reported that cold-rolling causes obvious atomic arrangement, which tends to either softening or strengthening of the metallic glasses [383]. The viscosity is reduced after the cold-rolling for metallic glasses. On the other hand, physical aging below the glass transition temperature  $T_g$  decreases the concentration of “defects” and crystallization induces atomic rearrangement in large scale, then increases the hardness and storage modulus.

It is worth noting that the sample density will be increased after structural relaxation [336]. For samples with the partial crystallization and crystallization at higher temperature, more uniform structure state may be formed. Similar phenomenon was observed in polymers. Plasticity in cold-rolling or compression is a result of geometry constraints that leads to development of a dense shear band structure. Intuitively, the structural state is more disordered and leads to a drastic atomic mobility via the deformation far below the glass transition temperature  $T_g$ .

In agreement with the concept of “flow units”, the concentration of flow units will decrease by physical aging below  $T_g$ . Above results confirm that the atomic configuration becomes more disordered after plastic deformation (i.e. cold-rolling at room temperature). On the other hand, structural relaxation process and the formation nanocrystal phases in glass matrix will cause the system shift to a more stable state. Therefore, it is suggested that the atomic mobility in metallic glasses is connected to the local energy landscape.

The dynamics of supercooled liquids is believed to be spatially heterogeneous [324, 384]. With decreasing temperature (or increasing density) the length scale of the dynamic correlation length increases, causing the slowing down of the dynamics that eventually bring to the glass transition. Since within the regions of correlated motion co-exist regions of slow and fast dynamics, ultimately with decreasing temperature also the heterogeneity increases. On approaching the glass transition the regions of

cooperative motions grow, while within these regions of slow and fast dynamic regions coexists. To determine experimentally the number of units within a correlating region have been proposed different metrics.

Donth put forward the number of correlating units (i.e. atoms in a metallic glass, segments in a polymer, molecules in a simple liquid) can be determined from thermodynamic quantities as [385]:

$$N_{\alpha} = \frac{RT^2}{m_0(\delta T)^2} \Delta c_p^{-1} \quad (4-12)$$

where  $m_0$  is the molecular weight of the relaxing unit, and  $\delta T$  can be determined from the  $c_p''$  as discussed in [386]. The values of  $N_{\alpha}$  of typical metallic glasses are listed in **Table 1**. It is interesting to note that  $N_{\alpha} \sim 600$  for the PdNiCuP metallic glasses without Cu and  $N_{\alpha} \sim 1100$  for the metallic glass with Cu. Interestingly, these values are significantly larger than those found for polymers and molecular liquids for which generally  $N_{\alpha} < 400$ .

Using a different approach Berthier *et al.* have derived an approximate formula for the number of correlated units [387, 388]:

$$N_c = \frac{R}{\Delta c_p} T^2 \left\{ \max_t \chi_T(t) \right\}^2 \quad (4-13)$$

where  $\chi_T$  is the time derivative of a suitable correlation function. In the case this correlation function has a stretched exponential form and it has been shown that it reduces to

$$N_c = \frac{R}{\Delta c_p m_0} \left( \frac{\beta_{KWW}}{e} \right)^2 \left( \frac{\partial \ln \tau_{\alpha}}{\partial \ln T} \right)^2 \quad (4-14)$$

where  $e$  is the Euler's number. The values of  $N_c$  calculated using Eq.(4-13) from the

mechanical measurements are reported in **Table 1**.  $N_c$  can be calculated from the thermodynamic data.

Taking into consideration Eqs.(4-12), (4-13) and (4-14) it follows that

$$\frac{N_\alpha}{N_c} \approx 6.45 \Delta c_p \Delta c_p^{-1} \quad (4-15)$$

For the cases included herein  $0.07 < \Delta c_p \Delta c_p^{-1} < 0.14$ , thus  $0.45 < \frac{N_\alpha}{N_c} < 0.9$ . The values of  $N_c$  calculated from the thermodynamic quantities using Eq.(4-15) are reported in Table 1 ( $N_c^{MDSC}$ ), and we can see that the values are very close to those found from the dynamics.

Like the values of  $N_\alpha$ , the values of  $N_c$  are also significantly larger than those observed for other types of glass formers, for which  $N_c < 570$  [389]. These large values of  $N_\alpha$  and  $N_c$  for metallic glass-forming liquids could indicate the existence of a short range order in metallic glasses, that is, atoms in metallic glasses could be organized into clusters, instead of moving independently [390].

**Table 1.** Thermodynamic quantities measured using Modulated Differential Scanning Calorimetry (MDSC) [148]. Reprinted with permission from reference[148]. Copyright (2014) American Chemical Society.

Metallic glass	$T^*$ [K]	$\delta T$ [K]	$c_p^{glass}$ [J/(gK)]	$c_p^{liquid}$ [J/(gK)]	$\Delta c_p^{-1}$ [(gK)/J]	$N_\alpha$	$N_c^{MDSC}$	$N_c^{G''}$	$\beta_{KWW}^{MDSC}$	$T_{shift}$ [ K]
Pd <sub>40</sub> Ni <sub>10</sub> Cu <sub>30</sub> P <sub>20</sub>	294.5	6.5	0.33	0.55	1.0	1040	730	710	0.61	7
Pd <sub>30</sub> Ni <sub>50</sub> P <sub>20</sub>	314.2	7.6	0.40	0.54	0.65	570	960	940	0.62	5.5
Pd <sub>40</sub> Ni <sub>40</sub> P <sub>20</sub>	312.6	7.5	0.39	0.51	0.60	590	1100	1060	0.61	6.5
Pd <sub>42.5</sub> Ni <sub>7.5</sub> Cu <sub>30</sub> P <sub>20</sub>	299.6	6.5	0.38	0.55	0.82	1090	970	1000	0.59	3.5

## 5. Structural heterogeneity and mechanical properties of amorphous alloys

In this chapter, our focus is on the possible correlations between structural heterogeneity and mechanical properties of amorphous metals. We will start with the elastic properties of amorphous metals, including shear modulus and Poisson ratio, and move to the properties associated with plasticity in amorphous metals, such as yield strength and plasticity. After that, we will review the recent works on the possible routes one may take to alter or introduce structural heterogeneity at different length scales to enhance the mechanical properties of amorphous metals.

### 5.1 Elastic constants and structural heterogeneity in amorphous alloys

At the macroscopic scale, amorphous metals are generally considered to be a homogeneous solid. The shear modulus of bulk amorphous metals is known to be 10-30% lower than that of their crystalline counterparts [11], while their bulk moduli are similar. The difference in shear moduli is commonly attributed to the presence of frozen-in defects in an amorphous structure. In the classic literature, these frozen-in defects were generally understood as free volume [207]; however, they were referred to as liquid-like regions [218, 391], non-affine deformation sites [392] or generally defect regions [366, 393] when structural heterogeneity was considered. Compared to an elastic (or solid-like) amorphous matrix, these defect (or liquid-like) regions cannot carry stress indefinitely and will release mechanical stress after the experimental or observation time exceeds their relaxation time, as illustrated in [Fig. 67\(a\)](#). The instant local stress relaxation leads to modulus reduction as well as anelasticity in amorphous metals. Furthermore, as a structural feature of the amorphous structure, existing liquid-like regions could grow and new liquid-like regions could nucleate under

mechanical stress, causing mechanical softening as noted by Huo et al.[218][see Fig. 67(b)].

Based on a mean-field theory, the overall elastic modulus of an amorphous metal can be derived as that of a solid-like elastic shell containing a liquid-like core [Fig. 67(c)]. The rheological behaviour of such a physical model is equivalent to the standard solid model or the three parameter model as shown in Fig. 67(d). As a result, the relaxed shear or Young’s modulus of an amorphous metal, which can be measured through regular mechanical tests, can be simply derived as [218]:

$$G = \frac{G_{\infty}}{1+\alpha} \quad (5-1)$$

where  $G_{\infty}$  is the shear or Young’s modulus of the elastic shell while  $\alpha = \frac{\beta\Omega G_{\infty}}{k_B T}$  can be viewed as a factor embodying the total effect of the aggregated liquid-like cores. Here  $\Omega$  stands for the average volume of the liquid-like cores,  $T$  for the ambient temperature and  $\beta$  for a strain sensitivity factor defined in Ref. [218]. According to (5-1), for a given temperature  $T$ , the shear or Young’s modulus of an amorphous metal decreases as the average volume of the liquid-like regions increases. Theoretically, this is consistent with the interstitalcy theory [331], according to which the shear modulus of an amorphous alloy decreases with the increasing volume fraction of structural defects.

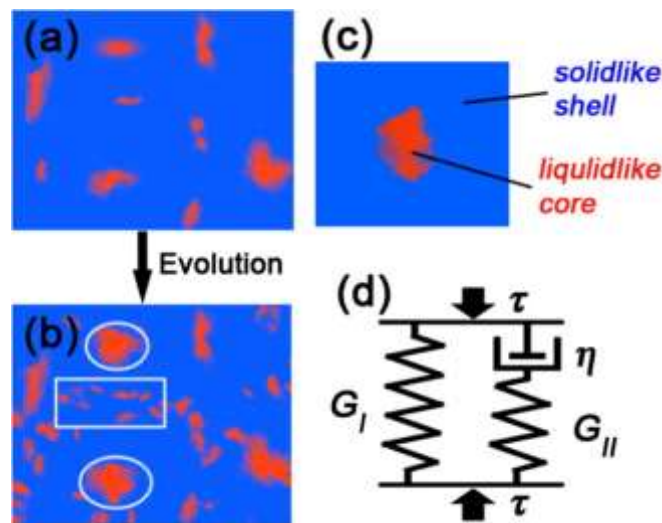


**Fig. 67.** (a) Schematic illustration of the zones of local heterogeneity being activated under stress in metallic glasses (the red regions represent the liquid-like cores and the blue surroundings the elastic matrix); (b) illustration of the evolution of the structural heterogeneity; (c) sketch of the core-shell deformation unit in metallic glasses; and (d) the three-parameter viscoelastic model[218]. Reprinted from reference [218], copyright (2013), with permission from Elsevier.

According to Dmowski *et al.* [265], the atomic fraction of the frozen-in liquid-like atoms is ~24.3% in the  $Zr_{52.5}Cu_{17.9}Ni_{14.6}Al_{10}Ti_5$  metallic glass. This estimation agrees with the atomic stress theory by Egami [71] in that glass transition would be triggered once the volume fraction of liquid-like regions in a supercooled liquid is lowered to below 25% during supercooling. Here, it is worth mentioning that, in the STZ theory developed by Falk and Langer[78, 215], it was estimated that the STZ density is only around 1% of the total atoms when yielding occurs. This STZ density is similar to that of free volume density estimated in other works [394] but is about one order of magnitude lower than the atomic fraction of liquid-like regions. In our opinion, this is not surprising considering that liquid-like atoms or regions are the essential character of an amorphous structure, being inherited from a heterogeneous supercooled liquid, while STZ is a transient event of local plasticity. In other words, if only 1% atoms constitute STZs and these STZs can be all correlated with the liquid-like regions or soft spots as discussed by Ding *et al.* [244], one may infer that only ~10% of the total liquid-like regions undergo STZs for yielding to take place in an amorphous alloy.

Aside from shear or Young's modulus, the Poisson's ratio of amorphous alloys is also important [395-398]. As already discussed in Chapter 2, it was previously observed that an amorphous alloys with a higher Poisson's ratio tends to exhibit a greater toughness and plasticity than otherwise [399-402]. This empirical rule was once rationalized by Lewandowski *et al.* [397] as simply the effect of the  $B/G$  ratio ( $B$  = bulk modulus and  $G$  = shear modulus), i.e., a high  $B/G$  ratio (a high Poisson's ratio) favors plastic or shear flow while a low  $B/G$  ratio (a low Poisson's ratio) favors

fracture. However, it was later recognized that this empirical rule does not hold for all amorphous metals. Some amorphous metals with a high Poisson's ratio, such as  $(\text{Pd}_{40}\text{Ni}_{40}\text{P}_{20})_{99.4}\text{Fe}_{0.6}$  [403] and  $\text{Pd}_{36}\text{Pt}_{9.3}\text{Cu}_{25}\text{Ni}_{9.3}\text{P}_{20.4}$  [404] turn out to be much more brittle than others with a relatively low Poisson's ratio, such as  $\text{Zr}_{53.8}\text{Cu}_{31.6}\text{Ag}_{7.0}\text{Al}_{7.6}$  [405] and  $\text{Zr}_{61.88}\text{Cu}_{18}\text{Ni}_{10.12}\text{Al}_{10}$  [212].

From the perspective of structural heterogeneity, Sun et al. [406] conceived that the overall Poisson's ratio of an amorphous metal should depend on how liquid-like regions respond to a mechanical perturbation. In general, the mechanical "softness" of a liquid-like region could manifest as shear softening (low shear modulus) or dilatational softening (low bulk modulus). Based on the Eshelby theory, Sun et al. showed that the overall Poisson's ratio ( $\nu$ ) of an amorphous metal can be derived as [406]:

$$\nu = \frac{(1+\nu_0)(1+B\nu_f)-(1-2\nu_0)(1+A\nu_f)}{2(1+\nu_0)(1+B\nu_f)+(1-2\nu_0)(1+A\nu_f)} \quad (5-2)$$

where  $\nu_0$  is the Poisson's ratio of the amorphous elastic matrix [Fig. 67(c)];  $\nu_f$  is the volume fraction of the liquid-like atoms;  $A = \frac{K_1-K_0}{2(K_0-K_1)\alpha-K_0}$  and  $B = \frac{G_1-G_0}{2(G_0-G_1)\beta-G_0}$ , in which  $K$  and  $G$  stand respectively for bulk and shear modulus while the subscript 0 and 1 for the solid- and liquid-like regions respectively [Fig. 67(c)]. Note that  $\alpha = \frac{1+\nu_0}{3(1-\nu_0)}$  and  $\beta = \frac{2(4-5\nu_0)}{15(1-\nu_0)}$  in the above expressions for  $A$  and  $B$ .

According to equation (5-2), the overall Poisson's ratio of an amorphous alloy increases with the increasing volume fraction ( $\nu_f$ ) of liquid-like regions if they are characterized by shear softening, or decreases with the increasing volume fraction ( $\nu_f$ ) of liquid-like regions if they are characterized by dilatational softening. Through sub- $T_g$  thermal annealing, Sun et al. [406] tuned the structural heterogeneity in various amorphous alloys and measured their elastic constants, including the bulk modulus, shear modulus and Poisson's ratio. Fig. 68 shows the variation of the measured Poisson's ratio with thermal annealing. Evidently, Eq. (5-1) fits the experimental data very well, according to which it can be concluded that the liquid-like regions in the

Zr-based amorphous alloys mainly cause shear softening while those in Ce- and La-based amorphous alloys mainly cause dilatational softening. These findings are important, which deliver a strong message that the Poisson's ratio of amorphous alloys depends on not only the amount but also the type of liquid-like sites or soft spots. As such, plasticity of amorphous alloys is unlikely to be solely determined by Poisson's ratio. Furthermore, one can also infer that the Poisson' ratio of an amorphous alloy would be independent of the volume fraction of the liquid like sites if they cause the same degree of shear and dilatational softening. Indeed, it was observed that the Poisson's ratio of the  $\text{Au}_{49}\text{Cu}_{26.9}\text{Si}_{16.3}\text{Ag}_{5.5}\text{Pd}_{2.3}$  amorphous alloy did not vary during sub  $T_g$  thermal annealing[407], which could be explained by the theory of Sun et al. [406]. Notably, Au-based amorphous alloys are generally brittle at room temperature but have a relatively high Poisson's ratio. Again, this fact suggests that which type of liquid-like sites or soft spots an amorphous alloy contains should be important to its plasticity. Interestingly, the notion of dilatational versus shear softening liquid-like sites, being proposed by Sun et al. [406], echoes well with the idea of tension transformation zone (TTZ) early proposed by Jiang et al. [408-410] as an alternative to shear transformation zone (STZ) as the atomic origin of fracture in amorphous alloys.

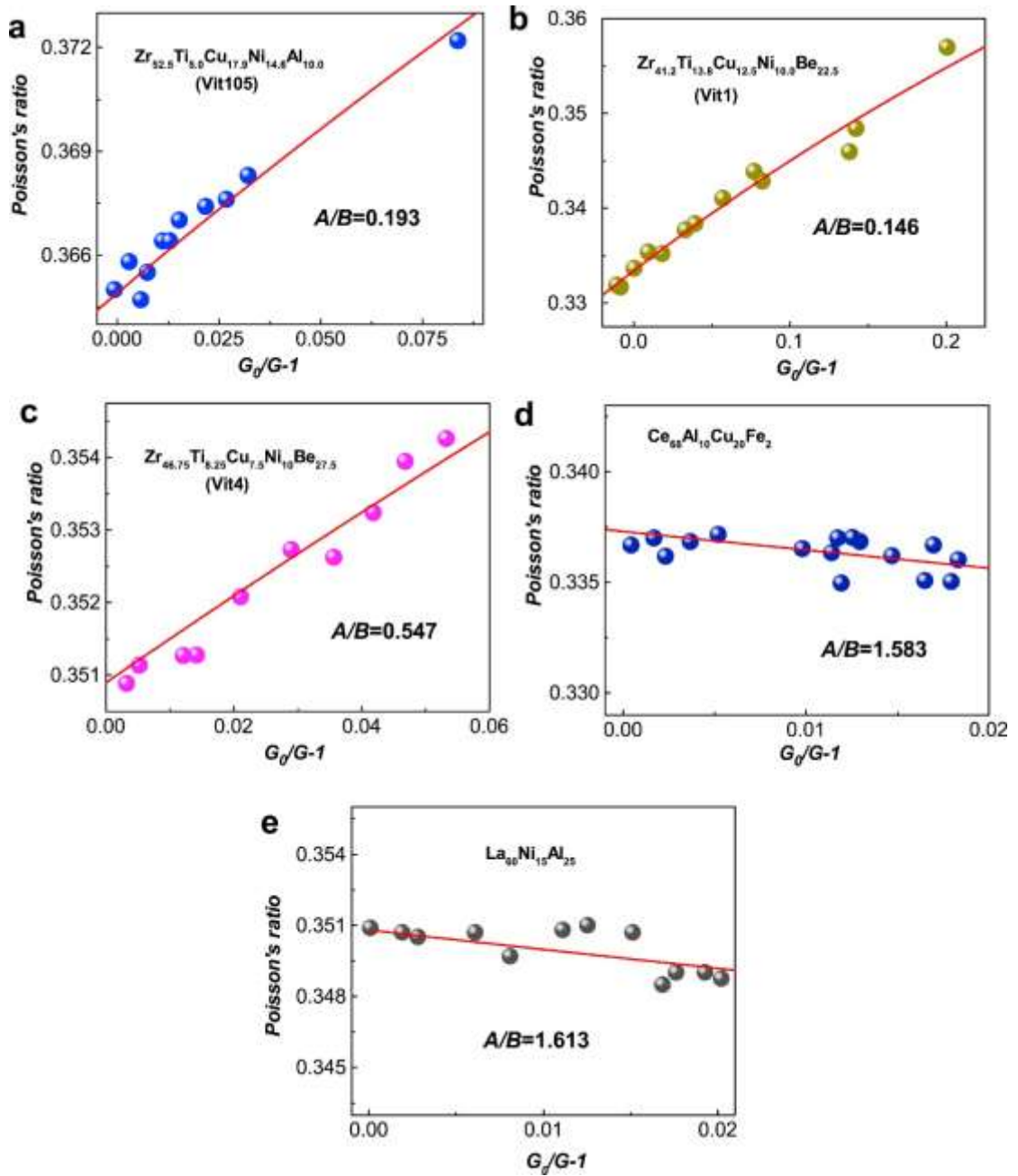


**Fig. 68.** The plot of measured Poisson's ratio,  $\nu$ , versus  $(G_0/G-1)$  upon annealing for different amorphous alloys: (a) Vit105; (b) Vit1; (c) Vit4; (d)  $Ce_{68}Al_{10}Cu_{20}Fe_2$ ; (e)  $La_{60}Ni_{15}Al_{25}$ . All data were well fitted by equation (5-2), with the fitting values  $A/B$  listed [406]. Reprinted from reference [406], copyright (2016), with permission from Elsevier.

## 5.2. Yield strength and structural heterogeneity in amorphous alloys

Unlike crystalline alloys, whose yielding strain is generally less than 0.005, a unique characteristic of yielding in amorphous alloys is that, regardless of their chemical compositions, the elastic strain limit or yielding strain,  $\varepsilon_y$ , at ambient temperature is distributed within a narrow range around 0.02 [323]. As seen in **Fig. 69**, one may view the elastic strain limit as a constant  $\varepsilon_y \sim 2.7\%$  when fitting a straight line to the data of shear modulus versus shear stress at yielding obtained for various amorphous alloys [323, 411]. Based on this observation, Johnson and Samwer developed the cooperative shearing model (CSM) by following the Frenkel assumption that the elastic energy  $\phi$  of a STZ subject to a shear strain  $\gamma$  can be described by  $\phi(\gamma) = \phi_0 \sin^2(\pi\gamma/4\gamma_c)$ , where  $\gamma_c$  is the yielding strain and  $\phi_0$  the total energy barrier density at  $\gamma=0$ . Thus, the critical yield stress can be derived as  $\tau_c = \left. \frac{\partial \phi_0}{\partial \gamma} \right|_{max} = \frac{\pi \phi_0}{4\gamma_c}$  without considering the strain rate effect. For plastic flows to occur on a given time scale or strain rate  $\dot{\gamma}$  at a finite temperature  $T$ , CSM gives [323]:

$$\varepsilon_Y = \frac{\tau_Y}{G} = \gamma_{C0} - \gamma_{C1} \left( \frac{T}{T_g} \right)^{2/3} \quad (5-3)$$

where  $\gamma_{C0}$  stands for the yielding strain at 0K and  $\gamma_{C1}$  is a parameter weakly dependent on the strain rate  $\dot{\gamma}$ . Through fitting the experimental data obtained from bulk amorphous alloys, it was shown that  $\gamma_{C0} \approx 0.036$  and  $\gamma_{C1} \approx 0.016$  [323].

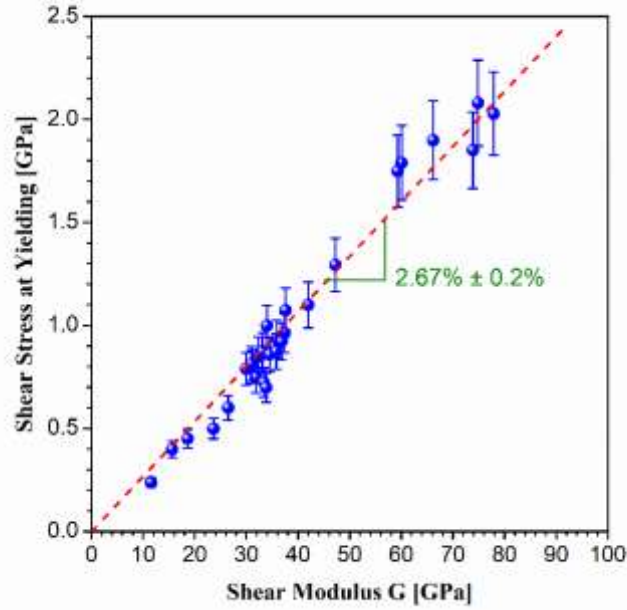


**Fig.69.** Experimental shear stress at yielding versus shear modulus  $G$  at room temperature in amorphous alloys [323]. Reprinted figures with permission from reference [323], copyright (2005) by the American Physical Society.

In the literature of amorphous alloys, the CSM model has been widely accepted in addition to the classic STZ models[67, 215] as the theoretical explanation for yielding in amorphous alloys. However, one question remains: what causes the constant yield strain ( $\sim 2\%$ ) of amorphous alloys? According to the RFOT theory [30], yielding occurs in amorphous solids once the energy barrier against the atomic arrangements in liquid-like sites (or beads) is tilted to a level such that local plastic flows become barrier-less. This is a yielding scenario without considering the effect of strain rate or time. As such, the yield stress  $\tau_y$  can be derived as[30]:

$$\tau_Y = \sqrt{\frac{2Gk_B T}{\kappa V_{bead}} \left[ \left( 3.20 \frac{T_K}{T} - 1.91 \right) - \frac{\Delta c_p(T_g) T_g}{k_B T} \ln \frac{T_g}{T_K} \right]} \quad (5-4)$$

where  $T_K$  is the Kauzmann temperature;  $\kappa = 3-6/(7-5\nu)$  is a constant with  $\nu$  the Poisson's ratio;  $G$  is the elastic shear modulus;  $\Delta c_p(T_g)$  is the jump in the heat

capacity at the glass transition temperature  $T_g$  and  $V_{bead}$  is the volume of a “bead” (i.e. liquid-like sites or movable units in the glass), which corresponds to the structural heterogeneity in glassy materials. By estimating vibrational displacements from Debye continuum theory and assuming a limiting Lindemann ratio for the maximum thermal excursions, Wistsorasak and Wolynes were able to show [30]:

$$G = 24.9k_B T_A / V_{bead} \quad (5-5)$$

where  $T_A$  ( $\approx T_M$  the melting temperature) is the mean field spinodal temperature and the size of the liquid-like site  $V_{bead}$  can be estimated according to Ref. [30], which is around 100 molecules or atoms for laboratory prepared glasses. Substituting (5-5) into (5-4) leads to

$$\frac{\tau_Y}{G} = 0.2 \sqrt{\frac{T}{T_M} \left[ \left( 3.20 \frac{T_k}{T} - 1.91 \right) - \frac{\Delta c_p(T_g) T_g}{k_B T} \ln \frac{T_g}{T_K} \right]} \quad (5-6)$$

Note that  $\nu$  and  $\kappa$  are approximated as 0.3 and 1.8 respectively in deriving the above equation. **Fig.70** shows the results of the strength versus shear modulus obtained from a variety of amorphous solids. Evidently, Eq. (5-6) fits the data very well, from which one can infer that the more or less constant yield strain as witnessed in amorphous alloys can be attributed to the events of local mechanical instability triggered at liquid-like sites. Furthermore, using the machine learning guided technique, Liu et al.[412] recently showed that yielding in amorphous solids, including amorphous alloys, could be attributed to the percolation of some “soft” spots in an amorphous structure. General speaking, this view is consistent with the broad idea of flow units [55, 334], liquid-like sites [71, 413, 414], quasi-point defects[377, 415] or GUM [73, 244], which suggests that structural heterogeneity be an essential basis to understand yielding in amorphous alloys.

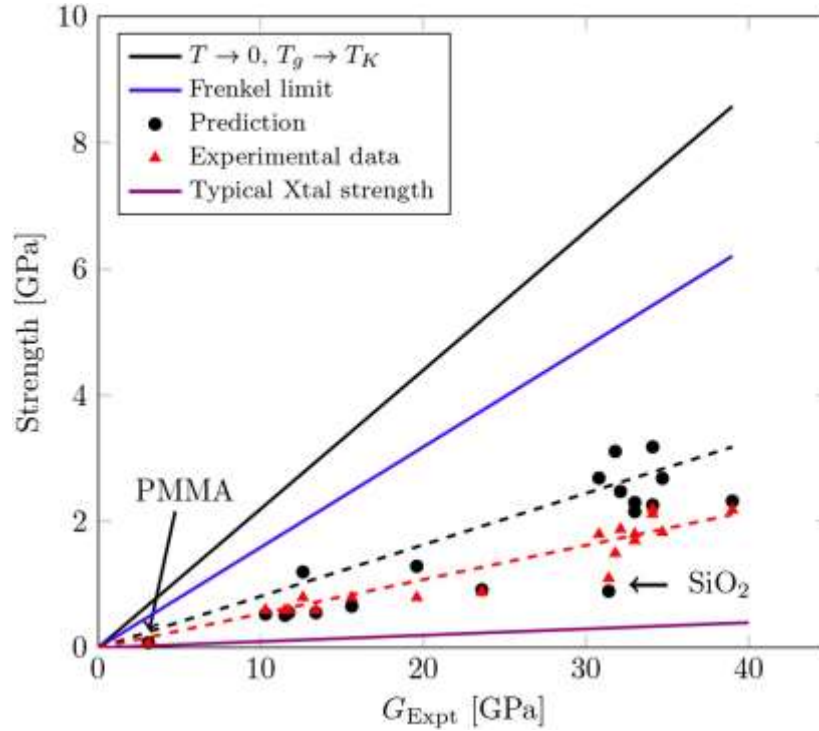


**Fig.70.** Strength as a function of shear moduli. The experimental strength (red triangle) and the predicted strength (black circle) have nearly the same slope and are quite different from Frenkel strength (blue solid line). Typical value of crystal strength (violet solid line) and strength in the limit  $T \rightarrow 0$ ;  $T_g \rightarrow T_K$  (black solid line) are also shown in comparison. Reprinted from reference[30], with permission from Proceedings of the National Academy of Sciences of the United States of America (PNAS). Copyright (2012) National Academy of Sciences.

In the above modeling, yielding in amorphous alloys is taken as a consequence of local energy barrier crossing events, either in the form of STZs or unstable structural rearrangements within liquid-like sites. However, yielding in amorphous alloys could be also attributed to the nucleation and growth of shear bands [416, 417], particularly so for bulk amorphous alloys. In that case, a size effect on yield strength comes about because of the finite size of a shear band embryo in amorphous alloys. According to the experimental results [418-421], the critical shear-band nucleation size was estimated to be  $\sim 100$  nm under tension[422, 423] while to range from  $\sim 200$  to  $\sim 500$  nm under compression[418-420, 424-426]. Obviously, the size effect on yield strength of amorphous alloys [299, 422, 427-430] involves a much wider length scale

than that in the elementary plasticity events, such as STZs [416]. Interestingly, through the high-angle annular dark-field scanning transmission electron microscopy (HAADF-STEM)[431], density fluctuations at the length scale of around 150 nm was recently observed inside the shear bands in the  $\text{Al}_{88}\text{Y}_7\text{Fe}_5$  and  $\text{Zr}_{52.5}\text{Cu}_{17.9}\text{Ni}_{14.6}\text{Al}_{10}\text{Ti}_5$  amorphous alloys in the post-deformation (i.e. cold-rolled or compression-deformed) states (as shown in Fig.71). These experimental results are interestingly, which suggest a hierarchy in the structural heterogeneity in deformed amorphous alloys.

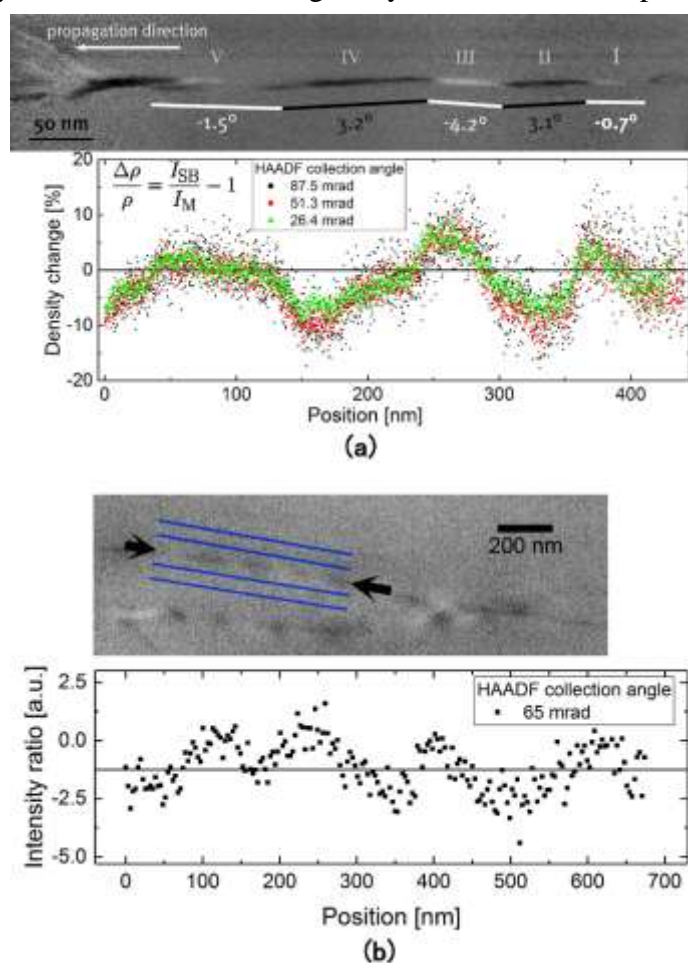


**Fig.71.** (a) Top: HAADF-STEM image showing contrast reversals (bright-dark-bright) in a shear band of cold-rolled  $\text{Al}_{88}\text{Y}_7\text{Fe}_5$  amorphous alloy. Bottom: Corresponding quantified density oscillations along the shear band for different collection angles of the HAADF detector. The results clearly indicate that the results are independent of the collection angle. Note that the amplitudes for the denser shear-band segments are about half of the dilated states. (b) Top: HAADF-STEM image showing contrast reversals (bright-dark-bright) in a shear band (see arrows) of a compression-deformed model alloy ( $\text{Zr}_{52.5}\text{Cu}_{17.9}\text{Ni}_{14.6}\text{Al}_{10}\text{Ti}_5$ ). Bottom: Corresponding quantified density

oscillations along the shear band[431]. Reprinted figures with permission from reference[431], copyright (2017) by the American Physical Society.

### **5.3. Ductility and structural heterogeneity in amorphous alloys**

Plasticity in crystalline solids is usually mediated through the creation and movement of crystalline defects, such as dislocations. However, due to the lack of long-range periodicity in noncrystalline solids, they do not possess structurally well-defined flow defects and therefore, their mechanism of plasticity has been long debated. As discussed in the previous sections, in the literature of amorphous metals, the widely accepted mean-field model for plasticity is the shear transformation zone (STZ) model [67, 215], according to which plasticity result from the thermal activation of STZs. However, the physical origin of STZs remains unspecified in the classic models [67] and STZ activation is usually taken as a randomly occurring event, which is usually perceived to be associated with loosely packed (free volume) regions or over-packed (the so called anti-free volume[71]) regions. More interestingly, aside from STZs, the notion of “tension transformation zone” (TTZ) was also proposed to rationalize the yielding and fracture behavior of amorphous metals at a crack tip [408, 409]. If one follows the line of reasoning in the STZ and TTZ model, he may infer that the form of atomic scale plasticity event in amorphous metals is seemingly dependent on the local stress state. Furthermore, because of its mean field nature, the only length scale involved in the STZ and TTZ model is the size of STZ or TTZ, which ranges from tens to hundreds of atoms [416, 417, 432-434] or around 1 nm [435-437].

However, plasticity in amorphous alloys is a multi-scaled phenomenon. One example is the emergence of nano-scale corrugation on the fracture surface of commonly perceived brittle amorphous alloys, such as Mg-based amorphous alloy, as shown in [Fig.72](#). Physically, the corrugated morphology originates from the meniscus instability as discussed in reference [438]. At the crack tip of an amorphous alloy

which is fluidized due to the local high stress, it has been shown that corrugation forms once there is a perturbation of local properties with the wavelength  $\lambda$  satisfying the following equation [438]:

$$\frac{\sigma_{th}}{\delta} \geq \gamma \frac{2\pi}{\lambda^2} \quad (5-7)$$

where  $\sigma_{th}$  is the theoretical strength ( $=E/10$ );  $\delta$  is a range parameter which equals 0.1-0.4 nm for typical brittle solids and  $\gamma$  is the surface tension ( $\sim 1 \text{ J/m}^2$  for amorphous alloys). For Dy- and Mg-based amorphous alloys, it was estimated that the critical wave length for causing nano-scale corrugation should be  $\lambda_{Dy} = 65 \text{ nm}$  and  $\lambda_{Mg}=92 \text{ nm}$ . Interestingly, these estimates from the experiments agree quite well with the wave length of density fluctuation in the shear band in amorphous alloys.

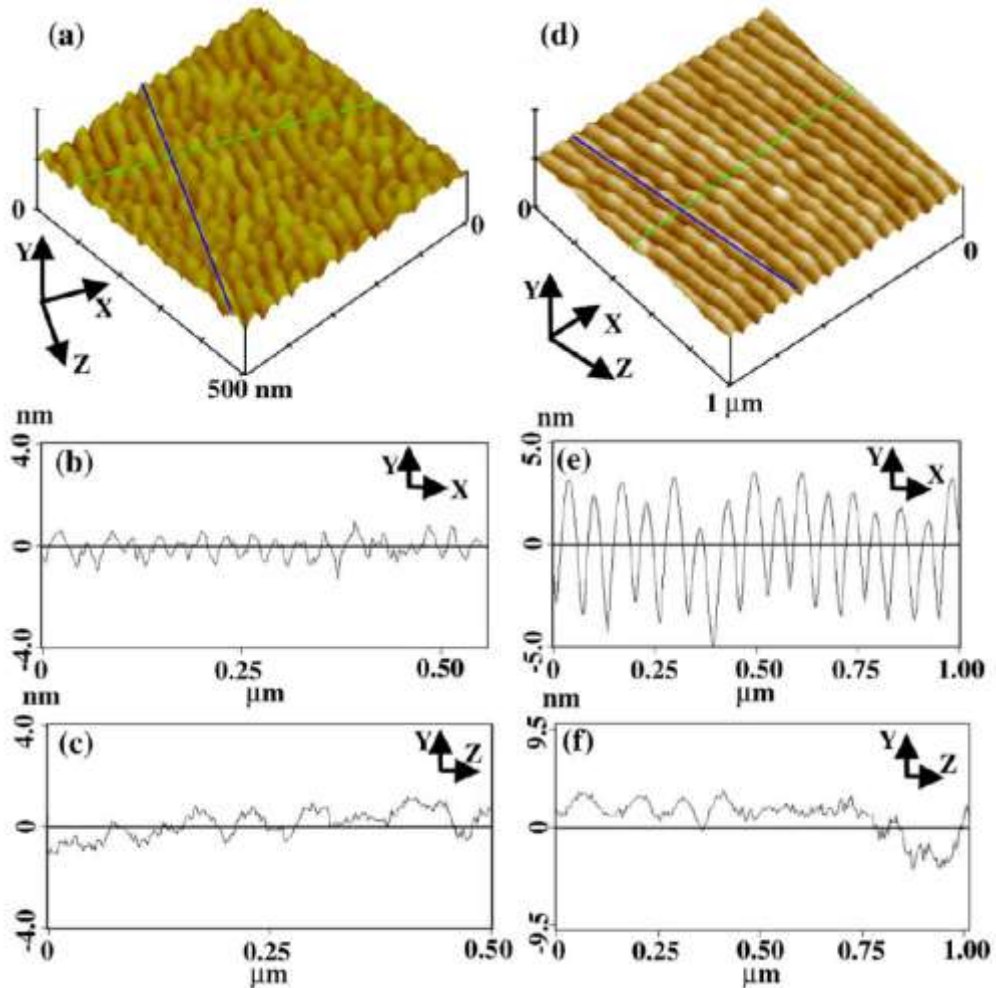


**Fig.72.** AFM results for the mirror zone on the fracture surface of two amorphous alloys. Cracks propagate along the X direction. (a) 3D image for the Dy-based amorphous alloy. (b) Section shape of the corrugation being along a dashed line in (a), i.e., the crack propagation direction. (c) Section shape of the corrugation being along a solid line in (a), i.e., perpendicular to the crack propagation direction. (d) 3D image for the Mg-based amorphous alloy. (e) Section shape of the corrugation being along a dashed line in (d), i.e., the crack propagation direction. (f) Section shape of the corrugation being along a solid line in (d), i.e., perpendicular to the crack propagation direction. Reprinted figures with permission from reference[438], copyright (2007) by the American Physical Society.

In the framework of the RFOT theory [30, 41, 43], density fluctuation is the intrinsic feature of a heterogeneous supercooled liquid, which can be inherited by the corresponding glass after glass transition. Wisitsorasak and Wolynes[439] recently extended the RFOT theory to study the formation of shear bands in amorphous alloys. **Fig.73** shows the deformation fields in the typical Vitreloy 1 amorphous alloy at various shear strains. Their results indicate that the applied stress can cause the fluctuation in local atomic mobility to intensify, ultimately giving rise to shear banding with an initial thickness of 10 nm. Their results are in good agreement with the experimental findings on amorphous alloys [440-443]. More importantly, the authors pointed out that the local regions of high atomic mobility which leads to shear band nucleation could be the same site to initiate local crystallization and cavitation. If that is the case, one may infer that STZ and TTZ are simply the mechanical response of a same local region of high atomic mobility subject to a different stress state.

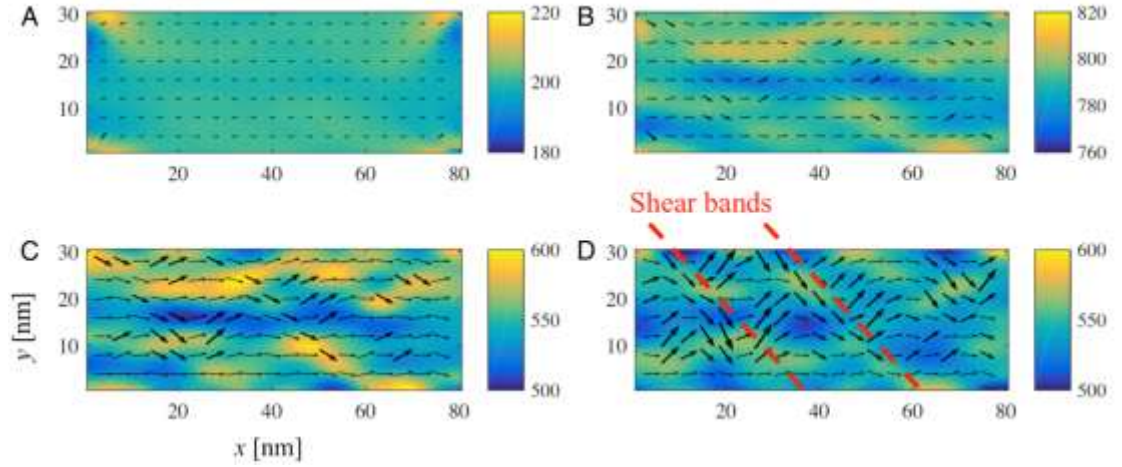


**Fig.73.** Predictions of the various deformation fields in the Vitreloy 1 model under the applied strain rate of  $0.01 \text{ s}^{-1}$  at various stages of deformation[439]. The ambient temperature  $T=643 \text{ K}$ . Each plot shows the equivalent stress overlaid with the strain field. The color bar on the right of each plot shows the magnitude of the stress in units of MPa. (A) The strain  $\epsilon=0.01$ , (B)  $\epsilon = 0.03$ , (C)  $\epsilon = 0.1$ , and (D)  $\epsilon=0.2$ . Reprinted from reference[439], with permission from Proceedings of the National Academy of Sciences of the United States of America (PNAS). Copyright (2017) National Academy of Sciences.

Based on the notion of density fluctuation or structural heterogeneity, Furukawa and Tanaka[444] developed a coarse grained continuum model to study plasticity and failure in amorphous alloys. Since amorphous alloys can be viewed as “frozen” metallic liquids, the deformation of amorphous alloys can be described by using the general Navier-Stokes constitutive equation:

$$\left(\frac{\partial}{\partial t} + \mathbf{v} \cdot \nabla\right) \boldsymbol{\sigma} - (\nabla \mathbf{v}^\dagger \cdot \boldsymbol{\sigma} + \boldsymbol{\sigma} \cdot \nabla \mathbf{v}) = G(\rho)(\nabla \mathbf{v}^\dagger + \nabla \mathbf{v}) - \frac{1}{\tau(\rho)} \boldsymbol{\sigma} \quad (5-8)$$

where  $\mathbf{v}$  is the velocity,  $\boldsymbol{\Pi}(r, t)$  the pressure tensor,  $\boldsymbol{\sigma}(r, t)$  the stress,  $\tau$  the structural relaxation time,  $G$  the shear modulus. Note that  $\tau(\rho)$  and  $G(\rho)$  are both functions of local density  $\rho$ . According to Furukawa and Tanaka [444], shear banding in amorphous alloys is due to the amplification of density fluctuation under mechanical deformation, which is consistent with the prediction of the RFOT theory [41, 439].

More importantly, Furukawa and Tanaka pointed out that there are three types

of mechanical instability in amorphous alloys, as demonstrated in Fig.74, which include (i) the liquid-type instability, for which the intrinsic structure relaxation time is much shorter than the characteristic deformation time scale, i.e.  $\tau_0 \ll t$ , (ii) the solid-type instability ( $t \ll \tau_0$ ), and (iii) the viscoelastic-type instability, for  $\tau_0[(\partial \ln G / \ln \rho)(\ln \tau / \ln \rho)] < t \ll \tau_0$ . Note that by increasing the applied strain rate  $\dot{\gamma}$  or reducing the temperature  $T$ , the type of mechanical instability could change gradually from the liquid-type to the viscoelastic-type and finally to the solid-type[444]. Since brittle fracture conforms to the solid-type instability, the dynamic phase diagram (Fig. 74) also suggests a temperature or rate controlled ductile to brittle transition.

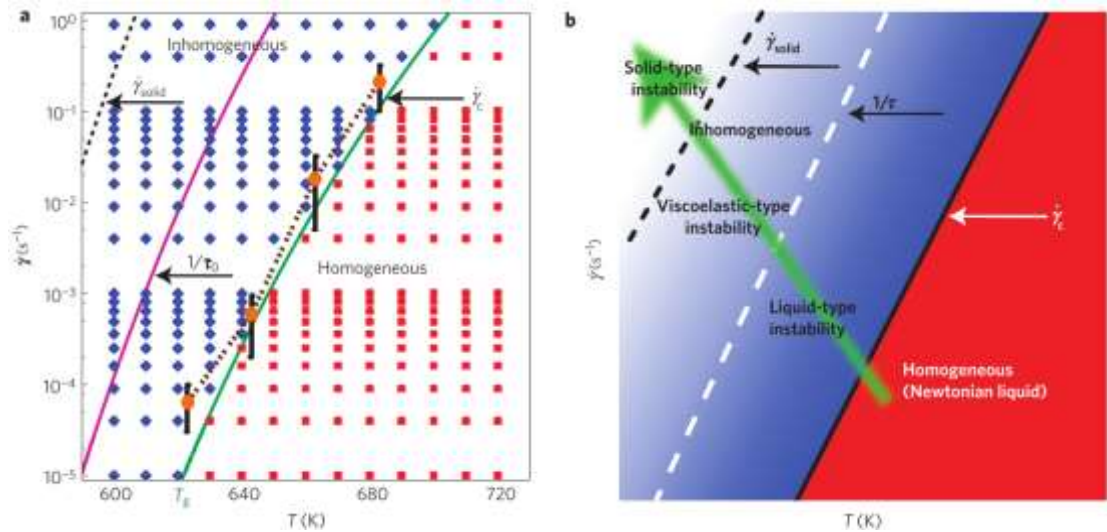


**Fig. 74.** Dynamic phase diagram for a sheared compressible viscoelastic liquid. **(a)** Dynamic phase diagram for Vitreloy 1 ( $Zr_{41.2}Ti_{13.8}Cu_{12.5}Ni_{10}Be_{22.5}$ ). The red and blue points indicate stable and unstable homogeneous states, respectively, estimated from the full numerical linear stability analysis. The black dotted curve represents  $\dot{\gamma}_{solid}$  predicted by the theory of Furukawa and Tanaka, above which the solid-type instability should occur. The green and red solid curves represent predicted critical shear rate in the viscous regime,  $\dot{\gamma}_c = (\partial \eta / \partial \rho)_T$ , and the inverse of the relaxation time,  $1/\tau_0$ , respectively. The orange circles represent the experimentally observed crossover shear rates  $\dot{\gamma}_c$  from Newtonian to non-Newtonian shear thinning behavior[445]. **(b)** Schematic dynamic phase diagram. Reprinted by permission from Nature Materials, reference[444], copyright (2009).

According to the dynamic phase diagram shown above (Fig. 74), the physical

origin of shear banding in amorphous alloys subject to a conventional strain rate is likely to be a viscoelastic-type instability. Recently, Liu et al. studied shear banding in amorphous alloys at a constant stress in microcompression [446]. Their results clearly showed that, prior to shear banding, the amorphous alloys already flowed as a viscous liquid and the measured overall viscosity fell in the range between  $10^{11}$  to  $10^{14}$  Pa s, which decreased with the increasing applied stress as shown in Fig.75. This experimental finding corroborates the theoretical prediction based on density fluctuation in amorphous alloys [444] and is also consistent with the view that yielding in amorphous alloys is essentially a phenomenon of stress induced glass transition in conventional mechanical tests [447].

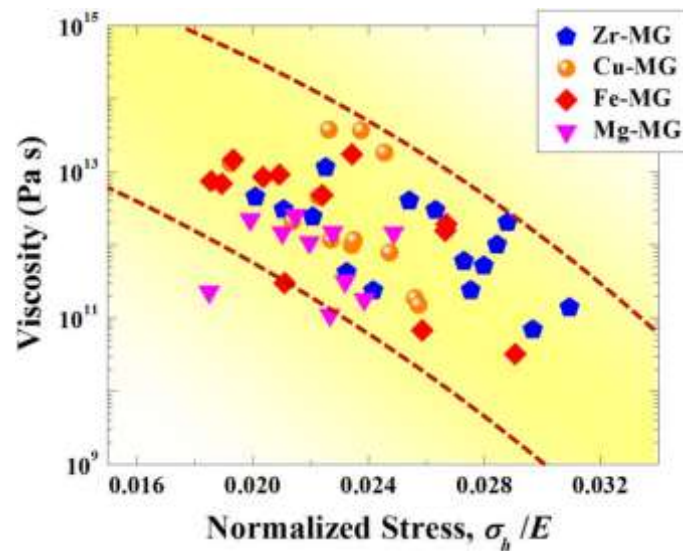


**Fig.75.** The extracted viscosity of the steady-state viscous flow showing a “shear thinning” behavior of the different types of amorphous alloys prior to shear instability[446]. Reprinted from reference[446], with the permission of AIP Publishing.

Aside from the dynamic phase diagram constructed by Furukawa et al. [444] (as shown in Fig. 74), Yu et al. [448] also developed a deformation mode map based on the  $\beta$  relaxation temperature of the La-based amorphous alloy, which is quite similar to Fig. 74 and shown in Fig. 76. According to Yu et al.[448], the critical temperature

and strain rate that trigger the ductile to brittle transition follow the Arrhenius equation, which yields an activation energy identical to that for the slow  $\beta$  relaxation in the amorphous alloy. This finding is very important, which suggests that plastic flow in amorphous alloys could be intrinsically correlated with the slow  $\beta$  relaxation in the amorphous alloy. In other words, the local region of high atomic mobility could be the source of slow  $\beta$  relaxation. More importantly, Yu et al. [448] found that the La-based amorphous alloy is of a heterogeneous amorphous structure and the length scale that characterizes the heterogeneity is around 100 nm, as shown in Fig. 77.

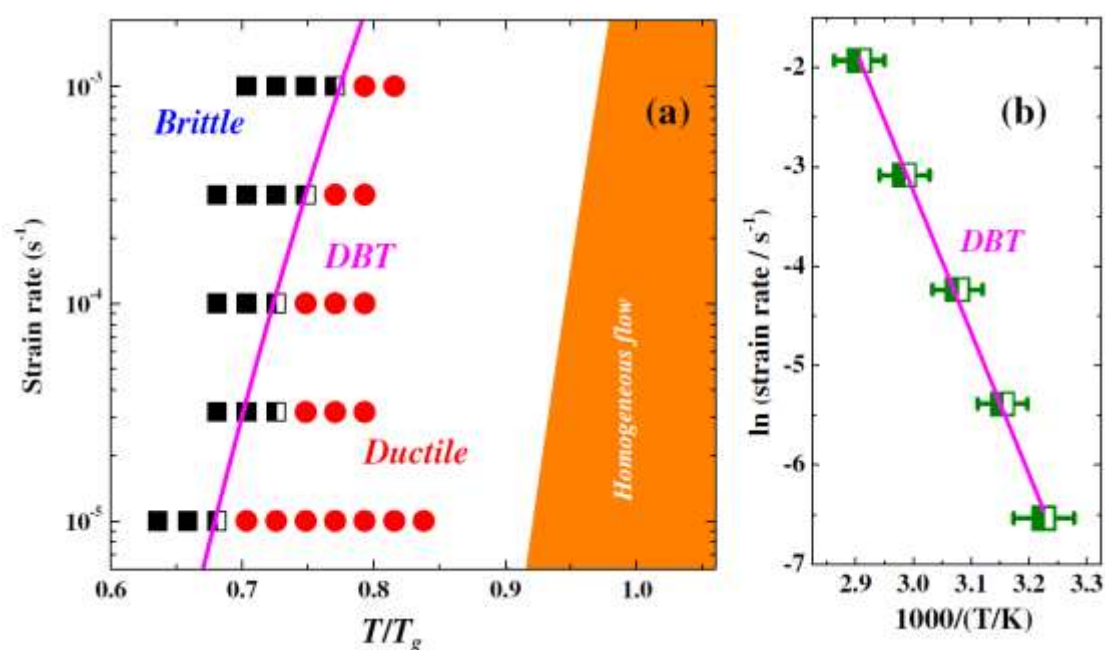


**Fig.76.** (a) The deformation mode map summarizing the tension tests at different temperature and strain rates; the filled squares denote the brittle fracture while filled circles are for the ductile fracture, and the ductile to brittle transition (DBT) is represented by half-filled squares. (b) The temperature and strain rate dependence of the temperature of DBT and fitted with the Arrhenius relation. Reprinted figures with permission from reference [448], copyright (2012) by the American Physical Society.

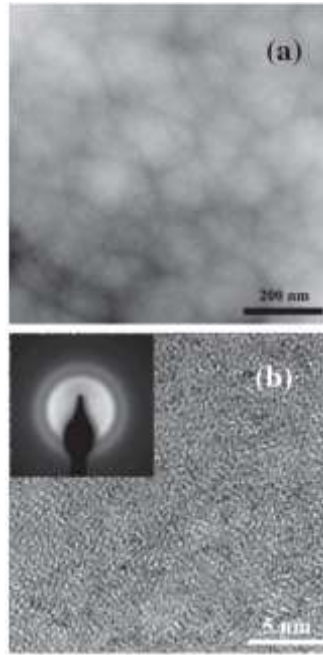


**Fig.77.** (a) A scanning transmission electron microscope (TEM) image of the as-cast  $\text{La}_{68.5}\text{Ni}_{16}\text{Al}_{14}\text{Co}_{1.5}$  amorphous alloy. (b) A high-resolution TEM micrograph of the as-cast  $\text{La}_{68.5}\text{Ni}_{16}\text{Al}_{14}\text{Co}_{1.5}$  amorphous alloy; the inset shows the selected-area electron diffraction. Reprinted figures with permission from reference [448], copyright (2012) by the American Physical Society.

However, in contrast to [Fig. 74](#) and [Fig. 76](#), Wang et al. [35] recently found that plasticity of amorphous alloys can be significantly improved at a particular temperature far below the room temperature, as seen in [Fig. 29\(a\)](#). This plasticity improvement at the low temperature is due to multiple shear banding and, more interestingly, this particular temperature is almost identical to the temperature of the fast  $\beta$  relaxation. Since the activation energy for the fast  $\beta$  relaxation is identical to that for anelasticity, this finding [[Fig. 29\(a\)](#)] prompted the idea that the elementary source of plasticity in amorphous alloys should be the local liquid-like regions that are responsible for the anelastic deformation or the elastic modulus reduction as discussed in [Section 5.1](#). In a such case, one can infer that elasticity and plasticity in amorphous alloys should be intrinsically correlated. Based on the experimental results on the slow and fast  $\beta$  relaxations, Wang and his co-workers further discovered that the

brittle and ductile amorphous alloys are indeed characterized by the ratio of the activation energy of fast ( $E_{\beta'}$ ) to slow  $\beta$  relaxation ( $E_{\beta}$ ). The insight that can be drawn from **Fig. 29(b)** is that the lower is the  $E_{\beta'}/E_{\beta}$  ratio the easier is to activate local liquid-like sites and, therefore, the better is the overall plasticity.

With the nanoindentation based dynamic modulus mapping (DMM) technique, Flores and co-workers revealed the elastic heterogeneity in a Zr-based amorphous alloy[449]. **Fig.78** shows the K-means clustering analysis for such an elastic microstructure in the Zr-based amorphous alloy. Interestingly, these authors found that the elastic microstructure is sensitive to the energy state of the amorphous alloy, which however exhibits a length scale of  $\sim 100$  nm. Notably, this length scale of the elastic modulus fluctuation is in good agreement with the length scale found for the density fluctuation within a shear band [431] or the length scale for shear band nucleation [423]. In general, this finding is consistent with the physical picture that shear banding in amorphous alloys should result from and, therefore, is closely connected with the density fluctuation or structural heterogeneity in amorphous alloys.

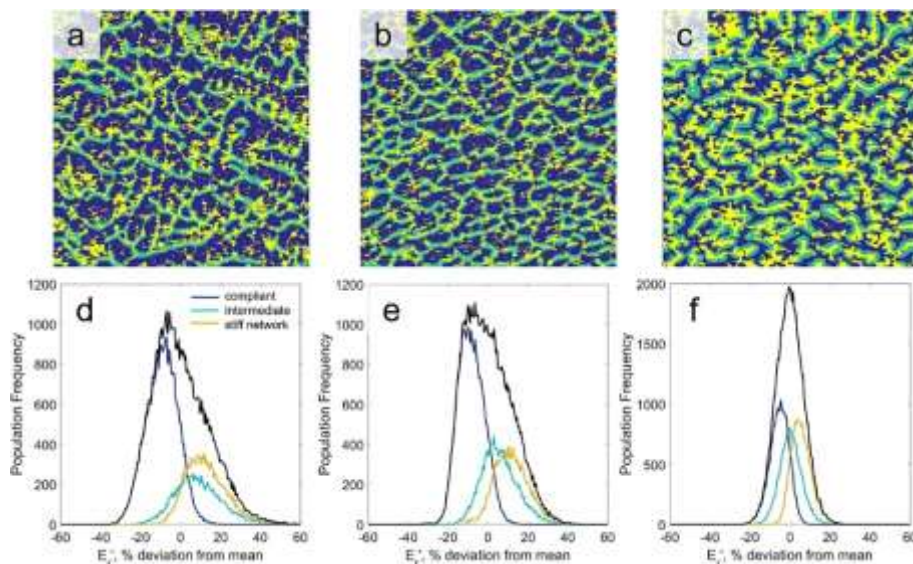


**Fig.78.** K-means clustering analysis for characterization of elastic microstructure[449]. (a-c) Example tricolor representations of the modulus maps with the pixels grouped according to the modulus category (blue = compliant, green = intermediate, and

yellow = stiff). Image (a) is from the central location of an as-cast sample, (b) is from the central location of the sample post-annealing, and (c) represents the map obtained from the sample pulsed with a 180 W laser. (d-f) Corresponding deconvolved histograms, showing the overlapping distribution of the storage modulus  $E_r'$  for the three categories of features. Reprinted from reference[449], copyright (2017), with permission from Elsevier.

Aside from density fluctuation, structural heterogeneity—could also manifest as chemical fluctuation, which has a profound effect on the plasticity of amorphous alloys with phase separation. In 2007, Du et al. [450] showed that plasticity can be significantly improved in two-glass-phase amorphous alloys. Physically, the chemical fluctuation originates from liquid phase separation and can be engineered by carefully controlling the chemical composition of amorphous alloys [451], as shown in **Fig. 79**. The reported length scale for the structural heterogeneity derived from chemical fluctuation ranges from 10 to 100 nm [450, 452, 453], which is similar to the length scale derived from density fluctuation. Regardless of the nature of structural heterogeneity (density versus chemistry), the general trend is that plasticity can be enhanced with the increasing degree of structural heterogeneity. Indeed, this view was already discussed in the early search for ductile amorphous alloys[212, 214, 454].

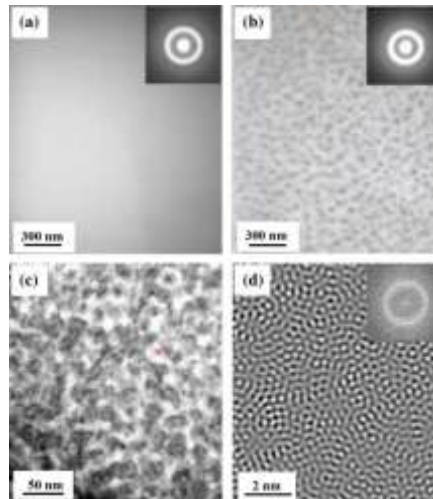


**Fig. 79.** Bright-field (BF)-transmission electron microscopy (TEM) images and selected-area diffraction patterns (SADPs) for the  $\text{Cu}_{47.2}\text{Zr}_{46.5}\text{Al}_{5.5}\text{Nb}_{0.8}$  amorphous alloy: (a) As-spun ribbon and (b) as-cast rod 2 mm in diameter. (c) Scanning transmission electron microscopy (STEM)-BF image showing the phase-separated

structure of as-cast rod 2 mm in diameter. (d)Inverse Fourier filtering (IFF) image showing an amorphous structure (inset is fast Fourier transformed image). Reprinted from reference[451], copyright (2014), with permission from Elsevier.

#### 5.4. Tuning structural heterogeneity for enhanced mechanical properties

Based on our previous discussions, it is clear that the mechanical properties of amorphous alloys are strongly affected by their density and/or chemical fluctuations. Now, we would like to discuss in this section the possible approaches people can utilize to tune the structural heterogeneity in order to enhance the mechanical properties of the amorphous alloys. According to the RFOT theory [30, 41-43, 314], the length scale  $\xi$  for the density fluctuation in a supercooled liquid at the temperature  $T$  can be written as:

$$\xi \sim \left( \frac{1}{T-T_K} \right)^{\frac{1}{d-\theta}} \quad (5-9)$$

where  $T_K$  is the Kauzmann temperature,  $d$  the Euclidean dimension of the overall heterogeneous liquid and  $\theta$  the dimension that characterizes the fractal shape of local “homogeneous” liquid droplets. Since the heterogeneous structure of the supercooled liquid can be quenched-in in its corresponding glass upon glass transition, Eq. (5-9)

suggests that the length scale  $\xi_{glass}$  in a glass scales with  $\xi_{glass} \sim \left( \frac{1}{T_g-T_K} \right)^{\frac{1}{d-\theta}}$ . As such, this length scale  $\xi_{glass}$  can be tuned by altering the thermal or thermomechanical history of the glass. Furthermore, one could also infer from the above equation that structural heterogeneity should vanish in amorphous alloys with  $T_g \gg T_K$  ( $\xi_{glass} \sim 0$ ) or with  $T_g \approx T_K$  ( $\xi_{glass} \rightarrow infinity$ ). Given such a large variation in  $\xi_{glass}$ , it seems that there is a large window to control the structural heterogeneity. However, it is known that the glass transition temperature  $T_g$  of laboratory prepared amorphous alloys can hardly vary by a significant amount with simple and conventional methods, such as changing the cooling rate. Therefore, new approaches are needed to tune the structural heterogeneity of amorphous alloys.

### 5.4.1 Cryogenic thermal cycling

In 2018, Ketov et al. showed that amorphous alloys can be rejuvenated by subjecting them to thermal cycling between ambient temperature and liquid nitrogen temperature (77K) [455]. The degree of rejuvenation depends on the number of thermal cycles as well as the initial energy state of the sample. As a result, the cryogenic thermal cycling led to a significant increase in the exothermal heat reaction below the glass transition temperature  $T_g$ , indicative of rejuvenation as shown in **Fig. 80 (a)**. In accord with the rejuvenation, the compressive plasticity of the thermally cycled amorphous alloy increased by around 50 % [**Fig. 80(b)**]. To rationalize these results, these authors conjectured that amorphous alloys are essentially inhomogeneous at the nanometer scale and contain local regions of varying thermal expansion coefficient. Consequently, the cryogenic thermal cycling leads to local thermal stress and local plastic strain, and hence introduces more structural heterogeneities in terms of a higher concentration of flow “defects” or soft spots, being illustrated as the dark regions in **Figs.80 (c)-(e)**, which then improves the overall plasticity of the amorphous alloy.

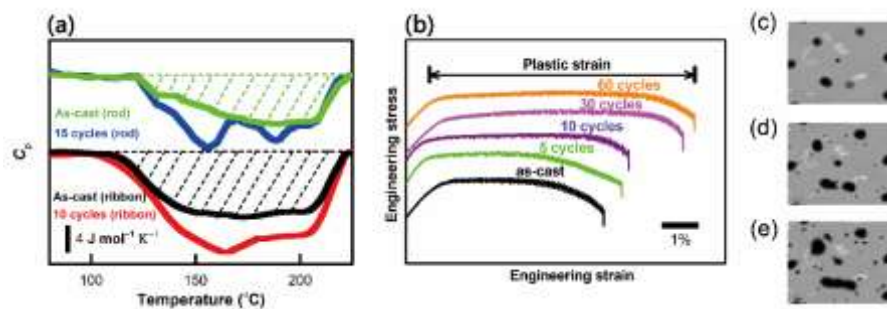


**Fig. 80.** (a) Specific heat  $C_p$  increased after thermal cycles (from room temperature to 77 K) of melt-spun ribbons of  $\text{La}_{55}\text{Ni}_{20}\text{Al}_{25}$  and bulk rods of  $\text{La}_{55}\text{Ni}_{10}\text{Al}_{35}$  amorphous alloys [456]. (b) Effect of thermal cycling treatment (338 K to 77 K thermal cycles) on  $\text{Zr}_{62}\text{Cu}_{24}\text{Fe}_5\text{Al}_9$  amorphous alloy. Schematic depictions of the degree of heterogeneity in an amorphous alloy in the as-cast state (c), and after increasing numbers of thermal cycles [(d), (e)]. The population and intensity of soft spots (dark), with lower elastic stiffness and higher coefficient of thermal expansion increases with cycling. Reprinted by permission from Nature, copyright (2015).

The hypothesis of Ketov et al. suggests that their rejuvenated amorphous alloy should be more heterogeneous than the relaxed counterpart. If this was true, one might infer that fast quenching could introduce more heterogeneities in laboratory prepared amorphous alloys. **Fig. 81** shows the recent finding of Zhu et al. on the cooling rate on the structural heterogeneity in the Zr-based amorphous alloy[6]. Clearly, the hyper-quenched amorphous alloy appear more heterogeneous than the relaxed one over the length scale of 5 nm. To a certain extent, this is consistent with the hypothesis of Ketov et al.[456]. However, one should be cautious that there is no necessary correlation between rejuvenation and structural heterogeneity. Indeed, all glasses are heterogeneous according to the RFOT theory [41]. In principle, rejuvenation of a glass can elevate the glass transition temperature  $T_g$  and therefore

lowers down the characteristic length scale  $\xi_{\text{glass}}$  given that  $\xi_{\text{glass}} \sim \left( \frac{1}{T_g - T_K} \right)^{\frac{1}{d-\theta}}$ .

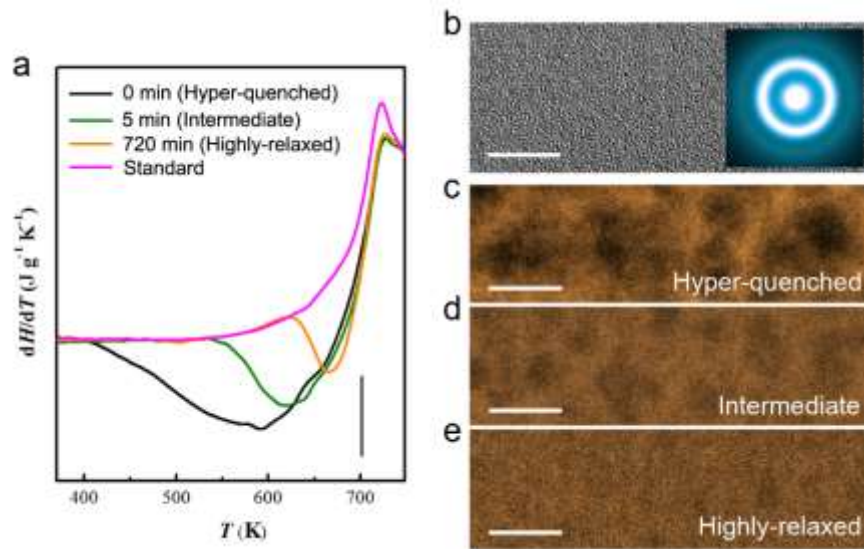


**Fig. 81.** Spatial heterogeneity of metallic glasses with different thermodynamic statuses[6]. (a) Heat flow traces of the as-prepared hyper-quenched sample and the samples annealed at 553 K ( $\sim 0.8T_g$ ) for 5 min (intermediate) and 720 min (highly relaxed). The heat flow trace of a standard samples is also plotted for reference. Scale bar, 0.2. (b) High-resolution TEM (HRTEM) image of the hyper-quenched metallic glass. The inset is the corresponding selected area electron diffraction pattern. Scale

bar, 5 nm. High-angle annular dark-field scanning TEM (HAADF-STEM) images of (c) the hyper-quenched, (d) the intermediate and (e) the highly relaxed samples. Scale bar, 5 nm. Reprinted by permission from Macmillan Publishers Ltd: Nature Communications, reference[6], copyright (2018).

In 2013, Saida et al. developed a novel recovery-annealing technique to rejuvenate a pre-relaxed  $Zr_{55}Al_{10}Ni_5Cu_{30}$  amorphous alloy [457]. They found that, once the relaxed amorphous alloys were reheated to a certain temperature above  $T_g$ , their glassy structure can be reset and the final state of the samples depended on the cooling rate just after the annealing. Later, Guo et al. applied the same technique to obtain a rejuvenated  $Cu_{47.5}Zr_{47.5}Al_5$  amorphous alloy [458]. Interestingly, they found that the rejuvenated samples were more brittle than the relaxed counterparts. Following Ketov et al.[456], deep cryogenic cycling treatment (DCT) was recently developed in light of its possibility for enhanced rejuvenation of amorphous alloys. To conduct DCT, amorphous alloys are cyclically cooled and heated between ambient and cryogenic temperature [459, 460]. Guo et al. applied DCT on the  $Zr_{55}Cu_{30}Al_{10}Ni_5$  amorphous alloy [459], and attempted to calculate the internal stress upon DCT which may contribute to the rejuvenation behavior based on the notion of structural heterogeneity. Their major finding is that the initial structure of glass before DCT plays an important role in rejuvenation and its effect on plasticity [461]. Lowering the casting temperature for a more initially relaxed glass can effectively improve the degree of rejuvenation. These authors also applied DCT on the Mg-based amorphous alloy[462]. Unfortunately, no macroscopic plasticity improvement could be observed.

Compared to other possible rejuvenation methods, such as severe plastic deformation, ion irradiation and shot peening, cryogenic thermo-cycling has several technical advantages[456]: it is non-destructive, does not lead to sample shape change and structural anisotropy, can be applied to any shape of sample (thin film, ribbon and bulk amorphous alloys), and does not lead to macroscopic internal stress and plastic strain. Most importantly, it is easy to control and the occurring internal stress is local

and far below the elastic limit of the amorphous alloy to be treated.

## 5.4. 2 Surface treatment

Aside from cyogenic thermal cycling, one can also improve the mechanical properties of amorphous alloys through various surface treatments. At the fundamental level, surface of glasses is softer and more liquid like than bulk [463] and therefore much easier to be altered in terms of its structure and mechanical properties. Recently, Wang et al. demonstrated that the surface of amorphous alloys can be easily softened or “rejuvenated” through contact resonance ultrasonic actuation (CRUA) [464] [Fig. 82(a)]. These authors hypothesized that, under the resonance actuation, atoms near the surface with a large vibration amplitude can reach higher energy states in the energy landscape, thereby reducing the local packing density and the local elastic modulus, as shown in Fig. 82(b). Furthermore, it was found that the size, pattern and extent of the local softened or “rejuvenated” zones could be tailored by adjusting the CRUA parameters. Interestingly, the local rejuvenation as reported by Wang et al. might be keyed to the fast  $\beta$  relaxation of amorphous alloys because the frequency of CRUA is close to that of the fast  $\beta$  relaxation ( $10^5 - 10^6$  Hz) at room temperature [35]. After CRUA, further nanoindentation tests revealed that shear band nucleation can be facilitated.

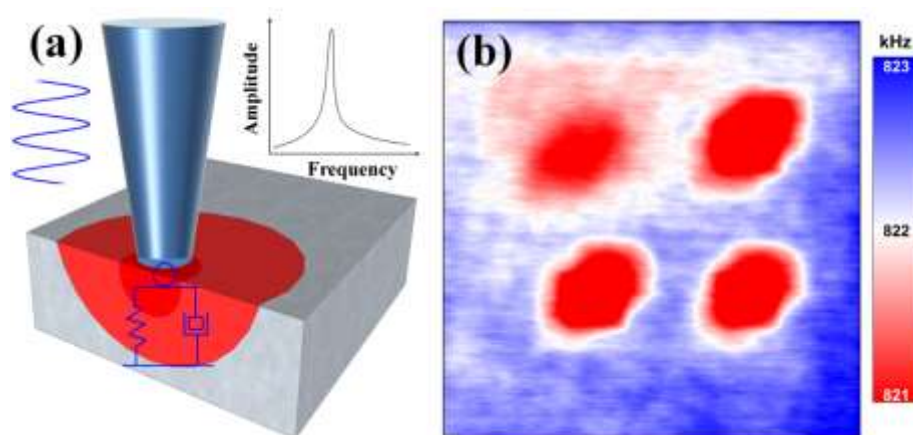


**Fig. 82.** (a) Schematic illustration of CRUA. The probe of AFM contacts with the surface of sample and vibrates in a resonance mode at the frequency of  $10^5$ -  $10^6$  Hz. (b) Map of the contact resonance frequency of the sample after CRUA for four positions. The lower contact resonance frequency implies the decreasing of elastic modulus for the treated sites, which corresponds to the local structural rejuvenation [464]. Reprinted figures with permission from reference, copyright (2017) by the American Physical Society.

Like shot-peening, surface mechanical attrition treatment (SMAT) is another low-cost surface processing technique, which could be applied on amorphous alloys to improve their mechanical properties. As discussed in reference [465], the SMATed amorphous alloy could show a pronounced tensile ductility even at room temperature, which is rare on the as-cast samples. It was envisioned that SMAT can severely deform the amorphous structure near its surface, causing the liquid-like atoms to percolate and enhance the structural heterogeneity nearby [466]. **Fig.83** shows the network-typed amorphous structure in the 25-minute SMATed  $\text{Cu}_{46}\text{Zr}_{47}\text{Al}_7$  amorphous alloy (**Fig.83** (b)-(d)). Note that the volume fraction of low density regions, manifested as the bright regions in **Fig.83** (b)-(d), can reach up to 50~70% near the surface after SMAT. As a result, structural heterogeneity increases, which promotes the atomic mobility and finally leads to a tensile plasticity in the SMATed amorphous alloys (as shown in **Fig.83** (f)). Ion irradiation is another technique that can tailor the mechanical properties of amorphous alloys through local rejuvenation. Magagnosc *et al.* [467] reported an increase in ductility and reduction in the yield stress of the  $\text{Pt}_{57.5}\text{Cu}_{14.3}\text{Ni}_{5.7}\text{P}_{22.5}$  amorphous alloy nanowires after ion irradiation, which leads to softening and a more heterogeneous structure [468].

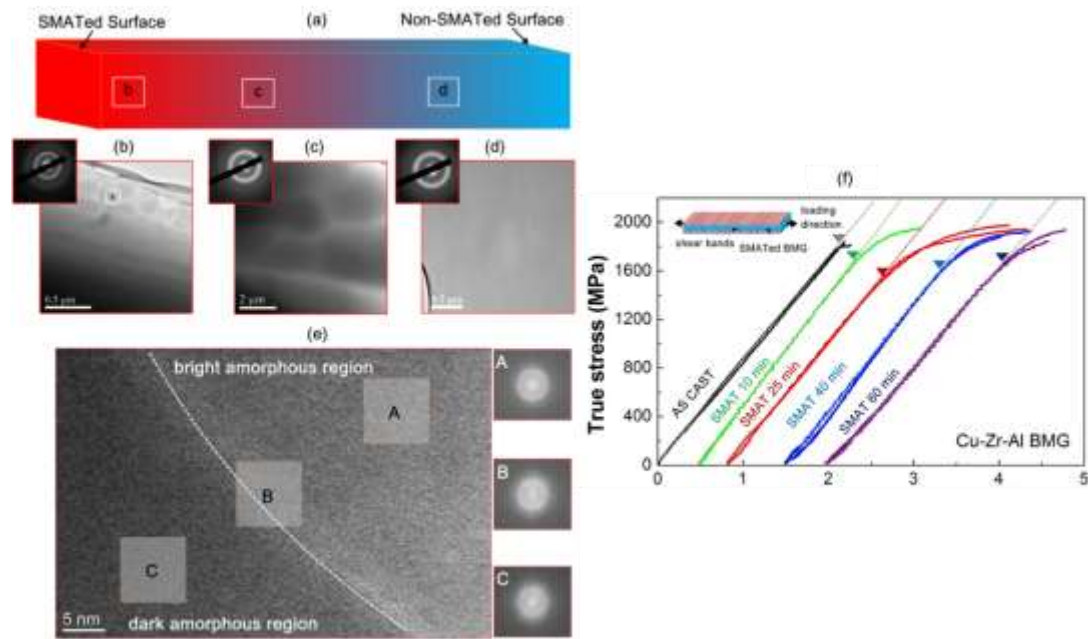


**Fig. 83.** The gradient amorphous structure in the 25-minute treated amorphous alloy[466]. (a) the schematics showing the SMATed amorphous alloy undergoing a varying degree of structural evolution at the different distances to the impacted surface, (b)-(d) the TEM images of the atomic structure at the different depths [inset = the selective area electron diffraction (SAED) pattern], and (e) the HRTEM image of the amorphous structure shown in (b). The inclined dashed line indicates the boundary between the dark amorphous region and the bright amorphous boundary-like region. The FFT patterns taken from the three random sites, labeled as A, B, and C, confirm that the atomic structures are all structurally amorphous. Reprinted by permission from Macmillan Publishers Ltd: Scientific Reports, reference[466], copyright (2014).

### 5.4.3 Liquid-liquid phase separation

Through liquid-liquid phase separation, chemical heterogeneity can be induced in amorphous alloys before glass transition occurs [92, 469, 470]. This is usually achieved by including in a metallic liquid atom pairs of large positive enthalpy of mixing. As a result, various types of amorphous microstructures, such as the droplet (**Fig. 84 (a)**[469]) or interconnected type (**Fig. 84 (b)**[471]) microstructure, can be formed in amorphous alloys upon quenching. Similar to density fluctuation, chemical fluctuation originating from phase separation occurs over a length scale ranging from

10 to 100 nm. In bulk amorphous alloys, such chemical fluctuation facilitates shear band formation [472] and even nanocrystallization[213], which leads to superior plasticity which is hardly seen in chemically homogeneous amorphous alloys. Furthermore, the recent study by He et al. [473] showed that the interplay between shear banding and chemical heterogeneity in the Zr-based bulk amorphous alloy could be rather complex, entailing structural evolution during shear band propagation (see Fig. 85).

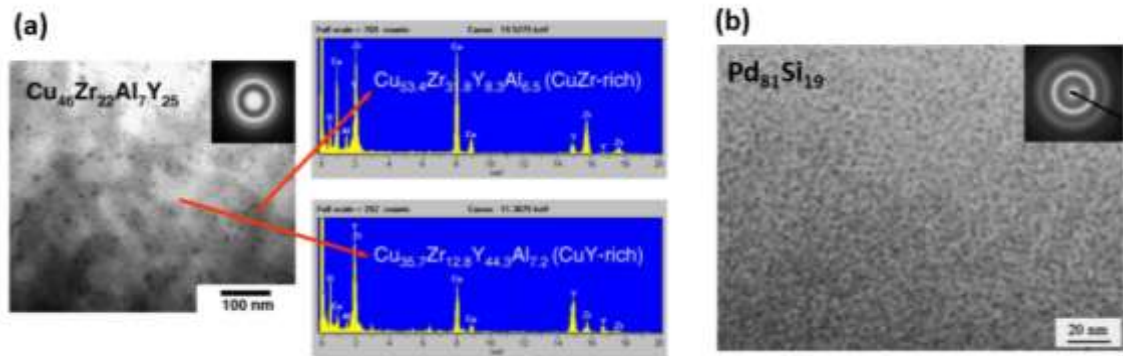


**Fig. 84.** (a) TEM bright-field image, selected area diffraction pattern (SADP), and EDS results obtained for the as-spun  $\text{Cu}_{46}\text{Zr}_{22}\text{Y}_{25}\text{Al}_7$  ribbon. Reprinted from reference[469], copyright (2006), with permission from Elsevier. (b) The bright field TEM image of the as-prepared  $\text{Pd}_{81}\text{Si}_{19}$  binary amorphous alloy, shows a fine networklike contrast morphology with a length scale of 3–6 nm. The inset is the related selected area electron diffraction (SAED) pattern. Reprinted from[471], with the permission of AIP Publishing.

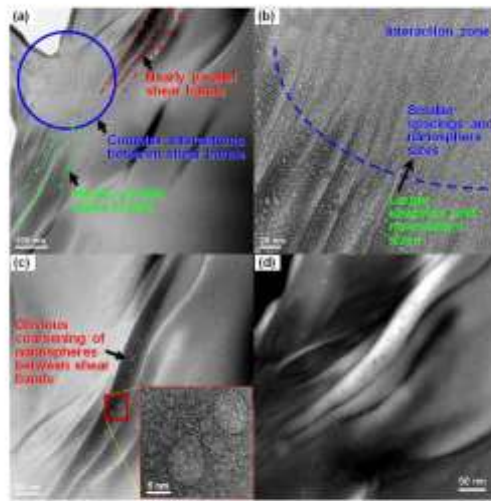


**Fig.85.** (a) TEM image of  $(\text{Fe}_{0.45}\text{Cu}_{0.55})_{33}\text{Al}_8\text{Zr}_{59}$  amorphous alloy compressed uniaxially to a thin-disc shape ( $\sim 110\%$  plastic strain), showing numerous shear bands (lines) and an interaction zone (circle). (b,c) HRTEM micrographs of the shear bands near the green and red lines in (a). The inset in (c) is a higher-magnification image of the region marked by the red rectangle. (d) STEM image corresponding to the TEM image in (c), further verifying chemical heterogeneity[473]. Reprinted by permission from Macmillan Publishers Ltd: Scientific Reports, reference[473], copyright (2016).

#### 5.4.4. Nanograined amorphous alloy (nano-glass)

Aside from quenching from metallic liquids, amorphous alloys can be also obtained through the consolidation of nano-sized glassy droplets, as first reported by Jing et al. in 1989 [474]. This generates a nano-grained morphology, which looks similar to nanocrystalline alloy, but without any crystallinity inside the nanograins, as illustrated in **Fig.86**. The amorphous alloys so obtained were also termed as

nano-glass (NG). Conceptually, it was perceived that the inter-granular phases between two amorphous nano-grains should be of a low density[475] or full of excess free volume[476, 477], which brings about a density fluctuation analogous to that caused by shear banding in an otherwise homogeneous glassy structure (**Fig. 86**). In other words, the density fluctuations in NGs could go far beyond those in regular un-deformed amorphous alloys. According to the recent work of Liu et al.[478], the volume fraction of low density regions or the so-called liquid-like sites can reach ~29% in the  $\text{Sc}_{75}\text{Fe}_{25}$  NG, which is very close to the theoretical limit of ~25% according to the atomic stress theory [265, 479]. More importantly, compared to rapid cooling, one can more easily tune the nanostructure of NGs through the inert-gas condensation (IGC) technique. As of today, NGs with various chemical compositions have been synthesized [480-482].

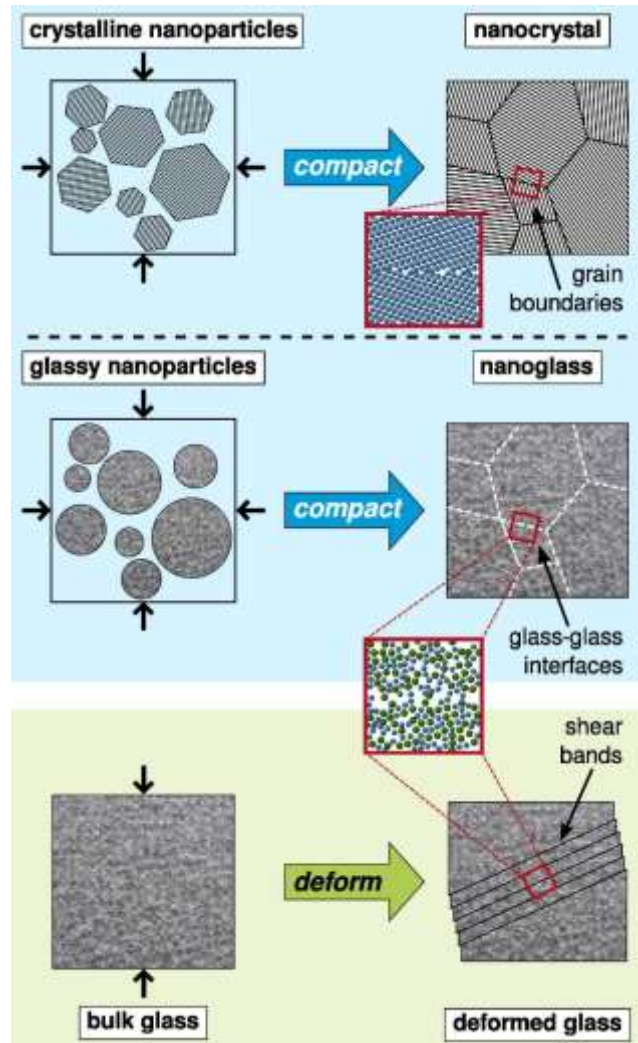


**Fig.86.** Different ways for tuning the structure of amorphous alloys: nanoglasses containing grain-boundary-like interfaces can be obtained by powder consolidation (middle), similar to the synthesis of nanocrystalline materials (top). Another approach to modifying the glass structure is to introduce shear bands by pre-plastic deformation (bottom). Both shear bands and interfaces are planar defects with modified topology[476]. Reprinted from reference[476], copyright (2011), with permission from Elsevier.

Given the engineered structural heterogeneity in NGs, considerable research has been dedicated to studying the effect of structural heterogeneity on the mechanical properties of amorphous alloys. Sopy et al. revealed that the low density inter-granular phases can act as preferred regions for the formation of shear bands [483]. Through molecular dynamics simulations, Adibi et al. found a drastic change in

the deformation mode of NGs, from a single shear band ( $d \sim 15$  to  $10$  nm), to cooperative shear failure ( $d \sim 10$  to  $5$  nm) and to homogeneous superplastic flow ( $d \sim 5$  nm), as shown in Fig. 87 (a-b) [484]. These simulation results suggest that the glassy grain size can be an effective design parameter to tune the plasticity of amorphous alloys, which is supported by the recent experimental result of Wang et al. [485]. However, compared to regular amorphous alloys, the presence of a large density fluctuation also reduces the yield strengths of NGs [475, 480, 481, 485-488]. Mechanistically, this softening effect can be attributed to the shear band widening in NGs [486, 489]. Very recently, Sha et al. proposed that NGs with the superior ductility could be used to toughen amorphous alloys or to make the so-called NG-MG nanolaminate composites. They evaluated the effects of NG layer thickness and separation as well as the loading direction on the mechanical properties of NG-nanolaminate composites [490, 491] and identified the most effective MG-NG nanolaminate structure that has the best combination of overall plasticity and failure stress [490]. These results indicate that NGs could be a promising structural material, particularly useful for micro- and nano-devices.

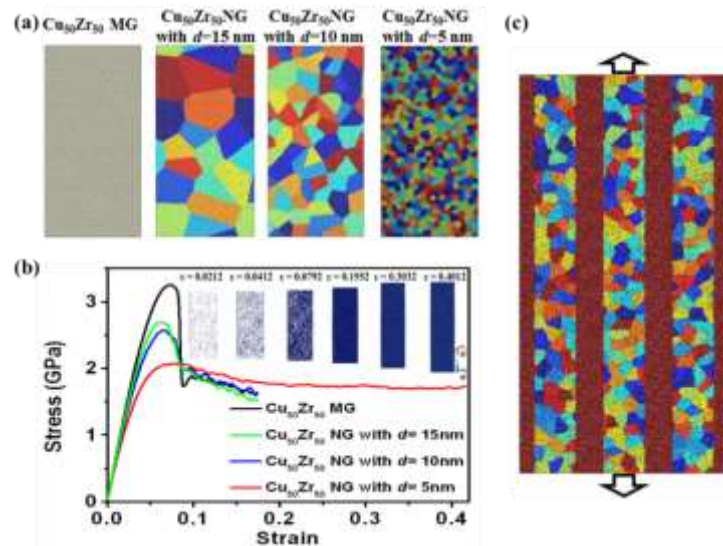


**Fig. 87.** (a)  $\text{Cu}_{50}\text{Zr}_{50}$  amorphous alloy and  $\text{Cu}_{50}\text{Zr}_{50}$  NG with average glassy grain sizes  $d = 15$ ,  $10$ , and  $5$  nm. Grains are shown in different colors to highlight the

architectures [484]. Reprinted from [484], with the permission of AIP Publishing. (b) Engineering tensile stress-strain curves for NG with  $d = 15, 10,$  and  $5$  nm, as well as for the MG. A drastic change in the mechanical response of NG (from localized shear banding to homogeneous plastic deformation) is observed by decreasing  $d$  from 15 to 5 nm. The large strain ( $>0.4$ ) attained by  $d = 5$  nm NG indicates super plasticity. The inset shows a sequence of snapshots that capture the deformation process for the NG with  $d = 5$  nm. The colors indicate the atomic shear strain [484]. Reprinted from [484], with the permission of AIP Publishing (c) Atomic configuration of MG-NG nanolaminate composite [490]. Reprinted from reference [490]. Copyright (2017), with permission from Elsevier.

## 6. Summary and outlook

In the current review article, we discussed the state-of-art research on the mechanical behavior and structural heterogeneities in amorphous alloys, with a focus on the use of mechanical relaxation to probe such heterogeneities. From a theoretic viewpoint, structural heterogeneities are intrinsic to supercooled liquids and inherited by the corresponding glasses upon rapid cooling. Various theories about glass transition, such as the RFOT [30, 41, 314, 439] or the two-order parameter model [46-48, 58, 315], were developed over the past decades to understand the thermodynamic origin of structural heterogeneities in supercooled liquids. General speaking, these models are supported by the recent experimental and computational work on metallic liquids [30, 439, 492-494].

In theory, the structural heterogeneity in amorphous alloys can be viewed as a quenched-in structural feature from the supercooled metallic liquids, which is characterized by either density or chemical fluctuation or both. Upon mechanical agitations, such structural heterogeneities could manifest as a wide distribution of local elastic moduli, local energy dissipation, local hardness or local viscosity. At the fundamental level, these fluctuations in the local properties can be amplified under mechanical loading, thereby causing mechanical instabilities [444] and yielding of amorphous alloys. This physical picture about yielding and plasticity is in sharp contrast to the classic mean field model, such as the free volume [67, 207] or STZ

model [78, 215], and could be formulated within the framework of the Navier-Stokes equation after taking density fluctuations into account. Here, it may be worth mentioning that different definitions of “flow defects” were recently proposed in the amorphous alloy literature in order to understand the origin of yielding in amorphous alloys. However, from the perspective of structural heterogeneity, local plasticity events are simply their responses to external mechanical loadings. Furthermore, the occurrence of the local plasticity events could appear stochastic because of many-body interactions and the form of these events could vary with the local stress tensor. As of today, it is still a challenging issue to trace back the structural origin of these local plasticity events, if there is any, in amorphous alloys. In our opinion, if plasticity of amorphous alloys is governed by the Navier-Stokes equation, it would be difficult to pinpoint a particular static geometric order or disorder as the origin of plasticity in amorphous alloys because a “flowing” amorphous structure must evolve constantly as dictated by the Navier-Stokes equation.

Under thermal agitations, such as in a typical mechanical relaxation experiment, amorphous alloys exhibit secondary relaxation modes. In the literature, these secondary relaxation modes were usually associated with the structural heterogeneities in amorphous alloys. Many investigations also indicated that the secondary relaxation in amorphous alloys is sensitive to physical aging and heat treatment. Interestingly, it was recently found that amorphous alloys could possess two secondary relaxation modes. This finding is intriguing, which suggests that the structural heterogeneity in amorphous alloys could be multi-scaled and even hierarchical. However, it remains unclear whether or under what conditions such a multi-scaled structural heterogeneity could be beneficial or detrimental to the mechanical properties of amorphous alloys.

Based on the results documented in the literature, it is reasonable to conclude that secondary relaxation modes in amorphous alloys could result either from the rattling motions of atoms within an elastic cage or from the string-like cooperative

motion of atoms after their escape from the elastic cage. However, this is a rather local view of dynamic heterogeneity in amorphous alloys, which occurs over a length scale of a few atomic distances ( $\sim 1$  nm) at most. Notably, this is far below either the length scale for density/chemical fluctuations or the length scale for shear band formation (10-100 nm) in amorphous alloys. Further research is therefore needed to decode the signals of secondary relaxation, such as the peak, width and skewness of a relaxation profile, in light of its possible connections with the heterogeneities at different length scales.

From the structural perspective, plasticity of an amorphous alloy can be improved if it could be enhanced with the help of rejuvenation, surface treatment and liquid-liquid phase separation. However, it is worth noting that rejuvenation and surface treatment do not necessarily lead to plasticity improvement if both methods fail in enhancing structural heterogeneity. A systematic study is still needed to study the structural evolution in amorphous alloys subject to different thermal or thermo-mechanical treatments. In terms of the volume fraction of low density regions, nano-glass or nano-grained amorphous alloy, obtained via inert gas condensation, exhibit a higher degree of structural heterogeneities than regular amorphous alloys. Most importantly, the structural heterogeneities of nano-glass can be easily tuned and altered, thereby enabling a systematic study of structure-property correlation in amorphous alloys.

Finally, we would like to reiterate that, according to the RFOT theory [41, 43, 439], the length scale of structural heterogeneity varies with the thermal history of amorphous alloys. Therefore, it is likely that the amorphous alloys obtained at an extremely fast cooling rate are closer to a homogeneous glass. On one hand, this poses a big challenge to study the structural heterogeneity of amorphous alloys with molecular dynamics (MD) simulations because the cooling rate utilized in MD simulations is usually unrealistically high. On the other hand, we believe that, with the notion of “varying structural heterogeneities”, it may be worth revisiting the concepts

and ideas on the structure-property correlation of amorphous alloys we developed through the tremendous studies carried out over the past nearly six decades.

### **Acknowledgements**

JCQ is indebted to Professor W.H Wang, Professor V. A. Khonik, Professor L.H. Dai, Professor Z.D. Sha, Professor Y.J. Wang, Dr. S.D. Feng for valuable discussions. The research of JCQ was supported by the Fundamental Research Funds for the Central Universities (Nos. 3102018ZY010 and 3102017JC1003). JCQ is also supported by the Hong Kong Scholar Program (Grant No. XJ2015056). JCQ thanks J. Wang and Q.F. He for their assistance. The research of YY was supported by the Research Grant Council (RGC), the Hong Kong Government, through the General Research Fund (GRF) with the Grant Nos. 11209317, 11213118 and 11207215. This work is a collaborative program (Proposal No.18GK0004) of the CRDAM-IMR, Tohoku University. QW acknowledges the financial supports provided by Natural Science Foundation of China (Grant No. 51871140), Natural Science Foundation of Shanghai (Grant No. 18ZR1414700) and the MOST 973 Program of China under the grant 2015CB856800. YYao acknowledges the financial supports from Natural Science Foundation of China (Grant No. 11572249, 11772257) and the Alexander von Humboldt Foundation. D.C. and E.P. acknowledge financial support from MINECO (grant FIS2017-82625-P) and Generalitat de Catalunya (grant 2017SGR0042).

### **References**

- [1] Klement W, Willens RH, Duwez POL. Non-crystalline Structure in Solidified Gold–Silicon Alloys. *Nature* 1960;187:869-70.
- [2] Inoue A. Stabilization of metallic supercooled liquid and bulk amorphous alloys. *Acta Materialia* 2000;48:279-306.
- [3] Hufnagel TC, Schuh CA, Falk ML. Deformation of metallic glasses: Recent developments in theory, simulations, and experiments. *Acta Materialia* 2016;109:375-93.

[4] Lan S, Ren Y, Wei XY, Wang B, Gilbert EP, Shibayama T, et al. Hidden amorphous phase and reentrant supercooled liquid in Pd-Ni-P metallic glasses. *Nature Communications* 2017;8:14679.

[5] He Y, Yi P, Falk ML. Critical Analysis of an FeP Empirical Potential Employed to Study the Fracture of Metallic Glasses. *Physical Review Letters* 2019;122:035501.

[6] Zhu F, Song S, Reddy KM, Hirata A, Chen M. Spatial heterogeneity as the structure feature for structure–property relationship of metallic glasses. *Nature Communications* 2018;9:3965.

[7] Smith HL, Li CW, Hoff A, Garrett GR, Kim DS, Yang FC, et al. Separating the configurational and vibrational entropy contributions in metallic glasses. *Nature Physics* 2017;13:900.

[8] Gao Y, Bei H. Strength statistics of single crystals and metallic glasses under small stressed volumes. *Progress in Materials Science* 2016;82:118-50.

[9] Schuh CA, Hufnagel TC, Ramamurty U. Mechanical behavior of amorphous alloys. *Acta Materialia* 2007;55:4067-109.

[10] Sun BA, Wang WH. The fracture of bulk metallic glasses. *Progress in Materials Science* 2015;74:211-307.

[11] Wang WH. The elastic properties, elastic models and elastic perspectives of metallic glasses. *Progress in Materials Science* 2012;57:487-656.

[12] Trexler MM, Thadhani NN. Mechanical properties of bulk metallic glasses. *Progress in Materials Science* 2010;55:759-839.

[13] Cheng YQ, Ma E. Atomic-level structure and structure-property relationship in metallic glasses. *Progress in Materials Science* 2011;56:379-473.

[14] Inoue A, Takeuchi A. Recent development and application products of bulk glassy alloys. *Acta Materialia* 2011;59:2243-67.

[15] Johnson WL. Bulk Glass-Forming Metallic Alloys: Science and Technology. *MRS Bulletin* 2013;24:42-56.

[16] Qiao JW, Jia HL, Liaw PK. Metallic glass matrix composites. *Mater Sci Eng R-Rep* 2016;100:1-69.

[17] Zhang ZF, Eckert J, Schultz L. Difference in compressive and tensile

fracture mechanisms of Zr<sub>59</sub>Cu<sub>20</sub>Al<sub>10</sub>Ni<sub>8</sub>Ti<sub>3</sub> bulk metallic glass. *Acta Materialia* 2003;51:1167-79.

[18] Waseda Y, Okazaki H, Masumoto T. Current views on the structure and crystallization of metallic glasses. *Journal of Materials Science* 1977;12:1927-49.

[19] Masumoto T, Hashimoto K. Chemical Properties of Amorphous Metals. *Annual Review of Materials Science* 1978;8:215-33.

[20] Zhu F, Hirata A, Liu P, Song S, Tian Y, Han J, et al. Correlation between Local Structure Order and Spatial Heterogeneity in a Metallic Glass. *Physical Review Letters* 2017;119:215501.

[21] Sun YL, Qu DD, Sun YJ, Liss KD, Shen J. Inhomogeneous structure and glass-forming ability in Zr-based bulk metallic glasses. *Journal of Non-Crystalline Solids* 2010;356:39-45.

[22] Li W, Bei H, Tong Y, Dmowski W, Gao YF. Structural heterogeneity induced plasticity in bulk metallic glasses: From well-relaxed fragile glass to metal-like behavior. *Applied Physics Letters* 2013;103:171910.

[23] Li W, Gao Y, Bei H. On the correlation between microscopic structural heterogeneity and embrittlement behavior in metallic glasses. *Scientific Reports* 2015;5:14786.

[24] Yang Y, Ye J, Lu J, Wang Q, Liaw PK. Revelation of the effect of structural heterogeneity on microplasticity in bulk metallic-glasses. *Journal of Materials Research* 2010;25:563-75.

[25] Ichitsubo T, Matsubara E, Yamamoto T, Chen HS, Nishiyama N, Saida J, et al. Microstructure of Fragile Metallic Glasses Inferred from Ultrasound-Accelerated Crystallization in Pd-Based Metallic Glasses. *Physical Review Letters* 2005;95:245501.

[26] Tian L, Volkert CA. Measuring Structural Heterogeneities in Metallic Glasses Using Transmission Electron Microscopy. *Metals* 2018;8:1085.

[27] Ke H, Liu C, Yang Y. Structural heterogeneity and deformation rheology in metallic glasses. *Science China Technological Sciences* 2015;58:47-55.

[28] Liu C, Maaß R. Elastic Fluctuations and Structural Heterogeneities in Metallic Glasses. *Advanced Functional Materials* 2018;28:1800388.

[29] Huang B, Ge TP, Liu GL, Luan JH, He QF, Yuan QX, et al. Density

fluctuations with fractal order in metallic glasses detected by synchrotron X-ray nano-computed tomography. *Acta Materialia* 2018;155:69-79.

[30] Wisitsorasak A, Wolynes PG. On the strength of glasses. *Proceedings of the National Academy of Sciences* 2012;109:16068-72.

[31] Shintani H, Tanaka H. Frustration on the way to crystallization in glass. *Nature Physics* 2006;2:200.

[32] Egami T. Understanding the properties and structure of metallic glasses at the atomic level. *JOM* 2010;62:70-5.

[33] Zhu F, Nguyen HK, Song SX, Aji DPB, Hirata A, Wang H, et al. Intrinsic correlation between beta-relaxation and spatial heterogeneity in a metallic glass. *Nature Communications* 2016;7:11516.

[34] Cheng YQ, Ma E. Atomic-level structure and structure–property relationship in metallic glasses. *Progress in Materials Science* 2011;56:379-473.

[35] Wang Q, Liu JJ, Ye YF, Liu TT, Wang S, Liu CT, et al. Universal secondary relaxation and unusual brittle-to-ductile transition in metallic glasses. *Materials Today* 2017;20:293-300.

[36] Qiao JC, Liu XD, Wang Q, Liu CT, Lu J, Yang Y. Fast secondary relaxation and plasticity initiation in metallic glasses. *National Science Review* 2018;5:616-8.

[37] Zhu F, Nguyen HK, Song SX, Aji DPB, Hirata A, Wang H, et al. Intrinsic correlation between  $\beta$ -relaxation and spatial heterogeneity in a metallic glass. *Nature Communications* 2016;7:11516.

[38] Yu H-B, Wang W-H, Samwer K. The  $\beta$  relaxation in metallic glasses: an overview. *Materials Today* 2013;16:183-91.

[39] Berthier L, Biroli G. Theoretical perspective on the glass transition and amorphous materials. *Reviews of Modern Physics* 2011;83:587-645.

[40] Adam G, Gibbs JH. On the Temperature Dependence of Cooperative Relaxation Properties in Glass - Forming Liquids. *The Journal of Chemical Physics* 1965;43:139-46.

[41] Lubchenko V, Wolynes PG. Theory of Structural Glasses and Supercooled Liquids. *Annual Review of Physical Chemistry* 2007;58:235-66.

[42] Kirkpatrick TR, Wolynes PG. Connections between some kinetic and

equilibrium theories of the glass transition. *Physical Review A* 1987;35:3072-80.

[43] Xia X, Wolynes PG. Fragilities of liquids predicted from the random first order transition theory of glasses. *Proceedings of the National Academy of Sciences* 2000;97:2990-4.

[44] Kirkpatrick TR, Thirumalai D, Wolynes PG. Scaling concepts for the dynamics of viscous liquids near an ideal glassy state. *Physical Review A* 1989;40:1045-54.

[45] Kirkpatrick TR, Wolynes PG. Stable and metastable states in mean-field Potts and structural glasses. *Physical Review B* 1987;36:8552-64.

[46] Tanaka H. Two-order-parameter description of liquids. I. A general model of glass transition covering its strong to fragile limit. *The Journal of Chemical Physics* 1999;111:3163-74.

[47] Tanaka H. Relation between Thermodynamics and Kinetics of Glass-Forming Liquids. *Physical Review Letters* 2003;90:055701.

[48] Tanaka H. Roles of local icosahedral chemical ordering in glass and quasicrystal formation in metallic glass formers. *Journal of Physics: Condensed Matter* 2003;15:L491-L8.

[49] Wool RP. Twinkling fractal theory of the glass transition. *Journal of Polymer Science Part B: Polymer Physics* 2008;46:2765-78.

[50] Wool RP. Self-healing materials: a review. *Soft Matter* 2008;4:400-18.

[51] Granato AV. Interstitialcy model for condensed matter states of face-centered-cubic metals. *Physical Review Letters* 1992;68:974-7.

[52] Granato AV. A Comparison with empirical results of the interstitialcy theory of condensed matter. *Journal of Non-Crystalline Solids* 2006;352:4821-5.

[53] Perez J. Homogeneous flow and anelastic/plastic deformation of metallic glasses. *Acta Metallurgica* 1984;32:2163-73.

[54] Perez J. Theories of liquid-glass transition. *Journal of Food Engineering* 1994;22:89-114.

[55] Liu ST, Wang Z, Peng HL, Yu HB, Wang WH. The activation energy and volume of flow units of metallic glasses. *Scripta Materialia* 2012;67:9-12.

[56] Liu ST, Jiao W, Sun BA, Wang WH. A quasi-phase perspective on flow

units of glass transition and plastic flow in metallic glasses. *Journal of Non-Crystalline Solids* 2013;376:76-80.

[57] Stillinger FH, Debenedetti PG. Glass Transition Thermodynamics and Kinetics. *Annual Review of Condensed Matter Physics* 2013;4:263-85.

[58] Tanaka H, Kawasaki T, Shintani H, Watanabe K. Critical-like behaviour of glass-forming liquids. *Nature Materials* 2010;9:324.

[59] G Debenedetti P, M Truskett T, P Lewis C, H Stillinger F. Theory of supercooled liquids and glasses: Energy landscape and statistical geometry perspectives 2001.

[60] Ediger MD, Harrowell P. Perspective: Supercooled liquids and glasses. *The Journal of Chemical Physics* 2012;137:080901.

[61] Wang Q, Zhang ST, Yang Y, Dong YD, Liu CT, Lu J. Unusual fast secondary relaxation in metallic glass. *Nature Communications* 2015;6:7876.

[62] Yu HB, Wang WH, Bai HY, Samwer K. The  $\beta$  relaxation in metallic glasses. *National Science Review* 2014;1:429-61.

[63] Zhao ZF, Wen P, Shek CH, Wang WH. Measurements of slow  $\beta$ -relaxations in metallic glasses and supercooled liquids. *Physical Review B* 2007;75:174201.

[64] Pelletier JM, Van de Moortèle B, Lu IR. Viscoelasticity and viscosity of Pd–Ni–Cu–P bulk metallic glasses. *Materials Science and Engineering: A* 2002;336:190-5.

[65] Küchemann S, Maaß R. Gamma relaxation in bulk metallic glasses. *Scripta Materialia* 2017;137:5-8.

[66] Wang XD, Zhang J, Xu TD, Yu Q, Cao QP, Zhang DX, et al. Structural Signature of  $\beta$ -Relaxation in La-Based Metallic Glasses. *The Journal of Physical Chemistry Letters* 2018:4308-13.

[67] Argon AS. Plastic deformation in metallic glasses. *Acta Metallurgica* 1979;27:47-58.

[68] Langer JS. Dynamics of shear-transformation zones in amorphous plasticity: Formulation in terms of an effective disorder temperature. *Physical Review E* 2004;70:041502.

[69] Ding J, Cheng YQ, Ma E. Quantitative measure of local solidity/liquidity in metallic glasses. *Acta Materialia* 2013;61:4474-80.

[70] Zhong C, Zhang H, Cao QP, Wang XD, Zhang DX, Ramamurty U, et al. Deformation behavior of metallic glasses with shear band like atomic structure: a molecular dynamics study. *Scientific Reports* 2016;6:30935.

[71] Egami T. Atomic level stresses. *Progress in Materials Science* 2011;56:637-53.

[72] Fan Y, Iwashita T, Egami T. How thermally activated deformation starts in metallic glass. *Nature Communications* 2014;5:5083.

[73] Ma E, Ding J. Tailoring structural inhomogeneities in metallic glasses to enable tensile ductility at room temperature. *Materials Today* 2016;19:568-79.

[74] Feng S, Qi L, Wang L, Pan S, Ma M, Zhang X, et al. Atomic structure of shear bands in Cu<sub>64</sub>Zr<sub>36</sub> metallic glasses studied by molecular dynamics simulations. *Acta Materialia* 2015;95:236-43.

[75] Feng SD, Chan KC, Chen SH, Zhao L, Liu RP. The role of configurational disorder on plastic and dynamic deformation in Cu<sub>64</sub>Zr<sub>36</sub> metallic glasses: A molecular dynamics analysis. *Scientific Reports* 2017;7:40969.

[76] Perepezko JH, Imhoff SD, Chen M-W, Wang J-Q, Gonzalez S. Nucleation of shear bands in amorphous alloys. *Proceedings of the National Academy of Sciences of the United States of America* 2014;111:3938-42.

[77] Greer AL, Cheng YQ, Ma E. Shear bands in metallic glasses. *Mater Sci Eng R-Rep* 2013;74:71-132.

[78] Falk ML, Langer JS. Deformation and Failure of Amorphous, Solidlike Materials. *Annual Review of Condensed Matter Physics* 2011;2:353-73.

[79] Wang WH. Correlation between relaxations and plastic deformation, and elastic model of flow in metallic glasses and glass-forming liquids. *Journal of Applied Physics* 2011;110:053521.

[80] Ruta B, Pineda E, Evenson Z. Relaxation processes and physical aging in metallic glasses. *Journal of Physics-Condensed Matter* 2017;29:503002.

[81] Liu C, Pineda E, Crespo D. Mechanical Relaxation of Metallic Glasses: An Overview of Experimental Data and Theoretical Models. *Metals* 2015;5:1073.

[82] Hu Y-C, Li Y-W, Yang Y, Guan P-F, Bai H-Y, Wang W-H. Configuration correlation governs slow dynamics of supercooled metallic liquids. *Proceedings of the National Academy of Sciences* 2018;115:6375.

[83] Debenedetti PG, Stillinger FH. Supercooled liquids and the glass transition. *Nature* 2001;410:259-67.

[84] Busch R, Schroers J, Wang WH. Thermodynamics and Kinetics of Bulk Metallic Glass. *Mrs Bulletin* 2007;32:620-3.

[85] Böhmer R, Ngai KL, Angell CA, Plazek DJ. Nonexponential relaxations in strong and fragile glass formers. *Journal of Chemical Physics* 1998;99:4201-9.

[86] Perera DN. Compilation of the fragility parameters for several glass-forming metallic alloys. *Journal of Physics Condensed Matter* 1999;11:3807-12.

[87] Kelton KF. Kinetic and structural fragility—a correlation between structures and dynamics in metallic liquids and glasses. *Journal of Physics: Condensed Matter* 2016;29:023002.

[88] Mauro NA, Blodgett M, Johnson ML, Vogt AJ, Kelton KF. A structural signature of liquid fragility. *Nature Communications* 2014;5:4616.

[89] Novikov VN, Sokolov AP. Poisson's ratio and the fragility of glass-forming liquids. *Nature* 2004;431:961-3.

[90] Lewandowski JJ, Wang WH, Greer AL. Intrinsic plasticity or brittleness of metallic glasses. *Philosophical Magazine Letters* 2005;85:77-87.

[91] Park ES, Lee JY, Kim DH, Gebert A, Schultz L. Correlation between plasticity and fragility in Mg-based bulk metallic glasses with modulated heterogeneity. *Journal of Applied Physics* 2008;104:023520.

[92] Kim DH, Kim WT, Park ES, Mattern N, Eckert J. Phase separation in metallic glasses. *Progress in Materials Science* 2013;58:1103-72.

[93] Ediger MD, Angell CA, Nagel SR. Supercooled Liquids and Glasses. *Jphyschem* 1999;100:13200-12.

[94] Qiao JC, Pelletier JM. Dynamic mechanical analysis in La-based bulk metallic glasses: Secondary ( $\beta$ ) and main ( $\alpha$ ) relaxations. *Journal of Applied Physics* 2012;112:083528--6.

[95] Wang Z, Sun BA, Bai HY, Wang WH. Evolution of hidden localized flow

during glass-to-liquid transition in metallic glass. *Nature Communications* 2014;5:5823.

[96] Chen HS, Leamy HJ, Barmatz M. The elastic and anelastic behavior of a metallic glass. *Journal of Non-Crystalline Solids* 1971;5:444-8.

[97] Chen HS, Goldstein M. Anomalous Viscoelastic Behavior of Metallic Glasses of Pd–Si- based Alloys. *Journal of Applied Physics* 2003;43:1642-8.

[98] Murata T, Kimura H, Masumoto T. Anelastic strain recovery of amorphous metals. *Scripta Metallurgica* 1976;10:705-9.

[99] Qiao JC, Pelletier JM, Yao Y. Creep in bulk metallic glasses. Transition from linear to non linear regime. *Materials Science and Engineering: A* 2019;743:185-9.

[100] Kimura H, Murata T, Masumoto T. Viscoelastic Behavior of Amorphous Metals. 1976;26:270-82.

[101] Chen HS. Atomic Transport Behavior in Metallic Glasses. 1979;27:97-109.

[102] Hettwer KJ, Haessner F. Influence of heat treatment on the internal friction of metglas Fe 32 Ni 36 Cr 14 P 12 B 6. *Materials Science & Engineering* 1982;52:147-54.

[103] Liu C, Pineda E, Crespo D, Qiao J, Evenson Z, Ruta B. Sub-T-g relaxation times of the alpha process in metallic glasses. *Journal of Non-Crystalline Solids* 2017;471:322-7.

[104] Taub AI, Spaepen F. The kinetics of structural relaxation of a metallic glass. *Acta Metallurgica* 1980;28:1781-8.

[105] Havriliak S, Negami S. A complex plane representation of dielectric and mechanical relaxation processes in some polymers. *Polymer* 1967;8:161-210.

[106] Cole KS, Cole RH. Dispersion and Absorption in Dielectrics I. Alternating Current Characteristics. *Journal of Chemical Physics* 2004;9:341-51.

[107] Svanberg C. Correlation function for relaxations in disordered materials. *Journal of Applied Physics* 2003;94:4191-7.

[108] Kohlrausch R. Theorie des elektrischen Rückstandes in der Leidener Flasche. *Annalen Der Physik* 1854;167:179–214.

[109] Williams G, Watts DC. Non-symmetrical dielectric relaxation behaviour arising from a simple empirical decay function. *Transactions of the Faraday Society* 1970;66:80-5.

[110] Alvarez F, Alegria A, Colmenero J. Relationship between the time-domain Kohlrausch-Williams-Watts and frequency-domain Havriliak-Negami relaxation functions. *Physical Review B* 1991;44:7306-12.

[111] Wang LM, Liu R, Wang WH. Relaxation time dispersions in glass forming metallic liquids and glasses. *Journal of Chemical Physics* 2008;128:164503.

[112] Qiao JC, Pelletier JM. Dynamic universal characteristic of the main ( $\alpha$ ) relaxation in bulk metallic glasses. *Journal of Alloys & Compounds* 2014;589:263-70.

[113] Qiao JC, Pelletier JM. Mechanical relaxation in a Zr-based bulk metallic glass: Analysis based on physical models. *Journal of Applied Physics* 2012;112:033518.

[114] Pineda E, Bruna P, Ruta B, Gonzalez-Silveira M, Crespo D. Relaxation of rapidly quenched metallic glasses: Effect of the relaxation state on the slow low temperature dynamics. *Acta Materialia* 2013;61:3002-11.

[115] Liu C, Pineda E, Crespo D. Characterization of mechanical relaxation in a Cu-Zr-Al metallic glass. *Journal of Alloys & Compounds* 2014;643:S17-S21.

[116] Yao ZF, Qiao JC, Pelletier JM, Yao Y. Characterization and modeling of dynamic relaxation of a Zr-based bulk metallic glass. *Journal of Alloys and Compounds* 2017;690:212-20.

[117] Ju JD, Jang D, Nwankpa A, Atzmon M. An atomically quantized hierarchy of shear transformation zones in a metallic glass. *Journal of Applied Physics* 2011;109:053522.

[118] Ju JD, Atzmon M. A comprehensive atomistic analysis of the experimental dynamic-mechanical response of a metallic glass. *Acta Materialia* 2014;74:183-8.

[119] Qiao JC, Wang YJ, Zhao LZ, Dai LH, Crespo D, Pelletier JM, et al. Transition from stress-driven to thermally activated stress relaxation in metallic glasses. *Physical Review B* 2016;94:104203.

[120] Perera DN, Tsai AP, Perera DN. Thermal and viscoelastic properties of a strong bulk metallic glass former. *Journal of Physics D Applied Physics* 2000;33:1937-46.

[121] Jeong HT, Kim JH, Kim WT, Kim DH. The mechanical relaxations of a Mm 55 Al 25 Ni 10 Cu 10 amorphous alloy studied by dynamic mechanical analysis. *Materials Science & Engineering A* 2004;385:182-6.

[122] Jeong HT, Fleury E, Kim WT, Kim DH, Hono K. Study on the Mechanical Relaxations of a Zr<sub>36</sub>Ti<sub>24</sub>Be<sub>40</sub> Amorphous Alloy by Time-Temperature Superposition Principle. *Journal of the Physical Society of Japan* 2007;73:3192-7.

[123] Pineda E, Serrano J, Bruna P, Crespo D. Fragility measurement of Pd-based metallic glass by dynamic mechanical analysis. *Journal of Alloys & Compounds* 2010;504:S215-S8.

[124] Zhai F, Pineda E, Ruta B, Gonzalez-Silveira M, Crespo D. Aging and structural relaxation of hyper-quenched Mg 65 Cu 25 Y 10 metallic glass. *Journal of Alloys & Compounds* 2014;615:S9-S12.

[125] Qiao J, Casalini R, Pelletier J-M, Kato H. Characteristics of the Structural and Johari–Goldstein Relaxations in Pd-Based Metallic Glass-Forming Liquids. *The Journal of Physical Chemistry B* 2014;118:3720-30.

[126] Taub AI, Spaepen F. Homogeneous flow of amorphous Pd 77.5 Cu 6 Si 16.5. *Scripta Metallurgica* 1980;14:1197-9.

[127] Hutchinson JM. Physical aging of polymers. *Progress in Polymer Science* 1995;20:703-60.

[128] Wolynes PG, Lubchenko V. *Structural glasses and supercooled liquids: Theory, experiment, and applications*: John Wiley & Sons; 2012.

[129] Busch R, Bakke E, Johnson WL. Viscosity of the supercooled liquid and relaxation at the glass transition of the Zr 46.75 Ti 8.25 Cu 7.5 Ni 10 Be 27.5 bulk metallic glass forming alloy. *Acta Materialia* 1998;46:4725-32.

[130] Ruta B, Chushkin Y, Monaco G, Cipelletti L, Pineda E, Bruna P, et al. Atomic-scale relaxation dynamics and aging in a metallic glass probed by x-ray photon correlation spectroscopy. *Physical Review Letters* 2012;109:165701.

[131] Csach K, Bobrov OP, Khonik VA, Lyakhov SA, Kitagawa K. Relationship between the shear viscosity and heating rate of metallic glasses below T<sub>g</sub>. *Physical Review B* 2006;73:092107.

[132] Munch E, Pelletier JM, Sixou B, Vigier G. Characterization of the drastic increase in molecular mobility of a deformed amorphous polymer. *Physical Review Letters* 2006;97:207801.

[133] Qiao JC, Pelletier JM, Kou HC, Zhou X. Modification of atomic mobility in a Ti-based bulk metallic glass by plastic deformation or thermal annealing. *Intermetallics* 2012;28:128-37.

[134] Qiao JC, Pelletier JM, Esnouf C, Liu Y, Kato H. Impact of the structural state on the mechanical properties in a Zr-Co-Al bulk metallic glass. *Journal of Alloys and Compounds* 2014;607:139-49.

[135] Cui B, Yang J, Qiao J, Jiang M, Dai L, Wang Y-J, et al. Atomic theory of viscoelastic response and memory effects in metallic glasses. *Physical Review B* 2017;96:094203.

[136] Daw MS, Baskes MI. Embedded-atom method: Derivation and application to impurities, surfaces, and other defects in metals. *Physical Review B* 1984;29:6443-53.

[137] Vashishta P, Kalia RK, Rino JP, Ebbsjö I. Interaction potential for  $\text{SiO}_2$ : A molecular-dynamics study of structural correlations. *Physical Review B* 1990;41:12197-209.

[138] Johari GP, Goldstein M. Viscous Liquids and the Glass Transition. II. Secondary Relaxations in Glasses of Rigid Molecules. *Journal of Chemical Physics* 1970;53:2372-88.

[139] Berry BS, Pritchett WC, Tsuei CC. Discovery of an Internal-Friction Peak in the Metallic Glass Nb<sub>3</sub>Ge. *Physical Review Letters* 1978;41:410-3.

[140] Yoon HN, Eisenberg A. Dynamic mechanical properties of metallic glasses *Journal of Non-Crystalline Solids* 1978;29:357-64.

[141] Berry BS, Pritchett WC. Hydrogen-related internal friction peaks in metallic glasses. *Scripta Metallurgica* 1981;15:637-42.

[142] Künzi HU, Agyeman K, Güntherodt HJ. Internal friction peaks in metallic glasses. *Solid State Communications* 1979;32:711-4.

[143] Khonik VA, Spivak LV. On the nature of low temperature internal friction peaks in metallic glasses. *Acta Materialia* 1996;44:367-81.

[144] Fukuhara M, Wang X, Inoue A, Yin F. Low temperature dependence of elastic moduli and internal friction for the glassy alloy Zr<sub>55</sub>Cu<sub>30</sub>Al<sub>10</sub>Ni<sub>5</sub>. *physica status solidi (RRL) - Rapid Research Letters* 2007;1:220–2.

[145] Hachenberg J, Bedorf D, Samwer K, Richert R, Kahl A, Demetriou MD, et

al. Merging of the  $\alpha$  and  $\beta$  relaxations and aging via the Johari–Goldstein modes in rapidly quenched metallic glasses. *Applied Physics Letters* 2008;92:131911.

[146] Wang Z, Yu HB, Wen P, Bai HY, Wang WH. Pronounced slow beta-relaxation in La-based bulk metallic glasses. *Journal of Physics-Condensed Matter* 2011;23:142202.

[147] Guo L, Wu X, Zhu Z. Mechanical relaxation studies of  $\alpha$  and slow  $\beta$  processes in Nd<sub>65</sub>Fe<sub>15</sub>Co<sub>10</sub>Al<sub>10</sub> bulk metallic glass. *Journal of Applied Physics* 2011;109:113524.

[148] Qiao JC, Casalini R, Pelletier JM, Kato H. Characteristics of the structural and Johari-Goldstein relaxations in Pd-based metallic glass-forming liquids. *Journal of Physical Chemistry B* 2014;118:3720-30.

[149] Rösner P, Samwer K, Lunkenheimer P. Indications for an “excess wing” in metallic glasses from the mechanical loss modulus in Zr<sub>65</sub>Al<sub>7.5</sub>Cu<sub>27.5</sub>. *Europhys Lett* 2004;68:226-32.

[150] Qiao JC, Chen YH, Casalini R, Pelletier JM, Yao Y. Main  $\alpha$  relaxation and slow  $\beta$  relaxation processes in a La<sub>30</sub>Ce<sub>30</sub>Al<sub>15</sub>Co<sub>25</sub> metallic glass. *Journal of Materials Science & Technology* 2019;35:982-6.

[151] Okumura H, Inoue A, Masumoto T. Glass Transition and Viscoelastic Behaviors of La<sub>55</sub>Al<sub>25</sub>Ni<sub>20</sub> and La<sub>55</sub>Al<sub>25</sub>Cu<sub>20</sub> Amorphous Alloys. *Mater Trans JIM* 1991;32:593-8.

[152] Okumura H, Chen HS, Inoue A, Masumoto T. Sub- T<sub>g</sub> mechanical relaxation of a La 55 Al 25 Ni 20 amorphous alloy. *Journal of Non-Crystalline Solids* 1991;130:304-10.

[153] Huang B, Zhu ZG, Ge TP, Bai HY, Sun BA, Yang Y, et al. Hand in hand evolution of boson heat capacity anomaly and slow beta-relaxation in La-based metallic glasses. *Acta Materialia* 2016;110:73-83.

[154] Slipenyuk A, Eckert J. Correlation between enthalpy change and free volume reduction during structural relaxation of Zr 55 Cu 30 Al 10 Ni 5 metallic glass. *Scripta Materialia* 2004;50:39-44.

[155] Haruyama O, Nakayama Y, Wada R, Tokunaga H, Okada J, Ishikawa T, et al. Volume and enthalpy relaxation in Zr<sub>55</sub>Cu<sub>30</sub>Ni<sub>5</sub>Al<sub>10</sub> bulk metallic glass. *Acta Materialia* 2010;58:1829-36.

[156] Evenson Z, Busch R. Equilibrium viscosity, enthalpy recovery and free

volume relaxation in a Zr<sub>44</sub>Ti<sub>11</sub>Ni<sub>10</sub>Cu<sub>10</sub>Be<sub>25</sub> bulk metallic glass. *Acta Materialia* 2011;59:4404-15.

[157] Kiss S, Posgay G, Harangozó IZ, Kedves FJ. Structural relaxation and crystallization of FeB and NiP metallic glasses followed by internal friction and modulus measurements. *J Phys Colloques* 1981;42:529-34.

[158] Morito N, Egami T. Internal friction and reversible structural relaxation in the metallic glass Fe<sub>32</sub>Ni<sub>36</sub>Cr<sub>14</sub>P<sub>12</sub>B<sub>6</sub>. *Acta Metallurgica* 1984;32:603-13.

[159] Chen HS, Morito N. Sub-T<sub>g</sub> relaxation in a PdCuSi glass; internal friction measurements. *Journal of Non-Crystalline Solids* 1985;72:287-99.

[160] Deng D, Argon AS. Structural relaxation and embrittlement of Cu<sub>59</sub>Zr<sub>41</sub> and Fe<sub>80</sub>B<sub>20</sub> glasses. *Acta Metallurgica* 1986;34:2011-23.

[161] Deng D, Argon AS. Analysis of the effect of aging on distributed relaxations, hardness, and embrittlement in Cu<sub>59</sub>Zr<sub>41</sub> and Fe<sub>80</sub>B<sub>20</sub> glasses. *Acta Metallurgica* 1986;34:2025-38.

[162] Evenson Z, Naleway SE, Wei S, Gross O, Kruzic JJ, Gallino I, et al. beta relaxation and low-temperature aging in a Au-based bulk metallic glass: From elastic properties to atomic-scale structure. *Physical Review B* 2014;89:174204.

[163] Xue RJ, Zhao LZ, Zhang B, Bai HY, Wang WH, Pan MX. Role of low melting point element Ga in pronounced beta-relaxation behaviors in LaGa-based metallic glasses. *Applied Physics Letters* 2015;107:241902.

[164] Luo P, Lu Z, Zhu ZG, Li YZ, Bai HY, Wang WH. Prominent beta-relaxations in yttrium based metallic glasses. *Applied Physics Letters* 2015;106:031907.

[165] Liu CR, Pineda E, Qiao JC, Crespo D. Modeling of the Sub-T<sub>g</sub> Relaxation Spectrum of Pd<sub>42.5</sub>Ni<sub>7.5</sub>Cu<sub>30</sub>P<sub>20</sub> Metallic Glass. *Journal of Physical Chemistry B* 2016;120:2838-44.

[166] Zhao ZF, Wen P, Shek CH, Wang WH. Measurements of slow beta-relaxations in metallic glasses and supercooled liquids. *Physical Review B* 2007;75:174201.

[167] Yu HB, Wang WH, Bai HY, Wu Y, Chen MW. Relating activation of shear transformation zones to beta relaxations in metallic glasses. *Physical Review B* 2010;81:220201.

[168] Cohen Y, Karmakar S, Procaccia I, Samwer K. The nature of the beta-peak in the loss modulus of amorphous solids. *Epl* 2012;100:36003.

[169] Yu HB, Samwer K, Wu Y, Wang WH. Correlation between beta Relaxation and Self-Diffusion of the Smallest Constituting Atoms in Metallic Glasses. *Physical Review Letters* 2012;109:095508.

[170] Yu H-B, Yang M-H, Sun Y, Zhang F, Liu J-B, Wang CZ, et al. Fundamental Link between  $\beta$  Relaxation, Excess Wings, and Cage-Breaking in Metallic Glasses. *The Journal of Physical Chemistry Letters* 2018:5877-83.

[171] Yu H-B, Richert R, Samwer K. Structural rearrangements governing Johari-Goldstein relaxations in metallic glasses. *Science Advances* 2017;3:e1701577.

[172] Yu H-B, Richert R, Samwer K. Correlation between Viscoelastic Moduli and Atomic Rearrangements in Metallic Glasses. *The Journal of Physical Chemistry Letters* 2016;7:3747-51.

[173] Liu YH, Fujita T, Aji DPB, Matsuura M, Chen MW. Structural origins of Johari-Goldstein relaxation in a metallic glass. *Nature Communications* 2014;5:3238.

[174] Louzguine-Luzgin DV, Seki I, Yamamoto T, Kawaji H, Suryanarayana C, Inoue A. Double-stage glass transition in a metallic glass. *Physical Review B* 2010;81:144202.

[175] Okumura H, Inoue A, Masumoto T. Heating rate dependence of two glass transitions and phase-separation for a La<sub>55</sub>Al<sub>25</sub>Ni<sub>20</sub> amorphous alloy. *Acta Metallurgica Et Materialia* 1993;41:915-21.

[176] Perez J, Gobin PF. Phénomènes de relaxation et frottement intérieur dans les solides vitreux. *Revue De Physique Appliquée* 1977;12:819-36.

[177] Yu H-B, Wang W-H, Samwer K. The beta relaxation in metallic glasses: an overview. *Materials Today* 2013;16:183-91.

[178] Johari GP. Source of JG Relaxation in the Entropy of Glass. *The Journal of Physical Chemistry B* 2019.

[179] Ngai KL, Capaccioli S. Relation between the activation energy of the Johari-Goldstein beta relaxation and T-g of glass formers. *Physical Review E* 2004;69:031501.

[180] Wang Z, Ngai KL, Wang WH. Understanding the changes in ductility and Poisson's ratio of metallic glasses during annealing from microscopic dynamics.

Journal of Applied Physics 2015;118:034901.

[181] Qiao JC, Wang Y-J, Pelletier JM, Keer LM, Fine ME, Yao Y. Characteristics of stress relaxation kinetics of La<sub>60</sub>Ni<sub>15</sub>Al<sub>25</sub> bulk metallic glass. *Acta Materialia* 2015;98:43-50.

[182] Qiao JC, Pelletier JM. Dynamic Mechanical Relaxation in Bulk Metallic Glasses: A Review. *Journal of Materials Science & Technology* 2014;30:523-45.

[183] Qiao JC, Casalini R, Pelletier JM. Main (alpha) relaxation and excess wing in Zr<sub>50</sub>Cu<sub>40</sub>Al<sub>10</sub> bulk metallic glass investigated by mechanical spectroscopy. *Journal of Non-Crystalline Solids* 2015;407:106-9.

[184] Qiao J, Casalini R, Pelletier J-M. Effect of physical aging on Johari-Goldstein relaxation in La-based bulk metallic glass. *Journal of Chemical Physics* 2014;141:104510.

[185] Casalini R, Roland CM. Aging of the Secondary Relaxation to Probe Structural Relaxation in the Glassy State. *Physical Review Letters* 2009;102:035701.

[186] Casalini R, Roland CM. Anomalous properties of the local dynamics in polymer glasses. *Journal of Chemical Physics* 2009;131:114501.

[187] Dyre JC, Olsen NB. Minimal model for beta relaxation in viscous liquids. *Physical Review Letters* 2003;91:155703.

[188] Zhao LZ, Wang WH, Bai HY. Modulation of beta-relaxation by modifying structural configurations in metallic glasses. *Journal of Non-Crystalline Solids* 2014;405:207-10.

[189] Qiao JC, Pelletier JM, Casalini R. Relaxation of Bulk Metallic Glasses Studied by Mechanical Spectroscopy. *Journal of Physical Chemistry B* 2013;117:13658-66.

[190] Zhao LZ, Xue RJ, Zhu ZG, Ngai KL, Wang WH, Bai HY. A fast dynamic mode in rare earth based glasses. *The Journal of Chemical Physics* 2016;144:204507.

[191] Barmatz M, Chen HS. Young's modulus and internal-friction in metallic glass alloys from 1.5 to 300 K. *Physical Review B* 1974;9:4073-83.

[192] Kato H, Ichitsubo T, Wang H, Wada T. Dynamic Relaxation of Pd<sub>42.5</sub>Ni<sub>7.5</sub>Cu<sub>30</sub>P<sub>20</sub> Metallic Glass. *Journal of the Japan Society of Powder and Powder Metallurgy* 2013;60:228-35.

- [193] Barmatz M, Chen HS. Young's modulus and internal friction in metallic glass alloys from 1.5 to 300 K. *Physical Review B* 1974;9:4073-83.
- [194] Bi QL, Lü YJ, Wang WH. Multiscale Relaxation Dynamics in Ultrathin Metallic Glass-Forming Films. *Physical Review Letters* 2018;120:155501.
- [195] Zhang T, Ye F, Wang YL, Lin JP. Structural relaxation of La<sub>55</sub>Al<sub>25</sub>Ni<sub>10</sub>Cu<sub>10</sub> bulk metallic glass. *Metallurgical and Materials Transactions a-Physical Metallurgy and Materials Science* 2008;39A:1953-7.
- [196] Hu L, Yue Y. Secondary relaxation behavior in a strong glass. *Journal of Physical Chemistry B* 2008;112:9053-7.
- [197] Hu L, Yue Y. Secondary Relaxation in Metallic Glass Formers: Its Correlation with the Genuine Johari-Goldstein Relaxation. *Journal of Physical Chemistry C* 2009;113:15001-6.
- [198] Chen HS. Method for evaluating viscosities of metallic glasses from rates of thermal transformations. *Journal of Non-Crystalline Solids* 1978;27:257-63.
- [199] Qiao JC, Pelletier JM. Enthalpy relaxation in Cu<sub>46</sub>Zr<sub>45</sub>Al<sub>7</sub>Y<sub>2</sub> and Zr<sub>55</sub>Cu<sub>30</sub>Ni<sub>5</sub>Al<sub>10</sub> bulk metallic glasses by differential scanning calorimetry (DSC). *Intermetallics* 2011;19:9-18.
- [200] Song L, Xu W, Huo J, Wang J-Q, Wang X, Li R. Two-step relaxations in metallic glasses during isothermal annealing. *Intermetallics* 2018;93:101-5.
- [201] He N, Song L, Xu W, Huo J, Wang J-Q, Li R-W. The evolution of relaxation modes during isothermal annealing and its influence on properties of Fe-based metallic glass. *Journal of Non-Crystalline Solids* 2019;509:95-8.
- [202] Wang WH, Dong C, Shek CH. Bulk metallic glasses. *Mater Sci Eng R-Rep* 2004;44:45-89.
- [203] Faupel F, Frank W, Macht MP, Mehrer H, Naundorf V, Ratzke K, et al. Diffusion in metallic glasses and supercooled melts. *Reviews of Modern Physics* 2003;75:237-80.
- [204] Tarjus G, Kivelson D. Breakdown of the stokes-einstein relation in supercooled liquids. *Journal of Chemical Physics* 1995;103:3071-3.
- [205] Ngai KL. Why the glass transition problem remains unsolved? *Journal of Non-Crystalline Solids* 2007;353:709-18.

[206] Bartsch A, Raetzke K, Meyer A, Faupel F. Dynamic Arrest in Multicomponent Glass-Forming Alloys. *Physical Review Letters* 2010;104:195901.

[207] Spaepen F. A microscopic mechanism for steady state inhomogeneous flow in metallic glasses. *Acta Metallurgica* 1977;25:407-15.

[208] Argon AS. Plastic-deformation in metallic glasses. *Acta Metallurgica* 1979;27:47-58.

[209] Perez J. Quasi-punctual defects in vitreous solids and liquid-glass transition. *Solid State Ionics* 1990;39:69-79.

[210] Hu YC, Guan PF, Li MZ, Liu CT, Yang Y, Bai HY, et al. Unveiling atomic-scale features of inherent heterogeneity in metallic glass by molecular dynamics simulations. *Physical Review B* 2016;93:214202

[211] Das J, Tang MB, Kim KB, Theissmann R, Baier F, Wang WH, et al. "Work-hardenable" ductile bulk metallic glass. *Physical Review Letters* 2005;94:205501.

[212] Liu YH, Wang G, Wang RJ, Zhao DQ, Pan MX, Wang WH. Super Plastic Bulk Metallic Glasses at Room Temperature. *Science* 2007;315:1385-8.

[213] Kim KB, Das J, Baier F, Tang MB, Wang WH, Eckert J. Heterogeneity of a Cu<sub>47.5</sub>Zr<sub>47.5</sub>Al<sub>5</sub> bulk metallic glass. *Applied Physics Letters* 2006;88:051911.

[214] Wang JG, Zhao DQ, Pan MX, Shek CH, Wang WH. Mechanical heterogeneity and mechanism of plasticity in metallic glasses. *Applied Physics Letters* 2009;94:031904.

[215] Falk ML, Langer JS. Dynamics of viscoplastic deformation in amorphous solids. *Physical Review E* 1998;57:7192-205.

[216] Gilman JJ. Mechanical-behavior of metallic glasses. *Journal of Applied Physics* 1975;46:1625-33.

[217] Flores KM, Sherer E, Bharathula A, Chen H, Jean YC. Sub-nanometer open volume regions in a bulk metallic glass investigated by positron annihilation. *Acta Materialia* 2007;55:3403-11.

[218] Huo LS, Zeng JF, Wang WH, Liu CT, Yang Y. The dependence of shear modulus on dynamic relaxation and evolution of local structural heterogeneity in a metallic glass. *Acta Materialia* 2013;61:4329-38.

- [219] Schuh CA, Hufnagel TC, Ramamurty U. Mechanical behavior of amorphous alloys. *Acta Materialia* 2007;55:4067-109.
- [220] Xu J, Ramamurty U, Ma E. The fracture toughness of bulk metallic glasses. *Jom* 2010;62:10-8.
- [221] Pan D, Yokoyama Y, Fujita T, Liu YH, Kohara S, Inoue A, et al. Correlation between structural relaxation and shear transformation zone volume of a bulk metallic glass. *Applied Physics Letters* 2009;95:141909.
- [222] Greer AL, Sun YH. Stored energy in metallic glasses due to strains within the elastic limit. *Philosophical Magazine* 2016;96:1643-63.
- [223] Johnson WL, Samwer K. A universal criterion for plastic yielding of metallic glasses with a  $(T/T_g)^{2/3}$  temperature dependence. *Physical Review Letters* 2005;95:195501.
- [224] Harmon JS, Demetriou MD, Johnson WL, Samwer K. Anelastic to plastic transition in metallic glass-forming liquids. *Physical Review Letters* 2007;99:135502.
- [225] Johnson WL, Demetriou MD, Harmon JS, Lind ML, Samwer K. Rheology and ultrasonic properties of metallic glass-forming liquids: A potential energy landscape perspective. *Mrs Bulletin* 2007;32:644-50.
- [226] Frenkel J. Zur Theorie der Elastizitätsgrenze und der Festigkeit kristallinischer Körper. *Zeitschrift für Physik* 1926;37:572-609.
- [227] Yu HB, Shen X, Wang Z, Gu L, Wang WH, Bai HY. Tensile Plasticity in Metallic Glasses with Pronounced beta Relaxations. *Physical Review Letters* 2012;108:015504.
- [228] Wang WH. Correlations between elastic moduli and properties in bulk metallic glasses. *Journal of Applied Physics* 2006;99:093506.
- [229] Greaves GN, Greer AL, Lakes RS, Rouxel T. Poisson's ratio and modern materials *Nat Mater* 2011;10:823-37.
- [230] Ngai KL, Wang LM, Liu R, Wang WH. Microscopic dynamics perspective on the relationship between Poisson's ratio and ductility of metallic glasses. *Journal of Chemical Physics* 2014;140:44511.
- [231] Wang Z, Ngai KL, Wang WH, Capaccioli S. Coupling of caged molecule dynamics to Johari-Goldstein beta-relaxation in metallic glasses. *Journal of Applied Physics* 2016;119:024902.

[232] Liang DD, Wang XD, Ge K, Cao QP, Jiang JZ. Annealing effect on beta-relaxation in a La-based bulk metallic glass. *Journal of Non-Crystalline Solids* 2014;383:97-101.

[233] Madge SV, Louzguine-Luzgin DV, Lewandowski JJ, Greer AL. Toughness, extrinsic effects and Poisson's ratio of bulk metallic glasses. *Acta Materialia* 2012;60:4800-9.

[234] Park K-W, Lee C-M, Wakeda M, Shibutani Y, Falk ML, Lee J-C. Elastostatically induced structural disordering in amorphous alloys. *Acta Materialia* 2008;56:5440-50.

[235] Sandor MT, Ke HB, Wang WH, Wu Y. Anelasticity-induced increase of the Al-centered local symmetry in the metallic glass La<sub>50</sub>Ni<sub>15</sub>Al<sub>35</sub>. *Journal of Physics-Condensed Matter* 2013;25:165701.

[236] Jiao W, Sun BA, Wen P, Bai HY, Kong QP, Wang WH. Crossover from stochastic activation to cooperative motions of shear transformation zones in metallic glasses. *Applied Physics Letters* 2013;103:081904.

[237] Maass R, Klaumuenzer D, Loeffler JF. Propagation dynamics of individual shear bands during inhomogeneous flow in a Zr-based bulk metallic glass. *Acta Materialia* 2011;59:3205-13.

[238] Lu Z, Jiao W, Wang W, Bai H. Flow unit perspective on room temperature homogeneous plastic deformation in metallic glasses. *Phys Rev Lett* 2014;113:045501.

[239] Wang Z, Sun B, Bai H, Wang W. Evolution of hidden localized flow during glass-to-liquid transition in metallic glass. *Nat Commun* 2014;5.

[240] Qiao JC, Wang Y-J, Zhao LZ, Dai LH, Crespo D, Pelletier JM, et al. Transition from stress-driven to thermally activated stress relaxation in metallic glasses. *Physical Review B* 2016;94:104203.

[241] Wang Q, Liu JJ, Ye YF, Liu TT, Wang S, Liu CT, et al. Universal secondary relaxation and unusual brittle-to-ductile transition in metallic glasses. *Materials Today* 2017.

[242] Zhang C, Qiao JC, Pelletier JM, Yao Y. Arrhenius activation of Zr<sub>65</sub>Cu<sub>18</sub>Ni<sub>7</sub>Al<sub>10</sub> bulk metallic glass in the supercooled liquid region. *Intermetallics* 2017;86:88-93.

[243] Zhao LZ, Xue RJ, Zhu ZG, Ngai KL, Wang WH, Bai HY. A fast dynamic

mode in rare earth based glasses. *Journal of Chemical Physics* 2016;144:204507.

[244] Ding J, Patinet S, Falk ML, Cheng Y, Ma E. Soft spots and their structural signature in a metallic glass. *Proceedings of the National Academy of Sciences* 2014;111:14052-6.

[245] Ke HB, Zeng JF, Liu CT, Yang Y. Structure Heterogeneity in Metallic Glass: Modeling and Experiment. *Journal of Materials Science & Technology* 2014;30:560-5.

[246] Hufnagel TC, Schuh CA, Falk ML. Deformation of metallic glasses: Recent developments in theory, simulations, and experiments. *Acta Materialia* 2016;109:375-93.

[247] Miracle DB. A structural model for metallic glasses. *Nat Mater* 2004;3:697-702.

[248] Sheng HW, Luo WK, Alamgir FM, Bai JM, Ma E. Atomic packing and short-to-medium-range order in metallic glasses. *Nature* 2006;439:419-25.

[249] Shen YT, Kim TH, Gangopadhyay AK, Kelton KF. Icosahedral Order, Frustration, and the Glass Transition: Evidence from Time-Dependent Nucleation and Supercooled Liquid Structure Studies. *Physical Review Letters* 2009;102:057801.

[250] Wang Q, Liu CT, Yang Y, Liu JB, Dong YD, Lu J. The atomic-scale mechanism for the enhanced glass-forming-ability of a Cu-Zr based bulk metallic glass with minor element additions. *Scientific Reports* 2014;4:4648.

[251] Ma E. Tuning order in disorder. *Nat Mater* 2015;14:547-52.

[252] Zhang Y, Wang CZ, Zhang F, Mendeleev MI, Kramer MJ, Ho KM. Strong correlations of dynamical and structural heterogeneities with localized soft modes in a Cu-Zr metallic glass. *Applied Physics Letters* 2014;105:151910.

[253] Ye JC, Lu J, Liu CT, Wang Q, Yang Y. Atomistic free-volume zones and inelastic deformation of metallic glasses. *Nat Mater* 2010;9:619-23.

[254] Yang Y, Zeng JF, Ye JC, Lu J. Structural inhomogeneity and anelastic deformation in metallic glasses revealed by spherical nanoindentation. *Applied Physics Letters* 2010;97:261905.

[255] Wagner H, Bedorf D, Kuechemann S, Schwabe M, Zhang B, Arnold W, et al. Local elastic properties of a metallic glass. *Nat Mater* 2011;10:439-42.

[256] Sun YT, Wang JQ, Li YZ, Bai HY, Li MZ, Wang WH. Effects of atomic interaction stiffness on low-temperature relaxation of amorphous solids. *Physical Chemistry Chemical Physics* 2016;18:26643-50.

[257] Shi YF, Falk ML. Strain localization and percolation of stable structure in amorphous solids. *Physical Review Letters* 2005;95:095502.

[258] Peng HL, Li MZ, Sun BA, Wang WH. Characterization of mechanical heterogeneity in amorphous solids. *Journal of Applied Physics* 2012;112:023516.

[259] Liu YH, Wang D, Nakajima K, Zhang W, Hirata A, Nishi T, et al. Characterization of Nanoscale Mechanical Heterogeneity in a Metallic Glass by Dynamic Force Microscopy. *Physical Review Letters* 2011;106:125504.

[260] Li M, Wang CZ, Hao SG, Kramer MJ, Ho KM. Structural heterogeneity and medium-range order in ZrxCu100-x metallic glasses. *Physical Review B* 2009;80:184201.

[261] Fujita T, Wang Z, Liu Y, Sheng H, Wang W, Chen M. Low temperature uniform plastic deformation of metallic glasses during elastic iteration. *Acta Materialia* 2012;60:3741-7.

[262] Fan C, Liaw PK, Liu CT. Atomistic model of amorphous materials. *Intermetallics* 2009;17:86-7.

[263] Ding J, Cheng YQ, Ma E. On the origin of elastic strain limit of bulk metallic glasses. *Applied Physics Letters* 2014;104:011912.

[264] Lu YM, Zeng JF, Wang S, Sun BA, Wang Q, Lu J, et al. Structural Signature of Plasticity Unveiled by Nano-Scale Viscoelastic Contact in a Metallic Glass. *Scientific Reports* 2016;6:29357.

[265] Dmowski W, Iwashita T, Chuang CP, Almer J, Egami T. Elastic Heterogeneity in Metallic Glasses. *Physical Review Letters* 2010;105:205502.

[266] Wang Z, Wen P, Huo LS, Bai HY, Wang WH. Signature of viscous flow units in apparent elastic regime of metallic glasses. *Applied Physics Letters* 2012;101:121906.

[267] Yang Y, Zeng JF, Volland A, Blandin JJ, Gravier S, Liu CT. Fractal growth of the dense-packing phase in annealed metallic glass imaged by high-resolution atomic force microscopy. *Acta Materialia* 2012;60:5260-72.

[268] Zeng JF, Chu JP, Chen YC, Volland A, Blandin JJ, Gravier S, et al. On the

use of atomic force microscopy for structural mapping of metallic-glass thin films. *Intermetallics* 2014;44:121-7.

[269] Fan Y, Iwashita T, Egami T. Evolution of elastic heterogeneity during aging in metallic glasses. *Physical Review E* 2014;89:062313.

[270] Ding J, Patinet S, Falk ML, Cheng Y, Ma E. Soft spots and their structural signature in a metallic glass. *Proceedings of the National Academy of Sciences of the United States of America* 2014;111:14052-6.

[271] Mayr SG. Relaxation kinetics and mechanical stability of metallic glasses and supercooled melts. *Physical Review B* 2009;79:060201.

[272] Tomida T, Egami T. Molecular-dynamics study of structural anisotropy and anelasticity in metallic glasses. *Physical Review B* 1993;48:3048-57.

[273] Leonforte F, Boissiere R, Tanguy A, Wittmer JP, Barrat JL. Continuum limit of amorphous elastic bodies. III. Three-dimensional systems. *Physical Review B* 2005;72:224206.

[274] Mizuno H, Mossa S, Barrat J-L. Elastic heterogeneity, vibrational states, and thermal conductivity across an amorphisation transition. *Epl* 2013;104:56001.

[275] Mizuno H, Mossa S, Barrat J-L. Measuring spatial distribution of the local elastic modulus in glasses. *Physical Review E* 2013;87:042306.

[276] Tsamados M, Tanguy A, Goldenberg C, Barrat J-L. Local elasticity map and plasticity in a model Lennard-Jones glass. *Physical Review E* 2009;80:026112.

[277] Weaire D, Ashby MF, Logan J, Weins MJ. Use of pair potentials to calculate properties of amorphous metals. *Acta Metallurgica* 1971;19:779-&.

[278] Suzuki Y, Egami T. Shear deformation of glassy metals - breakdown of cauchy relationship and anelasticity. *Journal of Non-Crystalline Solids* 1985;75:361-6.

[279] Poulsen HF, Wert JA, Neuefeind J, Honkimaki V, Daymond M. Measuring strain distributions in amorphous materials. *Nat Mater* 2005;4:33-6.

[280] Hufnagel TC, Ott RT, Almer J. Structural aspects of elastic deformation of a metallic glass. *Physical Review B* 2006;73:064204.

[281] Wang XD, Bednarcik J, Saksl K, Franz H, Cao QP, Jiang JZ. Tensile behavior of bulk metallic glasses by in situ x-ray diffraction. *Applied Physics Letters* 2007;91:081913.

- [282] Stoica M, Das J, Bednarcik J, Franz H, Mattern N, Wang WH, et al. Strain distribution in Zr<sub>64.13</sub>Cu<sub>15.75</sub>Ni<sub>10.12</sub>Al<sub>10</sub> bulk metallic glass investigated by in situ tensile tests under synchrotron radiation. *Journal of Applied Physics* 2008;104:013522.
- [283] Mattern N, Bednarcik J, Pauly S, Wang G, Das J, Eckert J. Structural evolution of Cu-Zr metallic glasses under tension. *Acta Materialia* 2009;57:4133-9.
- [284] Maloney C, Lemaitre A. Universal breakdown of elasticity at the onset of material failure. *Physical Review Letters* 2004;93:195501.
- [285] Maloney CE, Lemaitre A. Amorphous systems in athermal, quasistatic shear. *Physical Review E* 2006;74:016118.
- [286] Feder J. *Fractals*: Plenum Press; 1988.
- [287] Stauffer D, Aharony A. *Introduction To Percolation Theory*: 2nd Edition. London: Taylor & Francis, 1992.
- [288] Turnbull D, Cohen MH. Free volume model of amorphous phase-glass transition. *Journal of Chemical Physics* 1961;34:120-&.
- [289] Falk ML, Langer JS, Pechenik L. Thermal effects in the shear-transformation-zone theory of amorphous plasticity: Comparisons to metallic glass data. *Physical Review E* 2004;70:011507.
- [290] Garcia R, Perez R. Dynamic atomic force microscopy methods. *Surface Science Reports* 2002;47:197-301.
- [291] Garcia R, Magerle R, Perez R. Nanoscale compositional mapping with gentle forces. *Nat Mater* 2007;6:405-11.
- [292] Garcia R, Gomez CJ, Martinez NF, Patil S, Dietz C, Magerle R. Identification of nanoscale dissipation processes by dynamic atomic force microscopy. *Physical Review Letters* 2006;97:016103.
- [293] Bhushan B, Qi J. Phase contrast imaging of nanocomposites and molecularly thick lubricant films in magnetic media. *Nanotechnology* 2003;14:886-95.
- [294] Gomez CJ, Garcia R. Determination and simulation of nanoscale energy dissipation processes in amplitude modulation AFM. *Ultramicroscopy* 2010;110:626-33.

[295] Ackerman PJ, Smalyukh, II. Static three-dimensional topological solitons in fluid chiral ferromagnets and colloids. *Nat Mater* 2017;16:426-32.

[296] Johnson WL. Bulk glass-forming metallic alloys: Science and technology. *Mrs Bulletin* 1999;24:42-56.

[297] Pan D, Inoue A, Sakurai T, Chen MW. Experimental characterization of shear transformation zones for plastic flow of bulk metallic glasses. *Proceedings of the National Academy of Sciences of the United States of America* 2008;105:14769-72.

[298] Shi Y, Falk ML. Stress-induced structural transformation and shear banding during simulated nanoindentation of a metallic glass. *Acta Materialia* 2007;55:4317-24.

[299] Li Q-K, Li M. Assessing the critical sizes for shear band formation in metallic glasses from molecular dynamics simulation. *Applied Physics Letters* 2007;91:231905.

[300] Dasgupta R, Hentschel HGE, Procaccia I. Microscopic Mechanism of Shear Bands in Amorphous Solids. *Physical Review Letters* 2012;109:255502.

[301] Cleveland JP, Anczykowski B, Schmid AE, Elings VB. Energy dissipation in tapping-mode atomic force microscopy. *Applied Physics Letters* 1998;72:2613-5.

[302] Rabe U, Amelio S, Kopycinska M, Hirsekorn S, Kempf M, Goken M, et al. Imaging and measurement of local mechanical material properties by atomic force acoustic microscopy. *Surface and Interface Analysis* 2002;33:65-70.

[303] Srolovitz D, Maeda K, Vitek V, Egami T. Structural defects in amorphous solids statistical-analysis of a computer-model. *Philosophical Magazine a-Physics of Condensed Matter Structure Defects and Mechanical Properties* 1981;44:847-66.

[304] Kopycinska-Muller M, Caron A, Hirsekorn S, Rabe U, Natter H, Hempelmann R, et al. Quantitative evaluation of elastic properties of nano-crystalline nickel using atomic force acoustic microscopy. *Z Phys Chemie-Int J Res Phys Chem Chem Phys* 2008;222:471-98.

[305] Yuya PA, Hurley DC, Turner JA. Contact-resonance atomic force microscopy for viscoelasticity. *Journal of Applied Physics* 2008;104:074916.

[306] Wang Q, Liu CT, Yang Y, Dong YD, Lu J. Atomic-Scale Structural Evolution and Stability of Supercooled Liquid of a Zr-Based Bulk Metallic Glass. *Physical Review Letters* 2011;106:215505.

[307] Ding J, Cheng Y-Q, Ma E. Full icosahedra dominate local order in Cu<sub>64</sub>Zr<sub>34</sub> metallic glass and supercooled liquid. *Acta Materialia* 2014;69:343-54.

[308] Miracle DB, Sanders WS, Senkov ON. The influence of efficient atomic packing on the constitution of metallic glasses. *Philosophical Magazine* 2003;83:2409-28.

[309] Zhang Y, Mendeleev MI, Wang CZ, Ott R, Zhang F, Besser MF, et al. Impact of deformation on the atomic structures and dynamics of a Cu-Zr metallic glass: A molecular dynamics study. *Physical Review B* 2014;90:174101.

[310] Cances E, Legoll F, Marinica MC, Minoukadeh K, Willaime F. Some improvements of the activation-relaxation technique method for finding transition pathways on potential energy surfaces. *Journal of Chemical Physics* 2009;130:114711.

[311] Barkema GT, Mousseau N. Event-based relaxation of continuous disordered systems. *Physical Review Letters* 1996;77:4358-61.

[312] Fujita T, Guan PF, Sheng HW, Inoue A, Sakurai T, Chen MW. Coupling between chemical and dynamic heterogeneities in a multicomponent bulk metallic glass. *Physical Review B* 2010;81:140204.

[313] Wang L-M, Tian Y, Liu R, Richert R. Structural Relaxation Dynamics in Binary Glass-Forming Molecular Liquids with Ideal and Complex Mixing Behavior. *The Journal of Physical Chemistry B* 2010;114:3618-22.

[314] Stevenson JD, Wolynes PG. A universal origin for secondary relaxations in supercooled liquids and structural glasses. *Nature Physics* 2009;6:62.

[315] Tanaka H. Two-order-parameter model of the liquid–glass transition. II. Structural relaxation and dynamic heterogeneity. *Journal of Non-Crystalline Solids* 2005;351:3385-95.

[316] Dyre JC. Colloquium: The glass transition and elastic models of glass-forming liquids. *Reviews of Modern Physics* 2006;78:953-72.

[317] Angell CA, Ngai KL, McKenna GB, McMillan PF, Martin SW. Relaxation in glassforming liquids and amorphous solids. *Journal of Applied Physics* 2000;88:3113-57.

[318] Karmakar S, Dasgupta C, Sastry S. Growing Length Scales and Their Relation to Timescales in Glass-Forming Liquids. *Annual Review of Condensed Matter Physics* 2014;5:255-84.

[319] Wisitsorasak A, Wolynes PG. On the strength of glasses. Proceedings of the National Academy of Sciences of the United States of America 2012;109:16068-72.

[320] Stevenson JD, Wolynes PG. A universal origin for secondary relaxations in supercooled liquids and structural glasses. Nat Phys 2009;6:62-8.

[321] Laird BB, Schober HR. Localized low-frequency vibrational modes in a simple model glass. Phys Rev Lett 1991;66:636-9.

[322] Debenedetti PG, Stillinger FH. Supercooled liquids and the glass transition. NATURE 2001;410:259-67.

[323] Johnson WL, Samwer K. A Universal Criterion for Plastic Yielding of Metallic Glasses with a  $(T/T_g)^{2/3}$  Temperature Dependence. Physical Review Letters 2005;95:195501.

[324] Zhang P, Maldonis JJ, Liu Z, Schroers J, Voyles PM. Spatially heterogeneous dynamics in a metallic glass forming liquid imaged by electron correlation microscopy. Nature Communications 2018;9:1129.

[325] Qiao JC, Wang Q, Crespo D, Yang Y, Pelletier JM. Secondary relaxation and dynamic heterogeneity in metallic glasses: A brief review. Chinese Physics B 2017;26:016402.

[326] Lu Z, Shang BS, Sun YT, Zhu ZG, Guan PF, Wang WH, et al. Revealing beta-relaxation mechanism based on energy distribution of flow units in metallic glass. Journal of Chemical Physics 2016;144:144501.

[327] Duc N, Zhu Z-G, Pringle B, Lyding J, Wang W-H, Gruebele M. Composition-dependent metallic glass alloys correlate atomic mobility with collective glass surface dynamics. Physical Chemistry Chemical Physics 2016;18:16856-61.

[328] Zhu ZG, Li YZ, Wang Z, Gao XQ, Wen P, Bai HY, et al. Compositional origin of unusual beta-relaxation properties in La-Ni-Al metallic glasses. Journal of Chemical Physics 2014;141:084506.

[329] Casalini R, Roland CM. Pressure evolution of the excess wing in a type-B glass former. Physical Review Letters 2003;91:015702.

[330] Kobayashi Y, Zheng W, Meyer EF, McGervey JD, Jamieson AM, Simha R. Free-volume and physical aging of poly(vinyl acetate) studied by positron-annihilation. Macromolecules 1989;22:2302-6.

- [331] Khonik VA. Understanding of the Structural Relaxation of Metallic Glasses within the Framework of the Interstitialcy Theory. *Metals* 2015;5:504.
- [332] Doolittle AK. Studies in newtonian flow .2. the dependence of the viscosity of liquids on free-space. *Journal of Applied Physics* 1951;22:1471-5.
- [333] Wang Z, Sun BA, Bai HY, Wang WH. Evolution of hidden localized flow during glass-to-liquid transition in metallic glass. *Nat Commun* 2014;5:5823.
- [334] Wang WH, Yang Y, Nieh TG, Liu CT. On the source of plastic flow in metallic glasses: Concepts and models. *Intermetallics* 2015;67:81-6.
- [335] Xue RJ, Wang DP, Zhu ZG, Ding DW, Zhang B, Wang WH. Characterization of flow units in metallic glass through density variation. *Journal of Applied Physics* 2013;114:123514.
- [336] Xue RJ, Zhao LZ, Pan MX, Zhang B, Wang WH. Correlation between density of metallic glasses and dynamic fragility of metallic glass-forming liquids. *Journal of Non-Crystalline Solids* 2015;425:153-7.
- [337] Wang DP, Zhu ZG, Xue RJ, Ding DW, Bai HY, Wang WH. Structural perspectives on the elastic and mechanical properties of metallic glasses. *Journal of Applied Physics* 2013;114:173505.
- [338] Zhu ZG, Wen P, Wang DP, Xue RJ, Zhao DQ, Wang WH. Characterization of flow units in metallic glass through structural relaxations. *Journal of Applied Physics* 2013;114:083512.
- [339] Qiao JC, Pelletier JM. Kinetics of structural relaxation in bulk metallic glasses by mechanical spectroscopy: Determination of the stretching parameter beta(KWW). *Intermetallics* 2012;28:40-4.
- [340] Lu Z, Jiao W, Wang WH, Bai HY. Flow unit perspective on room temperature homogeneous plastic deformation in metallic glasses. *Physical Review Letters* 2014;113:045501.
- [341] Mei JN, Soubeyroux JL, Blandin JJ, Li JS, Kou HC, Fu HZ, et al. Structural relaxation of Ti<sub>40</sub>Zr<sub>25</sub>Ni<sub>8</sub>Cu<sub>9</sub>Be<sub>18</sub> bulk metallic glass. *Journal of Non-Crystalline Solids* 2011;357:110-5.
- [342] Hodge IM. Effects of annealing and prior history on enthalpy relaxation in glassy-polymers .4. comparison of 5 polymers. *Macromolecules* 1983;16:898-902.
- [343] Lunkenheimer P, Pimenov A, Dressel M, Goncharov YG, Bohmer R, Loidl

A. Fast dynamics of glass-forming glycerol studied by dielectric spectroscopy. *Physical Review Letters* 1996;77:318-21.

[344] Gupta S, Fischer JKH, Lunkenheimer P, Loidl A, Novak E, Jalarvo N, et al. Effect of adding nanometre-sized heterogeneities on the structural dynamics and the excess wing of a molecular glass former. *Scientific Reports* 2016;6:35034.

[345] Sasaki N, Enyo A. Viscoelastic properties of bone as a function of water-content. *Journal of Biomechanics* 1995;28:809-15.

[346] Hagenah JU, Meier G, Fytas G, Fischer EW. Distribution of retardation times from the photon-correlation spectra of glass forming systems. *Polymer Journal* 1987;19:441-9.

[347] Luo P, Wen P, Bai HY, Ruta B, Wang WH. Relaxation Decoupling in Metallic Glasses at Low Temperatures. *Physical Review Letters* 2017;118:225901.

[348] Jiao W, Wen P, Peng HL, Bai HY, Sun BA, Wang WH. Evolution of structural and dynamic heterogeneities and activation energy distribution of deformation units in metallic glass. *Applied Physics Letters* 2013;102:101903.

[349] Wu YC, Wang B, Hu YC, Lu Z, Li YZ, Shang BS, et al. The critical strain - A crossover from stochastic activation to percolation of flow units during stress relaxation in metallic glass. *Scripta Materialia* 2017;134:75-9.

[350] Raghavan R, Murali P, Ramamurty U. Influence of cooling rate on the enthalpy relaxation and fragility of a metallic glass. *Metallurgical and Materials Transactions a-Physical Metallurgy and Materials Science* 2008;39A:1573-7.

[351] Angell CA. Relaxation in liquids, polymers and plastic crystals - strong fragile patterns and problems. *Journal of Non-Crystalline Solids* 1991;131:13-31.

[352] Gallino I, Shah MB, Busch R. Enthalpy relaxation and its relation to the thermodynamics and crystallization of the  $Zr_{58.5}Cu_{15.6}Ni_{12.8}Al_{10.3}Nb_{2.8}$  bulk metallic glass-forming alloy. *Acta Materialia* 2007;55:1367-76.

[353] Zhang Y, Hahn H. Study of the kinetics of free volume in  $Zr_{45.0}Cu_{39.3}Al_{7.0}Ag_{8.7}$  bulk metallic glasses during isothermal relaxation by enthalpy relaxation experiments. *Journal of Non-Crystalline Solids* 2009;355:2616-21.

[354] Granato AV. Interstitialcy theory of simple condensed matter. *European Physical Journal B* 2014;87.

[355] Nordlund K, Ashkenazy Y, Averback RS, Granato AV. Strings and interstitials in liquids, glasses and crystals. *Europhysics Letters* 2005;71:625-31.

[356] Stillinger FH, Weber TA. Point-defects in bcc crystals - structures, transition kinetics, and melting implications. *Journal of Chemical Physics* 1984;81:5095-103.

[357] Zhang H, Khalkhali M, Liu Q, Douglas JF. String-like cooperative motion in homogeneous melting. *Journal of Chemical Physics* 2013;138:12A538.

[358] Safonova EV, Mitrofanov YP, Konchakov RA, Vinogradov AY, Kobelev NP, Khonik VA. Experimental evidence for thermal generation of interstitials in a metallic crystal near the melting temperature. *Journal of Physics-Condensed Matter* 2016;28:215401.

[359] Safonova EV, Konchakov RA, Mitrofanov YP, Kobelev NP, Vinogradov AY, Khonik VA. Contribution of interstitial defects and anharmonicity to the premelting increase in the heat capacity of single-crystal aluminum. *JETP Letters* 2016;103:765-8.

[360] Khonik VA. Interstitialcy theory of condensed matter states and its application to non-crystalline metallic materials. *Chinese Physics B* 2017;26:016401.

[361] Granato AV. Comparison with empirical results of the interstitialcy theory of condensed matter. *Journal of Non-Crystalline Solids* 2006;352:4821-5.

[362] Granato AV, Joncich DM, Khonik VA. Melting, thermal expansion, and the Lindemann rule for elemental substances. *Applied Physics Letters* 2010;97:171911.

[363] Granato AV. The specific heat of simple liquids. *Journal of Non-Crystalline Solids* 2002;307:376-86.

[364] Granato AV. A derivation of the Vogel-Fulcher-Tammann relation for supercooled liquids. *Journal of Non-Crystalline Solids* 2011;357:334-8.

[365] Goncharova EV, Konchakov RA, Makarov AS, Kobelev NP, Khonik VA. Identification of interstitial-like defects in a computer model of glassy aluminum. *Journal of Physics-Condensed Matter* 2017;29:305701.

[366] Khonik SV, Granato AV, Joncich DM, Pompe A, Khonik VA. Evidence of Distributed Interstitialcy-Like Relaxation of the Shear Modulus due to Structural Relaxation of Metallic Glasses. *Physical Review Letters* 2008;100:065501.

[367] Khonik VA, Mitrofanov YP, Makarov AS, Konchakov RA, Afonin GV,

Tsyplakov AN. Structural relaxation and shear softening of Pd- and Zr-based bulk metallic glasses near the glass transition. *Journal of Alloys and Compounds* 2015;628:27-31.

[368] Mitrofanov YP, Wang DP, Wang WH, Khonik VA. Interrelationship between heat release and shear modulus change due to structural relaxation of bulk metallic glasses. *Journal of Alloys and Compounds* 2016;677:80-6.

[369] Kobelev NP, Khonik VA. Theoretical analysis of the interconnection between the shear elasticity and heat effects in metallic glasses. *Journal of Non-Crystalline Solids* 2015;427:184-90.

[370] Mitrofanov YP, Wang DP, Makarov AS, Wang WH, Khonik VA. Towards understanding of heat effects in metallic glasses on the basis of macroscopic shear elasticity. *Scientific Reports* 2016;6:23026.

[371] Afonin GV, Mitrofanov YP, Makarov AS, Kobelev NP, Wang WH, Khonik VA. Universal relationship between crystallization-induced changes of the shear modulus and heat release in metallic glasses. *Acta Materialia* 2016;115:204-9.

[372] Gordon CA, Granato AV, Simmons RO. Evidence for the self-interstitial model of liquid and amorphous states from lattice parameter measurements in krypton. *Journal of Non-Crystalline Solids* 1996;205:216-20.

[373] Goncharova EV, Konchakov RA, Makarov AS, Kobelev NP, Khonik VA. On the nature of density changes upon structural relaxation and crystallization of metallic glasses. *Journal of Non-Crystalline Solids* 2017;471:396-9.

[374] Khonik VA, Kobelev NP. Alternative understanding for the enthalpy vs volume change upon structural relaxation of metallic glasses. *Journal of Applied Physics* 2014;115:093510.

[375] Makarov S, Mitrofanov YP, Afonin GV, Kobelev NP, Khonik VA. Shear susceptibility - A universal integral parameter relating the shear softening, heat effects, anharmonicity of interatomic interaction and "defect" structure of metallic glasses. *Intermetallics* 2017;87:1-5.

[376] Perez J, Etienne S, Tatibouet J. Determination of glass-transition temperature by internal-friction measurements. *Phys Status Solidi A-Appl Res* 1990;121:129-38.

[377] Cavaille JY, Perez J, Johari GP. Molecular theory for the rheology of glasses and polymers. *Physical Review B* 1989;39:2411-22.

[378] Gauthier C, Pelletier JM, David L, Vigier G, Perez J. Relaxation of non-crystalline solids under mechanical stress. *Journal of Non-Crystalline Solids* 2000;274:181-7.

[379] Rinaldi R, Gaertner R, Chazeau L, Gauthier C. Modelling of the mechanical behaviour of amorphous glassy polymer based on the Quasi Point Defect theory-Part I: Uniaxial validation on polycarbonate. *Int J Non-Linear Mech* 2011;46:496-506.

[380] Qiao JC, Feng SD, Pelletier JM, Crespo D, Pineda E, Yao Y. Physical aging effects on the dynamic relaxation behavior and mechanical properties of Cu<sub>46</sub>Zr<sub>46</sub>Al<sub>8</sub> metallic glass. *Journal of Alloys and Compounds* 2017;726:195-200.

[381] Song KK, Pauly S, Zhang Y, Scudino S, Gargarella P, Surreddi KB, et al. Significant tensile ductility induced by cold rolling in Cu<sub>47.5</sub>Zr<sub>47.5</sub>Al<sub>5</sub> bulk metallic glass. *Intermetallics* 2011;19:1394-8.

[382] Wu X, Guo L, Liu CS. Dynamics of Johari-Goldstein beta relaxation and its universal relation to alpha relaxation in bulk metallic glasses by mechanical spectroscopy. *Journal of Applied Physics* 2014;115:223506.

[383] Chen HS. EFFECTS OF COLD ROLLING ON YOUNGS MODULUS AND STRUCTURE OF METALLIC GLASSES. *Scripta Metallurgica* 1975;9:411-5.

[384] Yamamoto R, Onuki A. Dynamics of highly supercooled liquids: Heterogeneity, rheology, and diffusion. *Physical Review E* 1998;58:3515-29.

[385] Donth E. The size of cooperatively rearranging regions at the glass-transition. *Journal of Non-Crystalline Solids* 1982;53:325-30.

[386] Donth E. The size of cooperatively rearranging regions at the glass transition. *Journal of Non-Crystalline Solids* 1982;53:325-30.

[387] Berthier L, Biroli G, Bouchaud JP, Cipelletti L, El Masri D, L'Hote D, et al. Direct experimental evidence of a growing length scale accompanying the glass transition. *Science* 2005;310:1797-800.

[388] Berthier L, Biroli G, Bouchaud JP, Kob W, Miyazaki K, Reichman DR. Spontaneous and induced dynamic fluctuations in glass formers. I. General results and dependence on ensemble and dynamics. *Journal of Chemical Physics* 2007;126:184503.

[389] Capaccioli S, Ruocco G, Zamponi F. Dynamically correlated regions and configurational entropy in supercooled liquids. *Journal of Physical Chemistry B*

2008;112:10652-8.

[390] Hao SG, Wang CZ, Li MZ, Napolitano RE, Ho KM. Dynamic arrest and glass formation induced by self-aggregation of icosahedral clusters in  $Zr_{1-x}Cu_x$  alloys. *Physical Review B* 2011;84:064203.

[391] Ye JC, Lu J, Liu CT, Wang Q, Yang Y. Atomistic free-volume zones and inelastic deformation of metallic glasses. *Nature Materials* 2010;9:619.

[392] Zaccone A, Schall P, Terentjev EM. Microscopic origin of nonlinear nonaffine deformation in bulk metallic glasses. *Physical Review B* 2014;90:140203.

[393] Khonik VA. Amorphous physics and materials: Interstitialcy theory of condensed matter states and its application to non-crystalline metallic materials. *Chinese Physics B* 2017;26:016401.

[394] Egami T, Iwashita T, Dmowski W. Mechanical Properties of Metallic Glasses. *Metals* 2013;3.

[395] Ngai KL, Wang L-M, Liu R, Wang WH. Microscopic dynamics perspective on the relationship between Poisson's ratio and ductility of metallic glasses. *The Journal of Chemical Physics* 2014;140:044511.

[396] Yang GN, Sun BA, Chen SQ, Gu JL, Shao Y, Wang H, et al. Understanding the effects of Poisson's ratio on the shear band behavior and plasticity of metallic glasses. *Journal of Materials Science* 2017;52:6789-99.

[397] Lewandowski \* JJ, Wang WH, Greer AL. Intrinsic plasticity or brittleness of metallic glasses. *Philosophical Magazine Letters* 2005;85:77-87.

[398] Wang DP, Zhao DQ, Ding DW, Bai HY, Wang WH. Understanding the correlations between Poisson's ratio and plasticity based on microscopic flow units in metallic glasses. *Journal of Applied Physics* 2014;115:123507.

[399] Schroers J, Johnson WL. Ductile Bulk Metallic Glass. *Physical Review Letters* 2004;93:255506.

[400] Eckert J, Das J, Kim KB, Baier F, Tang MB, Wang WH, et al. High strength ductile Cu-base metallic glass. *Intermetallics* 2006;14:876-81.

[401] Yu P, Bai HY. Poisson's ratio and plasticity in CuZrAl bulk metallic glasses. *Materials Science and Engineering: A* 2008;485:1-4.

[402] Guo SF, Qiu JL, Yu P, Xie SH, Chen W. Fe-based bulk metallic glasses:

Brittle or ductile? Applied Physics Letters 2014;105:161901.

[403] Nollmann N, Binkowski I, Schmidt V, Rösner H, Wilde G. Impact of micro-alloying on the plasticity of Pd-based bulk metallic glasses. Scripta Materialia 2016;111:119-22.

[404] Kumar G, Prades-Rodel S, Blatter A, Schroers J. Unusual brittle behavior of Pd-based bulk metallic glass. Scripta Materialia 2011;65:585-7.

[405] Wang X, Cao QP, Chen YM, Hono K, Zhong C, Jiang QK, et al. A plastic Zr–Cu–Ag–Al bulk metallic glass. Acta Materialia 2011;59:1037-47.

[406] Sun BA, Hu YC, Wang DP, Zhu ZG, Wen P, Wang WH, et al. Correlation between local elastic heterogeneities and overall elastic properties in metallic glasses. Acta Materialia 2016;121:266-76.

[407] Evenson Z, Naleway SE, Wei S, Gross O, Kruzic JJ, Gallino I, et al.  $\beta$  relaxation and low-temperature aging in a Au-based bulk metallic glass: From elastic properties to atomic-scale structure. Physical Review B 2014;89:174204.

[408] Jiang MQ, Ling Z, Meng JX, Dai LH. Energy dissipation in fracture of bulk metallic glasses via inherent competition between local softening and quasi-cleavage. Philosophical Magazine 2008;88:407-26.

[409] Jiang MQ, Ling Z, Meng JX, Gao JB, Dai LH. Nanoscale periodic corrugation to dimple transition due to “beat” in a bulk metallic glass. Scripta Materialia 2010;62:572-5.

[410] Jiang MQ, Wilde G, Jiang F, Dai LH. Understanding ductile-to-brittle transition of metallic glasses from shear transformation zone dilatation. Theoretical and Applied Mechanics Letters 2015;5:200-4.

[411] Qu RT, Liu ZQ, Wang RF, Zhang ZF. Yield strength and yield strain of metallic glasses and their correlations with glass transition temperature. Journal of Alloys and Compounds 2015;637:44-54.

[412] Liu X, Li F, Yang Y. “Softness” as the structural origin of plasticity in disordered solids: a quantitative insight from machine learning. Science China Materials 2019;62:154-60.

[413] Cohen MH, Grest GS. Liquid-glass transition, a free-volume approach. Physical Review B 1979;20:1077-98.

[414] Suzuki Y, Egami T. Shear deformation of glassy metals: Breakdown of cauchy relationship and anelasticity. *Journal of Non-Crystalline Solids* 1985;75:361-6.

[415] Mangion MBM, Cavallé JY, Perez J. A molecular theory for the sub-tg plastic mechanical response of amorphous polymers. *Philosophical Magazine A* 1992;66:773-96.

[416] Perepezko JH, Imhoff SD, Chen M-W, Wang J-Q, Gonzalez S. Nucleation of shear bands in amorphous alloys. *Proceedings of the National Academy of Sciences* 2014;111:3938-42.

[417] Greer AL, Cheng YQ, Ma E. Shear bands in metallic glasses. *Materials Science and Engineering: R: Reports* 2013;74:71-132.

[418] Wang S, Ye YF, Sun BA, Liu CT, Shi SQ, Yang Y. Softening-induced plastic flow instability and indentation size effect in metallic glass. *Journal of the Mechanics and Physics of Solids* 2015;77:70-85.

[419] Ye JC, Chu JP, Chen YC, Wang Q, Yang Y. Hardness, yield strength, and plastic flow in thin film metallic-glass. *Journal of Applied Physics* 2012;112:053516.

[420] Volkert CA, Donohue A, Spaepen F. Effect of sample size on deformation in amorphous metals. *Journal of Applied Physics* 2008;103:083539.

[421] Schuh CA, Lund AC, Nieh TG. New regime of homogeneous flow in the deformation map of metallic glasses: elevated temperature nanoindentation experiments and mechanistic modeling. *Acta Materialia* 2004;52:5879-91.

[422] Guo H, Yan PF, Wang YB, Tan J, Zhang ZF, Sui ML, et al. Tensile ductility and necking of metallic glass. *Nature Materials* 2007;6:735.

[423] Jang D, Greer JR. Transition from a strong-yet-brittle to a stronger-and-ductile state by size reduction of metallic glasses. *Nature Materials* 2010;9:215.

[424] Chen CQ, Pei YT, De Hosson JTM. Effects of size on the mechanical response of metallic glasses investigated through in situ TEM bending and compression experiments. *Acta Materialia* 2010;58:189-200.

[425] Bharathula A, Lee S-W, Wright WJ, Flores KM. Compression testing of metallic glass at small length scales: Effects on deformation mode and stability. *Acta Materialia* 2010;58:5789-96.

[426] Yavari AR, Georgarakis K, Botta WJ, Inoue A, Vaughan G.

Homogenization of plastic deformation in metallic glass foils less than one micrometer thick. *Physical Review B* 2010;82:172202.

[427] Jang D, Gross CT, Greer JR. Effects of size on the strength and deformation mechanism in Zr-based metallic glasses. *International Journal of Plasticity* 2011;27:858-67.

[428] Shi Y. Size-dependent mechanical responses of metallic glasses. *International Materials Reviews* 2019;64:163-80.

[429] Liontas R, Jafary-Zadeh M, Zeng Q, Zhang Y-W, Mao WL, Greer JR. Substantial tensile ductility in sputtered Zr-Ni-Al nano-sized metallic glass. *Acta Materialia* 2016;118:270-85.

[430] Bharathula A, Flores KM. Variability in the yield strength of a metallic glass at micron and submicron length scales. *Acta Materialia* 2011;59:7199-205.

[431] Hieronymus-Schmidt V, Rösner H, Wilde G, Zaccone A. Shear banding in metallic glasses described by alignments of Eshelby quadrupoles. *Physical Review B* 2017;95:134111.

[432] Pan D, Inoue A, Sakurai T, Chen MW. Experimental characterization of shear transformation zones for plastic flow of bulk metallic glasses. *Proceedings of the National Academy of Sciences* 2008;105:14769-72.

[433] Limbach R, Kosiba K, Pauly S, Kühn U, Wondraczek L. Serrated flow of CuZr-based bulk metallic glasses probed by nanoindentation: Role of the activation barrier, size and distribution of shear transformation zones. *Journal of Non-Crystalline Solids* 2017;459:130-41.

[434] Mayr SG. Activation Energy of Shear Transformation Zones: A Key for Understanding Rheology of Glasses and Liquids. *Physical Review Letters* 2006;97:195501.

[435] Vempati UK, Valavala PK, Falk ML, Almer J, Hufnagel TC. Length-scale dependence of elastic strain from scattering measurements in metallic glasses. *Physical Review B* 2012;85:214201.

[436] Chen LY, Li BZ, Wang XD, Jiang F, Ren Y, Liaw PK, et al. Atomic-scale mechanisms of tension–compression asymmetry in a metallic glass. *Acta Materialia* 2013;61:1843-50.

[437] Zhang M, Wang YJ, Dai LH. Bridging shear transformation zone to the atomic structure of amorphous solids. *Journal of Non-Crystalline Solids*

2015;410:100-5.

[438] Wang G, Zhao DQ, Bai HY, Pan MX, Xia AL, Han BS, et al. Nanoscale Periodic Morphologies on the Fracture Surface of Brittle Metallic Glasses. *Physical Review Letters* 2007;98:235501.

[439] Wisitsorasak A, Wolynes PG. Dynamical theory of shear bands in structural glasses. *Proceedings of the National Academy of Sciences* 2017;114:1287.

[440] Zhang Y, Greer AL. Thickness of shear bands in metallic glasses. *Applied Physics Letters* 2006;89:071907.

[441] Chen M, Inoue A, Zhang W, Sakurai T. Extraordinary Plasticity of Ductile Bulk Metallic Glasses. *Physical Review Letters* 2006;96:245502.

[442] Zhang Y. Inhomogeneous deformation in metallic glasses. *Materials Science and Technology* 2008;24:379-91.

[443] Georgarakis K, Aljerf M, Li Y, LeMoulec A, Charlot F, Yavari AR, et al. Shear band melting and serrated flow in metallic glasses. *Applied Physics Letters* 2008;93:031907.

[444] Furukawa A, Tanaka H. Inhomogeneous flow and fracture of glassy materials. *Nature Materials* 2009;8:601.

[445] Lu J, Ravichandran G, Johnson WL. Deformation behavior of the Zr<sub>41.2</sub>Ti<sub>13.8</sub>Cu<sub>12.5</sub>Ni<sub>10</sub>Be<sub>22.5</sub> bulk metallic glass over a wide range of strain-rates and temperatures. *Acta Materialia* 2003;51:3429-43.

[446] Liu ZY, Chen MW, Liu CT, Yang Y. Origin of yielding in metallic glass: Stress-induced flow. *Applied Physics Letters* 2014;104:251901.

[447] Guan P, Chen M, Egami T. Stress-Temperature Scaling for Steady-State Flow in Metallic Glasses. *Physical Review Letters* 2010;104:205701.

[448] Yu HB, Shen X, Wang Z, Gu L, Wang WH, Bai HY. Tensile Plasticity in Metallic Glasses with Pronounced  $\beta$  Relaxations. *Physical Review Letters* 2012;108:015504.

[449] Tsai P, Kranjc K, Flores KM. Hierarchical heterogeneity and an elastic microstructure observed in a metallic glass alloy. *Acta Materialia* 2017;139:11-20.

[450] Du XH, Huang JC, Hsieh KC, Lai YH, Chen HM, Jang JSC, et al. Two-glassy-phase bulk metallic glass with remarkable plasticity. *Applied Physics*

Letters 2007;91:131901.

[451] Chen SS, Zhang HR, Todd I. Phase-separation-enhanced plasticity in a Cu<sub>47.2</sub>Zr<sub>46.5</sub>Al<sub>5.5</sub>Nb<sub>0.8</sub> bulk metallic glass. *Scripta Materialia* 2014;72-73:47-50.

[452] Ren YL, Zhu RL, Sun J, You JH, Qiu KQ. Phase separation and plastic deformation in an Mg-based bulk metallic glass. *Journal of Alloys and Compounds* 2010;493:L42-L6.

[453] Chen N, .., Louzguine-Luzgin DV, Xie GQ, Sharma P, .., Perepezko JH, Esashi M, .., et al. Structural investigation and mechanical properties of a representative of a new class of materials: nanograined metallic glasses. *Nanotechnology* 2013;24:045610.

[454] Sato K, Takenaka K, Makino A, Hirotsu Y. Direct imaging of structural heterogeneity of the melt-spun Fe<sub>85.2</sub>Si<sub>2</sub>B<sub>8</sub>P<sub>4</sub>Cu<sub>0.8</sub> alloy. *AIP Advances* 2015;5:067166.

[455] Ketov SV, Trifonov AS, Ivanov YP, Churyumov AY, Lubenchenko AV, Batrakov AA, et al. On cryothermal cycling as a method for inducing structural changes in metallic glasses. *NPG Asia Materials* 2018;10:137-45.

[456] Ketov SV, Sun YH, Nachum S, Lu Z, Checchi A, Beraldin AR, et al. Rejuvenation of metallic glasses by non-affine thermal strain. *Nature* 2015;524:200.

[457] Saida J, Yamada R, Wakeda M. Recovery of less relaxed state in Zr-Al-Ni-Cu bulk metallic glass annealed above glass transition temperature. *Applied Physics Letters* 2013;103:221910.

[458] Guo W, Yamada R, Saida J, Lü S, Wu S. Thermal rejuvenation of a heterogeneous metallic glass. *Journal of Non-Crystalline Solids* 2018;498:8-13.

[459] Guo W, Yamada R, Saida J. Rejuvenation and plasticization of metallic glass by deep cryogenic cycling treatment. *Intermetallics* 2018;93:141-7.

[460] Priezjev NV. The effect of cryogenic thermal cycling on aging, rejuvenation, and mechanical properties of metallic glasses. *Journal of Non-Crystalline Solids* 2019;503-504:131-8.

[461] Guo W, Yamada R, Saida J, Lü S, Wu S. Various Rejuvenation Behaviors of Zr-Based Metallic Glass by Cryogenic Cycling Treatment with Different Casting Temperatures. *Nanoscale Research Letters* 2018;13:398.

[462] Guo W, Saida J, Zhao M, Lü S, Wu S. Thermal Rejuvenation of an

Mg-Based Metallic Glass. *Metallurgical and Materials Transactions A* 2019;50:1125-9.

[463] Stevenson JD, Wolynes PG. On the surface of glasses. *The Journal of Chemical Physics* 2008;129:234514.

[464] Wang DP, Yang Y, Niu XR, Lu J, Yang GN, Wang WH, et al. Resonance ultrasonic actuation and local structural rejuvenation in metallic glasses. *Physical Review B* 2017;95:235407.

[465] Chan HL, Ruan HH, Chen AY, Lu J. Optimization of the strain rate to achieve exceptional mechanical properties of 304 stainless steel using high speed ultrasonic surface mechanical attrition treatment. *Acta Materialia* 2010;58:5086-96.

[466] Wang Q, Yang Y, Jiang H, Liu CT, Ruan HH, Lu J. Superior Tensile Ductility in Bulk Metallic Glass with Gradient Amorphous Structure. *Scientific Reports* 2014;4:4757.

[467] Magagnosc DJ, Kumar G, Schroers J, Felfer P, Cairney JM, Gianola DS. Effect of ion irradiation on tensile ductility, strength and fictive temperature in metallic glass nanowires. *Acta Materialia* 2014;74:165-82.

[468] Bian XL, Wang G, Chen HC, Yan L, Wang JG, Wang Q, et al. Manipulation of free volumes in a metallic glass through Xe-ion irradiation. *Acta Materialia* 2016;106:66-77.

[469] Park ES, Kim DH. Phase separation and enhancement of plasticity in Cu–Zr–Al–Y bulk metallic glasses. *Acta Materialia* 2006;54:2597-604.

[470] Zhang ZQ, Song KK, Sun BA, Wang L, Cui WC, Qin YS, et al. Dual self-organised shear banding behaviours and enhanced ductility in phase separating Zr-based bulk metallic glasses. *Philosophical Magazine* 2018;98:1744-64.

[471] Yao KF, Ruan F, Yang YQ, Chen N. Superductile bulk metallic glass. *Applied Physics Letters* 2006;88:122106.

[472] Park ES, Kyeong JS, Kim DH. Phase separation and improved plasticity by modulated heterogeneity in Cu–(Zr,Hf)–(Gd,Y)–Al metallic glasses. *Scripta Materialia* 2007;57:49-52.

[473] He J, Kaban I, Mattern N, Song K, Sun B, Zhao J, et al. Local microstructure evolution at shear bands in metallic glasses with nanoscale phase separation. *Scientific Reports* 2016;6:25832.

[474] Jing J, Krämer A, Birringer R, Gleiter H, Gonser U. Modified atomic structure in a Pd · Fe · Si nanoglass: A Mössbauer study. *Journal of Non-Crystalline Solids* 1989;113:167-70.

[475] Fang JX, Vainio U, Puff W, Würschum R, Wang XL, Wang D, et al. Atomic Structure and Structural Stability of Sc<sub>75</sub>Fe<sub>25</sub> Nanoglasses. *Nano Letters* 2012;12:458-63.

[476] Ritter Y, Şopu D, Gleiter H, Albe K. Structure, stability and mechanical properties of internal interfaces in Cu<sub>64</sub>Zr<sub>36</sub> nanoglasses studied by MD simulations. *Acta Materialia* 2011;59:6588-93.

[477] Şopu D, Albe K, Ritter Y, Gleiter H. From nanoglasses to bulk massive glasses. *Applied Physics Letters* 2009;94:191911.

[478] Liu W-H, Sun BA, Gleiter H, Lan S, Tong Y, Wang X-L, et al. Nanoscale Structural Evolution and Anomalous Mechanical Response of Nanoglasses by Cryogenic Thermal Cycling. *Nano Letters* 2018;18:4188-94.

[479] Egami T. Nano-glass Mechanism of Bulk Metallic Glass Formation. *MATERIALS TRANSACTIONS* 2002;43:510-7.

[480] Gleiter H. Our thoughts are ours, their ends none of our own: Are there ways to synthesize materials beyond the limitations of today? *Acta Materialia* 2008;56:5875-93.

[481] Gleiter H. Nanoglasses: A New Kind of Noncrystalline Material and the Way to an Age of New Technologies? *Small* 2016;12:2225-33.

[482] Gleiter H. Nanoglasses: a new kind of noncrystalline materials. *Beilstein Journal of Nanotechnology* 2013;4:517-33.

[483] Söpu D, Ritter Y, Gleiter H, Albe K. Deformation behavior of bulk and nanostructured metallic glasses studied via molecular dynamics simulations. *Physical Review B* 2011;83:100202.

[484] Adibi S, Sha Z-D, Branicio PS, Joshi SP, Liu Z-S, Zhang Y-W. A transition from localized shear banding to homogeneous superplastic flow in nanoglass. *Applied Physics Letters* 2013;103:211905.

[485] Wang XL, Jiang F, Hahn H, Li J, Gleiter H, Sun J, et al. Plasticity of a scandium-based nanoglass. *Scripta Materialia* 2015;98:40-3.

[486] Li FC, Wang TY, He QF, Sun BA, Guo CY, Feng T, et al. Micromechanical

mechanism of yielding in dual nano-phase metallic glass. *Scripta Materialia* 2018;154:186-91.

[487] Chen N, Frank R, Asao N, Louzguine-Luzgin DV, Sharma P, Wang JQ, et al. Formation and properties of Au-based nanograin metallic glasses. *Acta Materialia* 2011;59:6433-40.

[488] Guo C, Fang Y, Wu B, Lan S, Peng G, Wang X-l, et al. Ni-P nanoglass prepared by multi-phase pulsed electrodeposition. *Materials Research Letters* 2017;5:293-9.

[489] Li FC, Wang S, He QF, Zhang H, Sun BA, Lu Y, et al. The stochastic transition from size dependent to size independent yield strength in metallic glasses. *Journal of the Mechanics and Physics of Solids* 2017;109:200-16.

[490] Sha Z-D, Branicio PS, Lee HP, Tay TE. Strong and ductile nanolaminate composites combining metallic glasses and nanoglasses. *International Journal of Plasticity* 2017;90:231-41.

[491] Sha ZD, He LC, Pei QX, Liu ZS, Zhang YW, Wang TJ. The mechanical properties of a nanoglass/metallic glass/nanoglass sandwich structure. *Scripta Materialia* 2014;83:37-40.

[492] Tanaka H. Physical Origin of the Boson Peak Deduced from a Two-Order-Parameter Model of Liquid. *Journal of the Physical Society of Japan* 2001;70:1178-81.

[493] Kawasaki T, Tanaka H. Structural signature of slow dynamics and dynamic heterogeneity in two-dimensional colloidal liquids: glassy structural order. *Journal of Physics: Condensed Matter* 2011;23:194121.

[494] Tanaka H. Bond orientational order in liquids: Towards a unified description of water-like anomalies, liquid-liquid transition, glass transition, and crystallization. *The European Physical Journal E* 2012;35:113.